UNIVERSITÀ
DEGLI STUDI
DI PADOVA

Sede amministrativa: Università degli Studi di Padova

Dipartimento di Ingegneria Civile Edile ed Ambientale

DOTTORATO DI RICERCA IN SCIENZE DELL'INGEGNERIA CIVILE ED AMBIENTALE

CICLO: XXVII

STATIC AND SEISMIC PERFORMANCES OF R.C. SHEAR WALLS CAST INTO WOOD CHIP AND CEMENT FORMWORKS

- Experimental tests, theoretical interpretation and numerical validations -

Direttore della scuola: Ch.mo Prof. **STEFANO LANZONI**

Supervisore: Ch.mo Prof. **ROBERTO SCOTTA**

Controrelatori: Prof. **OLIVER FISCHER**
Prof. **KONRAD BERGMEISTER**

Dottorando: **DAVIDE GIRARDINI**

GENNAIO 2015

To Fernanda

Sommario

Lo scopo di questa tesi di dottorato è quello di studiare il comportamento del particolare sistema costruttivo che fa uso di pareti portanti in calcestruzzo armato con getto entro blocco cassero in legno mineralizzato. Viene studiato tale sistema costruttivo sia sotto l'azione di forze pseudo-statiche (per via sperimentale e numerica), sia in fase dinamica (per via numerica).

Le attività svolte fanno in generale fatto uso di apparecchiature sperimentali per la realizzazione di test su materiali e su provini che possono essere sia porzioni di pannello che muri in scala reale. Inoltre si è fatto uso di software commerciali per la modellazione numerica degli elementi che compongono il sistema costruttivo in esame.

In particolare, nei primi capitoli della tesi si è fornita una completa trattazione analitica basata su risultati sperimentali ottenuti sia negli anni precedenti all'inizio del dottorato sia negli anni del dottorato. Gli aspetti originali dal punto di vista sperimentale, sono state le due campagne sperimentali riguardanti porzioni di pannello sollecitate a taglio diretto e muri in scala reale sollecitati da forze orizzontali in sommità cicliche di carattere pseudo-statico. Inoltre la campagna sperimentale è stata completata con le prove su connessioni parete-parete e parete-solaio previste dalle LL.GG. del Min. dei LL.PP. (2011) e mirate allo studio di pareti portanti gettate entro blocchi cassero.

Le prove di taglio diretto hanno dimostrato un'incongruità dei risultati sperimentali con la trattazione analitica degli anni precedenti al 2012 e quindi si è ritenuto necessario integrarla con nuove considerazioni teoriche. È stata sviluppata una nuova ed originale trattazione analitica basata su meccanismi di tipo puntone-tirante.

Negli ultimi capitoli il sistema costruttivo è stato inquadrato dal punto di vista numerico.
Nella modellazione numerica del sistema costruttivo è stata impiegata la trattazione analitica sviluppata facendo uso sia di elementi a plasticità concentrata che distribuita capaci di riprodurre i principali meccanismi di rottura documentati nelle prove sperimentali. Tale modellazione è stata prima validata sui risultati delle prove sperimentali su muri in scala reale e successivamente utilizzata per simulare il comportamento di edifici multipiano regolari ed irregolari, rispettivamente con modelli bidimensionali e spaziali. Tali edifici sono stati assoggettati sia a spinte statiche incrementali sia a sollecitazioni dinamiche di natura sismica. I risultati numerici delle simulazioni uniti alle curve di capacità sperimentali hanno permesso di stimare il comportamento sismico del sistema costruttivo e, infine, il fattore di struttura che meglio lo sintetizza. La stima di tale parametro, di fondamentale importanza nella progettazione sismica, costituisce uno dei principali risultati della ricerca. Si è verificata la validità dell'impostazione assunta dalle normative ma, nello stesso tempo, si è dimostrato che il sistema costruttivo in esame ha un comportamento sismico più favorevole rispetto a quanto previsto dalle Linee Guida vigenti.

Summary

The purpose of this thesis is to study the behavior of the particular building system that makes use of load-bearing walls of reinforced concrete cast into mineralized wood. This construction system has been studied under the action of pseudo-static forces (experimentally and numerically) and under dynamic forces (only numerically).

The activities carried out, in general, employed experimental equipment for the realization of tests on materials and on specimens that can be both portions and real scale walls. Additionally, a commercial software has been used for the numerical modeling of the elements composing the construction system in object.

In particular, in the first chapters of the thesis, a complete analytical treatment based on experimental results obtained in the years before the Ph.D beginning and during the Ph.D is provided. The original aspects, from the experimental point of view, were the two experimental campaigns concerning portions of panel subjected to direct shear and real scale walls subjected to cyclic horizontal forces in a pseudo-static fashion.

In addition, the experimental campaign was completed with the tests on wall-to-wall and wall-to-floor connections required by LL. GG. Min. of Public Works (2011) and aimed at the study of load-bearing walls cast within formwork blocks.

The direct shear tests have shown an incongruity of the experimental results with the first analytical treatment developed in the years before 2012 and therefore it was necessary to revise it with new theoretical considerations. A new and original analytical treatment based on strut-and-tie mechanisms was developed.

In the last chapters, the construction system has been treated numerically. In the numerical modeling of the structural system the analytical treatment exposed in the first chapters was employed using elements with lumped and distributed plasticity able to simulate the main failure mechanisms documented in the experimental tests.

This modeling was first validated on the results of tests on full-scale walls and then used to simulate the behavior of multi-story buildings, regular and irregular, with bi-dimensional and spatial models. These buildings have been subjected to static and dynamic forces typical of seismic action. The numerical results of the simulations coupled with the capacity curves enabled the estimate of the seismic response of the building system and, finally, the behavior factor which best synthesizes it.

The estimate of this parameter is of fundamental importance in seismic design, it is one of the main research results. It is worth to notice that the Italian Guidelines prescriptions regarding the behavior factor are more conservative with respect to the results of this research.

Contents

Chapter 1. – Introduction

1.1. Background

Buildings made up of cast in-situ reinforced-concrete walls represent a structural typology that has been widely used in civil buildings. Load-bearing shear walls characterized by small wall thickness (15 - 30 cm) and by small percentage values of steel reinforcement have shown excellent strength resources even against strong earthquake ground motions.

In the last years, since construction objectives aimed to the realization of civil buildings characterized by very good thermo-acoustic properties and moderate costs, many innovative construction techniques were developed. Unfortunately, sometimes the technology innovation is faster than the law modernization causing difficulties in the expansion of new product markets. This is the case of the construction system based on RC walls cast into wood-chip and cement hollow blocks. Despite its wide diffusion in European countries (e.g. Austria and Germany) and its increasing appeal in Italy, the International Regulation does not explicitly include this new technology, generating doubts in the professional community.

The Guidelines of the Italian Ministry published in 2011 (LL. GG. 2011) is the only official, but not mandatory document, that treats this topic.

Also the scientific literature is poor of studies on this topic. The only documented results are those of (Ceccoli, Dallavalle, et al. 2000), (Tullini 2000) and (Malavolta 2008), researchers at the University of Bologna.

A number of experimental tests has been recently conducted and interpreted at the University of Bologna with cyclic horizontal loading and shaking table tests (conducted at the laboratory of the European Seismic Centre EUCENTRE in Pavia) and by the University of Padua. These last are described and interpreted in this thesis.

1.2. Thesis objectives

The main objectives of this Ph.D thesis on RC walls cast in wooden blocks are the following:

- Organize and present the experimental tests performed so far on this construction system
- Describe an analytical framework coherent with experimental results
- Develop a realistic modeling coherent with the behavior experienced in the tests
- Evaluate the seismic performances and coherent behavior factor of this construction system, by means of numerical extension of the experimental tests and analytical approach.

1.3. Dissertation overview

The thesis is subdivided in four parts, in particular:

- The first part describes in detail the construction system and its peculiarities, for example the types and shapes of blocks, the characteristics of the walls and the connection details between different structural elements
- The second part resumes the discussion about the construction system in the scientific literature and Building Codes.
- The third part describes the experiments carried out so far at the University of Padua. Each experiment treats a particular topic: out-of-plane behavior, in-plane behavior, flexural and shear failure. A theoretical proposal is presented for each test series in order to interpret the experimental results and give practical design rules for professionals.
- The fourth part regards the modeling and the strategies used to take into account the inelastic behavior of the structural elements, in particular when subjected to seismic horizontal forces. This is a fundamental step in order to evaluate the behavior factor of the construction system by means of numerical pushover and dynamic time history analyses.

PART I – Generalities about the construction system

Chapter 2. – Peculiarities of the construction system

2.1. Introduction to Part I

The part I of this Ph.D thesis describes the peculiarities of the construction system. The elements described are used in the construction of buildings employing reinforced concrete cast in mineralized wooden blocks.

The basic elements used for the realization of the investigate walls are mineralized wood-chip and cement hollow blocks (WCBs). The blocks themselves do not have a structural function. They are just hollow formworks that permit to realize cast in situ bearing reinforced concrete walls. The particular geometry of the blocks allows the realization of a grid type internal structure. The mass and thermal characteristics of WCBs, coupled with insulation panels inserted into them, result in an optimal combination of insulation and acoustic capacities of the finished walls.

The walls obtained are then connected each other by slab-floors and appropriate reciprocal connections in order to ensure a box type behavior of the whole structure.

2.2. The blocks: characteristics of the basic elements

The hollow blocks are obtained by a mixture of water, Portland concrete and woodchips; after a mineralization process the material obtained is cast in suitable molds in order to give to the product the desired shape.

Figure 2-1. Typical wooden blocks, without insulation (left) and with insulation (right)

The chemical process called mineralization destroys all the organic parts typical of the wood in order to have pure inorganic material. Thanks to this treatment the final block gains very important characteristics such as strength, inalterability, impermeability. As shown in Figure 2-1 the block has a specific shape with hollows both in the longitudinal and in the transversal section. The external rectangular shape is internally subdivided by ribs to form vertical continuous channels. The ribs themselves have holes in the upper part to create a continuous horizontal voids.. Moreover, the blocks without insulation are characterized by a double symmetry axis in order to ease the installation.

The next paragraph will clarify the function of this particular shape.

2.3. The wall as an assembly of blocks

The block is the basic element of the wall. Indeed the wall is built by combining blocks, line by line, and proceeding from the bottom to the top. The blocks can be easily cut with a band saw for a perfect installation in the desired position.

Figure 2-2. Residential building with curved wall surface (left), the first line of blocks (right)

Over the years special blocks have also been developed, named "ancillary blocks" in (EN 15498 2008), that permit the realization of curved surfaces to the delight of creative architects (see Figure 2-2).

After the blocks positioning, a single layer of horizontal and vertical re is placed inside the wall and the concrete is cast from the top. The wall usually is completed with two or more pouring sessions in order to allow adequate placement and compaction of the concrete inside the blocks.

Figure 2-3. Reinforcement inside the wall before casting (left) and internal RC grid (right)

As mentioned above, the holes inside the blocks have a particular function: form a grid type structure of reinforced concrete in the inner part of the wall. Initially, the ribs were designed to provide strength and stiffness to the formworks and also to allow transpiration of the wall, but the particular internal micro-frame allow also optimal mechanical balance between strength, stiffness, ductility and dissipative capacity.

An adequate number of integrative bars is placed where the static and seismic action can concentrate damage, e.g. at the openings frame (doors and windows), at the ends of a bearing wall. Typically, a concrete C25/30 (according to Eurocode 2) is used for wall casting with a slump S5 and an aggregate diameter not greater than 30 mm. The typical diameter for horizontal and vertical bars usually varies from 8 to 12 mm, but it is possible to use larger diameters where necessary according to the structural design.

In the case of a bearing wall, the thickness can reach 30 cm in the case without insulation and 40 cm ore more with the insulation layer.

2.4. The connection with foundations

The foundations are usually designed as a continuum slab or a net of beams in reinforced concrete in order to minimize the ground instability in seismic zones. The vertical bars of the first line of blocks laying on the ground level, can be prearranged during the foundation pouring or anchored to the foundation with chemical resins into post-drilled holes ensuring an appropriate anchor length.

The second solution usually is the most common because it eases the operations in the construction site. Prearranging the vertical bars in the foundation could result in a very difficult constraint to respect.

Figure 2-4. First line of blocks with the starting bars anchored in the foundation

2.5. Wall-to-wall connection

The cross-section of the wall is formed by a set of cells that form the vertical element (column) of the internal concrete frame.

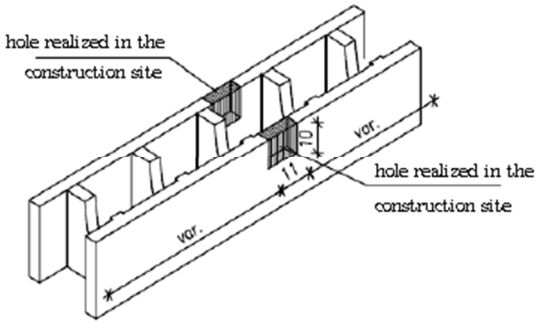

Figure 2-5. Modified block for the wall-to-wall connection

As shown in Figure 2-4 in the T or cross joint between two walls holes have to be realized in the external faces to allow continuous horizontal rebars.

2.6. Floor-to-wall connection

Usually the floor is realized with traditional techniques in order to obtain horizontal structures with adequate out-of-plane and in-plane stiffness and strength. These in-plane properties are fundamentals to distribute properly the horizontal forces (typical of seismic events) to the vertical walls.

A very useful structural provision is the ring-beam connecting all the perimeter walls in order to emphasize the confinement action already expressed by the floor. In this case the walls are directly connected with the ring-beam maintaining the casting continuity. In presence of an opening it is possible to use a special hollow block in order to realize a lintel connected with the upper ring-beam. This kind of solution was used in the experiments on real scale walls (see chapter 10).

Figure 2-6 shown a typical wall-to-floor connection with two openings at the top (window) and at the bottom. It is convenient the use of a special block that allows the continuity between lintel, floor and wall in the upper floor.

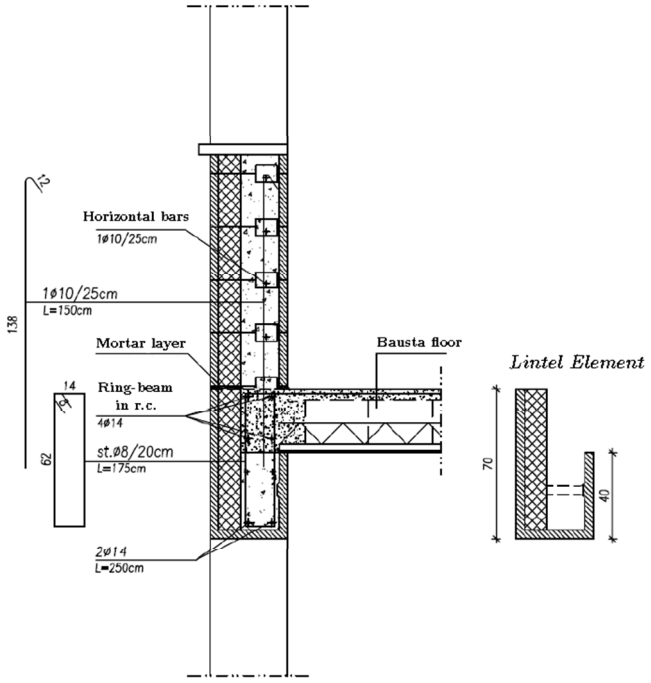

Figure 2-6. Wall-to-floor joint section (right) and lintel special block (left)

2.7. The general system

Thanks to each part described above, the obtained construction system has the following peculiarities:

- Each bearing wall is composed by a reinforced concrete grid cast in a continuous series of wood-chip blocks. The perimeter walls present an insulation layer that provides good thermodynamic properties to the structure
- The perimeter walls, properly connected with floor slab and ring beam, provide the *box behavior* to the structure
- The internal partition walls, properly connected with the perimeter ones, realize the *cellular behavior* of the structure (i.e. *bundled-tube behavior*)

The cellular/box behavior permits to realize structural systems with a great torsional stiffness and strength. When the structure is subjected to horizontal forces, the walls work on the *in-plane* direction.

This constructive system is generally adopted in the construction of residential buildings characterized by a small number of stories where walls length is equal or greater than the inter-story height. With this geometric configuration walls are generally considered squat (instead of slender).

In addition to the above characteristics it is worth noting that, in order to guarantee a high safety level regarding vertical loads and high ductility levels regarding horizontal forces:

- Axial forces are limited
- In a capacity design approach, ductile failures have to anticipate brittle ones
- The connections (wall-to-wall and wall-to-floor) are designed to remain in the elastic field even under rare seismic event.

PART II – The construction system in scientific literature and Building Codes

Chapter 3. – Introduction to Part II

The most salient features of the construction system at hand can be summarized as follows:

- *squat walls*;
- *bundled-tube behavior*;
- *RC walls cast in wood-chip shuttering.*

From deep analysis and interpretation of all the references, the following aspects have been observed. As far as the seismic behavior of concrete walls is concerned, most of the research work accomplished up to date is focused upon *slender cantilever walls* (for sake of conciseness, let us refer to (Coull e Stafford 1991) and (Paulay e Priestley 1992)) with little research works developed for *squat walls* despite they have already shown valuable strength resources towards earthquake of high intensity (as for example, in Montenegro and in Chile). Such works, i.e. (Salonikios, Kappos, et al. 1999), (Salonikios, Kappos, et al. 2000), (Hidalgo, Ledezma e Jordan 2002), (T. N. Salonikios 2002), (Chai e Anderson 2005), mainly regard the in-plane seismic behavior of a single squat concrete walls subjected to a cyclic load.

It is worth pointing out that all these researches regarding *squat walls* are relatively recent and this fact indicates the increasing interest in *structural systems composed of cast in situ squat concrete walls*. As far as the bundled-tube behavior is concerned, it is worth noting that all the mentioned research works testified that there is a good knowledge of the seismic behavior of bundled-tube systems but it is focused on high-rise framed structure and it does not concern the behavior of low-rise building completely composed of squat reinforced concrete walls.

Finally, as far as the behavior of *RC walls with wood-chip block shuttering* is concerned, the few research works mainly regard the in-plane behavior under vertical static loads and horizontal forces; see (Gasparini, et al. 2008), (Ceccoli, Dallavalle, et al. 2000), (Ceccoli, Diotallevi e Tullini 2001) and (Malavolta 2008). To the knowledge of the author, there is no research work available on out-of-plane action or which illustrates the behavior under seismic loads with a dynamic test of a full-scale building on a shaking table. In particular, several codes, e.g. (NTC

2008), (CNR 10025 1984), (CNR 10025 1998) and *Eurocodes,* have been analyzed in order to identify parts pertinent with the structural system at hand.

Chapter 4. – The construction system in the scientific literature

4.1.– State-of-art in European and Italian Building Codes

Building structures which make use of structural systems obtained by filling hollow blocks with concrete have had a wide employment in northern Europe (mainly in Germany, Austria and Belgium), especially in the last decades.

Despite the extensive use of this kind of concrete walls, to the author's knowledge, no Building Code outside of Europe handles the construction technique in question. The European Building Regulation deals this topic through a Guideline for European Technical Approvals, (ETAG009 2002), drawn up by the EOTA Working Group. This is the only reference that explicitly treats shuttering kits/systems bases on hollows blocks or panels and concrete, even if this document regards non load-bearing permanent walls. The same ETAG009 recognizes a strong lack of investigation into the current state of the art.

The European Regulation EN 15498 published by the Austrian Standards Institute prescribes a series of tests regarding the wood-chip block properties, e.g. thermal insulation, water vapor permeability, durability, etc., but does not treat the mechanical properties of the assembled walls including the internal RC structure cast into the formwork.

ETAG009 divides into three types this kind of walls: i) according to the intended use; ii) according to concrete infill structural pattern; iii) according to basic elements of the shuttering. This is the only specific classification in the literature.

Each category is subdivided in sub-categories:

i. Load-bearing (structural) walls, non-load-bearing (non-structural) walls, internal walls, external walls
ii. Continuous type, grid type, column type, other types
iii. Hollow blocks, panels

Quoting the *Grid type* description of ETAG009: "The structural pattern of the grid type consists of concrete columns connected by horizontal concrete ribs. Columns and ribs are formed by filling the voids of the shuttering hollow blocks or panels with concrete. The vertical columns extend the entire height of the wall without interruption or reduction of cross-sectional area."

According to this classification, the construction system at hand has a *grid type* concrete infill structural pattern assembled with *hollow blocks*.

In Annex B of ETAG009 three design methods for grid type shear walls are proposed:

– Frame model
– Continuous strut model
– Beam model

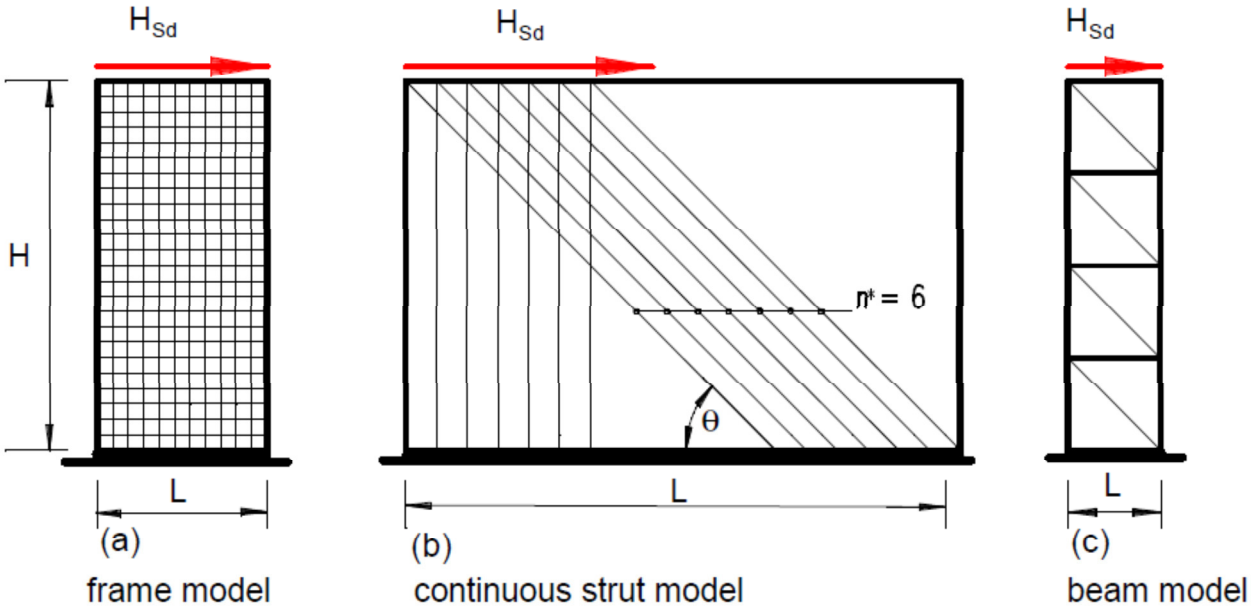

Figure 4-1. Load bearing models for horizontal shear forces H_{sd}

In the frame model, the design resistance H_{Rd} of the frame model depends on the tensile strength of the connecting beams (transverses). Assuming a parabolic shear stress distribution over the wall length L according to beam theory and assuming a zero point of moment at mid-span of the transverses the load carrying capacity of a connecting beam is reached when the tensile stress due to the maximum bending moment at the intersection connector/column exceeds the flexural tensile strength of concrete. It is worth to notice that connector section is made of an homogeneous linear

elastic material until reaching the tensile strength limit. The reinforcement is neglected and therefore also the possibility of establishing other resisting mechanisms, typical of RC structures.

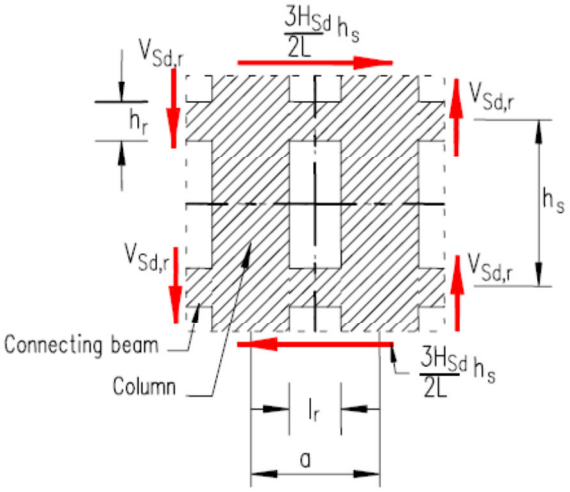

Figure 4-2. Unit cell used to compute the stress

In the continuous strut model, the design resistance of a strut is determined according to (ENV 1992-1-1:1991), clause 4.3.2, where a reduction factor ν is to be taken into account. The angle of inclination θ of the struts follows from Figure 4-3.

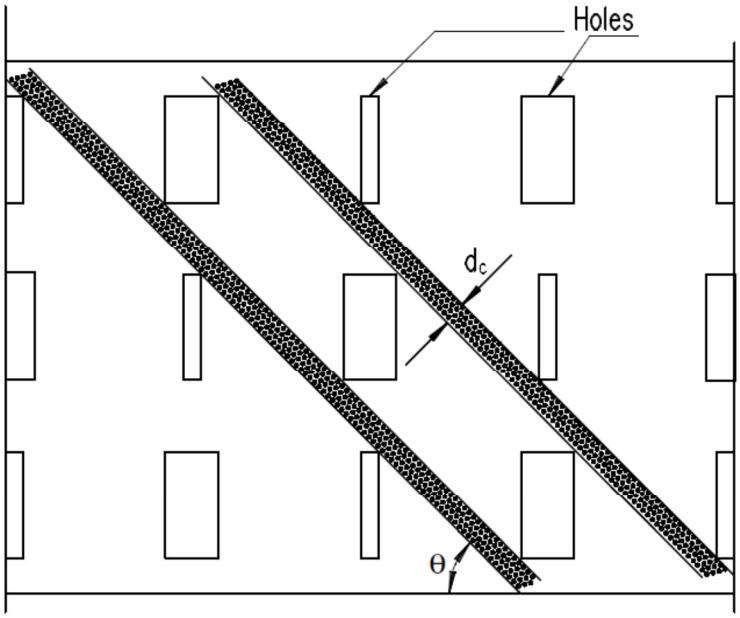

Figure 4-3. Depth d_c of a continuous strut

In the beam model, the design resistance H_{Rd} can be determined with the help of the design rules valid for reinforced concrete beams; the links are represented by horizontal bars passing along the connectors. A sufficient end anchorage of the horizontal bars – e.g. by hoop reinforcement – has to be verified according to (ENV 1992-1-1:1991), clause 5.2.

The Guideline document (LL. GG. 2011) issued in July 2011 by the Italian Ministry of Public Works allows the adoption of the system under discussion for the design and realization of load-bearing shear-walls. However, the Guideline mentioned above does not suggest a particular analytical procedure and it refers to the general Italian design rules (NTC 2008) for low ductility walls of reinforced concrete. This Guideline impose the execution of a reliable set of tests to investigate the actual behavior of these panels under various loads, especially under lateral forces simulating seismic effects. However, such document does not provide any test setup to study the behavior under out-of-plane loads. This document has been published in Italy under a strong pressure of the academic and professional engineering community that claimed a formal identification of the constructive system at hand inside the Italian Building Code. Unfortunately Italy is a seismic zone and structural designers are more sensitive to mechanical properties and behavior of materials not only in the elastic range but also in the inelastic one. For these reasons, European manufacturers of this products were pushed to investigate some important parameters, as ductility and behavior factor, in order to expand the their market also in Italy.

Regarding the structural elements without reinforcement or partially reinforced, usually employed in the industrial buildings as partitions or bearing walls, there was a chapter in (CNR 10025 1984); nevertheless this chapter was not inserted in the 1998's review, (CNR 10025 1998).

A few research works has been reported on shear, in-plane and out-of-plane behaviour of RC walls realized wood-chip formworks; moreover, there are no specific analytical formulation for compressed isolated members. In order to fill this lack, the Italian engineering and scientific communities, stimulated by the manufacturers, recently carried out experimental research on these aspects, in particular at the University of Bologna and Padua.

Section 4.2 resumes the tests performed by the University of Bologna at EUCENTRE and Distart (Dept. of Construction Technique) labs. That conduced at the University of Padova will be extensively described and interpreted in following chapters of this thesis.

4.2. Tests performed at the University of Bologna

In the tests performed at the University of Bologna a slightly different type of wood-chip blocks was used in which the length of transverses is not constant as in the constructive system studied in this thesis.

This affects, for example, the definition of the periodic unit cell in a model that uses the homogenization technique. Figure 4-5 shows the square unit cell employed by (Tullini 2000) where the two different lengths of transverses are evident. The results of this research are reported in §4.2.3.

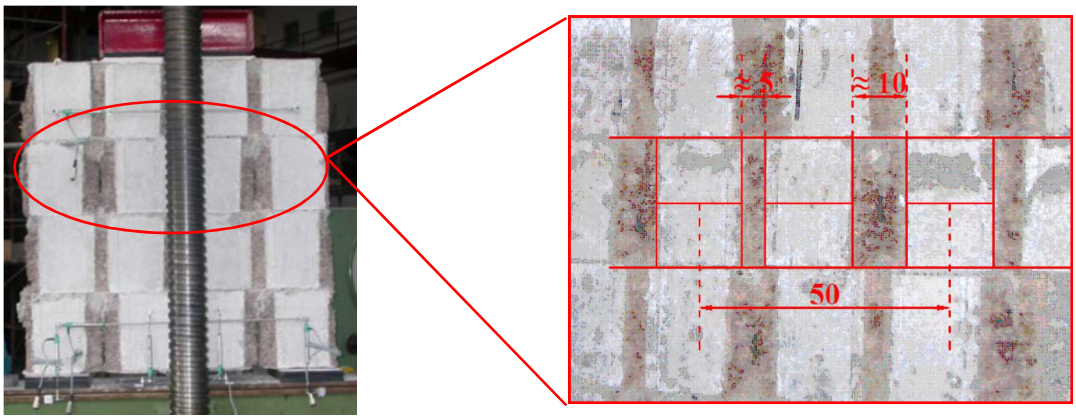

Figure 4-4. Internal concrete pattern of specimens studied by the University of Bologna: transverses with 2 different length

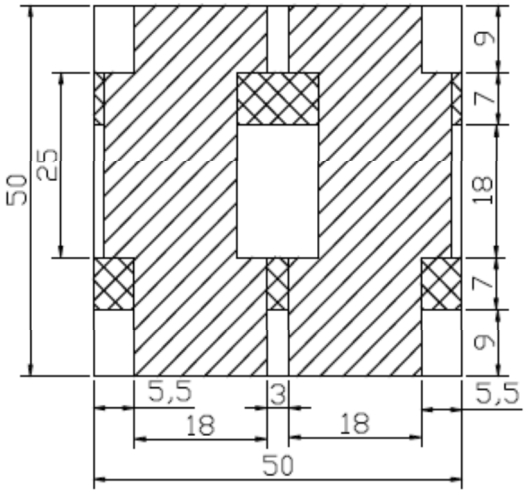

Figure 4-5. Unit two-dimensional cell employed by (Tullini 2000)

4.2.1. Cyclic axial tests on single walls with and without eccentricity in the out-of-plane direction

(Ceccoli, Dallavalle, et al. 2000) performed tests on 6 100x315 cm tall panels . The eccentricity ranged from 0 to 4.5 cm across the panel thickness. The effective buckling length L0 was 295 cm. The following table summarizes the concrete characteristics, loading eccentricities and ultimate resistant load:

	$\mathbf{R_c}$ [MPa]	$\mathbf{e_{inf}}$ [cm]	$\mathbf{e_{sup}}$ [cm]	$\mathbf{e_e}$ [cm]	N_u [kN]
C1	23.5	0	0	0	785
C2	23.5	0	0	0	959
C3	23.5	0	4.5	2.7	676
C4	23.5	3.5	3.5	3.5	480
C5	23.5	3.5	3.5	3.5	401
C6	23.5	3.5	4.5	4.1	230

Table 4-1. Results from axial load tests on tall panels (Ceccoli, Dallavalle, et al. 2000)

Results have been compared with the analytical ones obtained from the *model column* procedure according to (CEB/FIP Manual 1978) and with the proposal of (ENV 1992-1-1:1991). In the case of the last 4 panels the analytical results were reported in a graph giving a good matching with the experimental values.

4.2.2. Cyclic shear tests on single walls with axial constant load

(Ceccoli, Dallavalle, et al. 2000) performed two shear tests on two different panels with the same height, 315 cm, but with two different lengths, 100 and 200 cm. The panels were subjected to a first run of three cycles without vertical load and afterwards to a monotonic loading until panel failure.

The experimental results were compared in term of horizontal displacements with a numerical linear model where the internal concrete pattern was modeled with plain-stress elements. The Young modulus of concrete was 25 GPa and the Poisson coefficient was 0.15.

Only the first part of the experimental data was used for the comparison because of the limited capacity of the linear numerical model. In the first case, L=100 cm, the results matched very well the experimental ones with a relative error of 4%, but in the second case, L=200 cm, the numerical model underestimates the horizontal displacements. Possibly the micro-cracks involving the horizontal elements (transverses) decrease a lot the panel lateral stiffness and the linear elastic

model was not able to capture this effect. The lower is the H/L ratio, the greater is the damaging of transverses: this evidence can explain the worst results obtained with the larger panel.

4.2.3. Direct shear tests on wall portion (transverses strength)

(Ceccoli, Dallavalle, et al. 2000) performed 3 direct shear tests on 3 panel portions. Each specimen had 6 transverses reinforced with $\phi 8$ bars, one for each transverse with a spacing of 25 cm. The first cracking point was at 6 tons and the failure load recorded was 10 tons. The real stress state of the members and the failure modes were difficult to evaluate, in the author's opinion. They depend on the following variables:

- Position of the reinforcement
- Shape of the vertical elements and real span of the transverses
- Eventual asymmetrical deformation

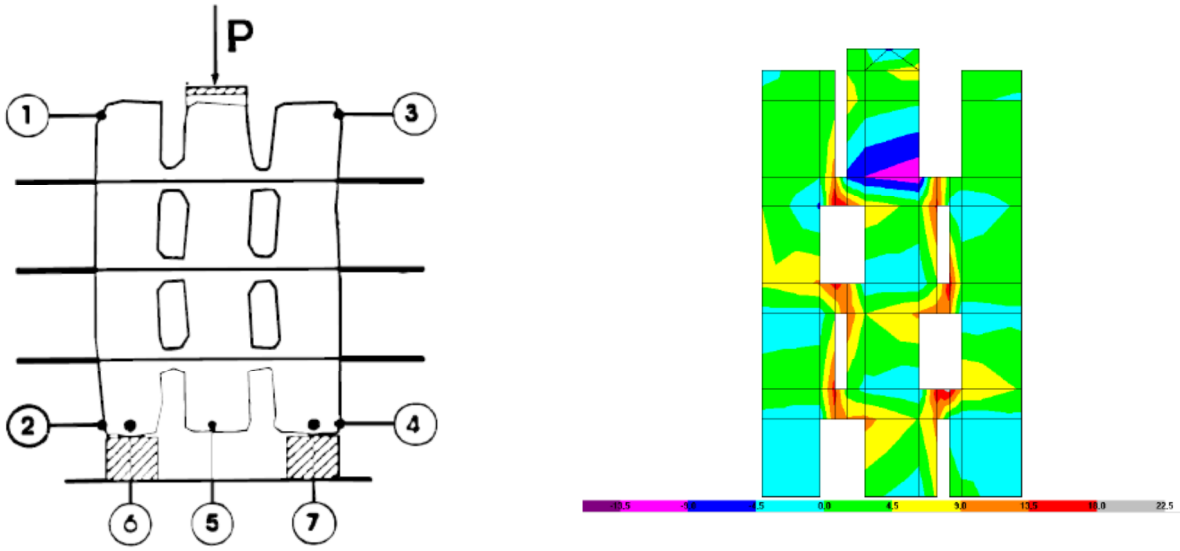

Figure 4-6. (Ceccoli, Dallavalle, et al. 2000) direct shear tests: setup (left) and numerical model (right)

It is worth to notice that the internal RC pattern in these tests was not perfectly regular but varies both the vertical section and the horizontal length of grid elements.

Some horizontal element behave like a double clamped beam with cracks in the tensile fibers, others behave like a squat beam with a unique diagonal crack typical of shear failure and others with a mixed behavior.

A linear numerical model with plain-stress elements was used in order to simulate the initial elastic part of the tests until the ultimate tensile stress of concrete. The homogenization technique was used in order to evaluate the following 3 parameter that identify a 2D orthotropic material:

	E_1/E	E_2/E	G_{12}/E	ν_{12}
2D cell	0.36	0.63	0.19	0.15
3D cell	0.34	0.63	0.19	0.15

Table 4-2. Elastic constants of the homogenized material

The numerical results in term of stress (see Figure 4-6) are in good agreement with the experimental ones: with an axial load of 6 tons the tensile strength of concrete was reached. Reinforcement in the numerical model was completely neglected.

(Malavolta 2008) performed 2 tests on 2 identical panel portions horizontally reinforced with $\phi 8$ bars (see Figure 4-4). 8 transverses, 4 for each side, connected the two lateral vertical elements with the two central ones. The tests where cyclic but not fully-reversed. The ultimate strength of specimens was about 320 kN, therefore on average 40 kN for each single transverse.

Two analytical procedures were proposed: one based on a strut-and-tie approach with an angle between the compressed an tensile elements of 55° evaluated *a posteriori* from the experimental results; one that sum the two contributes of steel and concrete sections in pure shear conditions.

In this case, (Malavolta 2008) proposed two types of modeling: one with mono-dimensional elements (*beams*) and the other with 2D *shell* elements. The model represents a square wall, 3 m long, subjected to dead loads and to an horizontal force of 300 kN. This model aimed to simulate another test performed by the author where, at this horizontal load threshold, the failure of transverses occurred. In both cases, the numerical results were in good agreement with experimental evidences.

4.2.4. Frequency analysis of a building by means of exciter action

In order to study the dynamical behavior of a wood-chip blocks RC building, (Tullini 2000) performed a dynamic test with a vibrodyne device on a 2 story building. The vibrodyne transmitted an horizontal force variable in time with a sinusoidal shape and a fixed frequency. This instrument was placed on the first floor with an horizontal action on two orthogonal directions and, after, on the roof in the direction with the lower stiffness. The building was schematized as a 2D dimensional structure with 3 degrees of freedom ξ_1, ξ_2 and φ (see Figure 4-7).

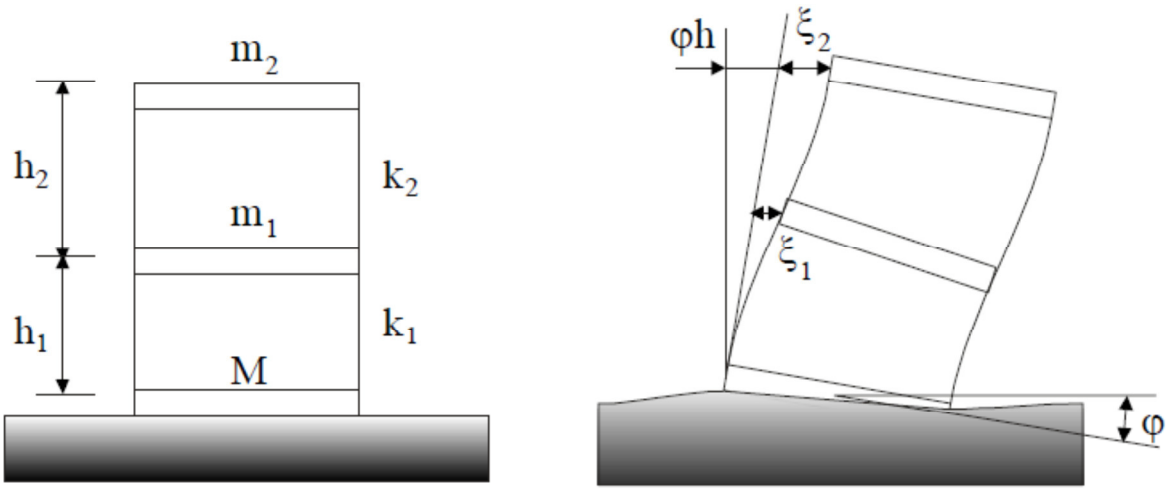

Figure 4-7. System with 3 d.o.f.

Wall and soil rigidities were computed using the elastic parameters in Table 4-2 and minimizing the error between experimental and analytical results due to the lack of information about the soil characteristics. The good agreement between experimental data and dynamic analysis confirmed that a POR linear modeling proposed by (Tomaževič 1978) can be used for the simulation of building realized with the system at hand.

4.2.5. Cyclic shear tests on real scale walls with and without openings

(Malavolta 2008) studied the behavior of single walls in real scale under a constant dead load and a variable horizontal cyclic force. He performed a test series of 5 walls without openings, 3 walls with openings, 3 walls with openings but with different reinforcement configuration and one 2 stories structure. All the multi-story specimens had an H plan section in order to avoid unwanted buckling effects.

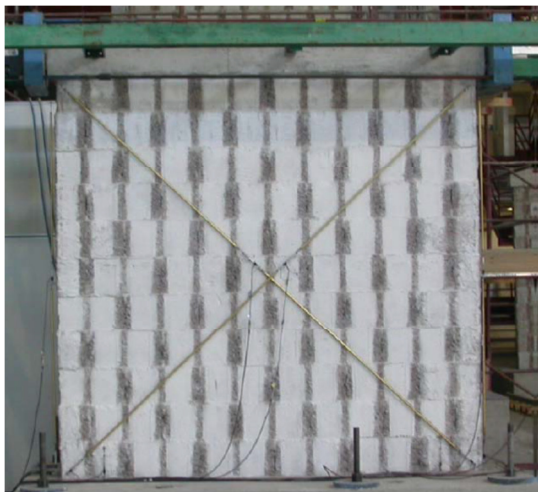

Figure 4-8. Quasi-static tests on single and assembled walls: wall with opening (top left); wall without openings (top right) and 2 stories structure without openings (left)

Applied dead load and reinforcement varied for each tested specimen.

The analytical formulation adopted to calculate the design strength of the structures was very similar to the classical one used for RC building. The bending moment-axial force (M-N) interaction diagram of a fictitious RC section equivalent to the actual grid section was built. The equivalent section had the same length and concrete area of the original one. The shear failure of the panels was checked through the analytical procedure described in §4.2.3 on the base of direct shear tests performed on wall portions.

For each tested specimen the ductility and the equivalent damping coefficients were evaluated obtaining quite high values: 8-12 and 3-15% respectively. On the base of these results (Malavolta 2008) estimated a behavior factor q equal to 3 for the construction system, in the case of regular buildings.

Chapter 5. – Definition of behavior factor q

5.1. Introduction

The European approach for a simplified seismic design of building using linear static or dynamic analyses is traditionally force-based. Available seismic codes for Europe area (Eurocode 8 2004) and for Italy (NTC 2008) refer to the Fundamental Mode Distribution (FMD) method (Chopra 1995) which requires the evaluation of the so-called behavior q-factor.

According to the definition given by (Eurocode 8 2004) this behavior q-factor is introduced to reduce the forces obtained from a linear-elastic analysis, in order to account for the non-linear response of a structure, associated with the material, the structural system and the design procedures. Once the elastic seismic actions are reduced by q, designers are allowed to verify stresses on structural elements and connections in comparison with the same capacity design values adopted for static action through the pertinent codes, e.g. (Eurocode 2 2004) for R.C., (Eurocode 3 2005) for steel, (Eurocode 5 2009) for wood. Based on such definition the q-factor represents the ability of the structure to dissipate energy and to withstand large deformations without ruin.

According to (Fajfar 1996) the reduction factor q used in the available seismic codes is composed by two different contributions: the first contribution q* takes into account the ductility and therefore the energy dissipation capacity of the structure while the factor Ω_d is the so-called overstrength. Based on such definition the behavior factor q is defined by [5.1]:

$$q = q^* \cdot \Omega_d \qquad [5.1]$$

q* is the ductility factor and represents the effective dissipative capacity due to the hysteretic behavior of the material in a ductile structure. According to (Fajfar 1996) an excellent overview about the definition of the ductility factor q* is reported in (Miranda e Bertero 1994). In detail, this paper gives the basic definition of the strength reduction factor and reports the specific elements with influence on its value. The factor q* depends firstly on the ductility of the structure

but it is also influenced by the principal elastic period of the structure and by the soil type. The most common relationship between the strength reduction factor q* and the principal elastic periods of the structure is given by (Vidic, Fajfar e Fischinger 1994). Otherwise the influence of the soil type over the strength reduction factor is given by (Miranda e Bertero 1994).

The definition of the strength reduction factor q* given by Fajfar P. for a Single Degree Of Freedom system summarized in the following equations [5.1] and [5.2]:

$$q^* = (\mu - 1) \cdot \frac{T}{T_0} + 1 \qquad if\ T < T_0 \qquad [5.1]$$

$$q^* = \mu \qquad if\ T \geq T_0 \qquad [5.2]$$

In the previous equation μ is the ductility of the system defined as the ratio between the maximum displacement and the yielding displacement (see Figure 5-1), T is the principal elastic period of the structure and T_0 is the transition period for which the constant acceleration part of the response spectrum transforms into the constant velocity portion of the spectrum. Generally the transition period T_0 is fixed equal to T_c (Fajfar 1996).

Research on the performance of buildings exposed to severe earthquakes indicated that structural overstrength plays a very important role in protecting buildings from collapse. According to (Elnashai e Mwafy 2002) the overstrength factor (Ω_d) may be defined as the ratio of the actual to the design lateral strength of the structure:

$$\Omega_d = \frac{V_y}{V_d} \qquad [5.3]$$

The component of the ratio are depicted in Figure 5-1 and termed the “observed” overstrength factor.

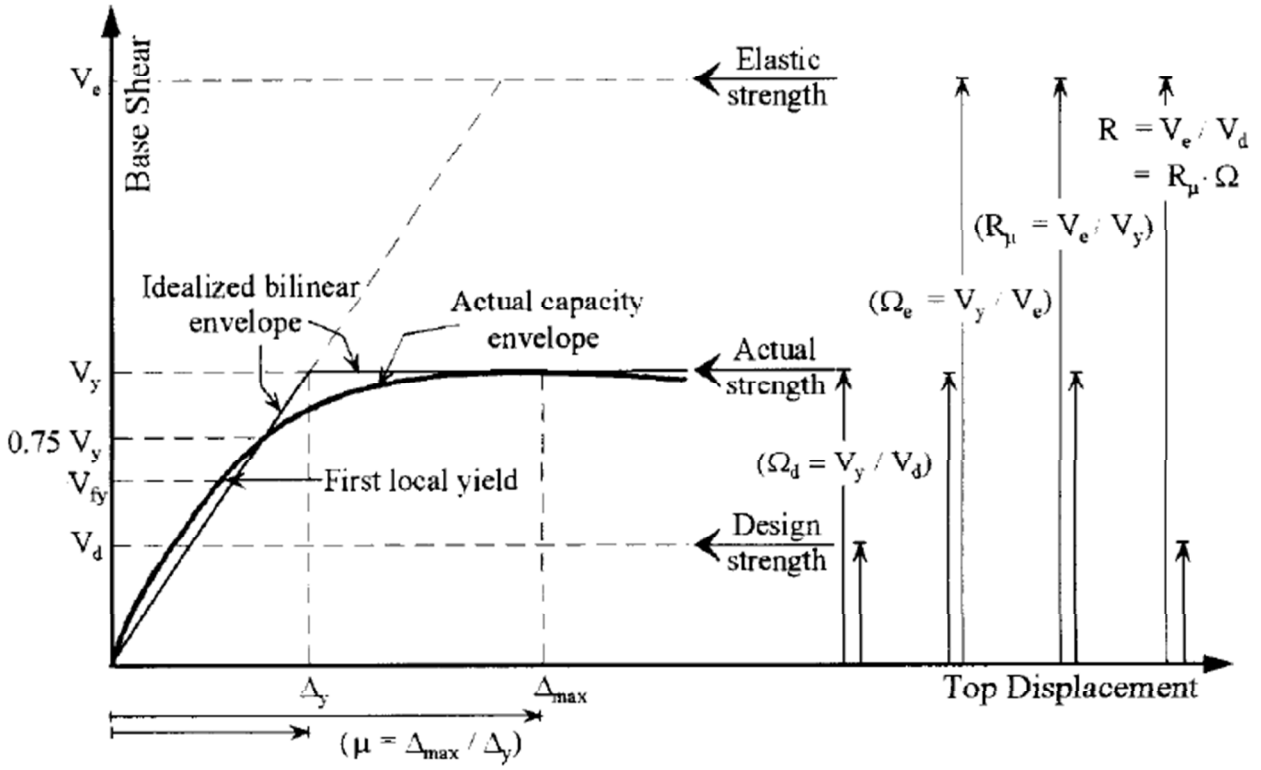

Figure 5-1. Relationships between the force reduction factor R, the structural overstrength Ω_d and the ductility reduction factor R_μ (Elnashai e Mwafy 2002)

According to (Elnashai e Mwafy 2002) quantification of the actual overstrength can be employed to reduce the forces used in the design, hence leading to more economical structures. The main sources of overstrength are reviewed in studies performed by (Uang 1991), (Mitchell e Paulter 1994), (Humar e Ragozar 1996) and (Park 1996). (Uang 1991) and (Humar e Ragozar 1996) studies focus on the difference between the actual and the design material strength; the conservatism of the design procedure and ductility requirements. Furthermore the effects of the participation of nonstructural elements and of structural elements not considered in predicting the lateral load capacity are taken into account by (Mitchell e Paulter 1994). Finally (Park 1996) gives some insight about the structural redundancy, the strain hardening and the use of the elastic period to obtain the design forces.

The results of researches reported above are implemented into the current seismic codes such as Eurocode 8, (FEMA 1997) etc...The q-factor can be subdivided into the following four factors [5.4]:

$$q = q_0 \cdot K_s \cdot K_r^p \cdot K_r^h \qquad [5.4]$$

where q_0 represent a basic value of the q-factor. (LL. GG. 2011) suggest a value of 2 that can be increased up to 3 in presence of test results supported by a reliable numerical analysis. K_s is a basic overstrength factor that should be multiplied by a reduction factor (K_r^p) in order to take into account the plan irregularity. In this way, the product between K_s and K_r^p is equivalent to the α_u/α_1 factor defined by (Eurocode 8 2004), (NTC 2008) and (LL. GG. 2011). The α_u/α_1 factor

resembles the overstrength factor Ω_d described by (Elnashai e Mwafy 2002) in Figure 5-1. The suggested value for K_s is 1.2 (LL. GG. 2011). K_r^h considers the regularity in elevation and varies from 1 (regular buildings) to 0.8 (irregular ones). In the European and Italian Codes is indicated with K_R. This notation is useful in order to describe properly the variables (type of structure, type of material, irregularity) that influence the assessment of the behavior factor.

A proper definition of these parameters represents a fundamental issue for a suitable seismic design of the building using the FMD method (Chopra 1995). Generally, these parameters are well defined by the standards for the more common building systems using traditional material such as steel, reinforced concrete and masonry.

5.1.1. Basic procedures for q-factor determination

A proper definition of the most suitable q behavior factor for the construction system at hand is a fundamental issue of the codes for structural seismic design. According to (Ceccotti e Sandhaas 2010) currently the q-factor is mainly evaluated by means of experimental methods based on quasi static tests on single wall specimens or on entire building shaking table tests. As reported in (Ceccotti e Sandhaas 2010) another procedure that can be used for the q-factor evaluation is based on numerical methods.

The standard experimental and numerical methods for the q-factor evaluation are summarized in (L. Pozza 2013) with the following scheme (see Figure 5-2).

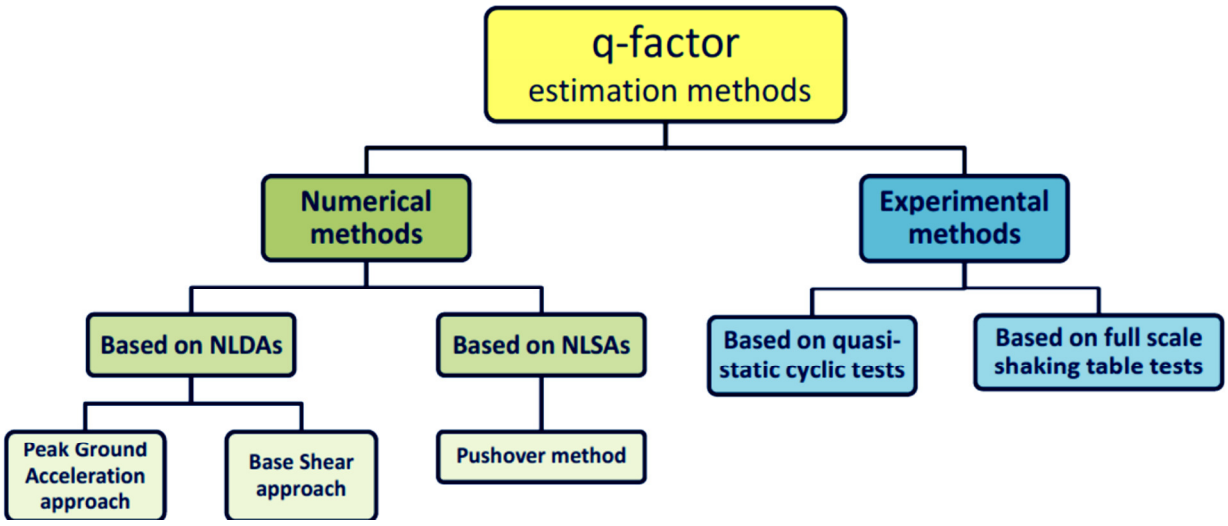

Figure 5-2. Scheme of methods used to evaluate the q-factor (L. Pozza 2013)

As concerning experimental methods only that based on quasi-static cyclic tests is used in this thesis due to the lack of shaking table tests on full scale buildings. In the last chapters also the

numerical procedure for estimation of the behavior factor with NLSA and NLDA analyses is applied to multistory building samples.

5.1.1.1. Q-factor definition by means of quasi-static cyclic tests

A first attempt to define the behavior q-factor was related to the concept of static ductility as the ratio of ultimate displacement over yield displacement. In (Eurocode 8 2004), construction typologies are assigned to ductility classes. Three ductility classes exist: Low Ductility Class with a correspondent upper limit value of q=1.5; Medium Ductility Class with a correspondent upper limit value of q=2.5; High Ductility Class with a correspondent upper limit value of q=5.

The three different classes must fulfill certain requirements of static ductility ratio in order to ensure that the given q-factors may be used. For instance, in Medium Ductility Class: "the dissipative zones shall be able to deform plastically for at least three fully reversed cycles at a static ductility ratio of 4". Otherwise, in High Ductility Class, "the dissipative zones shall be able to deform plastically for at least three fully reversed cycles at a static ductility ratio of 6". For both the ductility classes the strength degradation between first and third cycles should not exceed 20%.

However, this concept is difficult to use when load-displacement curves do not present a well-defined yield point. As an example Fig. 3.4 reports the typical load slip curve of a shear wall and the correspondent ductility levels evaluated according different bi-linearization criteria; (EN-12512 2001) and Equivalent Energy Strain Approach described by (Pozza, et al. 2012).

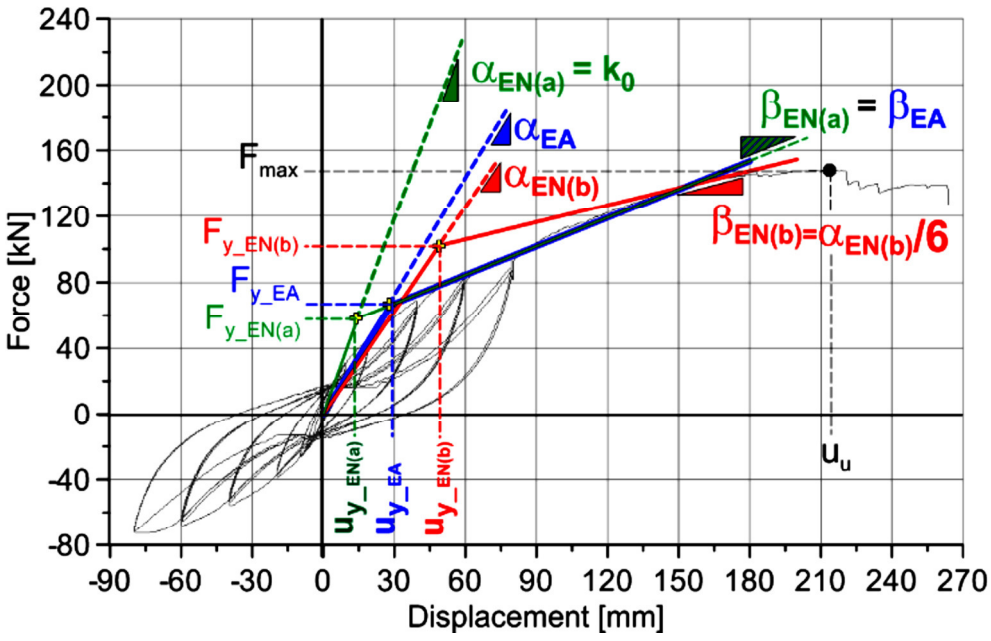

Figure 5-3. Shearwall load-slip curve and correspondent ductility levels: EN stands for EN12512 approach while E.A. stands for Equivalent Energy Strain Approach

As shown in Figure 5-3 there is a substantial variability between the yielding limits defined by the different bi-linearization criteria. As the ductility concept is very sensitive to the location of the yield point, the troubles deriving from the uncertainty in its definition are evident. Finally it should be pointed out that this procedure only allow to define the belonging of the investigated building system to a specific ductility class characterized by a q-factor range, but the exact definition of the q-values is not possible.

5.1.1.2. Conventional methods based on numerical simulations

According to (Eurocode 8 2004), numerical nonlinear model of buildings can be used to establish their behavior when subjected to earthquake loading. The main requirement for the applicability of this method is the availability of a numerical model suitable for reproducing the seismic response of an entire case study building.

Simplified models, such as wall-level models, calibrated on connection and element tests are more promising. Therefore, the most profitable approach seems to be that with higher-level element testing such as cyclic testing of wall elements, for instance in the timber structure case according to (EN-12512 2001), combined with numerical modeling using the test results as input parameters for complete building models.

Testing is necessary to establish system properties under fully-reversed cyclic loading. The complex loading conditions typical of an earthquake are thus simplified using cyclic loading protocols. A number of simplified numerical models of whole buildings validated on the output of experimental cyclic tests on wall specimens are reported in this thesis work (see chapter 13 and following).

Once provided the suitable model the numerical procedure is based on the following steps:

- choice of a representative case study building;
- design of the building with q=1 (elastic) with a chosen PGA_d (design peak ground acceleration) value according to the available seismic code (e.g. EC8);
- building modeling using test results as input parameters;
- execution of Non Linear Dynamic or Static Analyses to define the seismic response of the building.
- evaluation of the reduction factor q according to PGA approach or using the capacity curve from NLSA analyses.

The seismic response evaluation carried out with the nonlinear analyses allows assessing the most reliable q-factor of the investigated case study building. Two different independent procedures can be performed to define the q-factor: the first one based on the output from the NLDAs and the second one on the building load-displacement curve obtained by means of NLSAs. Below the main features of these two procedures are described.

5.1.1.2.1. Q-factor definition by means of NLDA analysis: PGA-based approach

The definition of the building seismic response using Non Linear Dynamic Analyses appear to be the most performing and suitable, because it is independent from the yielding limit definition and refers only to the first yielding condition (defined by PGA_d) and to the ultimate condition (defined by PGA_u) respectively for an elastic and an inelastic response.

It should be noted that the dissipative and displacement capacity of the building are strictly connected with the damping coefficient because the numerical models are sensitive to the assumed damping rate. However damping is difficult to evaluate on a global scale, it can vary between 2% and 15% according to (Newmark e Hall 1982). Usually a viscous damping of 5% is estimated (Chopra 1995).

Once defined the near collapse condition a series of NLDAs are performed with growing levels of PGA, e.g. starting from the design condition to the near collapse one. The outputs from the dynamic analyses at each levels of PGA represent the input parameters for the q-factor evaluation as described below.

The Peak Ground Acceleration approach refers to the PGA values used for the elastic seismic design of the building (i.e. PGA_{design}) and that one for which it is effectively achieved the near collapse condition (i.e. PGA_u). In the numerical method the PGA_u is obtained by means of nonlinear analyses performed on the numerical building models. The q-factor is then defined as the ratio between the PGA_u and the PGA_d according to the following equation:

$$q = \frac{PGA_u}{PGA_d} \qquad [5.5]$$

According to (Fajfar 1996) such a definition of the reduction factor q already includes the overstrength corrective factor, defined as the factor between the actual strength to the design strength of the structure.

The main limitation of this approach is that it is based on the hypothesis that the building reaches its first yielding condition under the PGA_d and it is constantly independent of the earthquake frequency content. While the near-collapse PGA_u determined through a nonlinear analysis, is function of the vibration period and of specific earthquake time history. Moreover, sometimes the model used for design is not the same as the one used for nonlinear analyses.

A way to avoid the assessment of first yielding condition is to consider a global yielding condition based on the bilinearization of the performance curve in the pushover analysis and defining

$$q = \frac{PGA_y}{PGA_u} \qquad [5.6]$$

In this way, only one nonlinear model is used, the errors on PGA_y (i.e. the seismic event that brings the structure to yielding condition) and on PGA_u estimation are compensated and a first yield condition is not needed at this stage.

The yielding condition depends on the criteria used for bi-linearization of the performance curve which is not univocally defined but usually related to a specific Building Code.

5.1.1.2.2. Q-factor definition by means of NLSA analysis: pushover method

The so called N2 pushover procedure defined by (Fajfar 1996) adopts an elastic perfectly plastic bi-linearization of the actual capacity curve behavior of the building. Usually, this procedure fits well regular structures having a clear change from elastic to inelastic behavior. The main passages of the procedure are hereafter explained.

The capacity curve is bi-linearized according to the reference Building Code. As instance the Italian Code fixes the elastic branch as passing through the point at the 60% of the maximum base shear and the plateau is chosen in order to have the same dissipation energy in the actual capacity curve and in the bi-linearized one (see Figure 5-4). The capacity curve cut off occurs when the descending branch reaches the 85% of the maximum base shear recorded.

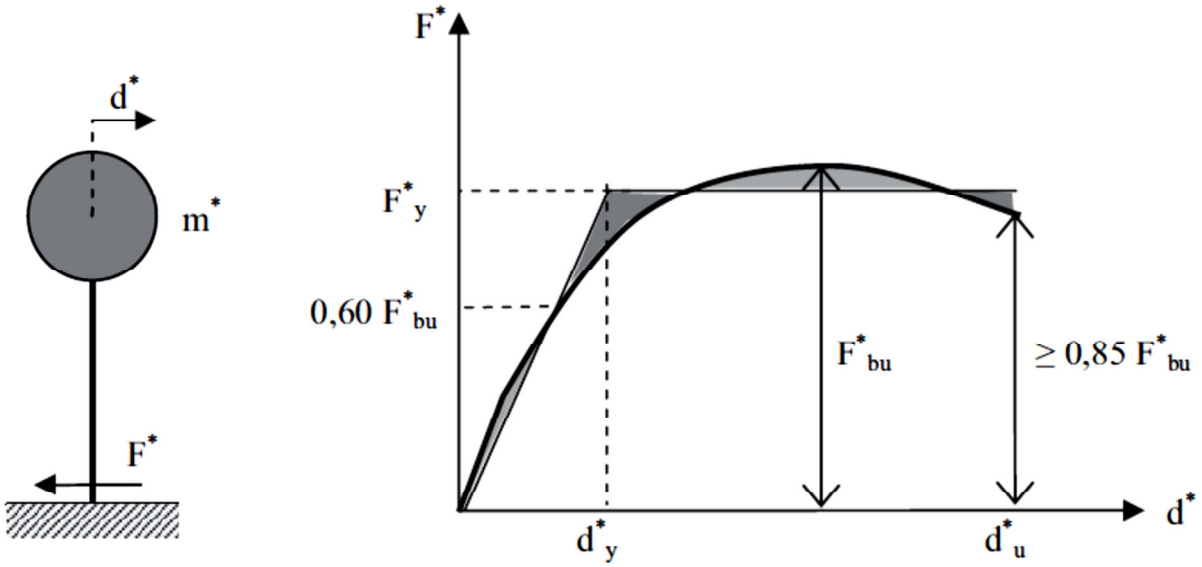

Figure 5-4. SDOF and capacity curve bi-linearization

The "star" in the symbols indicates, in general, a variable related to the idealized single degree of freedom system. The transformation factor Γ permits to convert the MDOF (multi-degree of freedom) system in the SDOF one (see EC8 Annex B §2 or NTC2008 §C7.3.4.1 for the determination of Γ).

The elastic spectrum is transformed in the ADRS (acceleration displacement response spectrum) format and the target displacement d_t* in the SDOF system is obtained with [5.7]:

$$d_t^* = \frac{d_{et}^*}{q_u} \cdot \left(1 + (q_u + 1) \cdot \frac{T_C}{T^*}\right) \qquad [5.7]$$

in the case of $T^* < T_C$ and $F_y^*/m^* < S_e(T^*)$ represented in Figure 5-5. The behavior factor q_u is the ratio between the acceleration in the structure with unlimited elastic behavior $S_e(T^*)$ and in the structure with limited strength F_y^*/m^*.

Observing that d_{et}^*/q_u is equal to d_y^* and imposing the target displacement d_t^*equal to d_m^*, the following expression for q_u, (also called q*), is obtained:

$$q_u = q^* = 1 + \left(\frac{d_m^*}{d_y^*} - 1\right) \cdot \frac{T_C}{T^*} = 1 + (\mu - 1) \cdot \frac{T_C}{T^*} \qquad [5.8]$$

where μ is the ductility.

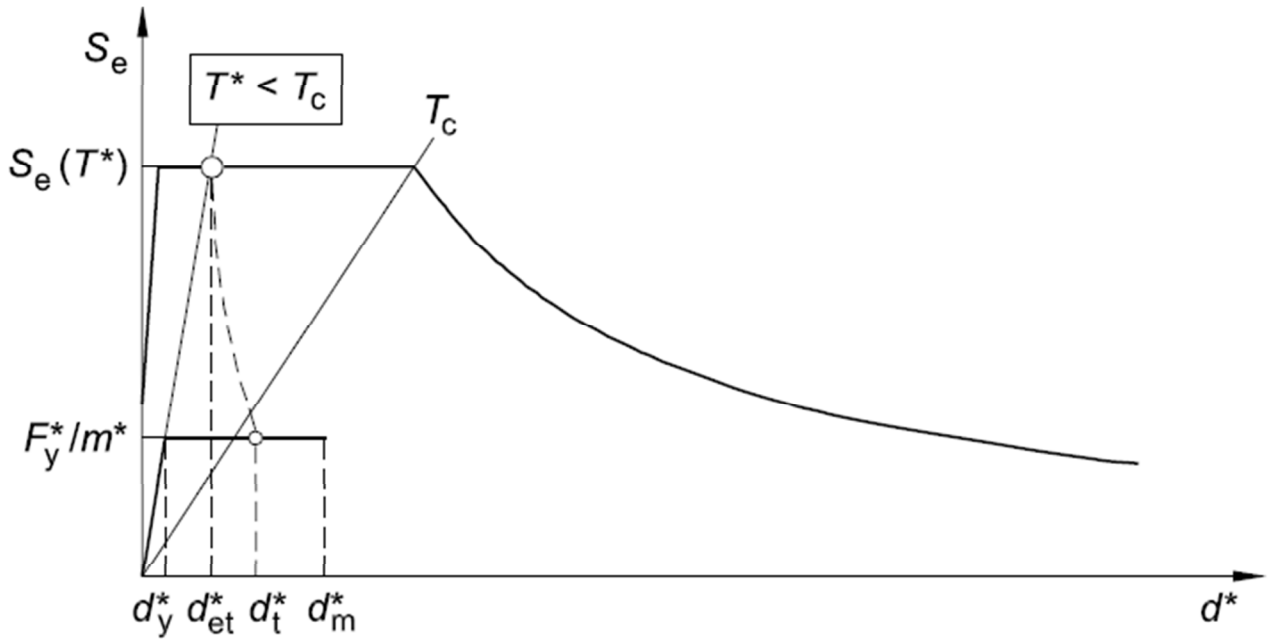

Figure 5-5. Acceleration displacement response spectrum and capacity curve

The definition of the q-factor using the pushover procedure depends on the bi-linearization criteria used to switch from the actual building pushover curve to the equivalent bi-linear curve. It should be noted that the bi-linearization procedure affects both the elastic branch of the pushover curve (and therefore the T* period) and the displacement capacity in term of ultimate displacement.

As a final remark, the q-factor defined according to the pushover procedure is coherent to that obtained to the PGA approach because both definitions are based on the design earthquake.

PART III – Experimental tests, analytical interpretations and theoretical framework

Chapter 6. – Introduction to part III

One of the objectives of this Ph.D thesis was to catalogue all the data and lab reports of the experimental tests performed so far at the University of Padua on the construction system at hand. All these tests have been classified in terms of typology and then logically organized.

For each test series, are presented: the objectives; the description of the experimental setup and the experimental results; the proposal of theoretical formulas for the analytical evaluation of the structural characteristics of the constructive system; the validation of the proposed theoretical formulas against experimental results.

In particular, the experimental tests concern:

- behavior of slender walls under axial centered and eccentric load (instability);
- behavior of panels under direct shear force;
- behavior of panels under diagonal compression, called *type 2* tests in (LL. GG. 2011);
- behavior of shear-walls under cyclic shear force; called *type 3* tests in (LL. GG. 2011);
- behavior of wall-to-floor and wall-to-wall connections under cyclic loading, called *type 4* tests in (LL. GG. 2011)

Different geometries of WCBs were used to realize the samples for the tests. The following table summarizes the geometrical characteristics of blocks.

TW30

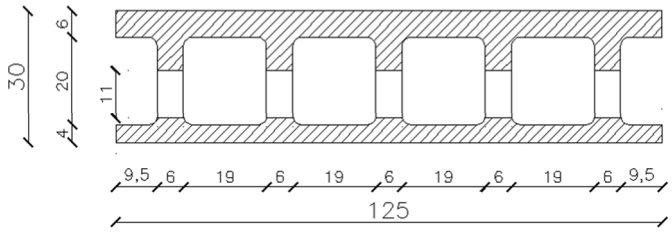

Total area	A_{cls}= 1520 cmq/m
Column spacing:	i_m=25 cm
Transverse spacing:	i_t=25 cm
Column thickness	t=20 cm
Effective thickness	t_{eff}=15.2 cm
Column area:	A_m=380 cmq
Transverse area:	A_t=110 cmq
Transverse height:	h=11 cm
Transverse length:	l=6 cm

N20

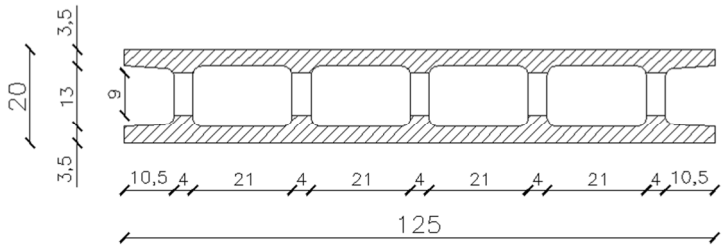

Total area A_{cls} = 1520 cmq/m
Column spacing: i_m=25 cm
Transverse spacing: i_t=25 cm
Column thickness t=13 cm
Effective thickness t_{eff}=10.92 cm
Column area: A_m=273 cmq
Transverse area: A_t=85 cmq
Transverse height: h=10 cm
Transverse length: l=4 cm

IL30

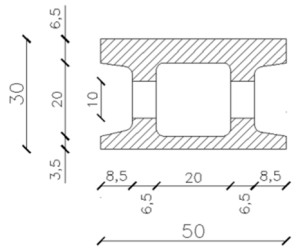

Total area A_{cls} = 1416 cmq/m
Column spacing: i_m=25 cm
Transverse spacing: i_t=25 cm
Column thickness t=20 cm
Effective thickness t_{eff}=14.8 cm
Column area: A_m=370 cmq
Transverse area: A_t=120 cmq
Transverse height: h=12 cm
Transverse length: l=6.5 cm

IL20

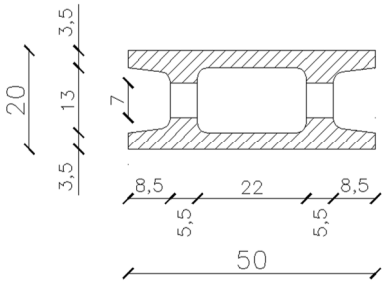

Total area A_{cls} = 966 cmq/m
Column spacing: i_m=25 cm
Transverse spacing: i_t=25 cm
Column thickness t=13 cm
Effective thickness t_{eff}=10.14 cm
Column area: A_m=253 cmq
Transverse area: A_t=96 cmq
Transverse height: h=12 cm
Transverse length: l=6.5 cm

N18

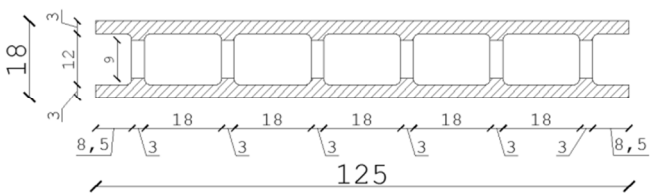

Total area A_{cls} = 1027 cmq/m
Column spacing: i_m=21 cm
Transverse spacing: i_t=25 cm
Column thickness t=12 cm
Effective thickness t_{eff}=10.27 cm
Column area: A_m=216 cmq
Transverse area: A_t=72 cmq
Transverse height: h=9 cm
Transverse length: l=3 cm

N25

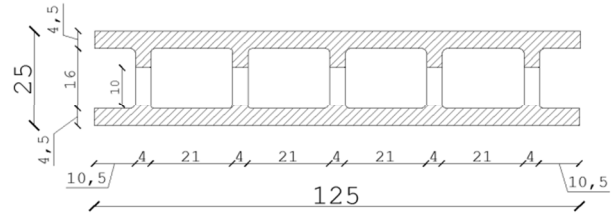

Total area A_{cls} = 1344 cmq/m
Column spacing: i_m=25 cm
Transverse spacing: i_t=25 cm
Column thickness t=16 cm
Effective thickness t_{eff}=13.44 cm
Column area: A_m=336 cmq
Transverse area: A_t=89.7 cmq
Transverse height: h=11 cm
Transverse length: l=4 cm

ISOSPAN I30

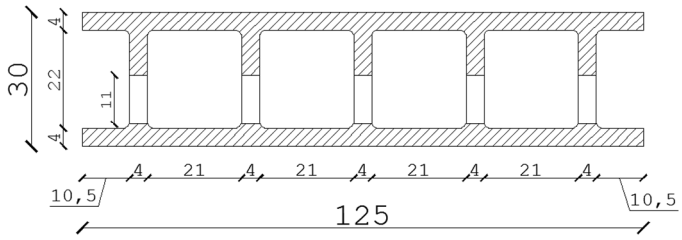

Total area A_{cls} = 1848 cmq/m
Column spacing: i_m=25 cm
Transverse spacing: i_t=25 cm
Column thickness t=22 cm
Effective thickness t_{eff}=18.48 cm
Column area: A_m=462 cmq
Transverse area: A_t=107.5 cmq
Transverse height: h=12 cm
Transverse length: l=4 cm

t_{eff} is defined as A_m/i_m and it is the thickness of an equivalent rectangular section having the same concrete area and length of the block.

Chapter 7. – Evaluation of mechanical behavior of slender walls under axial load with and without eccentricity (buckling)

The aim of the axial tests on slender walls was to evaluate the bearing capacity of tall walls that show instability effects. The experimental campaign has been performed in 2008 at the Material Tests Laboratory of the ICEA Department at the University of Padua. The experimental results are reported in the Laboratory official report n°29905.

7.1. Test setup and material properties

In order to investigate the behaviour of slender walls subjected to in-plane vertical compression and out-of-plane bending various panels have been subjected to an eccentric vertical load. This eccentricity gave an out-of-plane bending which played a very important role in the response of the wall due to its high slenderness.

The experiments performed at the University of Padua on eccentric compression encompassed 7 panels with a fixed height of 3 m, width and thickness variable depending on the type of block employed.

B450C steel type was employed with an average yielding stress f_{ym} of 501 MPa based on testing three steel coupons. The average 28-day compressive strength of the concrete f_{cm} was 25.1 MPa based on testing three cylinders.

Two different loading eccentricity have been applied: axial compression without eccentricity and with non-dimensional eccentricity e/t equal to 0,2; where t is a the thickness of the concrete core.

Both reinforced and unreinforced panels were tested. The bars were 10 mm diameter at 25 cm spacing in both directions and placed in the middle plane of the wall (see Table 7-1)

Sample number	Block type	Thickness t [cm]	Height h [cm]	Slenderness λ	Width L [cm]	Vertical bars	Relative eccentricity e/t
A	IL30	20	300	15	100	ϕ10/25x25	0
B	IL30	20	300	15	100	-	0.2
C	IL20	13	300	23	125	-	0
D	IL20	13	300	23	125	ϕ10/25x25	0.2
E	TW30	20	300	15	100	-	0
F	TW30	20	300	15	100	ϕ10/25x25	0.2
G	N20	13	300	23	125	-	0.2

Table 7-1. Characteristics of panels subjected to compression

The panel can be schematized as a cantilever beam simply supported at the top (see Figure 7-1).

During the test the following parameters have been continuously recorded:

- the vertical strain on both panel sides: $\varepsilon_{v\ int}$ and $\varepsilon_{v\ ext}$. The average vertical strain was obtained with:

$$\varepsilon_{avg} = \frac{\varepsilon_{int} + \varepsilon_{ext}}{2} \quad [7.1]$$

- the horizontal strain on only one side, in the middle of panel height ε_0:
- the out-of-plane displacement in the middle of panel height. Three different displacements have been measured: at the bottom f_{bottom}, at the top f_{top} and in the middle f_{mid} of the panels. The net out-of-plane displacement f has been obtained with:

$$f = f_{mid} - \frac{f_{top} + f_{bottom}}{2} \quad [7.2]$$

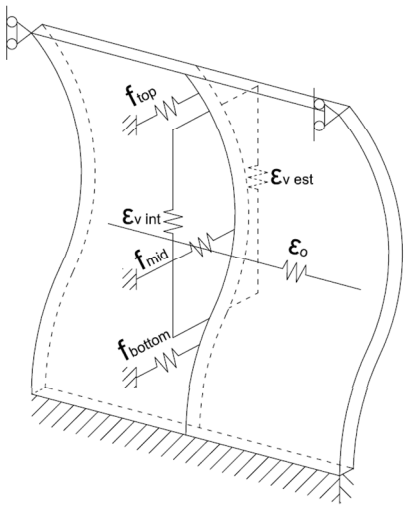

Figure 7-1. Measurements of internal and external deformation

The load has been transferred to the panel through a steel repartition beam and a metal plate in order to spread homogeneously the stress. Between the metal plate and the panel a plaster levelling layer was applied to provide a continuous and uniform contact (see Figure 7-2).

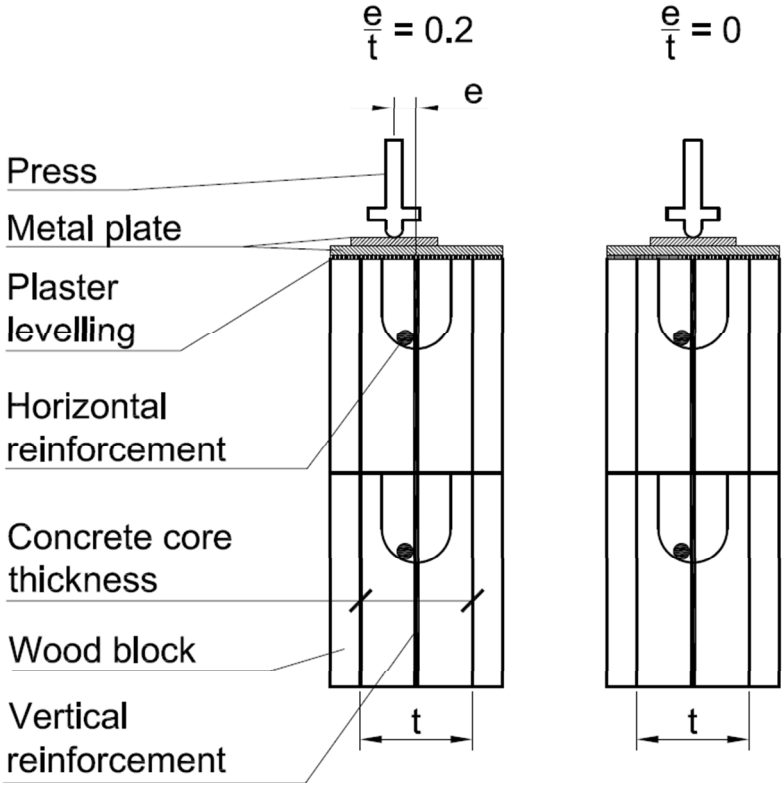

Figure 7-2. Test sketch

7.2. Results obtained

In this section the experimental measurements graphs obtained with different samples are presented; in particular the curves regarding:

- load-vertical ($\varepsilon_{v\ int}$, $\varepsilon_{v\ ext}$, and $\varepsilon_{v\ avg}$) and horizontal (ε_o) strains;
- load-out of plane displacement *f*.

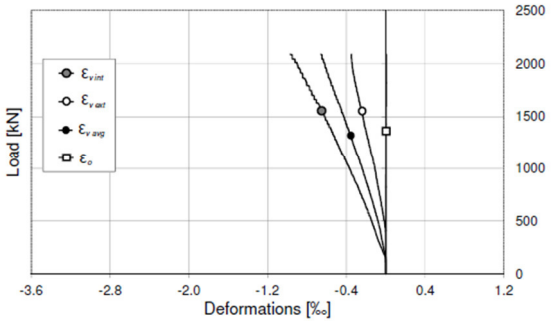

Figure 7-3. Load-deformations graph (panel A)

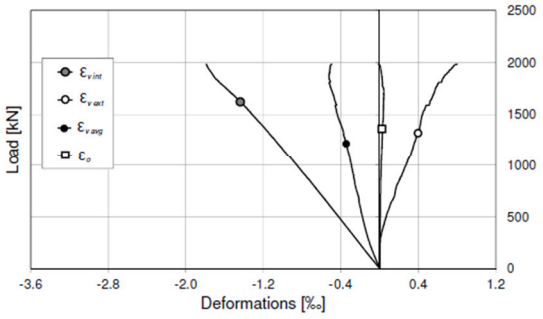

Figure 7-4. Load-deformations graph (panel B)

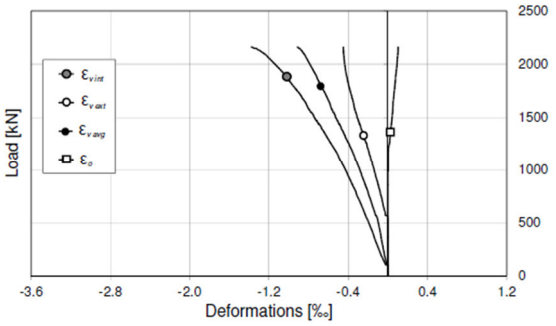

Figure 7-5. Load-deformations graph (panel C)

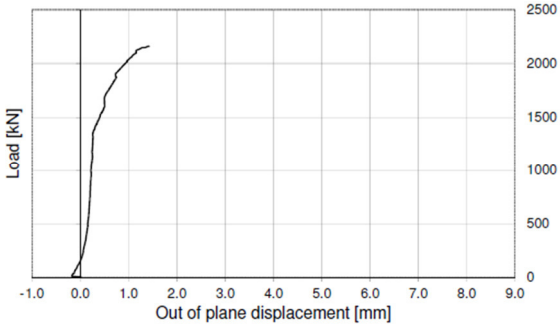

Figure 7-6. Out-of-plane displacements (panel C)

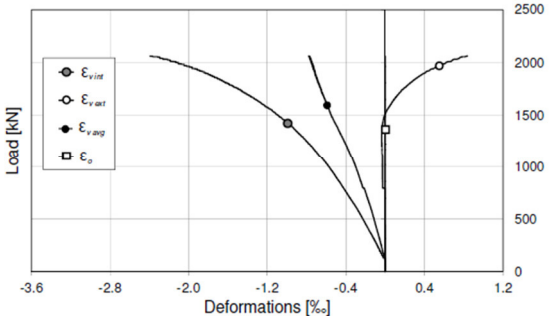

Figure 7-7. Load-deformations graph (panel D)

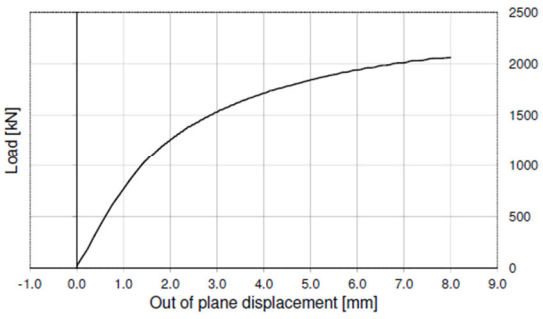

Figure 7-8. Out-of-plane displacements (panel D)

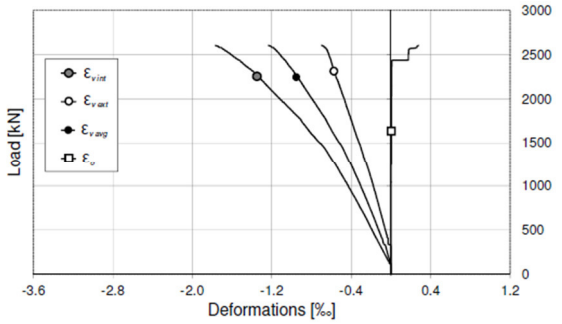

Figure 7-9. Load-deformations graph (panel E)

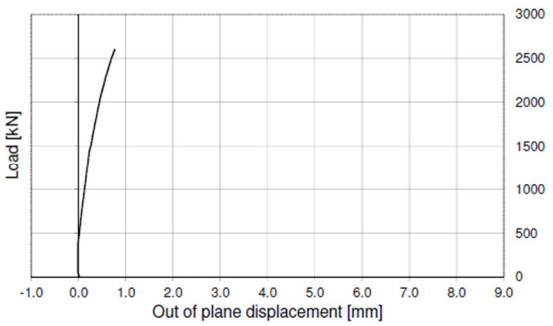

Figure 7-10. Out-of-plane displacements (panel E)

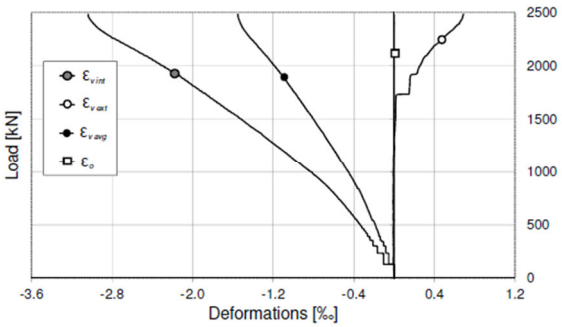

Figure 7-11. Load-deformations graph (panel F)

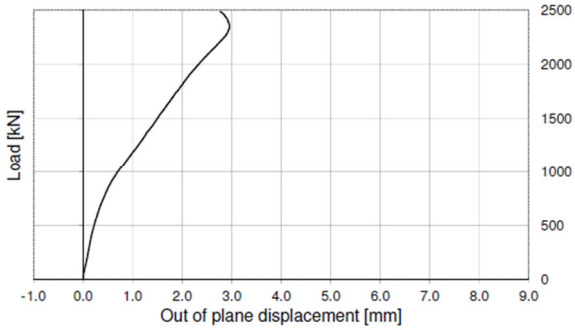

Figure 7-12. Out-of-plane displacements (panel F)

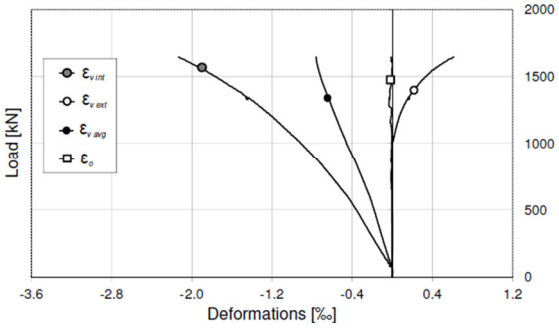

Figure 7-13. Load-deformations graph (panel G)

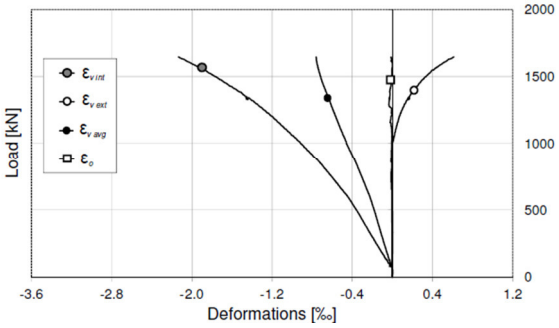

Figure 7-14. Out-of-plane displacements (panel G)

In each graph the ε_o strain is approximately null proving that the apparent "Poisson effect" of the structural grid can be neglected. Comparing the two different type of loading, with and without load eccentricity, it is clear that the out-of-plane bending moment produces a remarkable deformation. Table 7-2 summarizes the ultimate loads $N_{r,exp}$ measured in the experiments.

Sample number	Block type	Thickness t [cm]	Slenderness λ	Width L [cm]	Vertical bars	Relative eccentricity *e/t*	$N_{r,exp}$ [kN/m]
A	IL30	20	15	100	ϕ10/25x25	0	2764
B	IL30	20	15	100	-	0.2	2628
C	IL20	13	23	125	-	0	2160
D	IL20	13	23	125	ϕ10/25x25	0.2	2061
E	TW30	20	15	100	-	0	3471
F	TW30	20	15	100	ϕ10/25x25	0.2	3311
G	N20	13	23	125	-	0.2	1695

Table 7-2. Ultimate experimental load

Note that the eccentricity (e/t=0.2) is sufficient to produce compression only in a portion of the full concrete area, i.e. cracking of concrete uprights occurs.

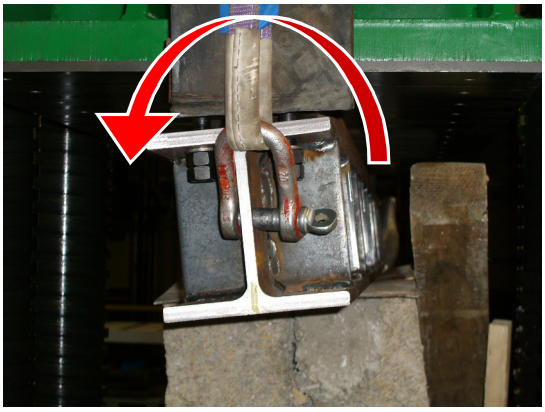

Figure 7-15. Steel beam for force distribution

Figure 7-16. LTDV at bottom

Figure 7-17. LTDV at top (left) and in horizontal position (right)

Figure 7-18. Failure of panel F

7.3. The analytical model

7.3.1. Theoretical approach

As written above, European Regulation does not provide a specific method to verify this kind of panels but it is very detailed about masonry (Eurocode 6 2006) and concrete (Eurocode 2 2004) structures. Here it is proposed an analytical method to compute the reinforced concrete panels at hand following an approach based on reduction factors similar to that proposed for masonry walls. Starting from the easier problem where the slenderness could be neglected up to the more complex case when the second order effects play an important role.

In analogy with the approach proposed by (Eurocode 6 2006) for ordinary masonries, two coefficients ϕ_t and ϕ_l, are introduced to take into account the impairment of bearing capacity in term of axial load due to the transversal and longitudinal load eccentricities and wall slenderness:

$$N_{rd} = \phi_t \cdot \phi_l \cdot N_{rd,0} \quad [7.3]$$

where $N_{rd,0}$ is the wall resistant axial load if no eccentricities and slenderness are accounted for. The "small displacements" assumption is implicitly included into the above formula.

In order to derive the relation between the reduction factors and all the variables involved, the equilibrium equation needs to be expressed in the deformed configuration (geometric non linearity), taking also into account the material non-linear behavior.

7.3.2. Definition of equivalent sections

Figure 7-19 describes the wall schematization used in the proposed analytical formulation: A_m is the area of a single upright, A_s is the reinforcement area, i_m is the uprights spacing, i_t is the transverses spacing.

The length and thickness of idealized longitudinal section are: (b_{eff} , t) considering the out-of-plane actions and (b, t_{eff}) considering the in-plane ones.

$$t_{eff} = \frac{A_m}{i_m} \quad [7.4]$$

$$b_{eff} = \frac{(number\ of\ uprights) \cdot A_m}{t} \quad [7.5]$$

In this way the idealization section area is equal to the real section area.

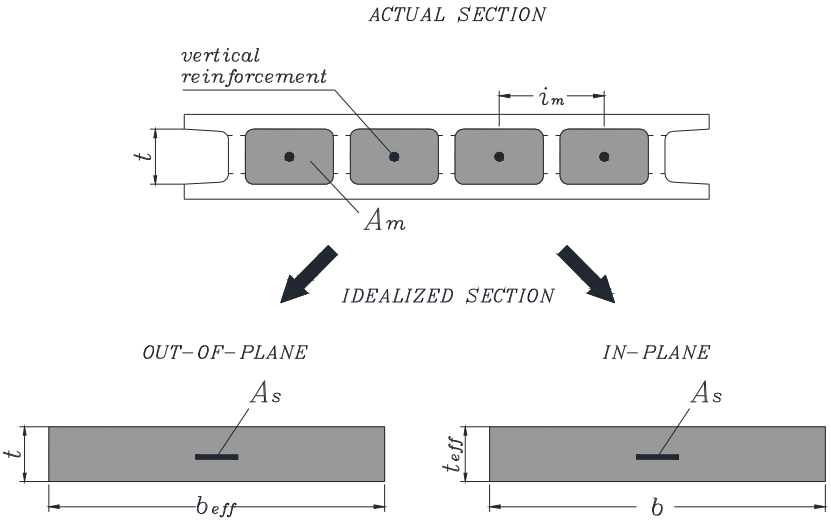

Figure 7-19. Module formwork: real section, idealized section

7.3.3. Interaction diagrams

The theoretical proposal is based on the following assumptions:

- sections remain plane during deformations
- that failure of section correspond to the attainment of a ultimate deformation of steel or concrete (say ±10 ‰ and -3.5 ‰ respectively)
- an elasto-plastic constitutive law for steel
- an stress-block constitutive law for concrete

the derivation of adimensionalized interaction diagrams μ-ν with increasing amount of steel mechanical ratio ω is straightforward using the usual formulas adopted for R.C. sections.

The height of the stress block region y is defined as a function of the neutral axis position:

$$y = \begin{cases} 0.8 \cdot x & if\ x \le t \\ \dfrac{x - 0.8t}{x - 0.75t}\, t & if\ x > t \end{cases} \qquad [7.6]$$

Defining $\xi = y/t$ and the steel stress $\sigma_s = kf_{yd}$ as a fraction of the yielding stress f_{yd}; all the internal forces could be expressed in non-dimensional form:

$$\nu_r = \frac{N_r}{b \cdot t \cdot f_{cd}} = \frac{y \cdot b \cdot f_{cd} - k \cdot A_s \cdot f_{yd}}{b \cdot t \cdot f_{cd}} = \xi - k \cdot \omega \qquad [7.7]$$

$$\mu_r = \frac{M_r}{b \cdot t^2 \cdot f_{cd}} = \frac{t-y}{2} \cdot \frac{y \cdot b \cdot f_{cd}}{b \cdot t^2 \cdot f_{cd}} = \frac{1-\xi}{2} \cdot \xi \qquad [7.8]$$

where μ is the mechanical reinforcement ratio defined as:

$$\omega_r = \frac{f_{yd} \cdot A_s}{f_{cd} \cdot A_c} = \frac{f_{yd} \cdot A_s}{f_{cd} \cdot b \cdot t} \qquad [7.9]$$

In the definition of mechanical reinforcement ratio, the material strengths are involved: $f_{cd} = a_{cc} f_{ck}/\gamma_c$ is the design cylindrical concrete strength; a_{cc}, generally equal to 0.85, considers the resistance reduction due to long term load effects; γ_c is the concrete partial safety factor. The r subscript marks the failure points in the μ-ν domain.

Figure 7-20 shows the interaction diagrams for different reinforcement ratios. When the neutral axis coincides with the reinforcement position, the adimensionalized bending moment μ-become independent from the reinforcement ratio; in this case the failure surface is reached with ν=0.4 and μ=0.12.

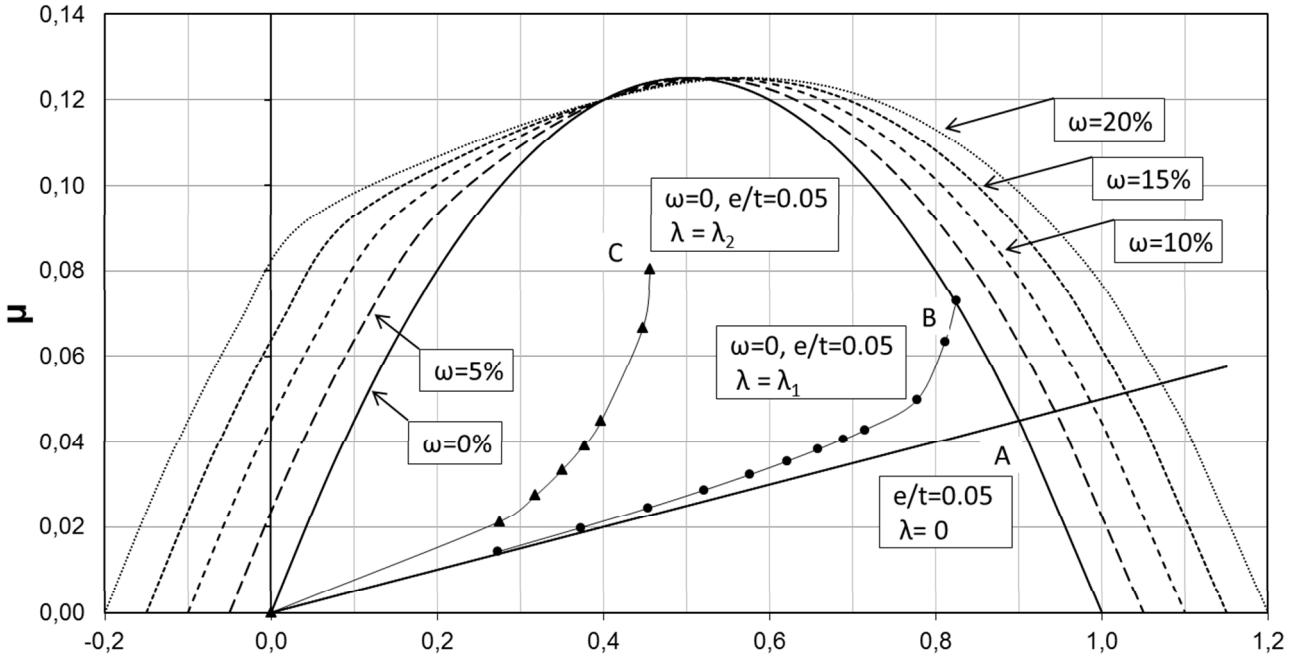

Figure 7-20. Interaction diagrams μ-ν

Let us assume the case with ω=0 and e/t =0.05. In Figure 7-20, the failure condition with different values of λ are represented. For λ=0 the bending moment μ-is simply proportional to the axial load ν (see straight continuous line with constant slope equal to e/t) and the point A marks the failure condition, for small values of λ (in figure indicated with λ_1) the section reaches the failure curve

with a smaller axial load (point B); for great λ values the section is not able to reach the failure curve due to the great second order eccentricity (point C). Section 7.3.4 treats with more details the case with large deformations.

7.3.4. The transversal eccentricity factor

The reducing factor ϕ_t accounting for load transversal eccentricity and slenderness is defined as the ratio of the normal load with a generic eccentricity to the maximum axial load applicable to the section. To start let us to consider the effect of transversal eccentricity only:

$$\phi_t = \frac{N_r}{N_{rd,0}} = \frac{N_r}{f_{cd} \cdot b \cdot t \cdot (1-\omega)} = \frac{\nu_r}{1+\omega} = \frac{\xi - k \cdot \omega}{1+\omega} \qquad [7.10]$$

For any given ξ it is possible to compute ϕ_t and e/t. Since k depends on ξ there is not a direct way to compute ϕ_t but, for any ω, the ϕ_t value can be plotted in function of eccentricity (see Figure 7-21).

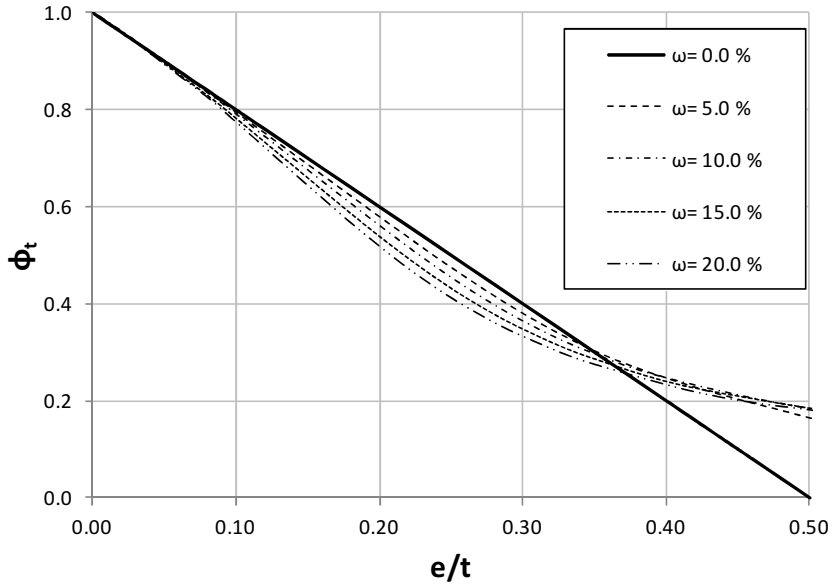

Figure 7-21. ϕ_t -e/t graph neglecting slenderness

Considering just the first order effect, the eccentricity could be expressed as:

$$\frac{e}{t} = \frac{\mu}{\nu} = \frac{\xi}{2} \cdot \frac{1-\xi}{\xi - k \cdot \omega} \qquad [7.11]$$

In a reinforced section some negative values of the ϕ_t factor are theoretically possible (walls undergoing traction axial forces) due to tensile strength supplied by the bars. But in practice such complication is useless.

In order to consider also the effect of slenderness, the proposed model employs the eccentricity-curvature graph and it is based on "nominal curvature" method as defined in (Eurocode 2 2004) with the same assumptions.

Let us consider the idealized rectangular section in Figure 7-22, where are presented the typical linear strain diagram (plane sections hypothesis), the concrete stress with the resultant force *C*, the reinforcement tensile force *Z*. Thanks to equilibrium equation and previous hypothesis, the eccentricity-curvature graph can be obtained.

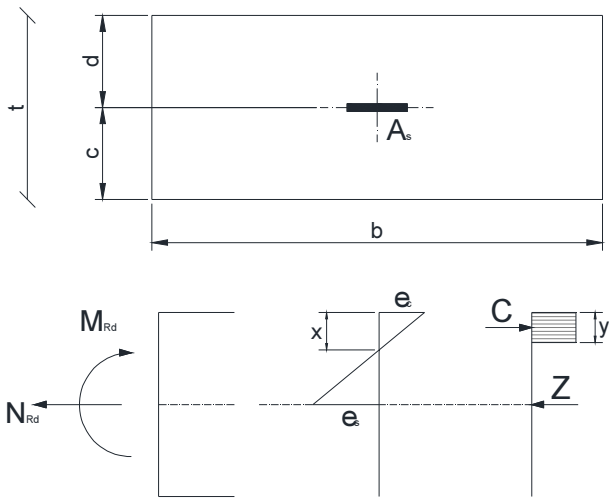

Figure 7-22. Scheme used to calculate internal forces of idealized section

The first order bending moment is constant, equal to the product of vertical load and eccentricity. The proposed method treats the deformation as a sinusoid and yields the following eccentricity:

$$\frac{e}{t} = \frac{e^I + e^{II}}{t} = \frac{e^I}{t} + \frac{1}{10} \cdot \frac{l_0^2}{t^2} \cdot (\chi \cdot t) = \frac{e^I}{t} + \frac{\lambda^2}{10} \cdot (\chi \cdot t) \qquad [7.12]$$

where l_0 is the effective panel height and χ is the curvature of the most stressed section. In the e/t-χ t graph second order effects are represented by a line with a slope equal to $\lambda^2/10$ that intercepts the eccentricity axis at e^I/t. The higher is the panel the greater is its slenderness, so increase panel height means increasing the second order eccentricity e^{II}. The external moment in terms of eccentricity can be computed as the sum of first and second order relative eccentricity, the internal forces give the concave curve in Figure 7-23 and the intersection points represent the equilibrium

between the external and internal forces. For example in Figure 7-23 for an axial load of 2000 kN there are two equilibrium conditions but, increasing the load until about 2072 kN, there is only one intersection that represents the tangency condition and the maximum load applicable. In fact for a greater load the curve shifts downward and there are no equilibrium conditions.

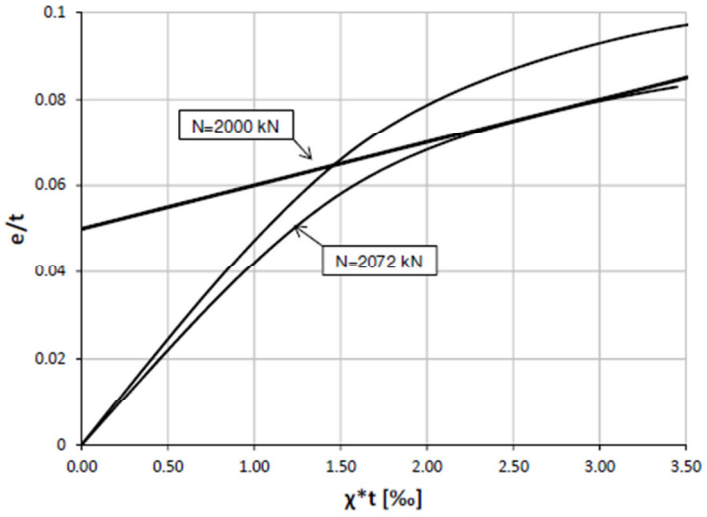

Figure 7-23. e/t - χ t graph for two fixed vertical loads

Coming back to Figure 7-20, some points of equilibrium derived from the eccentricity-curvature graph are plotted: with small loads the difference between first and second order moment is not significant but for greater values of ν the slenderness reduces the resisting domain.

With the procedure described above for any ω it is possible to plot a graph that describes the ϕ_t variation as a function of slenderness and relative eccentricity e/t.

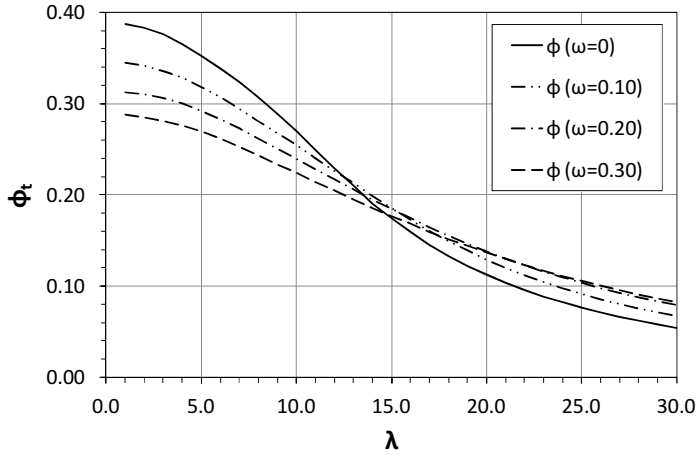

Figure 7-24. Convex hull of ϕ_t for e/t=0.30 and varying reinforcement ratio

Changing the reinforcement ratio the different curves barely shift; so we can consider only one graph helpful for all ω values which contains the minimum envelope of each curve. In Figure 7-24 the coefficient is evaluated for a given eccentricity and varying reinforcement ratio. The graph in Figure 7-30 represents the minimum envelope of ϕ_t over the different reinforcement ratio. It allows a simplified safe evaluation of the ultimate bearing capacity independently from the reinforcement ratio.

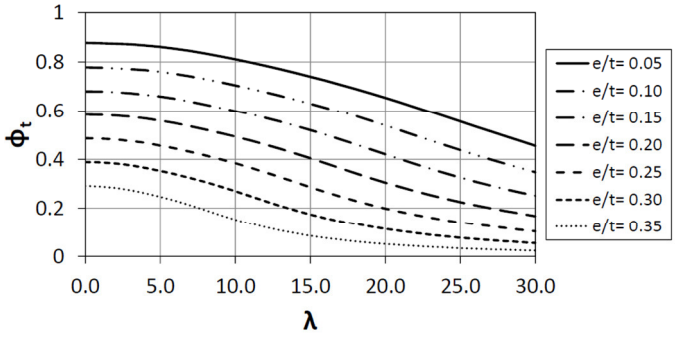

Figure 7-25. ϕ_t-λ graph (ω=0%)

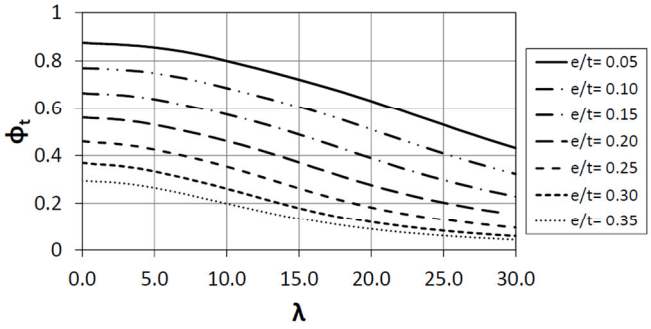

Figure 7-26. ϕ_t-λ graph (ω=5%)

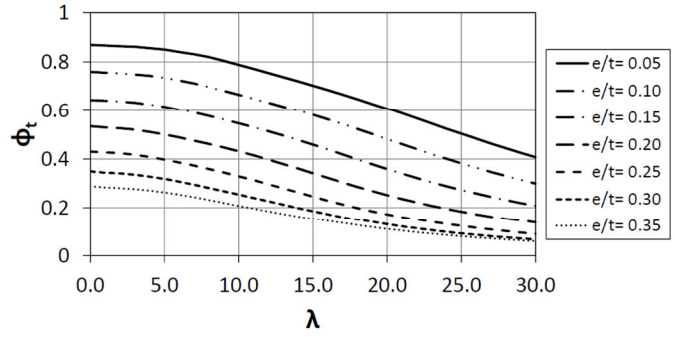

Figure 7-27. ϕ_t-λ graph (ω=10%)

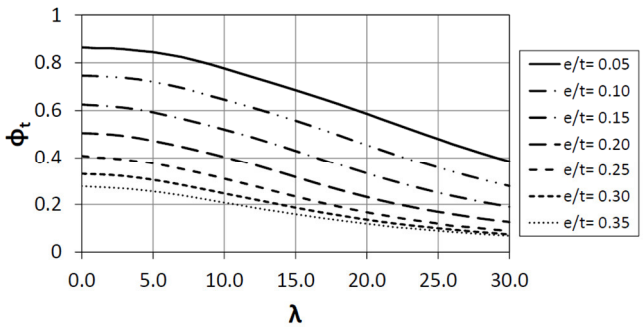

Figure 7-28. ϕ_t-λ graph (ω=15%)

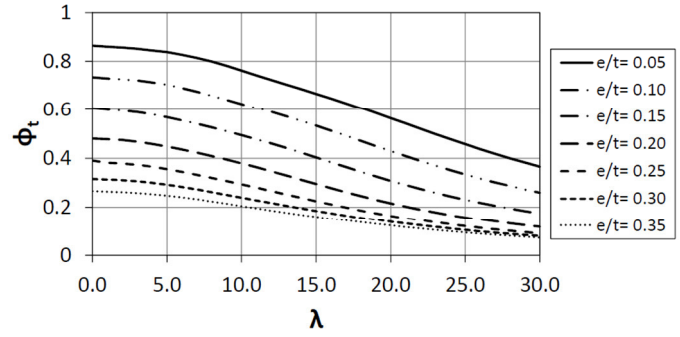

Figure 7-29. ϕ_t-λ graph (ω=20%)

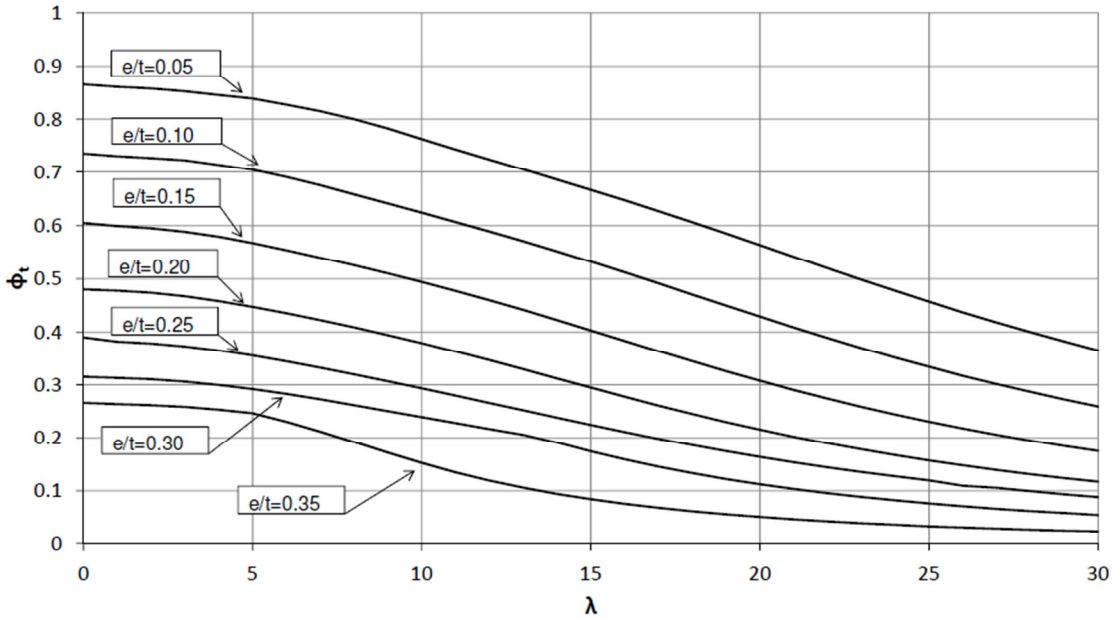

Figure 7-30. Transversal coefficient ϕ_t depending on eccentricity and slenderness (minimum envelope for varying reinforcement ratio)

There are three different cases for a moment-curvature graph where the sections are subjected only to bending moment (no axial load is applied): null tensile strength of concrete, null tensile strength of concrete in cracked conditions, null tensile strength of concrete in cracked conditions and "tension stiffening" effect. In the following the first case is assumed, which neglects completely the tensile strength of concrete during deformations.

7.3.5. The longitudinal eccentricity factor

An analytical model also for vertical load with an in-plane eccentricity is presented by means of a longitudinal eccentricity factor, even if no experiment was performed in that sense.

Dealing with the problem along the longitudinal axis, the reinforcement is uniformly distributed and the section can be simplified as a rectangle with the same concrete area of the actual section and the same length (see Figure 7-31).

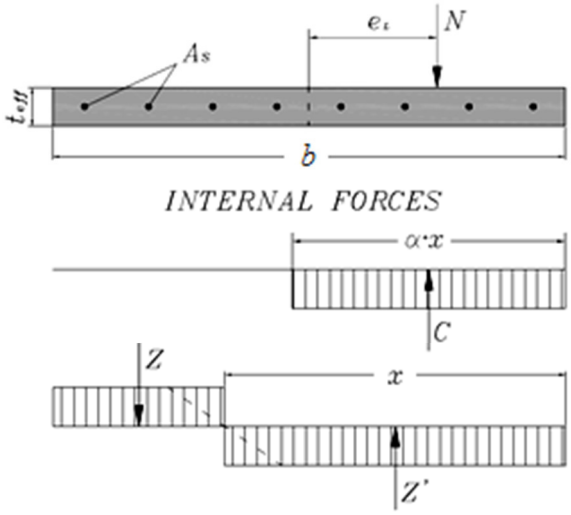

Figure 7-31. Section schematization

Considering the yielding strength at each bar (k=1) the equilibrium equations are:

$$\begin{cases} \sum F = 0 \\ \sum M = N \cdot e_L \end{cases} \Rightarrow \begin{cases} N - C + Z - Z' = 0 \\ C \cdot \dfrac{1-\alpha \cdot x}{2} + Z \cdot \dfrac{x}{2} + Z' \cdot \dfrac{1-x}{2} \end{cases} \qquad [7.13]$$

ϕ_l can be expressed as a function of the eccentricity but the expression is not very suitable, so it is more comfortable using the graph in Figure 7-32. In this graph the variables are all expressed in a non-dimensional way so it does not depend on panel length. For small eccentricity values, e.g. 20% of the length, the coefficient is almost the same for all the reinforcement ratios investigated. In first approximation the reinforcement can be neglect keeping the value:

$$\phi_l = 1 - 2 \cdot \frac{e_L}{t} \qquad [7.14]$$

Increasing the bending moment, i.e. for small loads and big eccentricity, the proposed method lacks in precision because it controls the axial load; so the interaction diagram is needed.

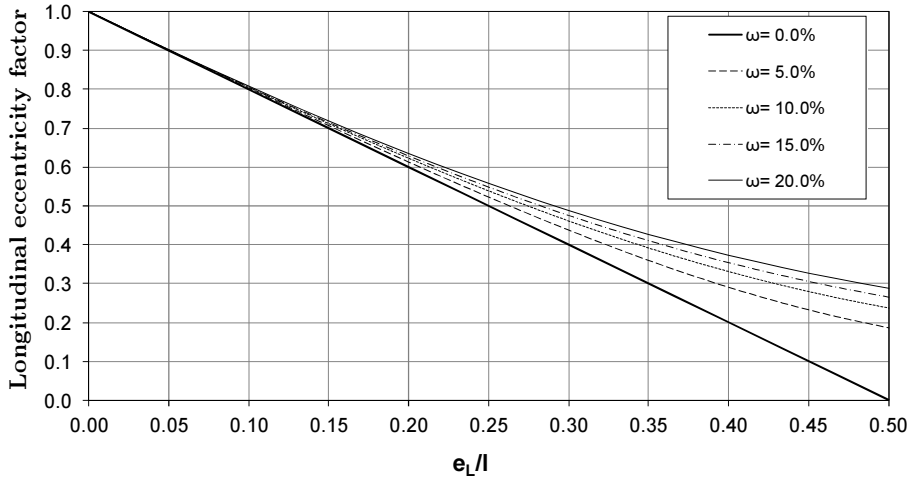

Figure 7-32. ϕ_l – e_L/l graph

7.3.6. Panels with a non-uniform reinforcement

The theoretical frame described above refers to sections with a uniform reinforcement along the panel width. In the case of panels with reinforcement concentrated in the ends, e.g. for a greater strength, the procedure is modified as follows:

- build the interaction diagram for the equivalent concrete rectangular section with width b and equivalent thickness t_{eff} , with the actual reinforcement
- scale the interaction diagram by a factor of ϕ_t which considers the transversal first and second order effects
- verify that the external forces, N_{sd} and M_{sd}, lie inside the interaction diagram

7.4. Comparison with experimental results and discussion

In this section the between experimental and analytical results is presented. The analytical predictions are based on the diagrams shown in the previous section, where the panel deformations are not negligible.

The test setup described at the beginning of the chapter presents the force distribution shown in Figure 7-33 applying a bending moment M_{top} to the wall. The top vertical force applied with the actuator lies on the boundary of the inertia core of the wall rectangular section. The compressed section in contact with the ground expresses a bending moment M_{low} equal to $M_{top}/2$. In this way,

the ground is able to express a fully clamped restraint (see Figure 7-34 on the left). This is possible in this particular situation because the top eccentricity of vertical load is very small.

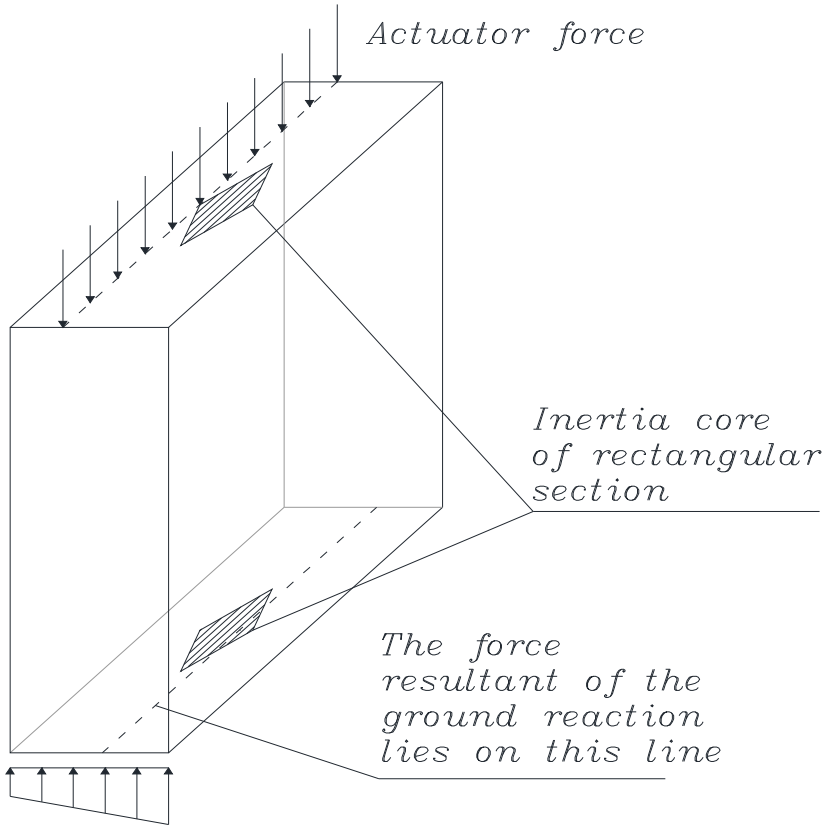

Figure 7-33. Test setup and force distribution

The tested panels can be seen as a cantilever beam with an external bending moment applied to the top (see Figure 7-34 on the left side). The out-of-plane translation is constrained by the friction between actuator and tested panel. Following a simplified method proposed by (Eurocode 2 2004), this static schematization can be simplified with a cantilever beam subjected to an equivalent moment:

$$M_{eq} = 0.6 \cdot M_{up} + 0.4 \cdot M_{low} = 0.6 \cdot P \cdot e + 0.4 \cdot \frac{P \cdot e}{2} = 0.4 \cdot P \cdot e = P \cdot e_{eq} \quad [7.15]$$

where

$$e_{eq} = 0.4 \cdot e \quad [7.16]$$

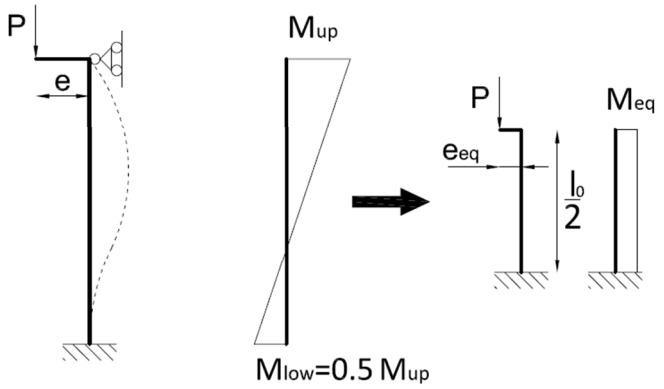

Figure 7-34. Derivation of e_{eq}: real panel (left) and equivalent cantilever beam (right)

In this section the comparison between experimental results and theoretical ones are presented. In the proposed formulas the followings parameters were inserted:

- the geometric test values (geometric samples dimensions, concrete areas, steel areas, eccentricity, etc.);
- the constraints: fixed at the bottom and hinged at the top (see chap.7 for constraints coefficients);
- no viscosity effects have been taken into account; viscosity in actual applications is treated in the following sections.

With these assumptions the results in Table 7-3 were obtained

Sample	**A**	**B**	**C**	**D**	**E**	**F**	**G**
Panel width [cm]	75.5	75.5	100	100	75	75	100
Block type	IL30	IL30	IL20	IL20	TW30	TW30	N20
$A_{cls,core}$ [cmq/m]	1413	1413	966	966	1520	1520	1092
Thickness t [cm]	20	20	13	13	20	20	13
Reinforcement	ϕ10/25x25	n.a.	n.a.	ϕ10/25x25	n.a.	ϕ10/25x25	n.a.
A_s [cmq/m]	3.16	0	0	3.16	0	3.16	0
ω [%]	4.43	0	0	6.47	0	4.11	0
$N_{rd,0}$ [kN]	3735	3577	2445	2604	3848	4006	2764
Effective length l_0 [cm]	225	225	225	225	225	225	225
Slenderness λ	11.25	11.25	17.31	17.31	11.25	11.25	17.31
Load eccentricity, e [cm]	0.0	4.0	0.0	2.6	0.0	4.0	2.6
Eq. eccentricity e_{eq} [cm]	0.0	1.6	0.0	1.04	0.0	1.6	1.04
Reducing factor ϕ_t	0.854	0.634	0.723	0.52	0.854	0.634	0.52
$\boldsymbol{N_{rd,th}=N_{rd,0} \cdot \phi_t}$	**3191**	**2269**	**1767**	**1353**	**3287**	**2542**	**1437**
$\boldsymbol{N_{rd,exp}}$ **[kN/m]**	**2764**	**2628**	**2160**	**2061**	**3471**	**3311**	**1695**
$\Delta_{th\text{-}exp}$ [%]	14.3	-14.6	-20.0	-41.5	-5.4	-26.3	-16.5

Table 7-3. Experimental and analytical results

Figure 7-35 gives a graphical representation of the comparison, the grey line shows the ideal condition of perfect matching between analytical and experimental results. Excluding only one case, the analytical predictions are always conservative compared with experimental recorded values; and in general quite close to the grey line.

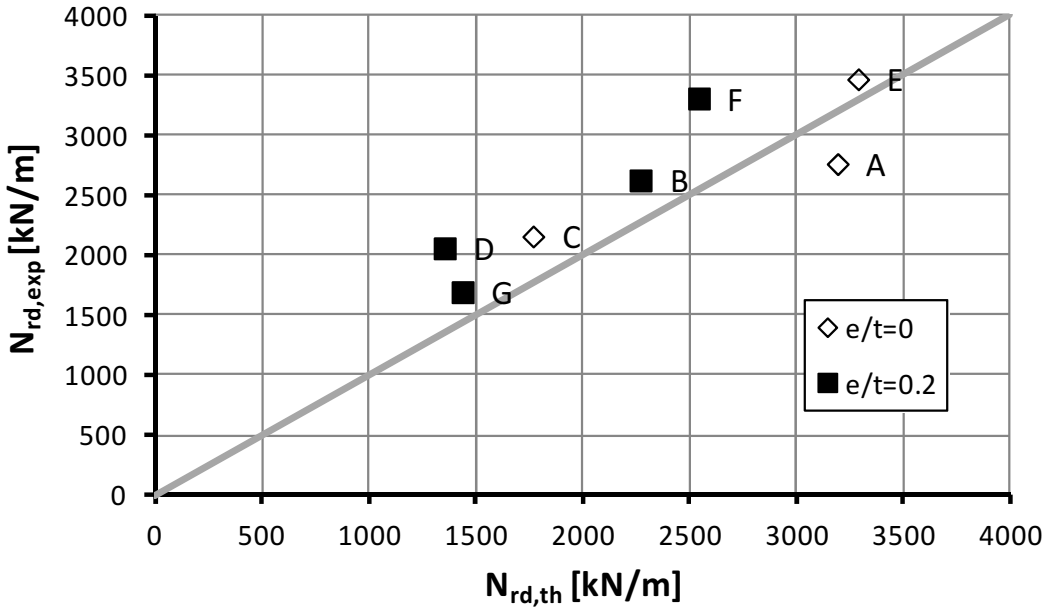

Figure 7-35. Comparison between experimental and theoretical results

7.4.1. Provisions for practical utilization and final considerations

In the previous paragraph no safety factors have been used regarding material resistance characteristics (γ_c=γ_s=1), because the theoretical framework should match exactly the real behavior of panels during the loading process. But, in practical applications, the standard codes impose to apply a reducing factor for each material resistance. In the case under investigation the partial factor for concrete is greater than the Italian coefficient proposed by (Eurocode 2 2004) and (NTC 2008), γ_c=1.5. Since the control on concrete integrity is not easy, and concrete compaction into the formworks is a difficult task, the partial factor has been increased.

The safety factor for steel corresponds to the Eurocode 1: γ_s=1.15. With this proposal the design strengths of materials are:

$$f_{cd} = \alpha_{cc} \cdot \frac{f_{ck}}{\gamma_c} = 0.85 \cdot \frac{f_{ck}}{1.8} \qquad [7.17]$$

and

$$f_{yd} = \frac{f_{yk}}{\gamma_s} = \frac{f_{yk}}{1.15} \quad [7.18]$$

respectively for concrete and steel; where f_{cd} is the characteristic cylindrical resistance of concrete and f_{yk} is the characteristic yielding point of steel.

In the experimental results interpretation, no viscosity effects have been taken into account and no concrete resistance reduction has been assumed for long term loading

In actual applications the effective height l_0 could be expressed in function of lateral constraints and viscosity effects:

$$l_0 = \beta \cdot \rho \cdot h \cdot \sqrt{1 + \Phi \cdot \xi} \quad [7.19]$$

Coefficient $\sqrt{1 + \Phi \cdot \xi}$ leads to an increased value of the buckling length l_0 considering that concrete viscosity tends to increase the out-of-plane displacement due to permanent loads. This factor is proposed in analogy with (CNR 10025 1998) and (CEB/FIP Manual 1978) considering:

- Φ the fluage coefficient, generally equal to 1.2;
- ξ the ratio between the long term load and the total load.

β and ρ depend respectively on vertical and lateral constraints; e.g. in the experiment configuration β =0.75 and ρ=1.0 (see (CNR 10025 1998) and (CEB/FIP Manual 1978) for more details about these coefficients).

Based on the experimental program and analysis of the test results, the following conclusions can be drawn:

- out-of-plane deformation is deeply affected by moment;
- the proposed theoretical framework based on the European Code matches quite well the experimental results and it is almost always conservative, especially in the evaluation of bearing capacity with transversal eccentric loading

The reason for the conservativeness of the theoretical proposal can be ascribed to the fact that the contribution of the formworks to bearing capacity has not been accounted for. This assumption is correct when considering the strength of the wall (since gaps between blocks are not perfectly closed). But in practice the lateral stiffness of the wall is significantly increased if the contribution of formworks is also considered.

The considerations in this chapter extend the theoretical framework of the European Code employed in masonry calculation to the technology under examination.

Chapter 8. – Direct shear tests

The aim of the direct shear tests was to evaluate the shear strength of the wall which is directly correlated to that of horizontal elements, also called transverses. The experimental campaign has been performed in 2012 at the Material Tests Laboratory of the ICEA Department at the University of Padua. The experimental results are reported in the Laboratory official report n°34570.

These kinds of tests are not prescribed by the Italian Ministry of Public Works Guidelines (2011) which proposes the execution of diagonal tests. As explained in the following chapter, the direct shear test is the more effective for the characterization of this construction system under shear forces.

8.1. Test matrix

Eighteen concrete specimens were tested. Among them only six were unreinforced. In the other tests, rebars were placed only in the horizontal elements (transverses) that in the test are subjected to shear forces.

The vertical elements are subjected only to axial force far lower than their compressive strength.

Specimens had a fixed height of 75 cm in order to avoid buckling effects.

Three different kind of block were employed: N18, N25 and I30. The number specifies the block thickness in centimetres, but the concrete core thickness into the columns was respectively 13, 18 and 22 cm. The section area of the transverses varies between 72, 90 and 107 mm^2 respectively.

Three reinforcement configuration were employed:

- without reinforcement;
- with single rebar in each transverse: ϕ8 mm@25 cm
- with single rebar in each transverse: ϕ12 mm@25 cm

Table 8-1 summarizes the specimens tested.

Sample number	Block type	Core thickness t [cm]	Horizontal bars	N° of strain gauges	Loading type
1	N18	13	-	-	monotonic
2	N18	13	-	-	mono.
3	N18	13	8mm @ 25cm	-	mono.
4	N18	13	12mm @ 25cm	-	mono.
5	N25	18	-	-	mono.
6	N25	18	-	-	mono.
7	N25	18	8mm @ 25cm	-	mono.
8	N25	18	12mm @ 25cm	-	mono.
9	I30	22	-	-	mono.
10	I30	22	-	-	mono.
11	I30	22	8mm @ 25cm	-	mono.
12	I30	22	12mm @ 25cm	-	mono.
13	N18	13	8mm @ 25cm	1	cyclic
14	N18	13	12mm @ 25cm	1	cyclic
15	N25	18	8mm @ 25cm	2	cyclic
16	N25	18	12mm @ 25cm	1	cyclic
17	I30	22	8mm @ 25cm	2	cyclic
18	I30	22	12mm @ 25cm	1	cyclic

Table 8-1. Characteristics of tested specimens

8.2. Material properties

B450C steel type was employed for the rebars with an average yielding stress f_{ym} of 544 MPa for the ϕ8 and 542 MPa for the ϕ12 one. These values were obtained by testing three steel coupons for each diameter according to (ISO 15630-1 2010). Normal weight C28/35 concrete was used to cast all the specimens. The average cylindrical compression strength f_{cm} was 29.1 MPa.

8.3. Loading test setup

All the specimens were brought to failure, the first 12 following a monotonic procedure loading history, whereas the last 6 were subjected to increasing cyclic shear loads applied with a prescribed

time history: 30%, 60% and 90% of the expected yielding point. The average loading rate was about 0.7 kN/s.

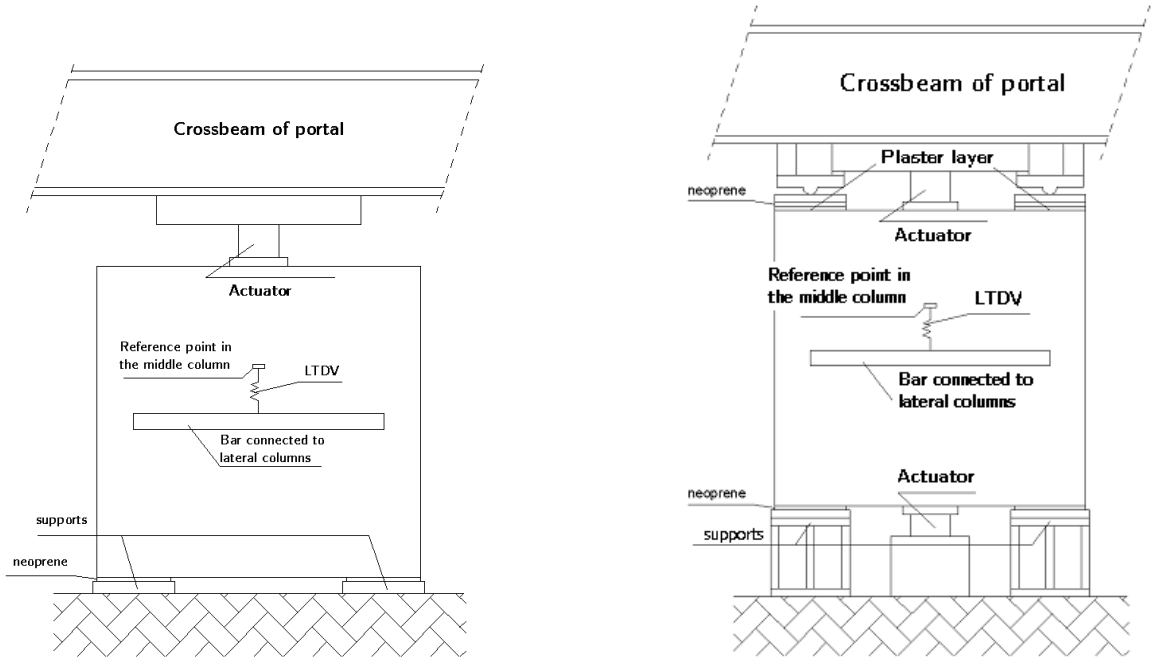

Figure 8-1. Direct shear: loading test setup

The data obtained in the monotonic tests were used to control and calibrate the successive cyclic tests.

The inner concrete structure was formed by three vertical columns laying on the same plane and by six horizontal transverse. The middle column was linked on each sides to the other two columns by three transverses (see Figure 8-2).

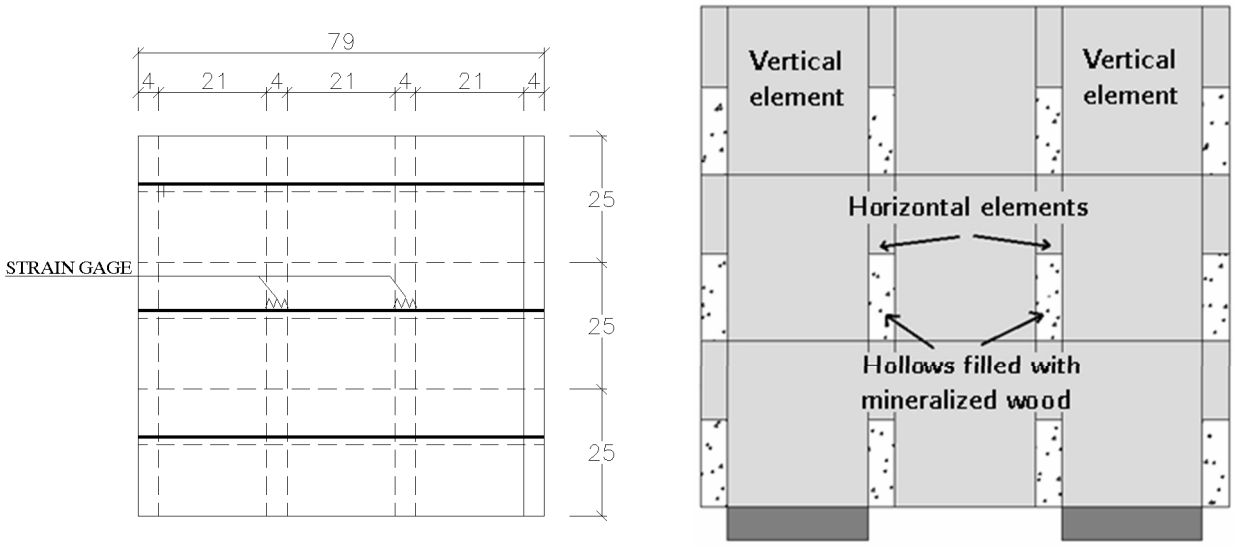

Figure 8-2. Strain gauge position (left) and internal concrete structure of specimens (right)

During the tests the external columns were constrained by two supports that worked as pinned ends. The vertical force was applied at the centre of the middle column ends; at the top in the monotonic cases and alternatively at both ends in the cyclic cases. To measure the vertical differential displacement between the columns, two linear variable differential transducers (LVDT) were used and located at mid-height under the loading point.

On each side of the specimen an aluminum bar was fixed to the lateral columns with hot melt glue. The external wooden shuttering block was removed in the support points in order to reach directly the concrete and obtain more accuracy. The transducer was fixed at the bar mid-span and the stem end was in contact with a steel angular placed above the bar. This angular was fixed at the middle column surface, in that way the transducer measured the relative displacements between the middle column and the lateral ones. Figure 8-3 shows the instruments employed to measure the vertical deflections.

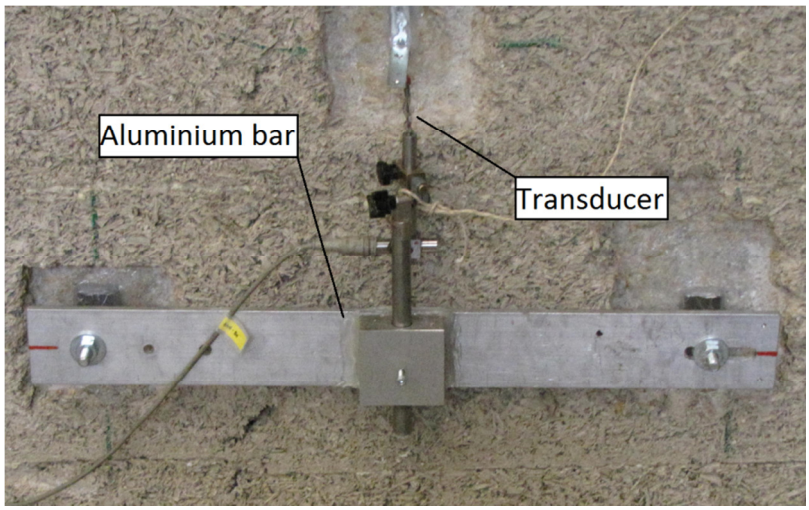

Figure 8-3. Instrumentation employed during the tests

The specimens subjected to cyclic loading were also instrumented with strain gauges applied to the reinforcement of the middle height transverses (see Figure 8-2).

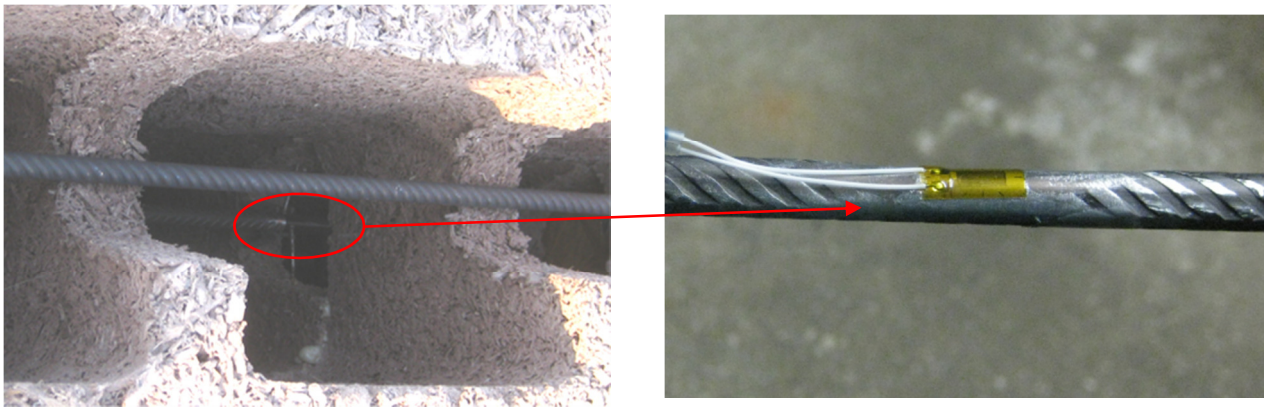

Figure 8-4. Particular of strain gauges

The load-deflection curves for all specimens are shown in the following graphs. For the cyclic tests also the load-strain curve of the bars are reported on the right.

8.4. Experimental results

During the test the following parameters have been continuously recorded:

- the vertical deflection of the middle column on both specimen sides: δ_{left} and δ_{right}. The average vertical deflection was obtained with:

$$\delta_{avg} = \frac{\delta_{int} + \delta_{ext}}{2} \qquad [8.1]$$

- the horizontal bars strain in the two middle transverses during the cyclic tests.

Two strain gauges placed in the horizontal middle bar measured the strains during the cyclic tests. The maximum elongation occurs in the two weak sections of the transverses.

Monotonic tests

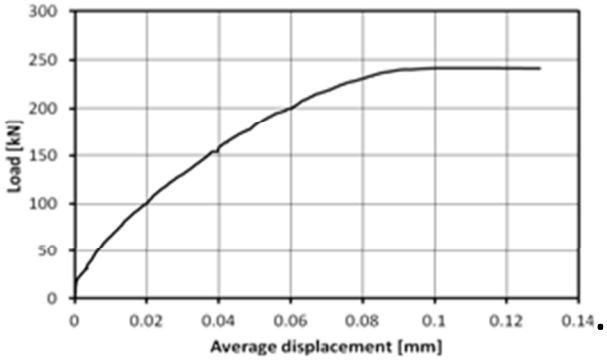

Figure 8-5. Load vs. distortion (panel 1)

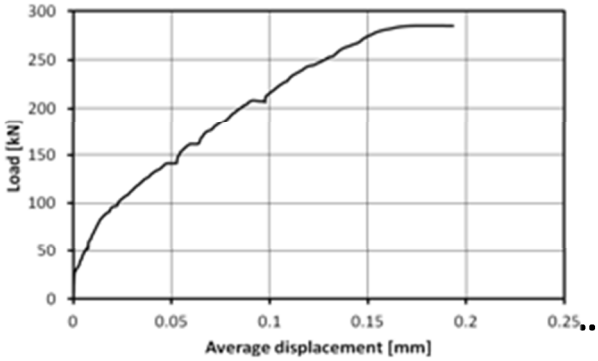

Figure 8-6. Load vs. distortion (panel 2)

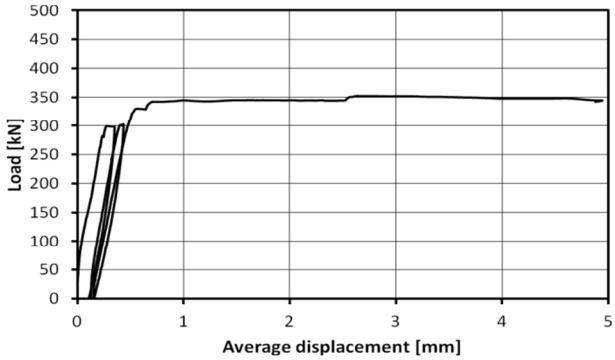

Figure 8-7. Load vs. distortion (panel 3)

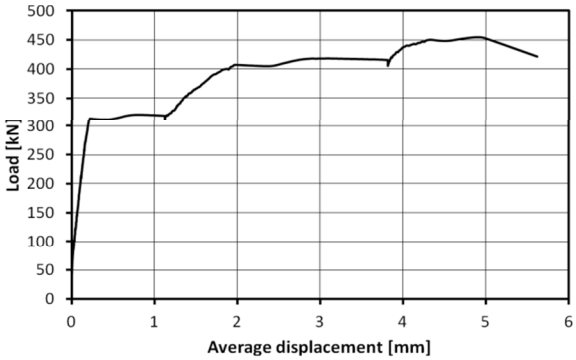

Figure 8-8. Load vs. distortion (panel 4)

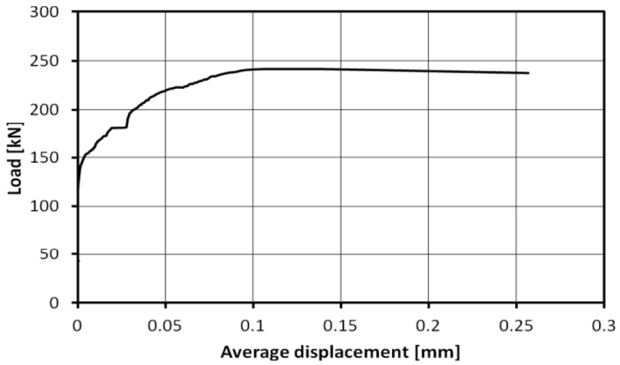

Figure 8-9. Load vs. distortion (panel 5)

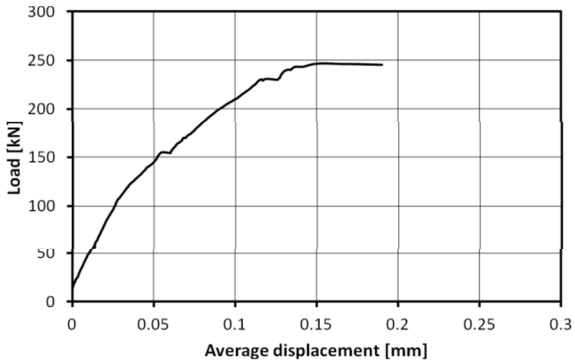

Figure 8-10. Load vs. distortion (panel 6)

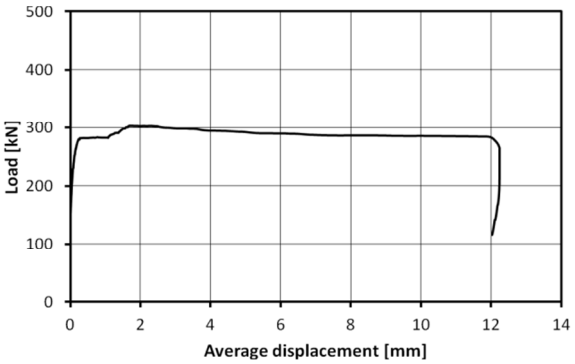

Figure 8-11. Load vs. distortion (panel 7)

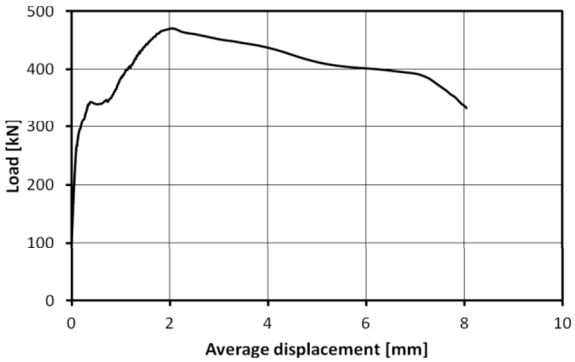

Figure 8-12. Load vs. distortion (panel 8)

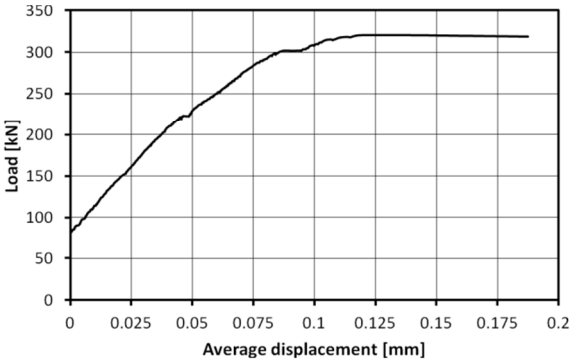

Figure 8-13. Load vs. distortion (panel 9)

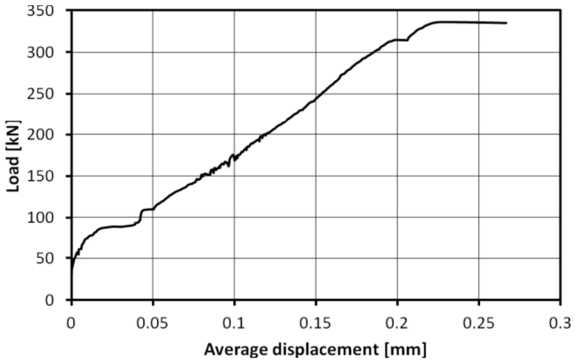

Figure 8-14. Load vs. distortion (panel 10)

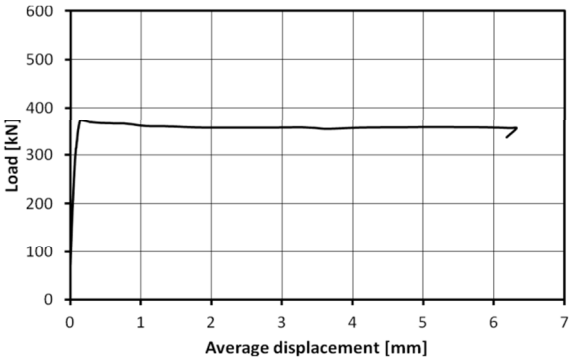

Figure 8-15. Load vs. distortion (panel 11)

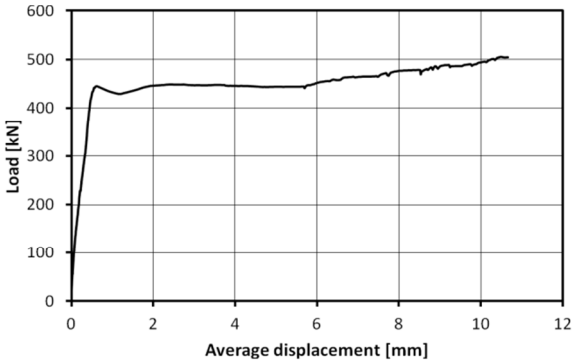

Figure 8-16. Load vs. distortion (panel 12)

Cyclic tests

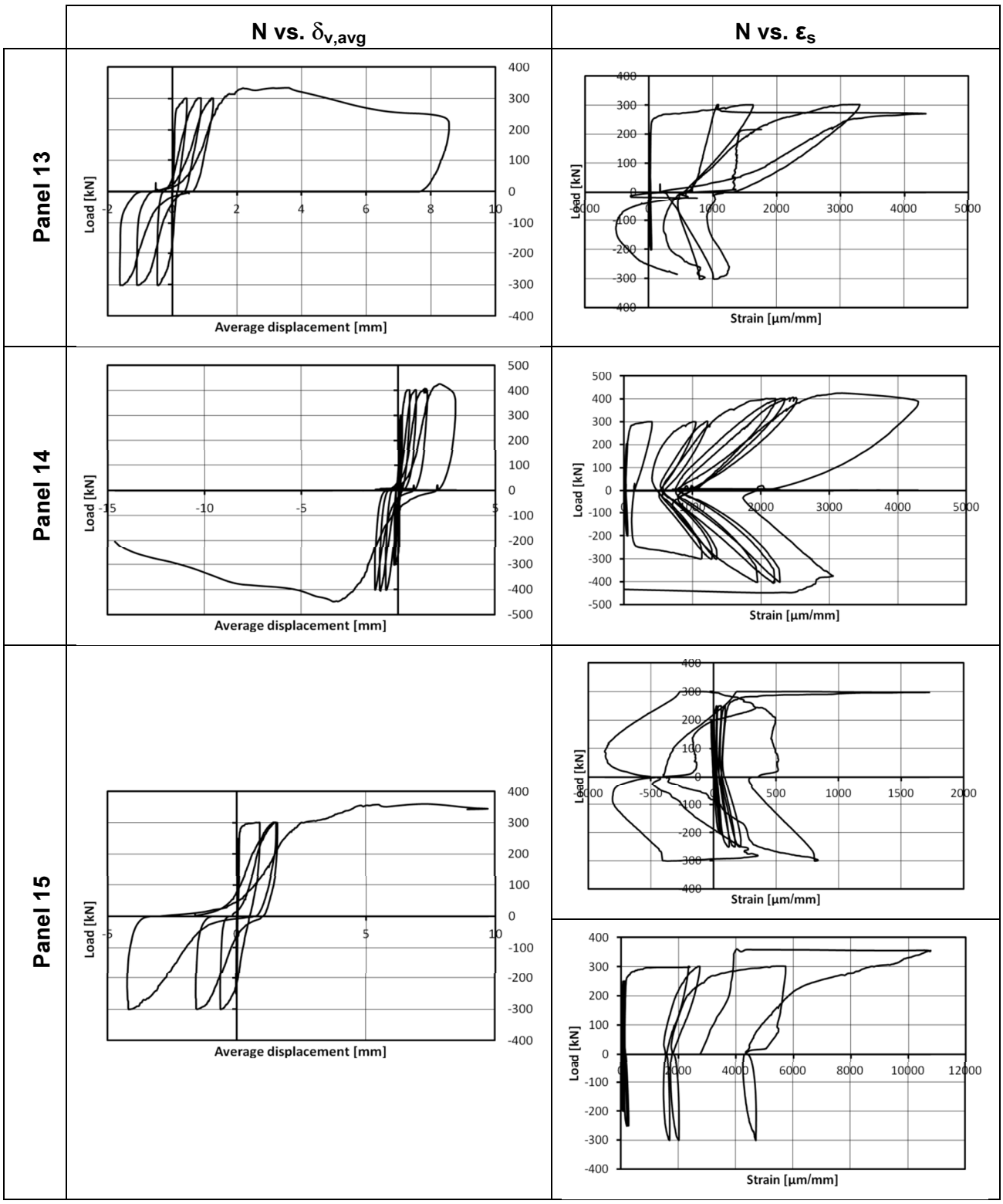

Figure 8-17. Cyclic tests: load vs. distortion and load vs. deformation graphs (panels 13-15)

	N vs. $\delta_{v,avg}$	N vs. ε_s
Panel 16	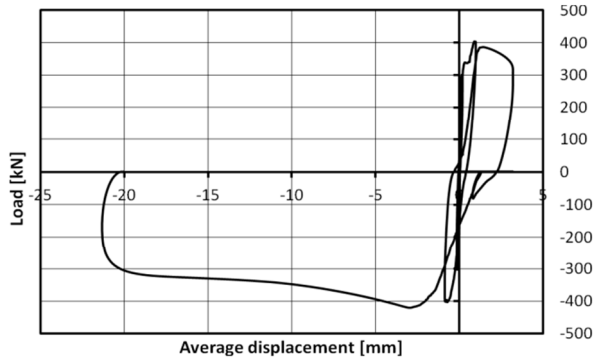	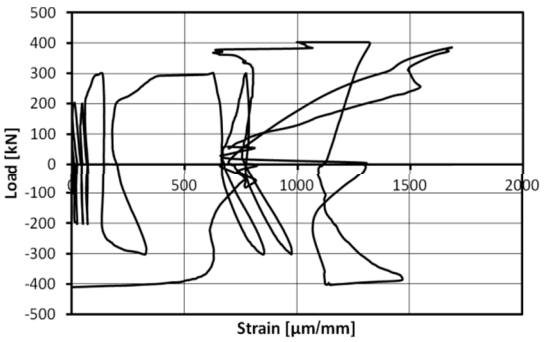
Panel 17 *	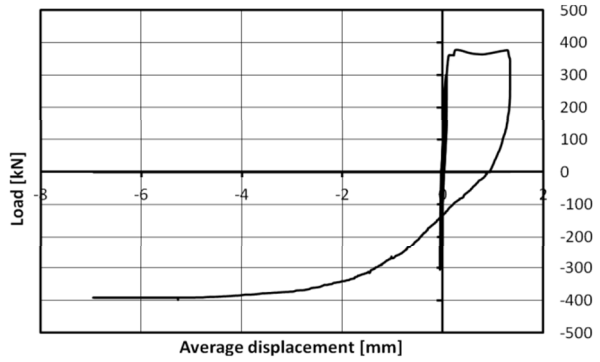 	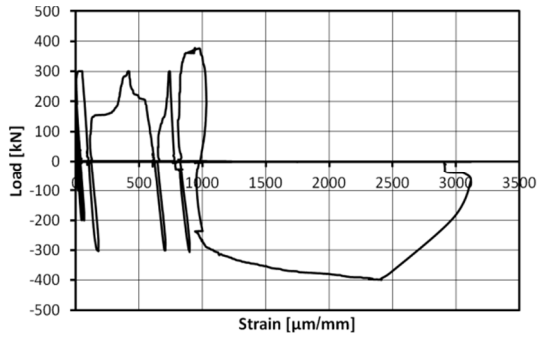 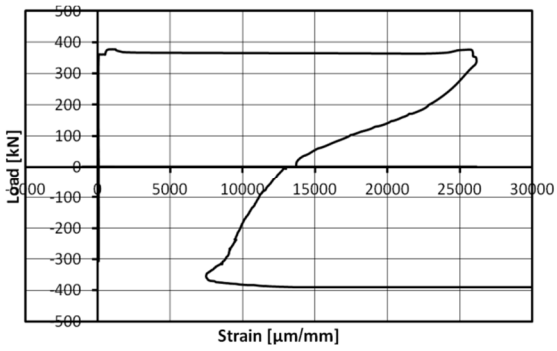
Panel 18	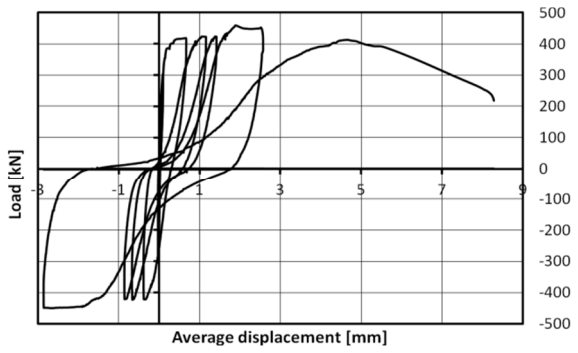	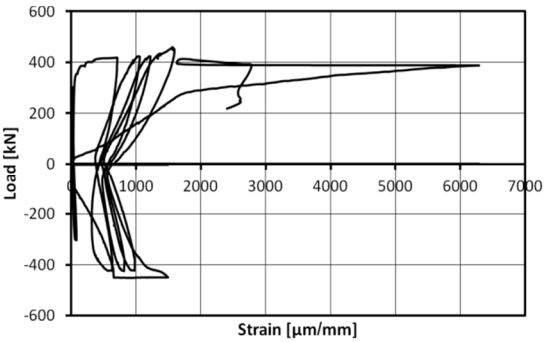

* The strain gauges graph and the figure at failure show that on the left side steel did not reach the yielding condition and the crack opened only on the right side.

Figure 8-18. Cyclic tests: load vs. distortion and load vs. deformation graphs (panels 16-18)

Sample number	Block type	Core thickness [cm]	Horizontal rebars	Ultimate load [kN]	Loading type
1	N18	13	-	240	monotonic
2	N18	13	-	285	mono.
3	N18	13	ϕ8 @ 25cm	353	mono.
4	N18	13	ϕ12 @ 25cm	455	mono.
5	N25	18	-	241	mono.
6	N25	18	-	247	mono.
7	N25	18	ϕ8 @ 25cm	303	mono.
8	N25	18	ϕ12 @ 25cm	471	mono.
9	I30	22	-	321	mono.
10	I30	22	-	336	mono.
11	I30	22	ϕ8 @ 25cm	372	mono.
12	I30	22	ϕ12 @ 25cm	523	mono.
13	N18	13	ϕ8 @ 25cm	334	cyclic
14	N18	13	ϕ12 @ 25cm	448	cyclic
15	N25	18	ϕ8 @ 25cm	360	cyclic
16	N25	18	ϕ12 @ 25cm	421	cyclic
17	I30	22	ϕ8 @ 25cm	399	cyclic
18	I30	22	ϕ12 @ 25cm	460	cyclic

Table 8-2. Maximum loads reached in direct shear tests

Table 8-2 reports the maximum loads values reached during the tests in the monotonic and cyclic case. These values are compared in the next paragraph with the results of an analytical model proposal.

8.5. Analytical model

The weak element in the ultimate shear state limit is the connecting element between columns, i.e the transverse. It limits the shear resistance of the whole wall. In the non-reinforced case, the failure is due to a pure shear action when the ultimate tensile strength of concrete is reached. In this case the failure is brittle.

If a horizontal reinforcement is present, the transverses behave like a coupling beam between the vertical elements and shear failure occurs due to the concrete strut or steel tie collapse. The horizontal reinforcement increments the shear resistance of transverses and provides more ductility to the system, avoiding a brittle failure.

Due to the grid pattern of the internal concrete structure, the level of axial vertical load does not affect the shear resistance. This behavior is different from the masonry one as described for example in (Vermeltfoort, Raijmakers e Janssen 1993). In a similar way, the vertical reinforcement does not increase the shear resistance of the panels

In the practical design the following condition must be satisfied:

$$v_{sd} \leq v_{rd} \quad [8.2]$$

v_{sd} and v_{rd} respectively being the shear demand and the shear capacity expressed as force per unit length. Multiplying these quantities by the length b of the wall we obtain the same condition in terms of forces.

8.5.1. Not reinforced transverses

The shear strength of not reinforced transverses subjected to a pure shear action is assure by the tensile stress capacity of concrete. Therefore it is possible to estimate the shear strength per unit length as:

$$v_{r,cls} = 0.25 \cdot \frac{A_t \cdot f_{ctd}}{i_t} \quad [8.3]$$

where:

- $f_{ctd} = 0.7 \cdot 0.3 \cdot f_{ck}^{2/3} / \gamma_c$ is the design tensile strength of concrete
- A_t is the transverse area
- i_t is the distance between transverses
- 0.25 is the coefficient that takes into account the low reliability of this mechanism based only on concrete tensile capacity

8.5.2. Reinforced transverses

The proposed model is a strut & one. The concrete strut forms a θ angle with the transverse axial that can vary between 0° to θ_{max}° where:

$$\theta_{max} = arctan\frac{h}{l} \quad [8.4]$$

The equilibrium condition is graphically represented in Figure 8-19, where V_s and N_s are shear and axial force acting on transverses. In actual shear-walls no axial force N_s acts on transverse (or are negligible) and therefore it would not be necessary to account for them. But, as we will see in the following chapter, accounting for axial force N_s is essential for the interpretation of diagonal compression test on square panels.

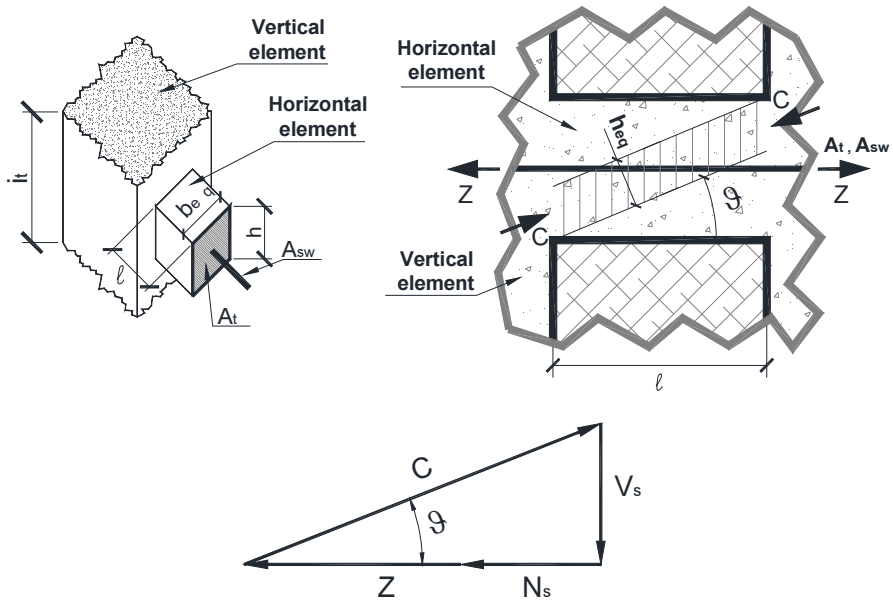

Figure 8-19. Strut-tie model with forces acting on the transverse

The transverse strength due to strut-tie mechanism $v_{r,s}$ is bounded by the tensile strength of the reinforcement v_s and by the compression strength of concrete strut v_c.:

$$v_{r,s}(\theta) = \min[v_s(\theta), v_c(\theta)] \qquad [8.5]$$

where

$$v_c(\theta) = \frac{b_{eq} \cdot h_{eq}(\theta) \cdot \nu \cdot f_{cd}}{i_t} \cdot sen\theta \qquad [8.6]$$

$$v_s(\theta) = \frac{f_{cd} \cdot A_{sw} + N_s}{i_t} \cdot tan\theta \qquad [8.7]$$

with the following notation:

- h transverse height
- $b_{eq}=A_t/h$ equivalent transverse width
- $h_{eq}(\theta)=[h \cdot \cos\theta - l \cdot sen\theta]$
- l transverse length
- A_{sw} transverse section
- f_{yd} design yielding stress of reinforcement
- $\nu = 0{,}7 - f_{ck}/200 \geq 0{,}5$ where f_{ck} is expressed in MPa (see (ETAG009 2002))
- f_{ck} characteristic compression strength of concrete

Varying the θ angle different values of v_c and v_s and therefore of $v_{r,s}$ are obtained. Ultimate shear strength is obtained for the optimal value of angle θ_{opt}, for which:

$$\nu_{r,s}(\theta_{opt}) = \nu_s(\theta_{opt}) = \nu_c(\theta_{opt}) = \max\ (\nu_{r,s}(\theta)) \qquad 0 < \theta \leq \theta_{max} \qquad [8.8]$$

Variation of v_c and v_s with θ is given in Figure 8-20, together with the definition of θ_{opt}.

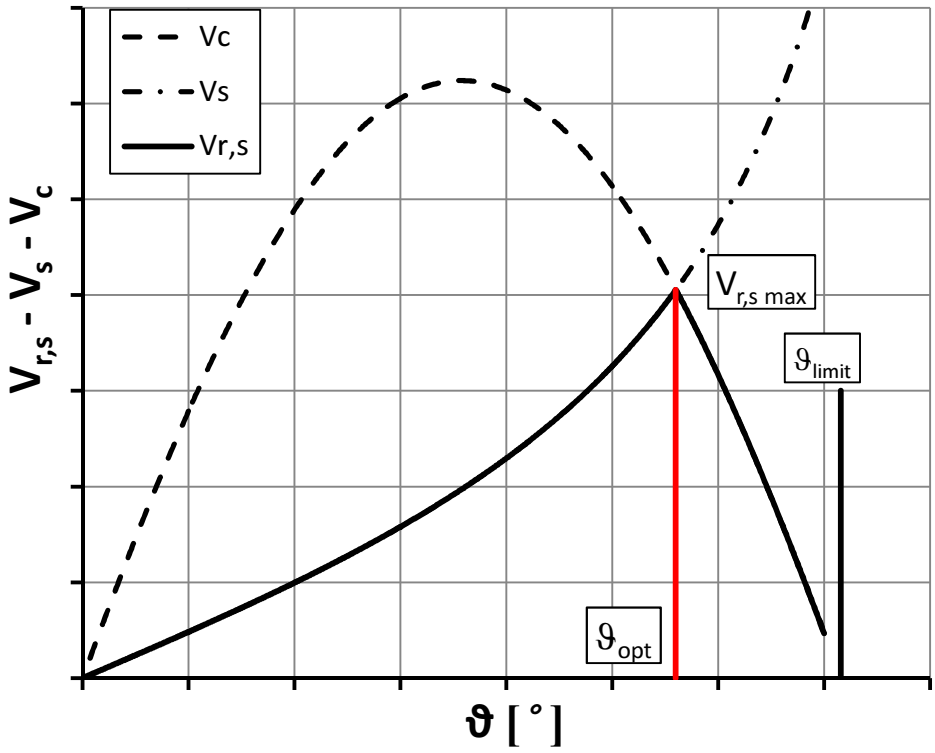

Figure 8-20. Strut-tie model: strength lower envelope

8.5.3. Total shear strength

Then the total shear strength v_{rd} is the sum of the two contributions above described, $v_{r,cls}$ due to concrete tensile strength and $v_{r,s}(\theta_{opt})$ due to strut-and-tie mechanism:

$$\nu_{rd} = \nu_{r,cls} + \nu_{r,s}(\theta_{opt}) \qquad [8.9]$$

8.6. Results and comparison

In this paragraph experimental and analytical results are compared. Therefore the following assumptions regarding the values used in the analytical calculations are adopted:

- actual dimensions for the horizontal element ("transverse") and for rebars steel section
- safety factor for steel and concrete, γ_c and γ_s, equal to 1 (i.e. actual strength of materials is used)
- actual average measured value of concrete compression strength f_c =29.1 MPa
- actual average measured value of steel yelding strength f_y=544 MPa and fy=542 MPa for reinforcement bars of 8 and 12 mm (values averaged on three steel samples for each diameter according to (ISO 15630-1 2010)
- the coefficient α_{cc} equal to 1 (long-term viscous effects neglected)

The analytical results are obtained following the procedure described in §8.5. Hereafter it is presented an example of V_{rd} calculation for the specimen realized with I30 block and reinforced with ϕ8 is presented.

Material characteristics			**Geometric characteristics: block I30**		
f_{cd} =	29.1	MPa	h_{trav} =	120	mm
f_{ctd} =	2.0	MPa	l =	40	mm
ν =	0.55		b_{eq} =	90	mm
f_{yd} =	542	MPa	A $_{trav}$ =	10745	mmq
$\gamma_c = \gamma_s$ =	1		n° $_{transverses}$ =	6	
V_r calculation (unreinforced panel)			**V_r calculation (reinforced panel)**		
$v_{r,cls}$ =	21.3	kN/tr.	ϕ =	8	mm
V_{rd} =	127.9	kN	Z =	27.3	kN/tr.
			ϑ_{opt} =	56°	
			$v_c(\vartheta_{opt})$ =$v_s(\vartheta_{opt})$ =	40.5	kN/trav
			v_{rd} = 21.3+40.5 =	61.9	kN/trav
			V_{rd} = 61.9 x 6 =	371.2	kN

Table 8-3. Analytical shear strength calculation for panels with I30 blocks with and without reinforcement

Specimen number	Type of test	Type of block	Type of reinforcement	n° of transverses	V_{exp} [kN] peak	V_d [kN] analitycal
1	monotonic	N18	-	6	240	86.1
2	mono.	N18	-	6	285	86.1
3	mono.	N18	8	6	353	287.9
4	mono.	N18	12	6	455	338.1
13	cyclic	N18	8	6	334	287.9
14	cyc.	N18	12	6	448	338.1
5	mono.	N25	-	6	241	106.8
6	mono.	N25	-	6	247	106.8
7	mono.	N25	8	6	303	323.4
8	mono.	N25	12	6	471	405.7
15	cyc.	N25	8	6	360	323.4
16	cyc.	N25	12	6	421	405.7
9	mono.	I30	-	6	321	127.9
10	mono.	I30	-	6	336	127.9
11	mono.	I30	8	6	372	371.2
12	mono.	I30	12	6	523	480.6
17	cyc.	I30	8	6	399	371.2
18	cyc.	I30	12	6	460	480.6

Table 8-4. Comparison between experimental and analytical values (direct shear tests)

Table 8-4 shows the analytical strength values for all the panels tested. The analytical and experimental values recorded during the experiments are reported in the last two columns. The experimental values are the maximum loads applied with the hydraulic actuator during the tests.

Experimental and analytical values are compared in Figure 8-21. The grey line represents the theoretical perfect matching between experimental values and analytical predictions of maximum shear strength. The majority of points lays in the upper part, it means that the analytical proposal is almost always conservative. The greatest variance occurs in the unreinforced panels, probably because the analytical proposal does not consider the confinement contribution of the block that could be important for small deformations. In the field of large deformations, close to the failure condition of reinforced panels, the blocks id cracked and this contribution is really small and therefore negligible. Indeed, in the reinforced panels case, the analytical proposal matches quite well the experimental values.

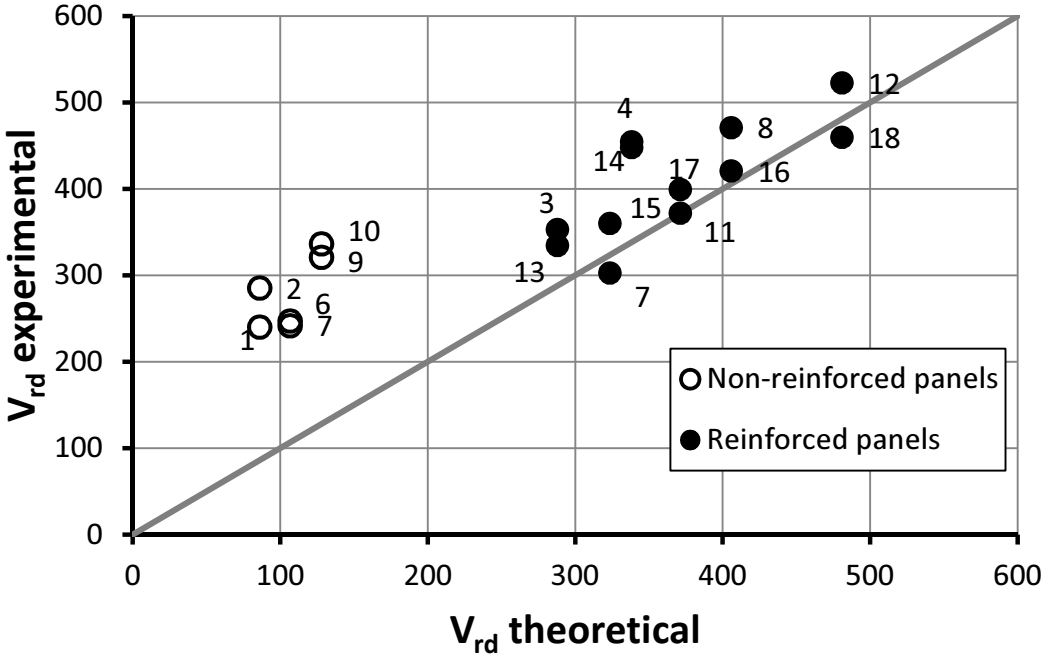

Figure 8-21. Comparison between experimental and analytical values (direct shear tests)

Chapter 9. – Diagonal compression tests

The aim of the diagonal compression tests was to evaluate the shear strength and stiffness. The experimental campaign has been performed in 2008 at the Material Tests Laboratory of the ICEA Department at the University of Padua. The experimental results are reported in the Laboratory official report n°29333.This kind of tests is also prescribed by the Italian Ministry of Public Works Guidelines (2011) where it is called *type 2 tests*.

This test series was carried out before the direct shear tests, indeed it is a standard procedure to evaluate the shear behavior also for other construction systems, for example masonry in (Page 1983). The orthotropic nature of the construction system at hand led to difficulties in the analytical test interpretation, described hereafter in this chapter. For this reason, it was clear the necessity of a different test setup able to study the behavior of horizontal elements, i.e. the direct shear tests.

9.1. Test matrix

A series of tests on 16 square specimens with a side of 1.25 m., with two different inclinations α of the internal concrete pattern: the transverse axis form an angle of 22.5 or 45 degrees with the ground plane. The panels were reinforced with different configurations and realized with different blocks:

- without reinforcement
- ϕ10 horizontal bars (only through the transverses), with a spacing of 25 cm
- ϕ10 bars in horizontal and vertical direction with a spacing of 25 cm

A description of the specimens tested is reported in Table 9-1.

Specimen number	Block type	Core thickness [cm]	Angle α [°]	Reinforcement type
1	IL20	13	45	w.r.
2	IL20	13	22.5	Φ10@25 (hor.)
3	IL20	13	22.5	Φ10@25/25
4	IL20	13	45	Φ10@25/25
5	IL30	20	22.5	w.r.
7	IL30	20	45	Φ10@25 (hor.)
6	IL30	20	22.5	Φ10@25/25
8	IL30	20	45	Φ10@25/25
13	TW30	20	45	w.r.
14	TW30	20	45	Φ10@25/25
15	N20	13	45	Φ10@25 (hor.)
16	N20	13	45	Φ10@25/25
17	TW30	20	22.5	Φ10@25 (hor.)
18	TW30	20	22.5	Φ10@25/25
19	N20	13	22.5	w.r.
20	N20	13	22.5	Φ10@25/25

Table 9-1. Description of specimens for diagonal compression tests

In the following figures dimensions, reinforcement bars and constructive details are described.

Figure 9-1. IL30 50x30 – 22.5°(ϕ10@25 only hor.)

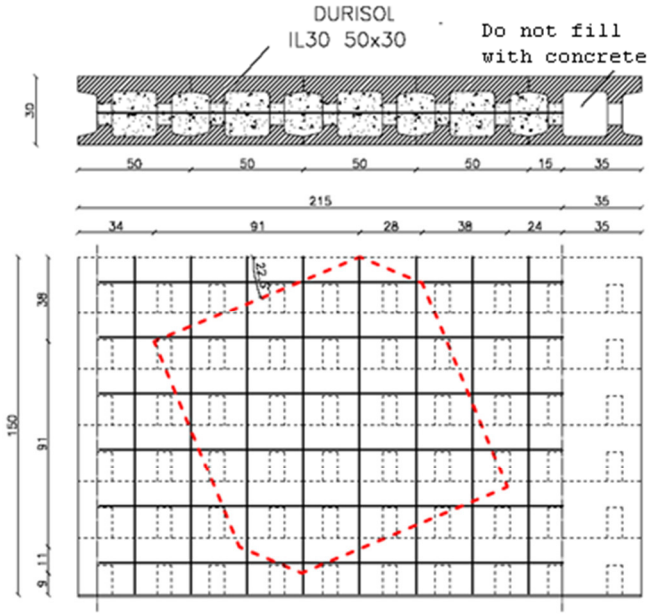

Figure 9-2. IL20 50x20 – 22.5°(ϕ10@25 hor./vert.)

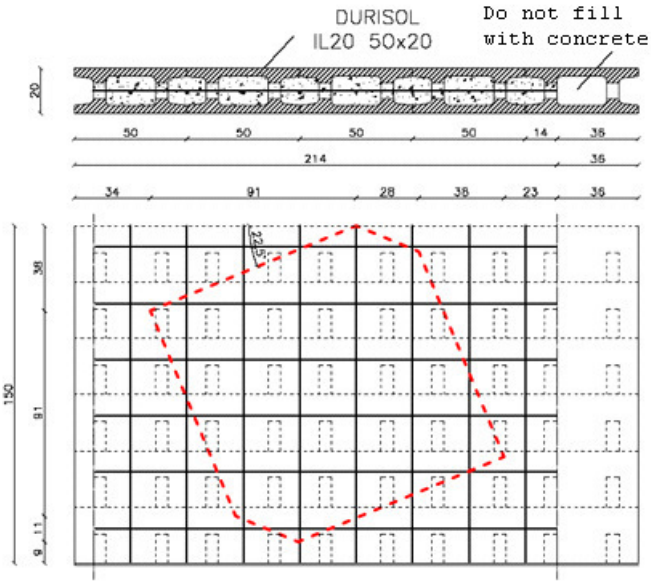

Figure 9-3. IL30 50x30 – 45°(ϕ10@25 only hor.)

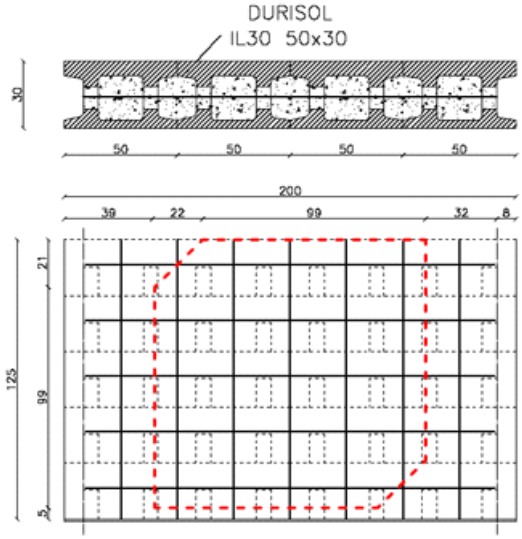

Figure 9-4. IL20 50x20 – 45°(ϕ10@25 hor./vert.)

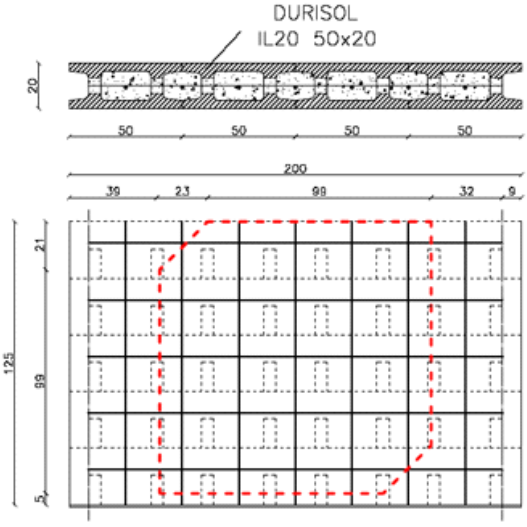

Figure 9-5 TW30 125x30 - 22.5°(ϕ10@25 only hor.)

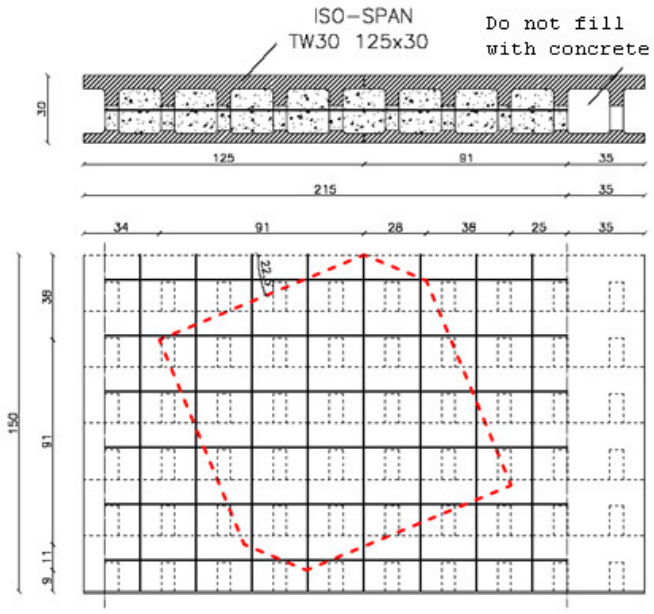

Figure 9-6. N20 125x20 – 22.5°(ϕ10@25 hor./vert.)

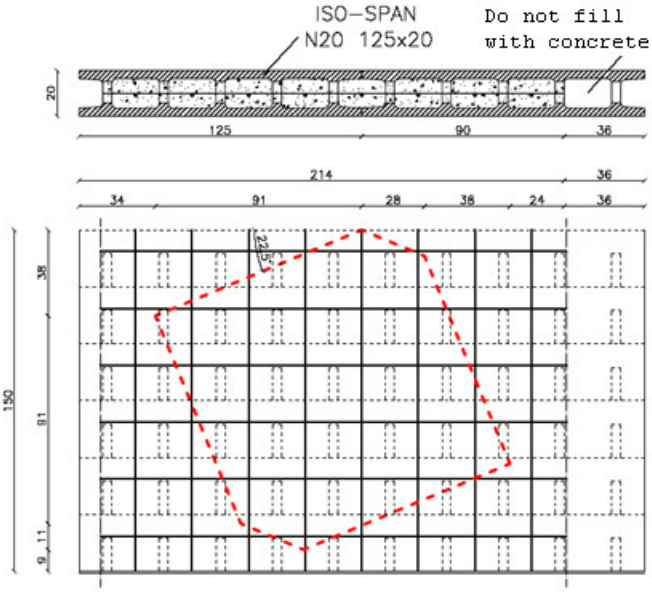

Figure 9-7. TW30 125x30 - 45°(ϕ10@25 only hor.)

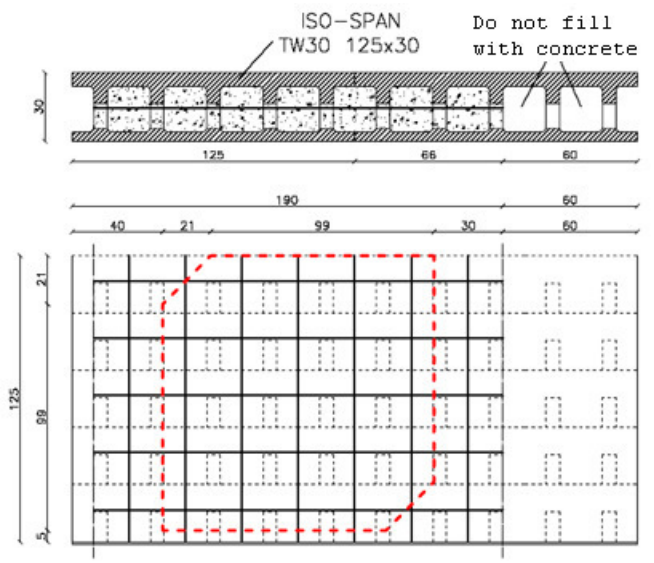

Figure 9-8. N20 125x20 – 45°(ϕ10@25 hor./vert.)

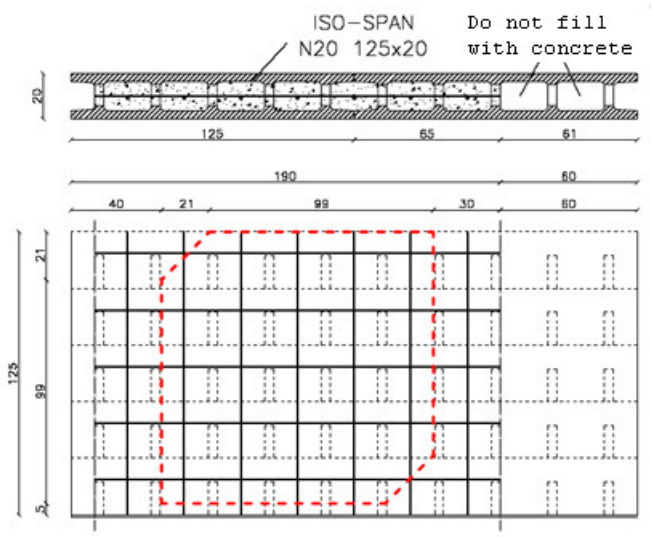

The specimens were cut from rectangular wall portions. The dashed red line in the figures represents the cutting line.

9.2. Material properties

Feb44k (now B450C) steel type was employed for the ϕ10 bars with an average yielding stress f_{ym} of 501 MPa and 599 MPa for the failure stress f_{tm} These values are based on testing six steel coupons according to (ISO 15630-1 2010) and reported in Table 9-2. The concrete used to cast all the specimens was C25/30 with normal weight. After the tests three cylindrical samples have been extracted with a diameter equal to 9.4 cm. The results obtained during the compression tests on these samples are reported in Table 9-3. The average compression strength f_{cm} recorded was 28.4 MPa.c

PROVE DI TRAZIONE E PIEGAMENTO
Decreto Ministeriale 14/09/2005 Min. Il. TT. - Norma UNI EN ISO 15630-1

Campione n.	Data di prova	Contrassegno	Marchio scheda n. C.A.	Trattamento termico	$ø_n$ [mm]	$ø_{eq}$ [mm]	Toll. [%]	f_y [N/mm^2]	f_t [N/mm^2]	A_{gt} [%]	Prova di piegamento
1	03/03/08		22	Non eseguito	10	10.5	9	537	623	10.3	Non richiesta
2	03/03/08		22	Non eseguito	10	10.2	3	489	585	15.3	Non richiesta
3	03/03/08		22	Non eseguito	10	10.2	4	489	587	12.8	Non richiesta
4	03/03/08		22	Non eseguito	10	10.1	3	486	583	12.8	Non richiesta
5	03/03/08		22	Non eseguito	10	10.2	4	487	602	12.8	Non richiesta
6	03/03/08		22	Non eseguito	10	10.5	10	515	612	10.3	Non richiesta
media								501	599	12.4	

Table 9-2. Tensile tests on reinforcement bars: f_{ym} and f_{tm} evaluation

PROVE DI COMPRESSIONE
Decreto Ministeriale 14/09/2005 Min. Il.TT. - Norma UNI EN 12390-3

Campione n.	Data di getto	Data di prova	Contrassegno	Rettifica	Requisiti provino	a [cm]	b [cm]	d [cm]	h [cm]	Sez. [cm^2]	M_u [Kg/dm^3]	R_c o f_c [MPa]	Tipo di rottura
1		30/05/08	19	NE	C	0.0	0.0	9.4	9.6	69	2.34	31.7	S
2		30/05/08	19	NE	C	0.0	0.0	9.4	9.6	69	2.33	32.5	S
3		30/05/08	5	NE	C	0.0	0.0	9.4	18.6	69	2.26	21.1	S

Table 9-3. Determination of compressive strength of concrete on three samples

9.3. Loading test setup

The specimens were subjected to a diagonal compression test, with a centered load, according to ASTM E519-81 adapted to the specific case. The surfaces of panels in contact with the press steel plates have been leveled with a plaster layer. The compression has been applied with a hydraulic actuator in displacement control measuring continuously the applied load. In some cases a monotonic load has been applied, in other cases a cyclic one. Each load cycle had a duration of about 1 hour in order to avoid effects related to load application velocity (quasi-static conditions).

During the tests the following data have been recorded:

- vertical deformation on the two panel sides: $\varepsilon_{v\ int}$ and $\varepsilon_{v\ ext}$. From this follows an average vertical deformation $\varepsilon_{v\ avg}$:

$$\varepsilon_{v\,avg} = \frac{\varepsilon_{v\,int} + \varepsilon_{v\,ext}}{2} \quad [9.1]$$

– horizontal deformation on the two panel sides: $\varepsilon_{h\ int}$ and $\varepsilon_{h\ ext}$. From this follows an average horizontal deformation $\varepsilon_{h\ avg}$:

$$\varepsilon_{v\,avg} = \frac{\varepsilon_{h\,int} + \varepsilon_{h\,ext}}{2} \quad [9.2]$$

– in the case of panels n° 7 and 13 the deformation along the two diagonal sides has also been recorded, obtaining in both cases values negligible compared with the horizontal and vertical deformations, these measurements are not reported in the following paragraphs.

The experimental results were elaborated in order to obtain the following significant quantities:

– shear deformation γ (average on the two sides):

$$\gamma = \varepsilon_{h\,avg} - \varepsilon_{v\,avg} \quad [9.3]$$

– the nominal shear tension τ, referred to the concrete area:

$$\tau = \frac{P\cos\alpha}{b \cdot t_{eff}} \quad [9.4]$$

being P the vertical load applied by the actuator and so $P\ cos\ \alpha$ the shear component on horizontal elements ("transverses"), b=120 cm is the base of the panel, t_{eff} is the effective concrete thickness. In this way the tension τ is uniformly distributed along the panel base with a t_{eff} thickness.

– the effective secant shear modulus G*:

$$G^* = \frac{\tau}{\gamma} \quad [9.5]$$

– the panel ductility μ, for deformation values higher than the peak strength, as:

$$\mu = \frac{\gamma}{\gamma_{max}} \quad [9.6]$$

being γ_{max} the shear deformation level at the peak shear stress τ_{max}.

The secant shear modulus is evaluated in correspondence of the peak shear stress τ_{max} and at 0.5 τ_{max}: this last value con be defined as the effective shear modulus G*, useful in the evaluation of the secant stiffness in cracking conditions.

9.4. Experimental results

The following figures illustrate the crack pattern observed during the tests. In the most cases cracks follow a vertical direction suggesting the formation of a compressed strut between the loading point and the ground.

Figure 9-9. Instrumentation (panel left side)

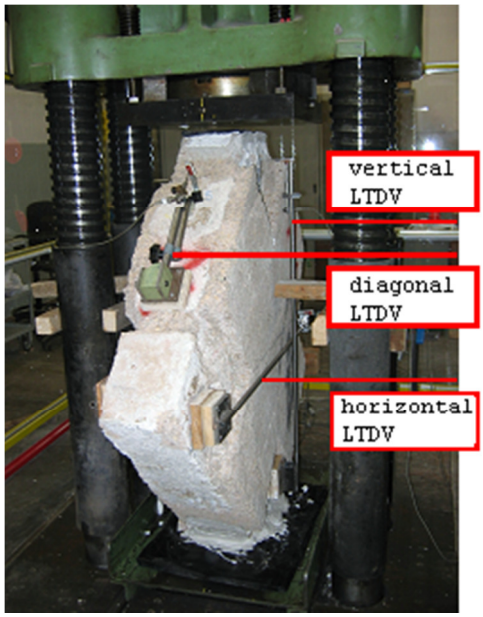

Figure 9-10. Instrumentation (panel rigth side)

Figure 9-11. Details of LTDV

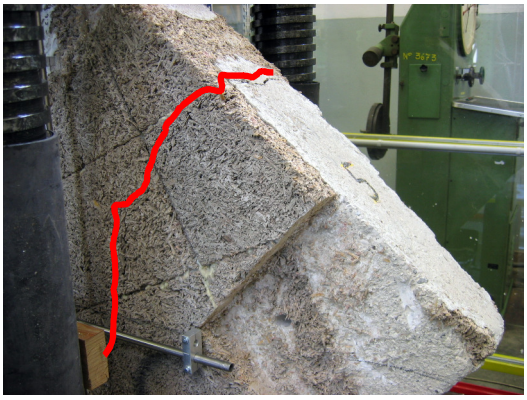

Figure 9-12. Failure of panel n.5

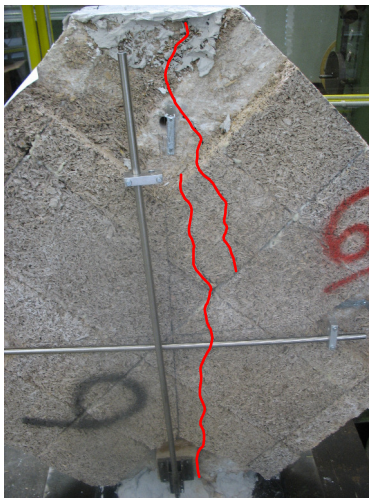

Figure 9-13. Failure of panel n.6

Figure 9-14. Cracks at failure of panel n.7

Figure 9-15. failure of panel n.7

Figure 9-16. Local failure of panel n.16

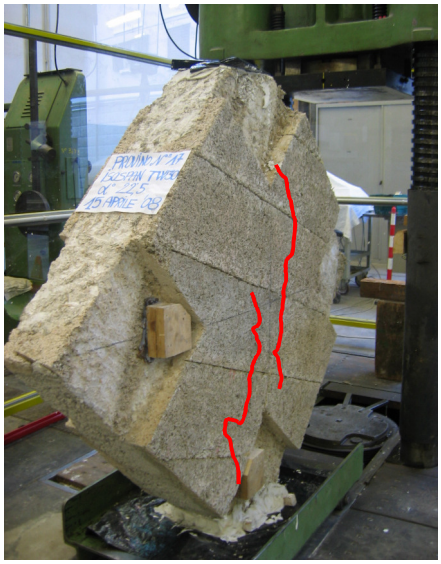

Figure 9-17. Failure of panel n.17

Figure 9-18. failure of panel n.18

In the following graphs of the experimental measurements are depicted for each specimen. The graphs also show elaborated quantities like shear stress and strain.

	P vs. $\varepsilon_{h\,avg}$ - $\varepsilon_{v\,avg}$	**τ – G* vs. γ**
Panel 1	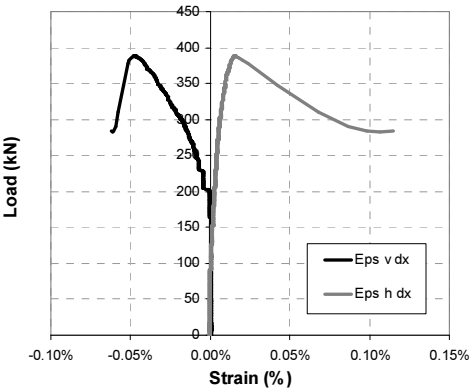	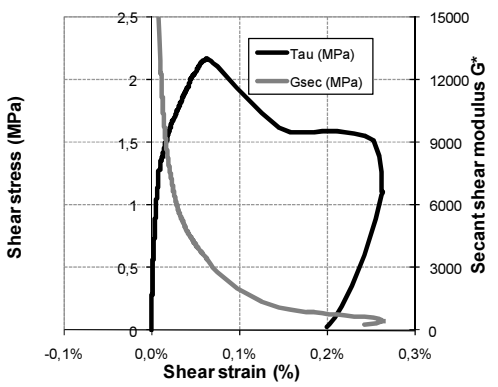
Panel 2	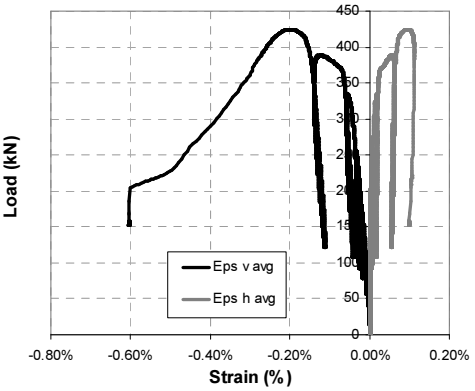	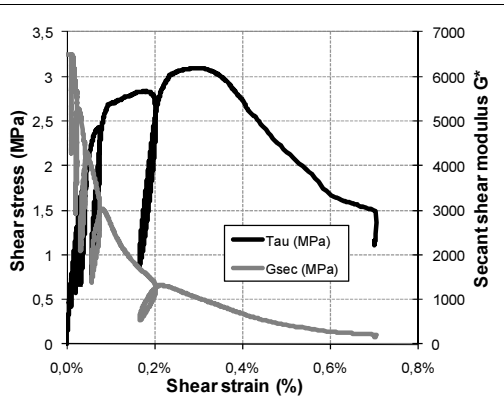
Panel 3	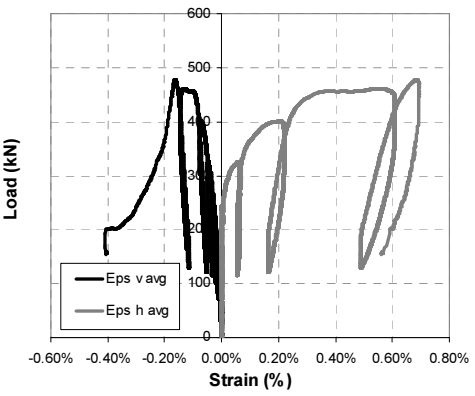	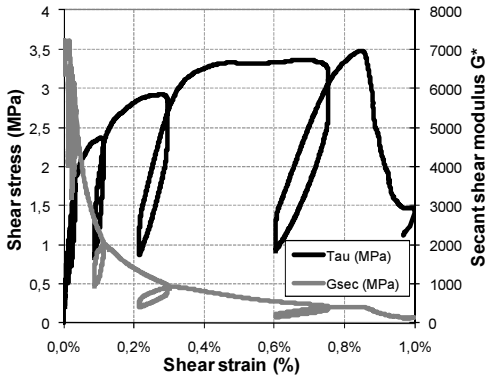

	P vs. $\varepsilon_{h\,avg}$ - $\varepsilon_{v\,avg}$	τ – G* vs. γ
Panel 4	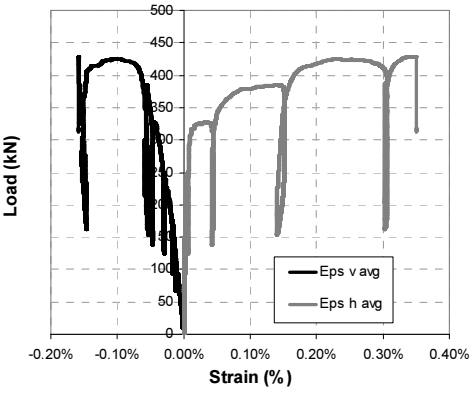	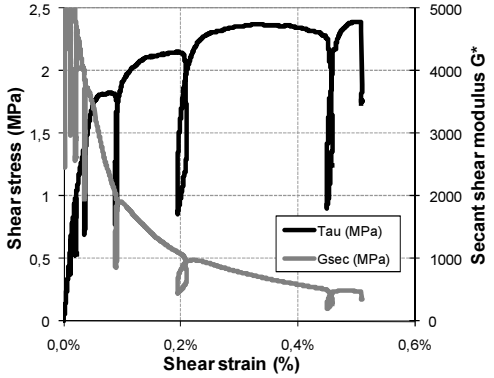
Panel 5	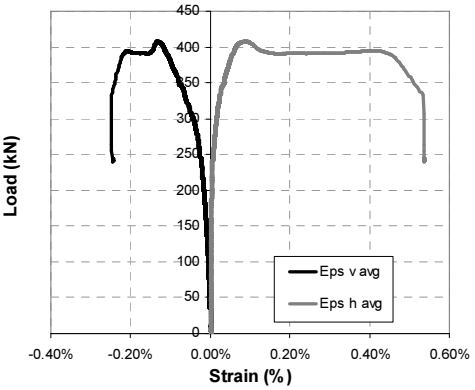	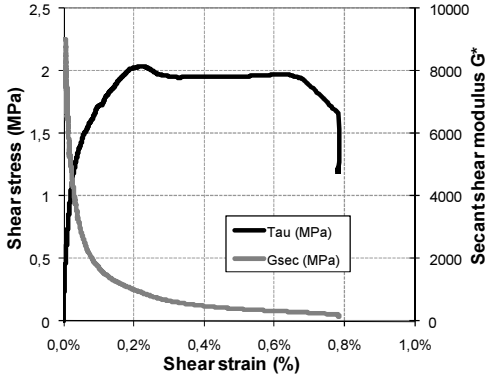
Panel 6	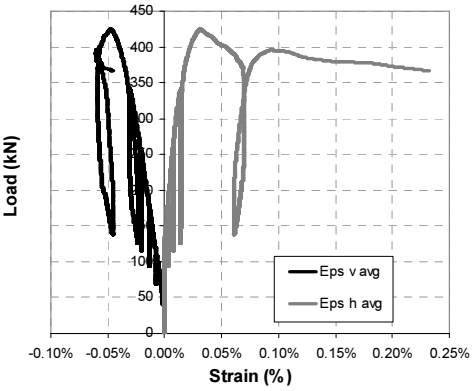	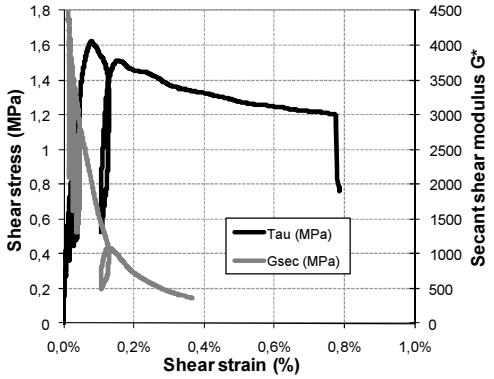
Panel 7	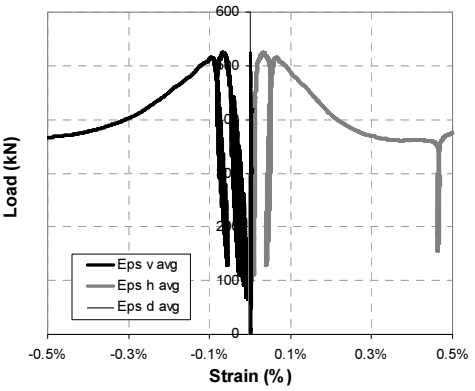	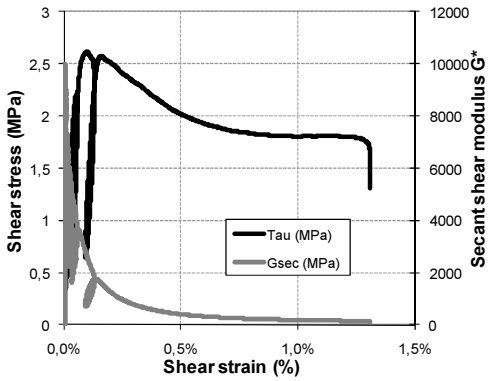

	P vs. $\varepsilon_{h\,avg}$ - $\varepsilon_{v\,avg}$	τ – G* vs. γ
Panel 8	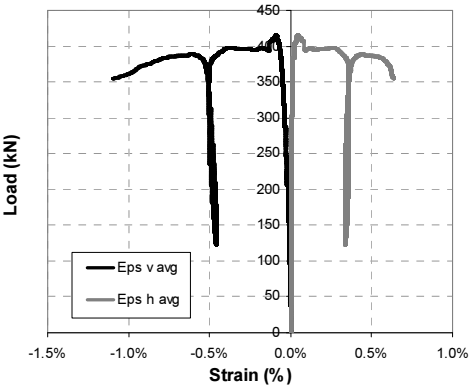	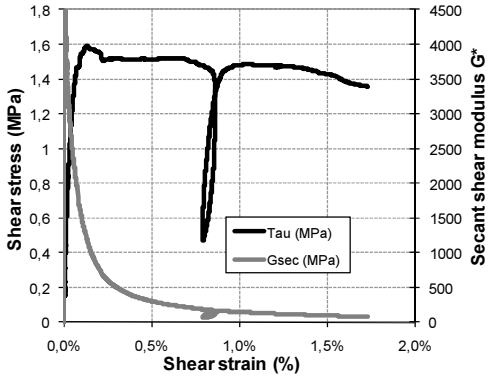
Panel 13	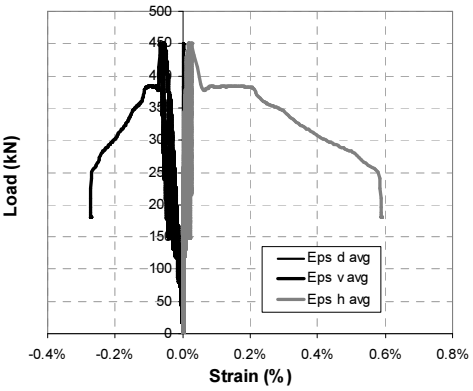	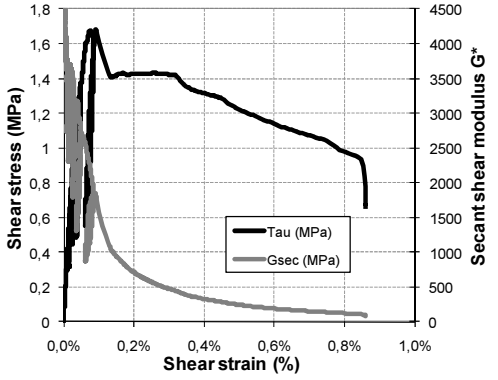
Panel 14	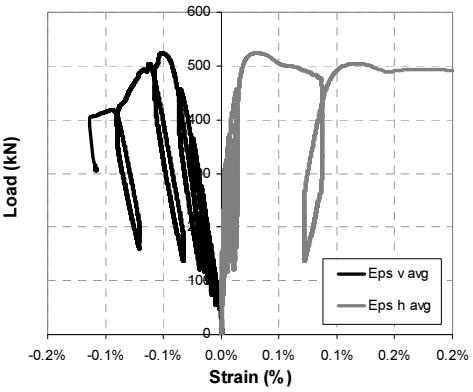	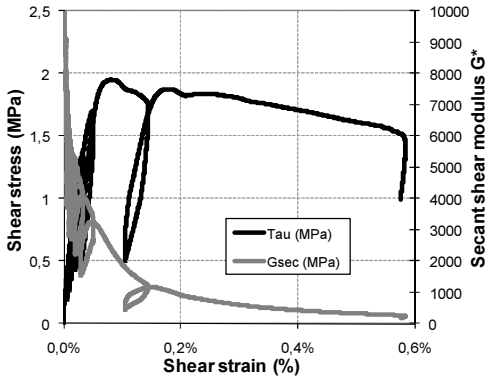
Panel 15	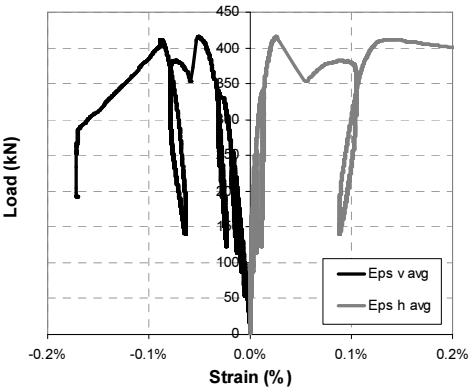	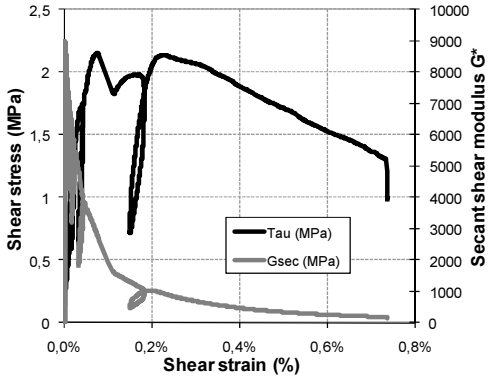

	P vs. $\varepsilon_{h\,avg}$ - $\varepsilon_{v\,avg}$	**τ – G* vs. γ**
Panel 16	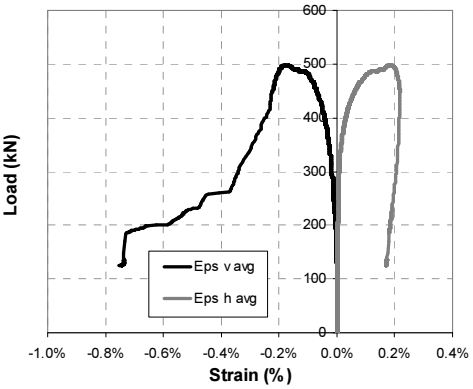	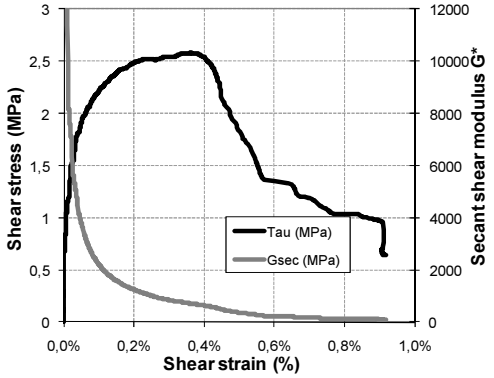
Panel 17	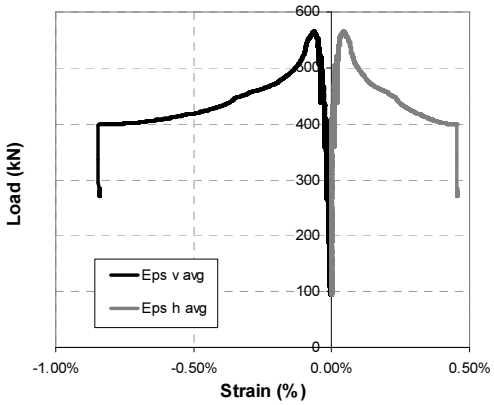	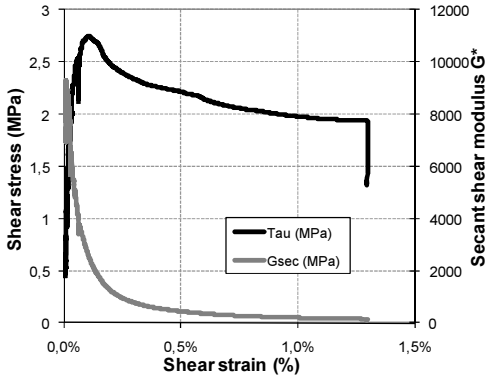
Panel 18	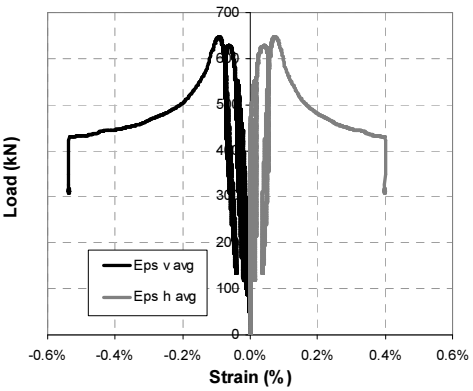	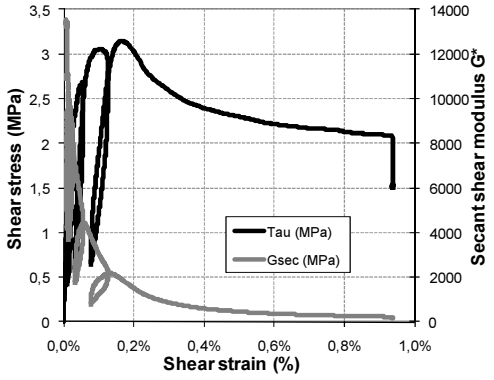
Panel 19	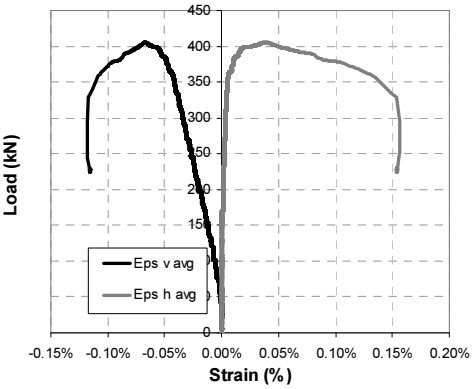	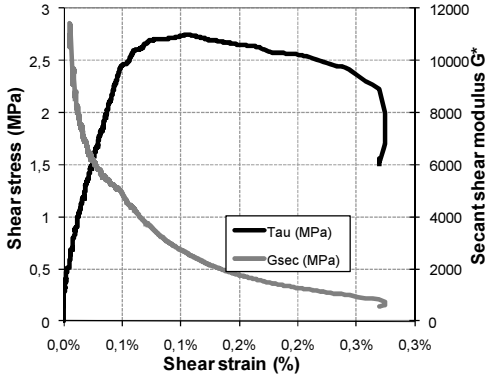

	P vs. $\varepsilon_{h\,avg}$ - $\varepsilon_{v\,avg}$	$\tau - G^*$ vs. γ
Panel 20	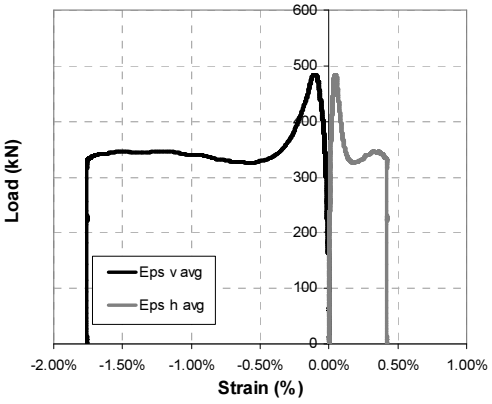	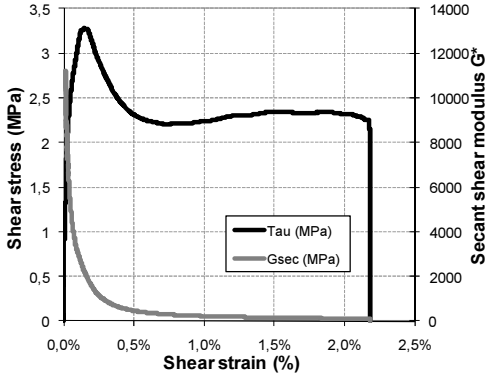

9.5. Discussion of the experimental results and analytical model

Table 9-4 summarizes the most significant results obtained. Moreover, the following graphs compare the τ-γ curves for each block type.

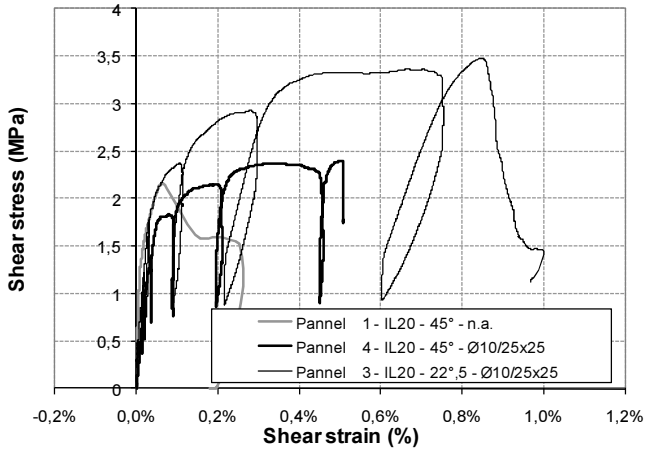

Figure 9-19. Comparison of τ-γ curves of panels 1,2 and 4 cast in IL20 block type

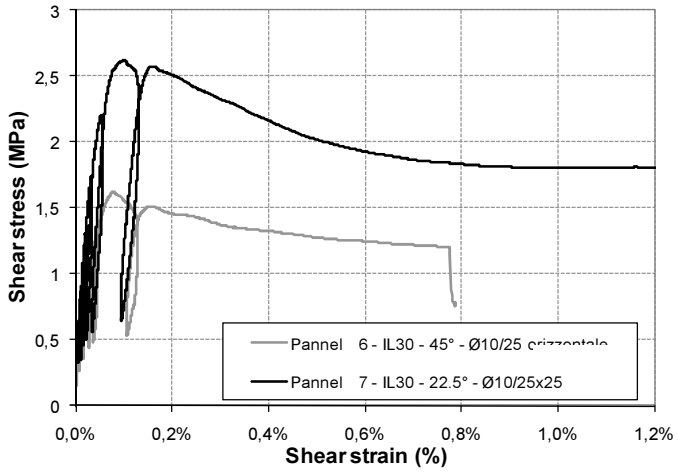

Figure 9-20. Comparison of τ-γ curves of panels 6 and 7 cast in IL30 block type

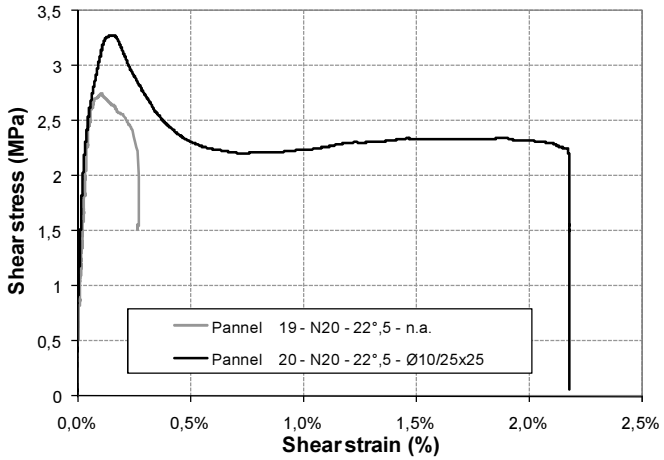

Figure 9-21. Comparison of τ-γ curves of panels 19 and 20 cast in N20 block type

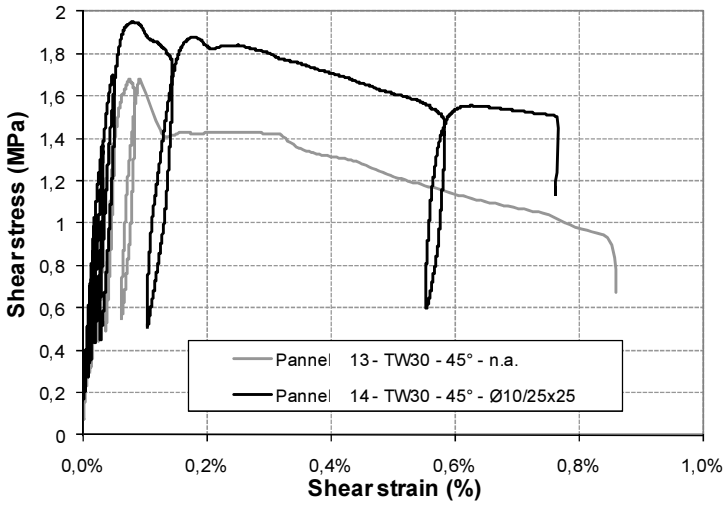

Figure 9-22. Comparison of τ-γ curves of panels 13 and 14 cast in TW20 block type

Specimen n°	Block type	Thickness t [cm]	Thickness t_{eff} [cm]	Angle a [°]	Reinforcement	P_{peak} [kN]	Type of load	50% P_{peak}			P_{peak}			80% P_{peak}			$P_{failure}$			Type of failure
								τ (MPa)	γ [%]	G* [Mpa]	τ (MPa)	γ [%]	G* [Mpa]	τ (MPa)	γ [%]	μ	τ (MPa)	γ [%]	μ	
1	IL20	13	10.14	45	-	388	mono.	1.08			2.17	0.07%		1.74	0.13%	1.99	1.52%	0.25%	4.01	vert. splitting
2	IL20	13	10.14	22.5	f10@25 hor.	424	cycl.	1.55	0.030%	5175	3.1	0.29%	1057	2.48	0.44%	1.51	1.49%	0.70%	2.4	local at top
3	IL20	13	10.14	22.5	f10@25 /25	477	cycl.	1.74	0.029%	6031	3.48	0.85%	410							local at top
4	IL20	13	10.14	45	f10@25 /25	429	mono.	1.2	0.028%	4335	2.39	0.50%	481							vert. splitting
5	IL30	20	14.8	22.5	-	407	mono.	1.02			2.04	0.22%	942	1.63	0.78%	3.62				vert. splitting
6	IL30	20	14.8	45	f10@25 hor.	424	cycl.	0.81	0.021%	3792	1.62	0.08%	2074	1.3	0.46%	5.83	1.20%	0.77%	9.9	vert. splitting
7	IL30	20	14.8	22.5	f10@25 /25	525	cycl.	1.31	0.022%	5989	2.62	0.10%	2609	2.1	0.44%	4.38	1.75%	1.30%	12.89	vert. splitting
8	IL30	20	14.8	45	f10@25 /25	416	cycl.	0.8	0.024%	3336	1.59	0.14%	1173	1.36	1.71%	12.60				vert. splitting
13	TW30	20	15.2	45	-	451	cycl.	0.84	0.023%	3598	1.68	0.09%	1819	1.34	0.36%	3.91	0.90%	0.85%	9.25	vert. splitting
14	TW30	20	15.2	45	f10@25 /25	524	cycl.	0.98	0.019%	5241	1.95	0.08%	2419	1.56	0.55%	6.88	1.45%	0.77%	9.51	vert. splitting
15	N20	13	10.92	45	f10@25 hor.	415	cycl.	1.08	0.016%	6567	2.15	0.08%	2796	1.72	0.49%	6.43	1.30%	0.74%	9.36	vert. splitting
16	N20	13	10.92	45	f10@25 /25	498	mono.	1.29	0.016%	7850	2.58	0.36%	711	2.06	0.46%	1.28	0.96%	0.91%	2.51	local at bottom
17	TW30	20	15.2	22.5	f10@25 hor.	564	cycl.	1.37	0.016%	8721	2.75	0.10%	2618	2.2	0.52%	5.00	1.94%	1.30%	12.37	vert. splitting
18	TW30	20	15.2	22.5	f10@25 /25	647	cycl.	1.57	0.019%	8319	3.15	0.16%	1927	2.52	0.33%	2.00	2.06%	0.94%	5.74	vert. splitting
19	N20	13	10.92	22.5	-	405	mono.	1.37	0.021%	6454	2.75	0.11%	2595	2.2	0.27%	2.55				vert. splitting
20	N20	13	10.92	22.5	f10@25 /25	484	mono.	1.64	0.017%	9773	3.28	0.13%	2249	2.62	0.34%	2.30	2.14%	2.18%	14.96	vert. splitting
Average on non-reinforced panels with a=45°								0.96		3598	1.92	0.09%			0.24%	2.63				
Average on non-reinforced panels with a=22.5°								1.2		6454	2.39	0.16%			0.53%	3.57				
Average on reinforced panels with a=45°								1.02		5187	2.05	0.21%			0.74%	3.58				
Average on reinforced panels with a=22.5°								1.53		7334	3.06	0.28%			0.41%	1.50				
General average								1.23		6084	2.46	0.19%			0.52%	2.82				

Table 9-4. Summary of experimental results of diagonal compression tests

Therefore the experimental curves above show 3 different behaviors:

- the non-reinforced panels present a peak (P_{peak}) followed by a brittle and sudden failure because the ultimate tensile strength of concrete is reached (pure shear mechanism);
- the panels with an inclination α equal to 22.5° show a peak strength (P_{peak}) followed by a *plateau* where the deformation increases maintaining a constant vertical force V_u until the failure condition;
- the panels with an inclination α equal to 45° show a greater peak strength (P_{peak}), compared with equal to 22.5°, followed by a brittle failure of concrete due to the high compression in the transverses.

It is worth to notice that the applied vertical load P induces a compression load on the transverses. Such compression does not only decrease the normal tensile stress on the concrete section but also it is equivalent to a reinforcement increment. This compression component is lower in the tests with an α of 22.5°, where the transverses are closer to the pure shear condition and the limited compression stress apparently increases the own shear strength. In the case with α equal to 45° this component becomes predominant and causes a premature failure of concrete strut due to high level of compression. This evidence is confirmed by the high ductility levels at the failure state reached with α equal to 22.5°.

A 2D numerical model of the internal concrete pattern loaded with the same force configuration used in the tests, described in (Vianello 2009), shows that the main amount of stress concentrates only in the 4 central transverses in the 45° case, whereas stress and shear strain distribute along the panel section in the 22.5° case, involving 5 connection elements (see circled area in Figure 9-23 and Figure 9-24). The greater resistance of the 22.5° panels can be explained in this way.

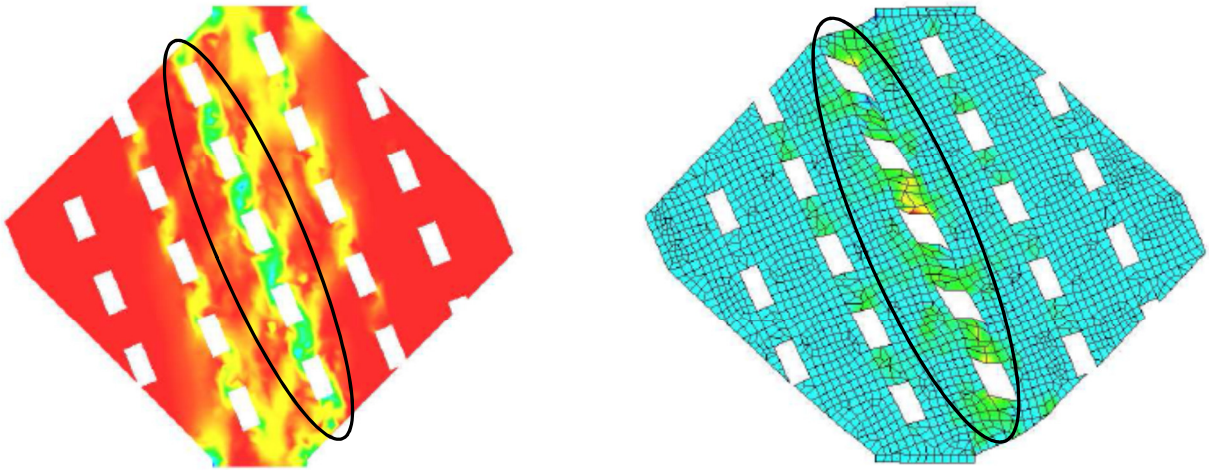

Figure 9-23. Stress (left) and strain (right) levels with α=22.5° (Vianello 2009)

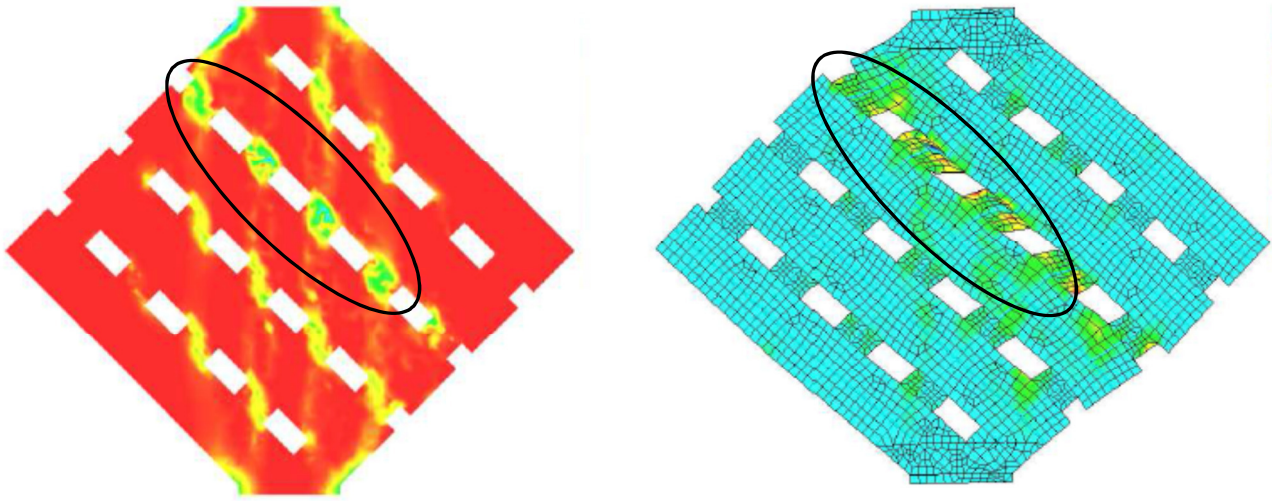

Figure 9-24. Stress (left) and strain (right) levels with α=45° (Vianello 2009)

In the non-reinforced panels, given the shear and normal forces applied on transverse section (V_s, N_s), the principal tensile stress can be computed as follows:

$$\sigma_1 = -\frac{N_s}{2 \cdot A_t} + \sqrt{\left(\frac{V_s}{A_t}\right)^2 + \left(\frac{N_s}{2 \cdot A_t}\right)^2} < f_{ctd} \qquad [9.7]$$

In this kind of test V_s and N_s are linked by α angle. Equation [8.3] can be extended in following way that takes into account the panel inclination α:

$$v_{r,cls} = \frac{f_{ctd} \cdot A_t}{i_t} \cdot \frac{\tan\alpha + \sqrt{4 + tan^2\alpha}}{2} \qquad [9.8]$$

The derivation of [9.8] is described in Appendix. The coefficient 0.25 in [8.3] accounted for since we want to compare experimental data with analytical prevision (we are not in a design phase). The design parameters are the characteristic ones. In the case of reinforced transverses eq. [8.9] remains valid. For each specimen tested the analytical strength computed with the formulas above, $V_{r,peak}$, is compared with the experimental peak shear resistance V_{peak}. Moreover, in the case of α equal to 22.5°, the only contribution to the resistance given by the strut-&-tie mechanism $V_{r,failure}$ is compared with the post-peak force $V_{failure}$ on the *plateau*.

Table 9-5 shows, for example, the detailed calculations to estimate the shear strength in a 22.5° and in a 45° case.

Material parameters		**Geometrical parameters IL20**	
f_{cd} =	28.4 MPa	h_{trav} =	120 mm
f_{ctd} =	2.0 MPa	l =	55 mm
ν =	0.56	b_{eq} =	80 mm
f_{yd} =	501 MPa	A $_{trav}$ =	9600 mmq
$\gamma_c = \gamma_s$ =	1.0		
V_r calculations (panel n.2)		**V_r calculations (panel n.4)**	
n° $_{trav}$ =	5	n° $_{trav}$ =	4
α =	22.5 °	α =	45°
ϕ (reinforcement) =	10 mm	ϕ (reinforcement) =	10 mm
N_s =	19.5 kN/trav	N_s =	48.9 kN/trav
Z =	39.3 kN/trav	Z =	39.3 kN/trav
$v_{r,cls}$ =	23.1 kN/trav	$v_{r,cls}$ =	30.4 kN/trav
ϑ_{opt} =	38.7 °	ϑ_{opt} =	32.7 °
$v_s(\vartheta_{opt}) = v_c(\vartheta_{opt})$ =	47.0 kN/trav	$v_s(\vartheta_{opt}) = v_c(\vartheta_{opt})$ =	48.9 kN/trav
v_{rd} = 23.1+47.0 =	70.1 kN/trav	v_{rd} = 30.4+48.9 =	79.3 kN/trav
$V_{r,peak}$ = 5 x 70.1 =	350.5 kN	$V_{r,peak}$ = 4 x 79.3 =	317.2 kN
$V_{r,failure}$ = 5 x 47.0 =	235.0 kN		

Table 9-5. V_r calculation examples for panel 2 (left) and panel 4 (right)

Since V_s and N_s are related by the geometrical condition $tan\ \alpha = N_s/V_s$; an iterative procedure is needed in order to estimate v_{rd}. Table 9-6 and the graphs reported in Figure 9-25 and Figure 9-26 show the comparison between analytical and experimental results in terms of peak and failure strength.

Specimen number	Block type	Angle α [°]	n° transv.	Reinf. type	P peak exper.	P failure exper.	V_{peak} exper.	$V_{failure}$ exper.	$V_{r,peak}$ analyt.	$V_{r,failure}$ analyt.
1	IL20	45	4	n.a.	388	-	274	-	121.5	-
4	IL20	45	4	10	429	-	303	-	317.2	-
2	IL20	22.5	5	10	424	205	392	189	350.5	235.0
3	IL20	22.5	5	10	477	200	441	185	350.4	235.1
5	IL30	22.5	5	n.a.	407	-	376	-	144.2	-
7	IL30	22.5	5	10	525	350	485	323	398.6	254.4
6	IL30	45	4	10	424	-	300	-	378.6	-
8	IL30	45	4	10	416	-	294	-	378.6	-
19	N20	22.5	5	n.a.	405	-	374	-	102.1	-
20	N20	22.5	5	10	484	316	447	292	331.5	229.4
15	N20	45	4	10	415	-	293	-	293.4	-
16	N20	45	4	10	498	-	352	-	293.4	-
13	TW30	45	4	n.a.	451	-	319	-	136.0	-
14	TW30	45	4	10	524	-	371	-	346.7	-
17	TW30	22.5	5	10	564	400	521	370	374.9	245.8
18	TW30	22.5	5	10	647	429	598	396	374.9	245.8

Table 9-6. Comparison between experimental and analytical results in the diagonal compression tests

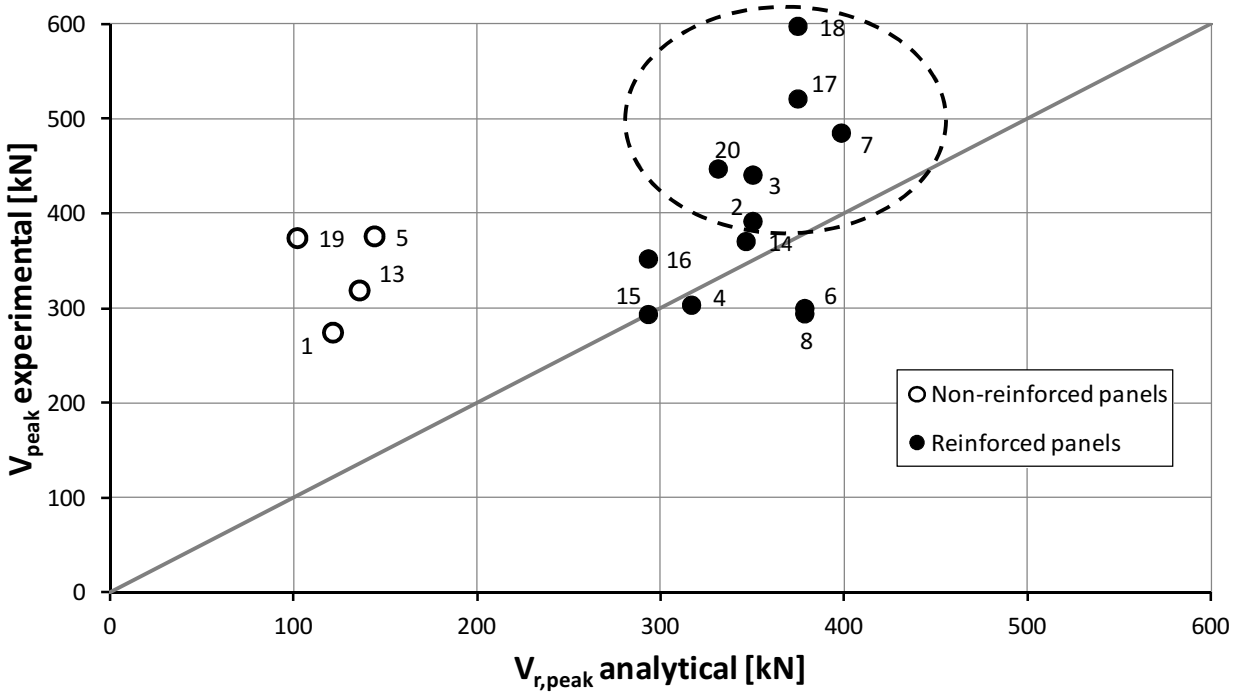

Figure 9-25. Comparison between experimental and analytical peak values (V_{peak}) in the diagonal compression tests (panels with α=22.5° are circled with a dashed line)

The dashed line in Figure 9-25 contains the points of reinforced panels with an inclination angle of 22.5°. As in case of the direct shear tests, the analytical proposal developed in this thesis is able to match better the reinforced panels strength than the non-reinforced one. Nevertheless the analytical values in this case are always conservative with respect to experimental results, because they lay above the grey line of perfect matching.

Figure 9-26 compares the experimental shear force at the ductility branch, $V_{failure}$, typical of the panels with α equal to 22.5°, with the analytical strength evaluated only with the strut-and-tie mechanism. The experimental results are in accordance with the analytical ones, because all the points lay in the proximity of the grey line.

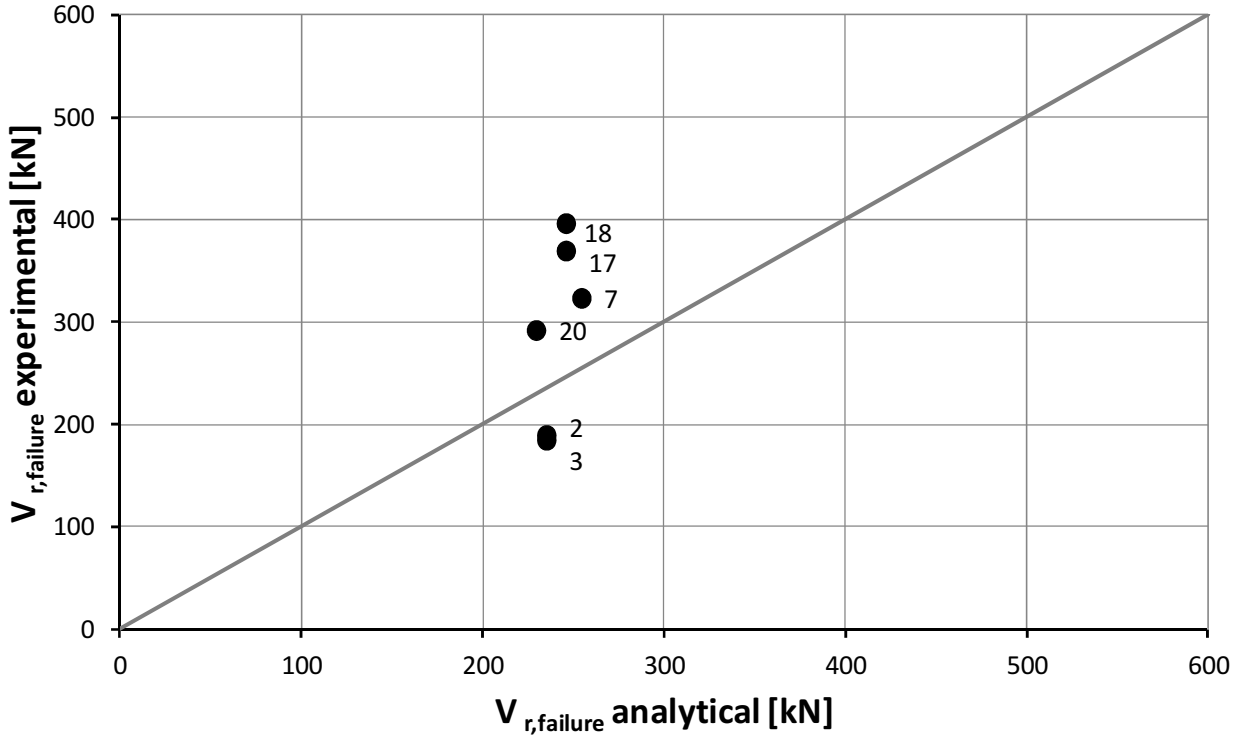

Figure 9-26. Comparison between experimental and analytical $V_{failure}$ values

The good approximation of the experimental shear strength with the analytical ones confirms the robustness and validity of the analytical proposal, even in presence of an axial force on the transverses. The little dispersion is very difficult to avoid because of the large number of variables involved, nevertheless it is extensively balanced by the partial safety factors for materials used in practical design, that were not considered in the analytical calculations.

In conclusion, some general considerations can be drawn:

a) the vertical reinforcement is not decisive for the shear resistance of this kind of panels, also in the diagonal compression tests where a compression component in the transverses is present;

b) the horizontal reinforcement definitely increases the shear strength and, above all, enhances the ductility of the system. In any case, even the non-reinforced panels showed a non-brittle failure thanks to the friction and interlocking effects on concrete surfaces. These effects are amplified by the compression on transverses. Moreover, the neglected formwork contribute could give an additional contribute to shear strength;
c) the dispersion of G* value, secant shear modulus, is quite wide and furthermore is affected by the block type, inclination α and the loading history (cyclic or monotonic). In this study, G* is evaluated as the average of the obtained values. Implicitly, the continuum material is considered isotropic whereas a more sophisticated approach would treat the system as orthotropic. Indeed, the internal concrete pattern has two principal axes of symmetry (horizontal and vertical) and the mechanical properties are different along each axis. The G* modulus estimated at 50% for the P_{peak} vertical load, theoretically, belongs to the factitious isotropic linear elastic material that fits in the best way the experimental evidences. The effective shear modulus G* is approximately 6000 MPa, i.e. G/2.2 where G is the theoretical shear modulus of concrete.

From these final considerations arises a great difficulty for the interpretation of diagonal compression tests of structure with a grid type internal pattern. This is due especially to the compression generated in the horizontal elements (transverses); that stress configuration occurs very rarely in the practical application.

As mentioned at the beginning of this chapter, the orthotropic nature of this construction system suggests to study independently the behavior of horizontal and vertical elements. For this reason, in the author's opinion, the direct shear tests are more appropriate to study the shear strength because these experiments focus on vertical elements coupling without subjecting transverses to axial load. Moreover, the interpretation of these tests is easier and more consistent.

In this context, it is worth to underline the extreme unsuitableness of the continuum approach, implicitly suggested also by "type 2 tests" of (LL. GG. 2011), for a grid type wall treated along the same lines as a solid RC structure.

Chapter 10. – Tests on real scale walls

In this chapter the in-plane behavior of real scale walls is investigated. These tests are also referred to as *type 3 tests* in the (LL. GG. 2011) and were performed in June 2012 at Terrassa Padovana (PD – Italy).

10.1. Tested specimens

Eight reinforced concrete shear walls cast in hollow wood formworks were tested. Among these, four walls had openings (window or door). The specimens were subjected to constant vertical load and reversed cyclic lateral displacement to study the influence of openings, type of block and reinforcement.

Three different kinds of block were employed denoted with the following abbreviations: N20, I25 and I30. The number specifies the block thickness in centimetres, but the concrete core thickness belonging to the columns were respectively 13, 18 and 22 cm. Transverse section area varies between the three blocks: 72, 90 and 107 mm^2. Bars with a diameter of 12 mm were used for walls with openings and a diameter of 10 mm for the remaining set.

The details of sections, reinforcement and façades are reported in Appendix.

The following table summarizes the characteristics of tested walls:

Wall number	Block type	Bar diameter [mm]	Core area [cmq]	Transverse area [cmq]	Total wall length L [cm]	Upright length b [cm]	Opening type
1	I25	12	378	90	325	87.5	Window
2	I25	12	378	90	425	137.5	Door
3	I30	12	462	107	335	92.5	Window
4	I30	12	462	107	435	142.5	Door
5	N20	10	273	85	415	-	-
6	I25	10	378	90	425	-	-
7	N20	10	273	85	315	-	-
8	I25	10	378	90	325	-	-

Table 10-1. Characteristics of full scale wall tested

10.2. Material properties

B450C steel type was employed for the bars with an average yielding stress f_{ym} of 580 MPa for ϕ10 (no openings) and 545 MPa ϕ12 (walls with openings). These values were derived from tests on three steel coupons for each diameter according to (ISO 15630-1 2010).

Six cylinders were cast along with each batch of specimens and tested in order to get an accurate record of the unconfined concrete strength. The obtained average compressive strength f_{cm} was 29.75 MPa.

10.3. Loading test setup

The testing frame setup is shown in Figure 10-1. The walls were cast on a reinforced concrete foundation in two sets of four each due to space limitations. The wall was anchored to the foundations through the vertical reinforcement with an anchorage length of 20 cm. An RC reaction wall, resting on the same foundation, was realized between two tested shear-walls.

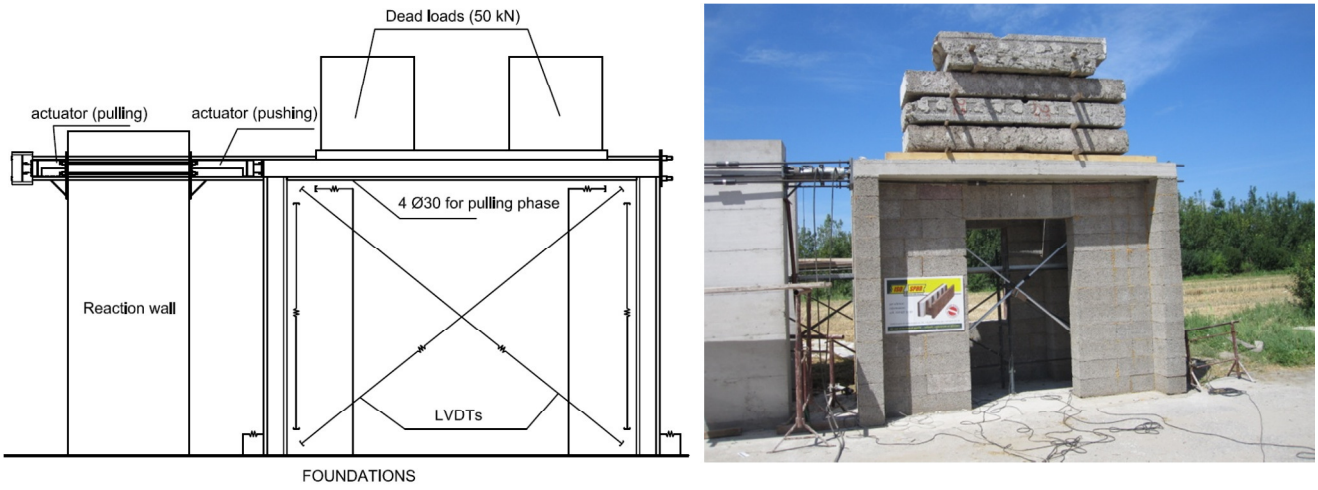

Figure 10-1. Test setup: scheme (left) and real view (right)

Each shear-wall has a double T section in order to prevent out-of-plane displacements (see Figure 12-1). In the upper part of the wall a portion of slab floor was realized, incorporating the lintel in case of walls with openings.

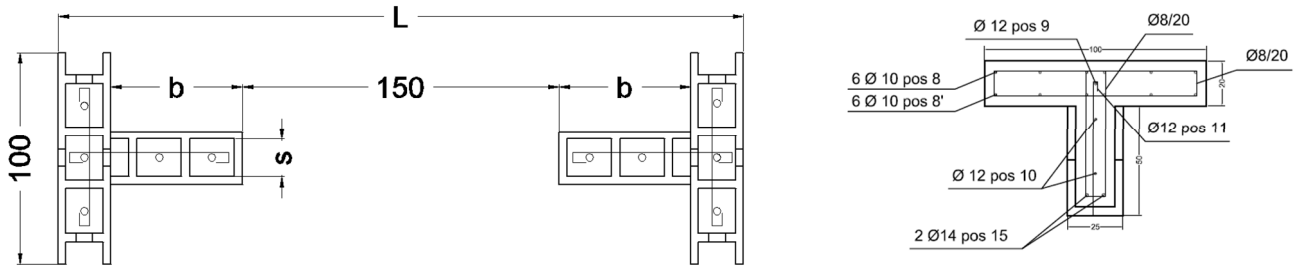

Figure 10-2. Double T section of a wall with opening (left) and lintel section (right)

As shown in Figure 10-1, a couple of actuators acting alternatively were used to apply the cyclic lateral forces (pushing and pulling phase) at the floor level.. Four threaded bars with a diameter of 30 mm allowed to apply the pulling forces, while the pushing actuator directly contrasted between the top of the reaction wall and the lateral surface of slab.

Four LVDTs were mounted to the base to measure relative rotation (vertical ones) and sliding (horizontal ones) if any. Four LVDTs were mounted to the top to measure horizontal and diagonal displacements of the top floor. Readings of the LVDT displacements and actuator forces were recorded at every load increment of 1 kN.

A constant vertical dead load of 50 kN was applied on the top of each wall to simulate the permanent loads. The horizontal applied load was progressively increased until failure of the specimens.

10.4. Experimental results

10.4.1. Load vs. displacements graphs

During the test the following parameters have been continuously recorded:

- the horizontal top displacements, both sides: δ_{left} and δ_{right}. The average horizontal top displacement was obtained with:

$$\delta_{avg} = \frac{\delta_{left} + \delta_{right}}{2} \quad [10.1]$$

- the horizontal base displacements
- the vertical displacements at the right and left end
- the two diagonal displacements

The base sliding is very small and has been neglect in the horizontal displacement computations. The most significant displacements are the horizontal and the vertical ones that are plotted for each panel in the figures below.

Wall number 1

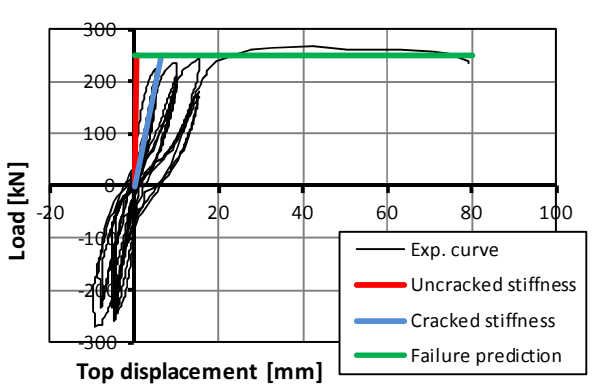

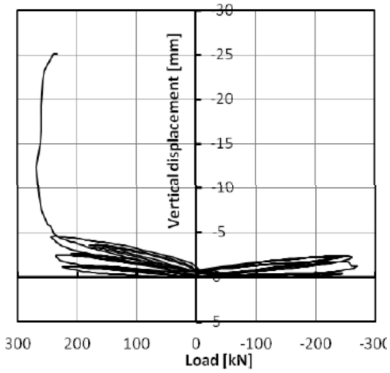

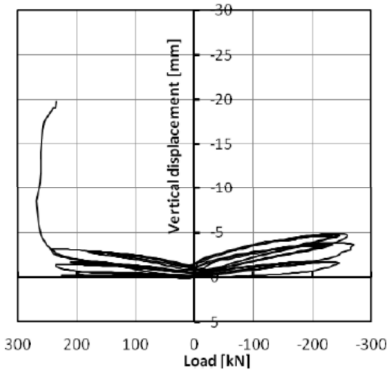

Wall number 2

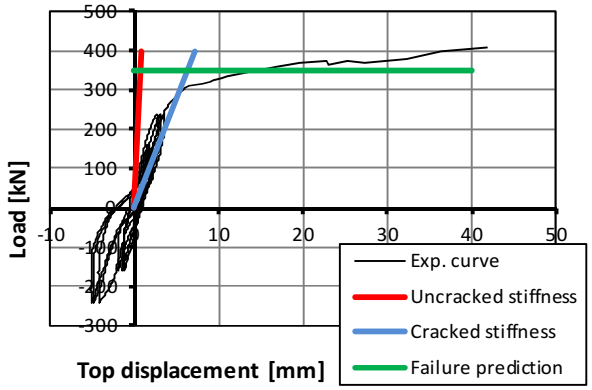

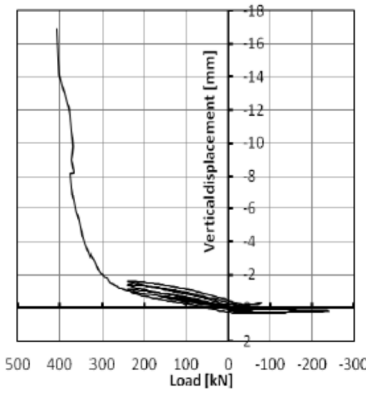

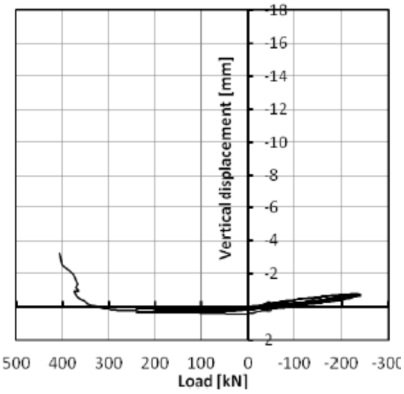

Wall number 3

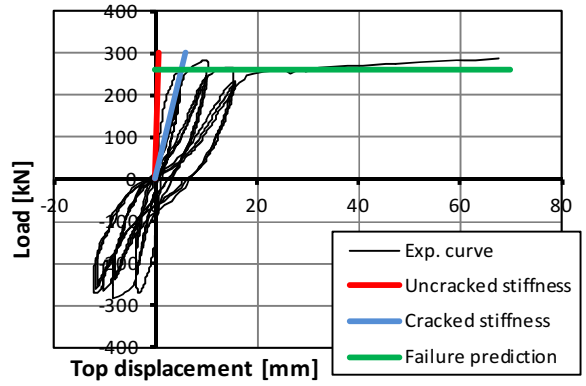

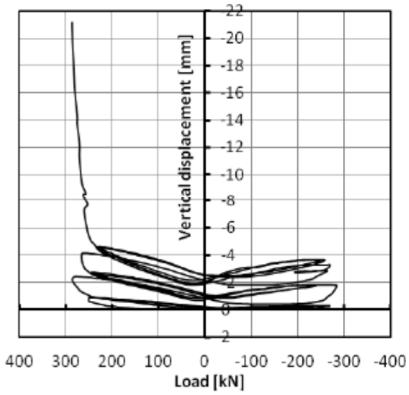

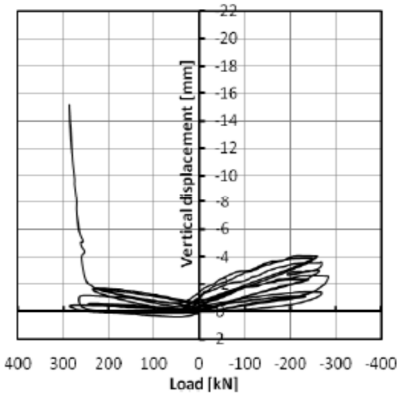

Wall number 4

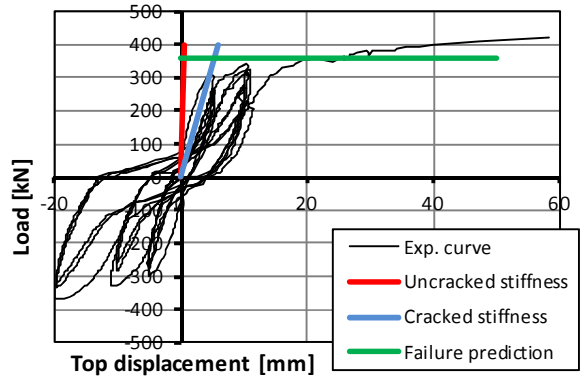

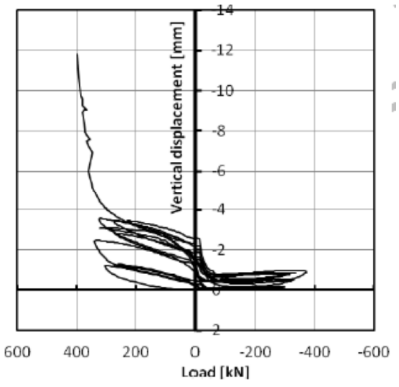

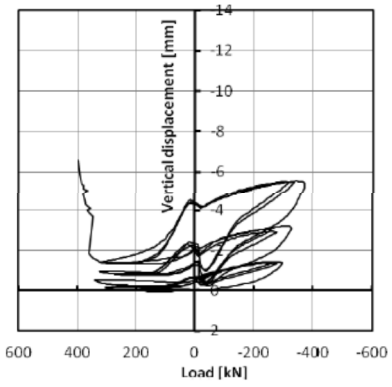

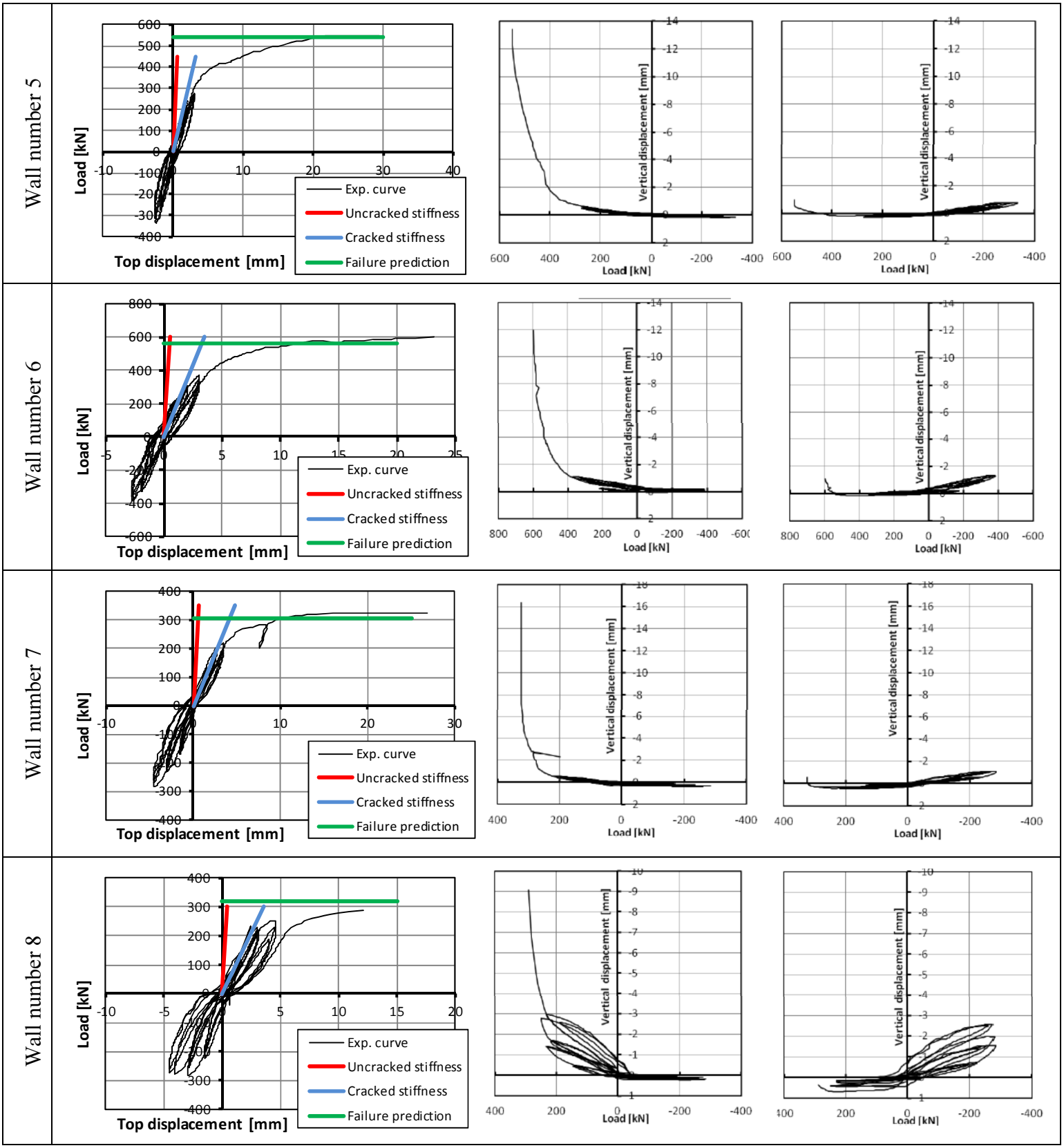

Figure 10-3. Base shear force vs. top horizontal displacement (left), vertical displacement on pushing side (middle), vertical displacement on pulling side (right)

The large vertical displacements recorded at both ends of walls denote a large rotation capacity of vertical elements, particularly in the case of walls with openings where the high H/B (height over length) ratio facilitates the rocking effect.

The vertical displacement near the reaction wall is larger because the LTDV was farther from the neutral axis that can be considered the rotational axis of the plastic hinge at upright ends (see Figure 10-4).

Figure 10-4. Geometrical explanation of great vertical displacement on the left upright

10.4.2. Failure mechanism

Walls without openings are subjected to a strong rocking effect and they form a plastic hinge at the base section. In the other cases, i.e. walls with openings, the plastic rotational hinge formation at the upright ends was the dominant cinematic mechanism. It is clear from the formation of diagonal cracks close to the opening corners with an angle between 30° and 45° degrees (see Figure 10-5).

The failure is due to vertical reinforcement collapse in all the cases. This collapse is due to the bending moment at the ends of the vertical elements where the plastic hinge formation induces the yielding and, at a later stage, the collapse of the external reinforcement. The height over length ratio (H/B) of vertical elements is lower in the walls without openings and it constraints the rotation capacity of the plastic hinge due to rocking effect. In the walls with door or window H/B is greater and the plastic hinge rotation increases generating a longer inelastic branch in term of displacements.

Not any failure of horizontal elements has been observed, confirming the analytical results. The transverses provided a perfect coupling between vertical elements transforming the resisting bending moment of frame vertical uprights in a sum of axial forces on the vertical grid elements. If the horizontal elements remain in the elastic field the grid type structure can reach its maximum resistance.

Figure 10-5. Diagonal cracks on the upright ends in a wall with window

10.5. Analytical model

10.5.1. Equivalent frame method

The equivalent frame method, namely "SAM method", proposed for masonry buildings by (Magenes 2000) is adequate for the interpretation of the failure modes and loads.

Considering a multistory wall loaded in plane by horizontal forces, if the geometry of the openings is sufficiently regular, it is possible to idealize the wall as an equivalent frame made by pier elements, spandrel beam elements, and joint elements (Figure 10-5).). The pier elements and the spandrel elements are modeled as beam elements with shear deformation, while the joint elements are supposed infinitely resistant and stiff, and are modeled by means of rigid offsets at the ends of the pier and spandrel elements. The length of these parts of spandrels is equal to the opening length and the pier height is calculated with the following formula:

$$h_{eff} = h' + \frac{b \cdot (h - h')}{3 \cdot h'} \qquad [10.2]$$

according to (Dolce 1989). In this way the deformation joint capacity is taken into account.

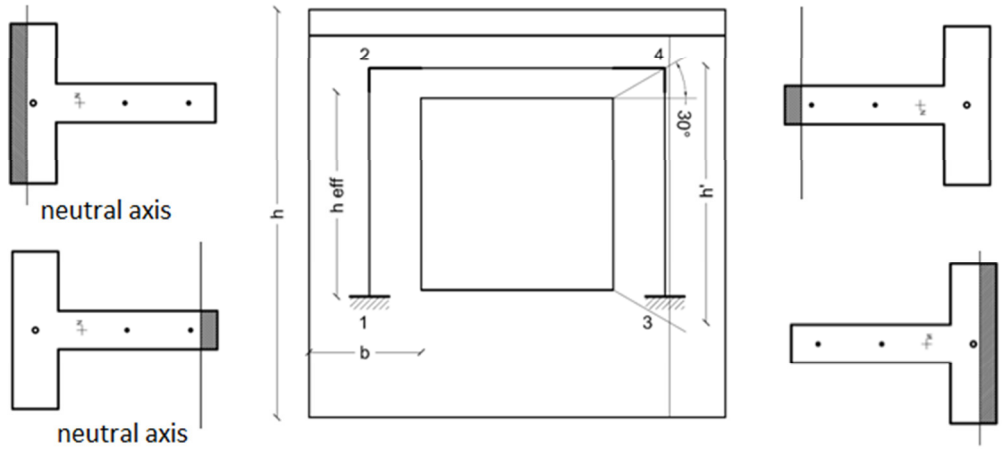

Figure 10-6. Equivalent frame example and parameters for h_{eff} calculation. Critical sections at upright ends and neutral axis in ultimate state

The spandrel can be considered rigid because the opening width is very small. The failure mechanism takes place at the formation of four plastic hinges at the upright ends. Then the ultimate shear force due to bending failure can be calculated as:

$$V_{r,flex} = \frac{M_1 + M_2 + M_3 + M_4}{h} \qquad [10.3]$$

where M_i are the ultimate bending moments at the four ends of the two uprights. These moments depend on the axial force N acting on the uprights that has been estimated as:

$$N = N_G \pm \frac{V \cdot H_{eff}}{2 \cdot l} \qquad [10.4]$$

where N_G are the dead loads placed on the top and l is the span between the two uprights.

The second term, due to the frame redundancy, is added in the compressed upright and subtracted in the other one. The substitution of [10.4] in [10.3] leads to an iterative procedure to evaluate the ultimate shear force.

The equivalent frame approach has been employed in the walls with openings. In the other cases the idealization is simpler since the wall can be seen as a clamped vertical beam; in this case

$$V_{r,flex} = \frac{M_{r,flex}}{h} \qquad [10.5]$$

where $M_{r,flex}$ is the ultimate bending moment at the wall base and h the wall height.

The shear resistance $V_{r,shear}$ of the walls was determined with the analytical strut-tie approach explained in chapter 8.

A commercial software, MIDAS Gen 2013 v2.1, that allows a fiber modeling of one dimensional elements, was used to investigate the uncracked and cracked frame stiffness. The "tension stiffening" effect is not considered in cracked conditions.

10.5.2. Stiffness prediction

In the case of walls with openings each specimen was modelled as an equivalent frame with rigid spandrels and nonlinear uprights. Walls without openings was considered as a base clamped column.

In each case, the gravity loads were included as self-weight. The uprights were modelled as equivalent "T" sections with a fibre damage model able to take into account the variation of flexural stiffness with cracking. The shear stiffness is assumed as constant (Timoshenko-type beam) and evaluated considering a reduced shear modulus G*=G/2.2, where G is the concrete shear modulus (see chapter 9).

Wall number	Block type	Bar diameter [mm]	Core area [cmq]	Uncracked stiffness [kN/mm]	Cracked stiffness [kN/mm]
1	I25	12	378	412.5	38.3
2	I25	12	378	517.7	56.0
3	I30	12	462	540.2	51.8
4	I30	12	462	661.7	66.3
5	N20	10	273	773.5	141.8
6	I25	10	378	1116.0	172.4
7	N20	10	273	511.9	73.1
8	I25	10	378	766.4	85.5

Table 10-2. Stiffness prediction of full scale wall tests

10.5.3. Comparison between experimental and theoretical results

The theoretical and the experimental ultimate shear force are compared in the following table and graph. In the table the analytical shear resistance $V_{r,shear}$ provided by transverses is also reported. As confirmed by experimental results, the ultimate shear strength was never reached due to anticipate flexular failure.

To be compared with the experimental results theoretycal values have been evaluauted considering the average effective mechanical properties of materials, without considering partial safety factors.

Wall n°	Block type	Bar diam. [mm]	Core area [cmq]	Trans-verse area [cmq]	Total wall length [cm]	Upright length [cm]	$V_{r,flex}$ [kN]	$V_{r,shear}$ [kN]	$V_{r,exp}$ [kN]	Rel. err. [%]
1	I25	12	378	90	325	87.5	250.6	466.8	260	3.6
2	I25	12	378	90	425	137.5	348	733.5	400	13.0
3	I30	12	462	107	335	92.5	263.4	559.8	280	5.9
4	I30	12	462	107	435	142.5	358.2	862.4	420	14.7
5	N20	10	273	85	415	-	537.7	1002.3	550	2.23
6	I25	10	378	90	425	-	558.4	1065.4	598	6.62
7	N20	10	273	85	315	-	308.3	760.8	320	3.66
8	I25	10	378	90	325	-	322.9	814.7	285*	-13.3

*pull-out failure of two bars

Table 10-3. Comparison between experimental and analytical ultimate lateral load

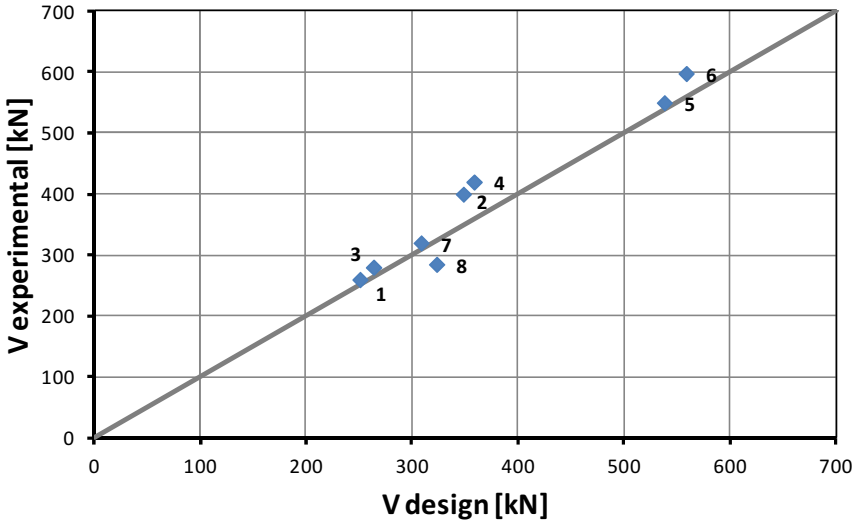

Figure 10-7. Comparison between experimental and analytical results

The experimental ultimate load bearing capacity was always greater than theoretical. The analytical predictions were always conservatives, except for wall number 8 where occurred a local pull-out failure of two vertical bars.

The analytical values slightly differ from the perfect match represented by the grey line in Figure 10-7 confirming the good accuracy of the model and of the analytical framework developed.

10.5.4. Ductility and behavior factor estimation

The term "ductility" in seismic design is used to mean the ability of a structure to undergo large amplitude cyclic deformations in the inelastic range without a substantial reduction in strength. It is a fundamental parameter for the seismic design. Generally, ductility is defined as the ratio between the ultimate displacement of a control point and the displacement at which yielding occurs. The control point is usually assumed as the roof barycenter.

When calculating ductility factors the definition of the yield deformation (displacement, rotation or curvature) often causes difficulties since the force-deformation relation of a structure may not have a well-defined yield point. This may occur, for example, due to nonlinear behavior of materials, or due to longitudinal bars at different depths in a reinforced concrete section reaching yield at different moment levels, or due to plastic hinges in different parts of a structure forming at different load levels.

All the walls tested present the characteristics described above and a criterion to define the yielding displacement is needed. The capacity curve, i.e. the upper envelope in the force-displacement graph, is transformed through the transformation factor Γ into a the single degree of freedom (SDOF) system. Actually, the walls tested are already SDOF systems because have only one story where the mass is concentrated and Γ is equal to 1.

According to (NTC 2008) the capacity curve is idealized with an elastic-perfectly plastic relationship where the initial stiffness k^* is fixed and the yielding force F_y^* is determined in order to have the same energy absorption of the real system (see Figure 10-8).

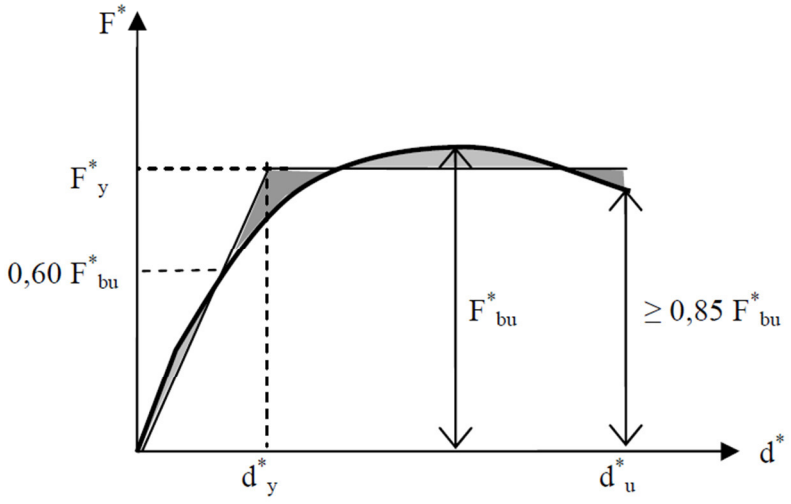

Figure 10-8. Determination of the bilinear curve of the idealized system

In this way the yielding and the ultimate displacement, d_y^* and d_u^*, are obtained. The natural period T* of the SDOF system is calculated as:

$$T^* = 2\pi\sqrt{\frac{m^*}{k^*}} \qquad [10.6]$$

where m^* is the equivalent mass of the SDOF system computed as the sum of the dead loads upon the roof and half of the self-weight divided by the gravity acceleration. For the calculation of the behavior factor q was chosen a design spectrum with a return period of 50 years. The site is L'Aquila (IT) with a type A soil according to (NTC 2008). The resulting T_C period is 0.346s.

According to Fajfar formulas [5.1] and [5.2], the following ductility and q-factor values are obtained:

Wall number	Period T* [s]	Ductility μ	Behaviour factor q
1	0.068	21.27	5.0
2	0.063	9.94	2.6
3	0.056	24.40	4.8
4	0.064	13.44	3.3
5	0.062	5.36	1.8
6	0.054	5.21	1.7
7	0.063	6.77	2.0
8	0.060	4.13	1.5

Table 10-4. Ductility and behavior factor for real scale walls tested

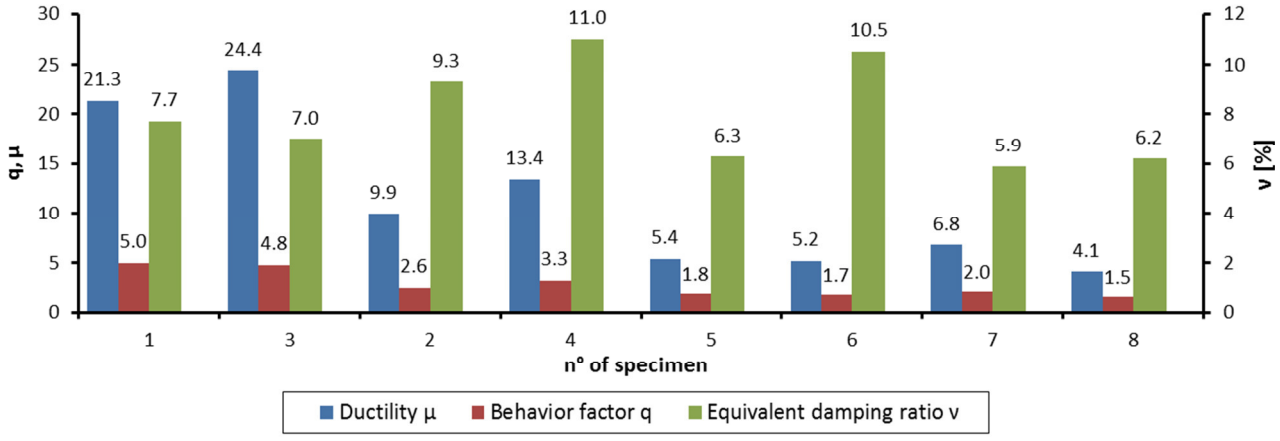

Figure 10-9. Ductility factor, behavior factor and equivalent damping ratio

It is clear that walls with openings (1-4), especially walls with doors (number 1 and 3), have demonstrated a larger displacement and ductility capacity thanks to the slenderness of uprights that provides more plastic rotation at the ends where plastic hinges localize. That yields to great values of the behavior factor q in the case of walls with openings. Walls without openings typically form a plastic hinge at the base but with a limited rotation capacity due to the low height-length ratio.

All the walls tested have a very small period T* of the equivalent SDOF system, if compared with T_C. This fact penalizes considerably the behavior factor estimation with the Vidic's formula because this approach considers the q-factor of structures with very small periods nearly not dependent on ductility. Given that, the q-factor estimation based on only 1-story buildings is not very reliable and, therefore, case studies with higher natural period are needed (see chapter 16 and 17).

10.5.5. Equivalent damping ratio and energy dissipation

In analogy to timber structures according to (EN-12512 2001), from the cyclic force-displacement curve an estimation of the equivalent damping ratio is obtained as:

$$\nu_{eq} = \frac{E_d}{2\pi \cdot E_p} \qquad [10.7]$$

where E_d is the dissipated energy and E_p is the potential energy available.

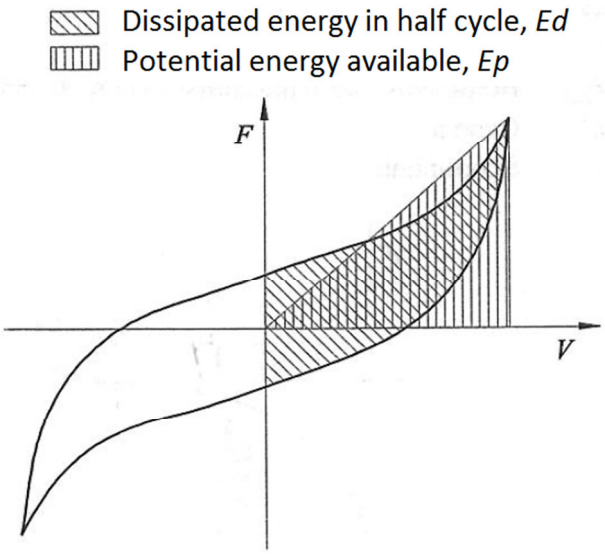

Figure 10-10. E_d and E_p graphical representation

The energy estimation regards the third cycle of the last ductility level of each wall.

The values regarding the equivalent dumping ratio are reported in Table 10-5 and are always greater than 5% that is the value suggested by European and Italian Code.

Wall number	E_d [kN mm]	E_p [kN mm]	ν_{eq} [%]
1	666	1379	7.7
2	241	414	9.3
3	784	1796	7.0
4	2118	3052	11.0
5	161	405	6.3
6	317	482	10.5
7	117	316	5.9
8	147	380	6.2

Table 10-5. Equivalent damping ratio

The equivalent damping ratio is closely related to the wall capacity of energy dissipation. The energy dissipation per load cycle is defined as the area enclosed by a hysteresis curve. The cumulative energy dissipation can be calculated by summing the energy associated with all the hysteresis loops. Figure 10-11 shows the cumulative energy dissipation of the test specimens versus the top drift ratio δ/h.

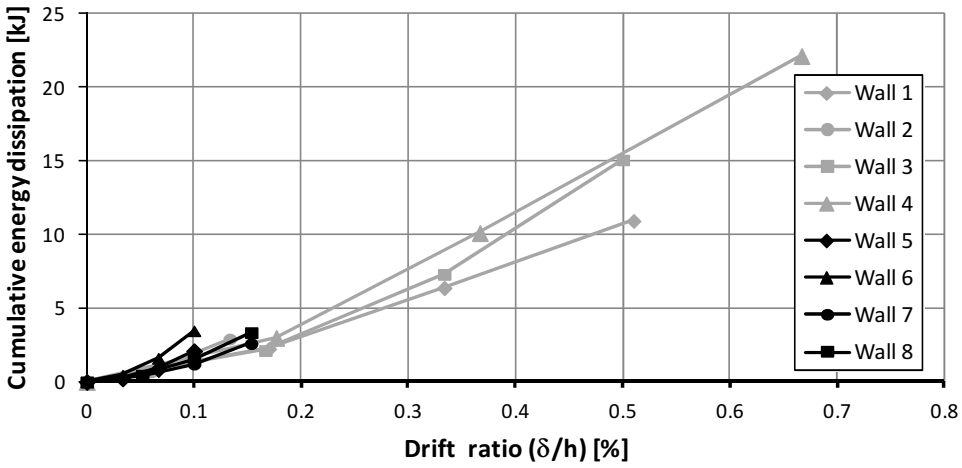

Figure 10-11. Cumulative energy dissipation of test specimens

The cumulative energy dissipation was calculated for each run of 3 cycles, without considering the last loading until the failure. Panels with openings have greater deformation and energy dissipation because the cycle runs were wider than the others.

The results of (Malavolta 2008) are reported in Table 10-6. These results are in good agreement with the results reported above. It is worth to noting that, even if the main part of these results are related to walls without openings, damping ratios are larger than 5% in all the cases that overcome a relatively small drift of 0.20%.

Interstory Drift	Test n°	3	4	5	6	8	9	10
	Type	*A (N=200 kN)*	*A (N=400 kN)*	*A (N=0 kN)*	*A (N=200 kN)*	*C (N=200 kN)*	*A (N=400 kN)*	*B* (N=240 kN)*
	0.10%	3.5	4.2	4.9	4.0	11.3	3.7	4.8
	0.20%	6.8	6.4	5.9	5.9	9.2	5.3	5.4
	0.40%	9.8	8.7	6.7	6.9	7.9	6.2	5.3
	0.60%	-	-	-	-	-	-	5.5
	0.75%	-	-	-	-	-	-	5.6
	0.80%	12.3	12.0	12.3	9.9	-	9.8	-
	1.00%	11.4	12.3	15.3	9.2	13.7	9.4	7.3
	1.20%	11.1	12.3	-	9.4	-	10.1	7.7
	1.50%	12.4	11.8	-	11.8	17.9	11.5	8.9
	1.70%	-	-	-	-	17.8	-	-
	1.80%	-	-	-	-	-	-	10.6
	2.00%	-	-	-	-	-	11.6	-

Legend:

Type A	No opening
Type B*	No hor. reinf. (window)
Type C	Multistory
-	< than 8
-	between 8 and 15
-	> than 15

Table 10-6. Damping ratios reported in (Malavolta 2008)

10.6. Conclusions

The behaviour of reinforced concrete bearing shear walls cast in mineralized wood shuttering kit has been investigated through cyclic loading tests. The analytical ultimate lateral load was estimated with an equivalent frame model and the results are in good agreement with the experimental ones. The analytical values are always conservative and the errors are smaller than 15% with respect to the experimental values.

The deformation capacity was studied through a pushover analysis performed with an equivalent frame model and fiber approach. It properly describes the experimental envelope curve and failure load in all cases. In the cases of walls without openings, where the shear deformation become dominant, the model overestimates the stiffness because it takes into account only for a constant uncracked shear elastic stiffness (Timoshenko beam theory).

The global experimental energy dissipation was investigated for each wall through the force-displacement experimental curve. The procedure described in this paper permits to estimate an equivalent damping coefficient for the construction system in object. All the obtained values are always greater than 5% which is the value suggested by European and Italian Code for seismic design.

Another important parameter in the seismic design codes is the behaviour factor q that can be computed applying a pushover procedure in the inverse order, maintaining q as a variable. The values obtained are always close to 2, the value suggested by (NTC 2008) for this particular construction system.

As already mentioned, the q-factor values in the test cases are not very reliable due to the small period of the 1-story tested structures. The Vidic's formula provides very low q-factor estimations despite the great ductility expressed by the tested specimens. Buildings with greater natural period should be analyzed in order to have a behavior factor assessment closer to reality. Great natural period means great values of mass and small lateral stiffness that are typically characteristics of tall buildings.

The analytical model adopted, despite its simplicity and advantages, is not able to properly describe the cyclic behaviour because the degrading of shear stiffness is neglected and energy dissipation is concentrated at upright ends. In reality, during the cyclic tests there is also a distributed damage along the transverses that provides a reduced stiffness especially in the unloading/reloading branches. This effect produces a remarkable pinching behaviour that leads to an underestimation of the energy dissipation.

To better simulate the real cyclic behavior of walls a more sophisticated model that considers also the nonlinear behavior of transverses is needed. A proposal for a nonlinear model in this direction is described in chapter 15.

Chapter 11. – Tests on connections

In this chapter the rotation capacity of floor-to-wall (T type) and wall-to-wall (L type) connections is investigated. This tests are also called as *type 4 tests* in the (LL. GG. 2011) and were performed in September 2012 at Terrassa Padovana (PD – Italy). The materials are the same used for the realization of the specimens described in chapter 10.

11.1. Test setup

Four RC connections were tested: 2 T-type and 2 L-type connections. Two different diameters, 10 and 12 mm, were used for the reinforcement of specimens. Table 11-1 summarizes the main characteristics of the tested connections:

Specimen number	Type of block	Reinforcement	Connection type
9	I30	Φ10@25/25	Floor-to-wall
10	I30	Φ12@25/25	Floor-to-wall
11	I30	Φ12@25/25	Wall-to-wall
12	I30	Φ10@25/25	Wall-to-wall

Table 11-1. Connections tested

The connections form in general an angle of 90° and a distortion cyclic force that tends to open and close the angle of the connection is applied until failure or the achievement of a maximum displacement condition. The force is applied with two actuators, one in the pushing phase and one in the pulling phase. The cyclic force was applied on one of the two elements forming the connection, whereas the other element was blocked to the ground with suitable restrains.

In the case of a floor-to-wall T connection, the plane formed by the wall was positioned horizontally and supported at both ends on two wood joists arranged orthogonally with respect to

the direction of the force imposed by the actuators. Another pair of joists anchored to the ground has been positioned on the upper part of the walls at both ends in order to create a simply supported scheme. The RC concrete slab (floor) has been placed vertically. The horizontal cyclic load was applied at the top of the slab with an eccentricity of 113 cm from the middle plane of the walls.

In order to simulate an axial load, the walls were compressed against the reaction wall with 4 threaded bars pre-tensioned with a force of 50 kN (see Figure 11-1).

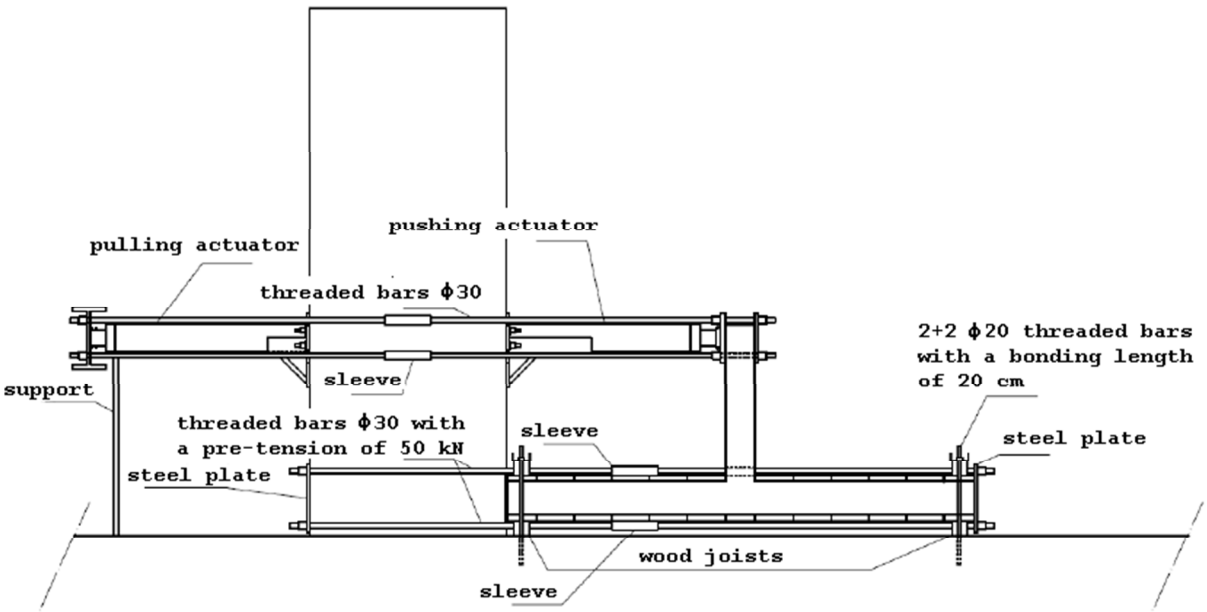

Figure 11-1.Test on floor-to-wall connection: setup

In the case of L connections (wall-to-wall) a RC block of 20 cm behind the vertical wall has been designed in order to create a restraint that blocks the rotation of the specimen in the pulling phase and its translation during the pushing phase. In the same way described in the T connection case, on both horizontal wall ends, a bilateral support restraint has been applied. These restraints block also the specimen horizontal translation. On the top of the vertical wall, the horizontal cyclic force was applied by the two actuators at 110 cm from the middle plane of the horizontal wall (see Figure 11-2).

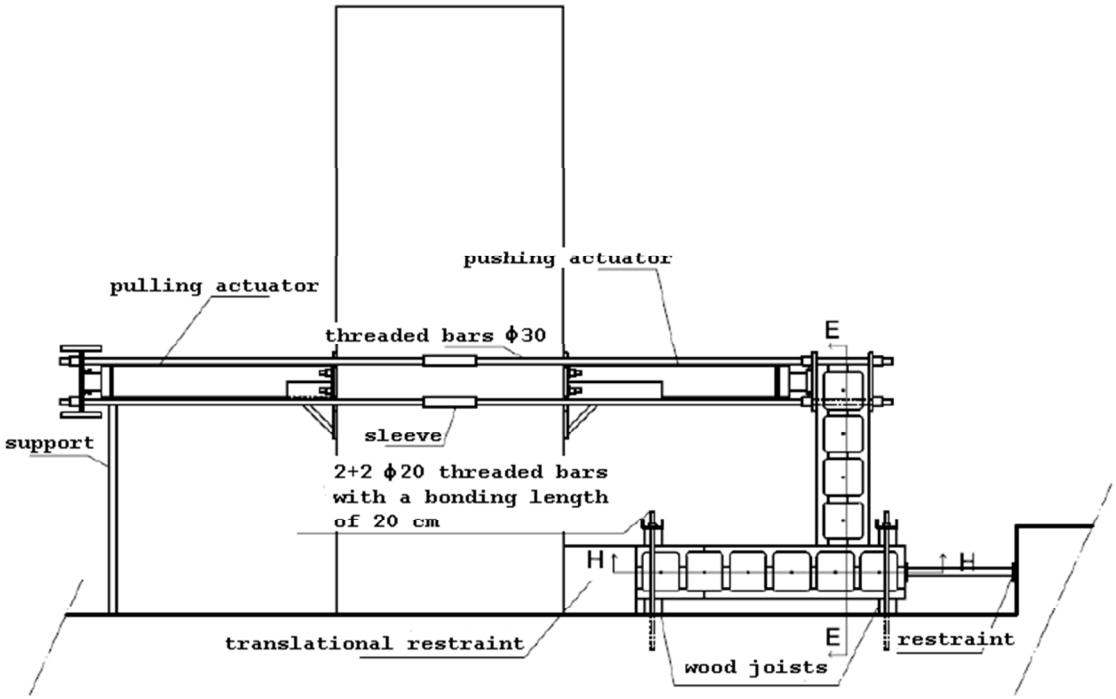

Figure 11-2. Test on wall-to-wall connection: setup

During the tests were recorded:

- the vertical displacements on the top of the vertical element
- the horizontal displacements on the top of the vertical element
- the horizontal displacements of the horizontal element

The horizontal displacements of the horizontal element were not always negligible, therefore a rigid body translation in the pushing force direction was measured. This rigid displacement component of the wall was subtracted from the maximum displacements of the vertical element.

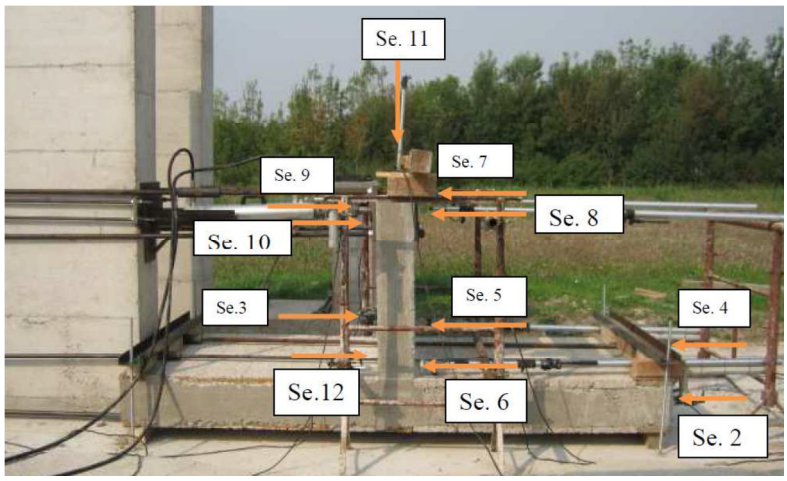

Figure 11-3. LTDV disposition on specimen

For each connection typology (T and L), a monotonic load was applied on the first specimen in order to calibrate the cyclic loading in the second specimen.

In the following, the general setup employed and the cracks developed in the weaker sections are presented with a series of pictures (see Figure 11-5 to Figure 11-10).

Figure 11-4. Actuators used during the tests on connections

A flexural failure of sections with the higher bending moment occurs in all the tested connections. All the specimens had demonstrated a great rotation capacity. Figure 11-9 shows a large lowering of the vertical element in the T connection after the cyclic load, due to the formation of two plastic hinges in the two sections of the walls close to the RC floor. This lowering is emphasized by the vertical dead load of the concrete slab.

Figure 11-5. Specimen 12: LTDV on top

Figure 11-6. Vertical sensor for vertical displacements

Figure 11-7. Sensor sliding during the test

Figure 11-8. Specimen 9 at failure

Figure 11-9. Specimen 10 at failure

Figure 11-10. Specimen 11 at failure

11.2. T connections: experimental results and comparisons

In the case of floor-to-wall connections, the critical section S are placed at ends of the walls, in proximity of the slab as marked in Figure 11-11. Out of plane bending failure of such sections was reached. The floor slab was designed to remain elastic during the test and it behaved accordingly.

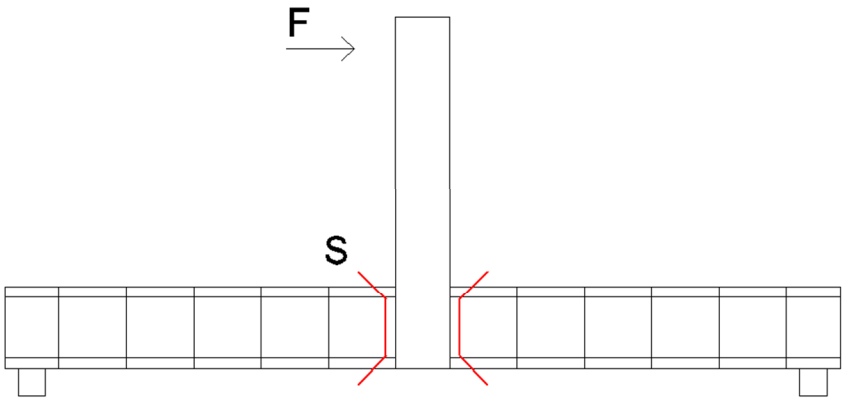

Figure 11-11. Critical sections in floor-to-wall tests

Experimental results from testing of floor-to-wall T connection are reported in Table 11-2 and Figure 11-12. In the case of specimen 9 the failure was not reached and the comparison of theoretical with experimental value of maximum strength is not possible.

Specimen number	Type of block	Reinforcement	Connection type	V_r [kN] analytical	V_r [kN] experim.	Difference [%]
9	I30	Φ10@25/25	Floor-to-wall	41.3	-	-
10	I30	Φ12@25/25	Floor-to-wall	52.4	68.4	23.4

Table 11-2. Analytical and experimental results of tests on T connections

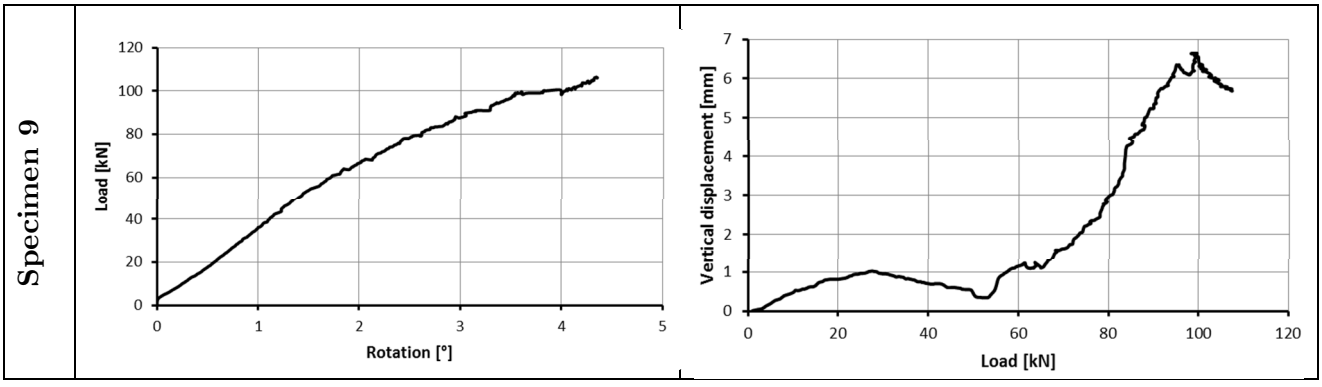

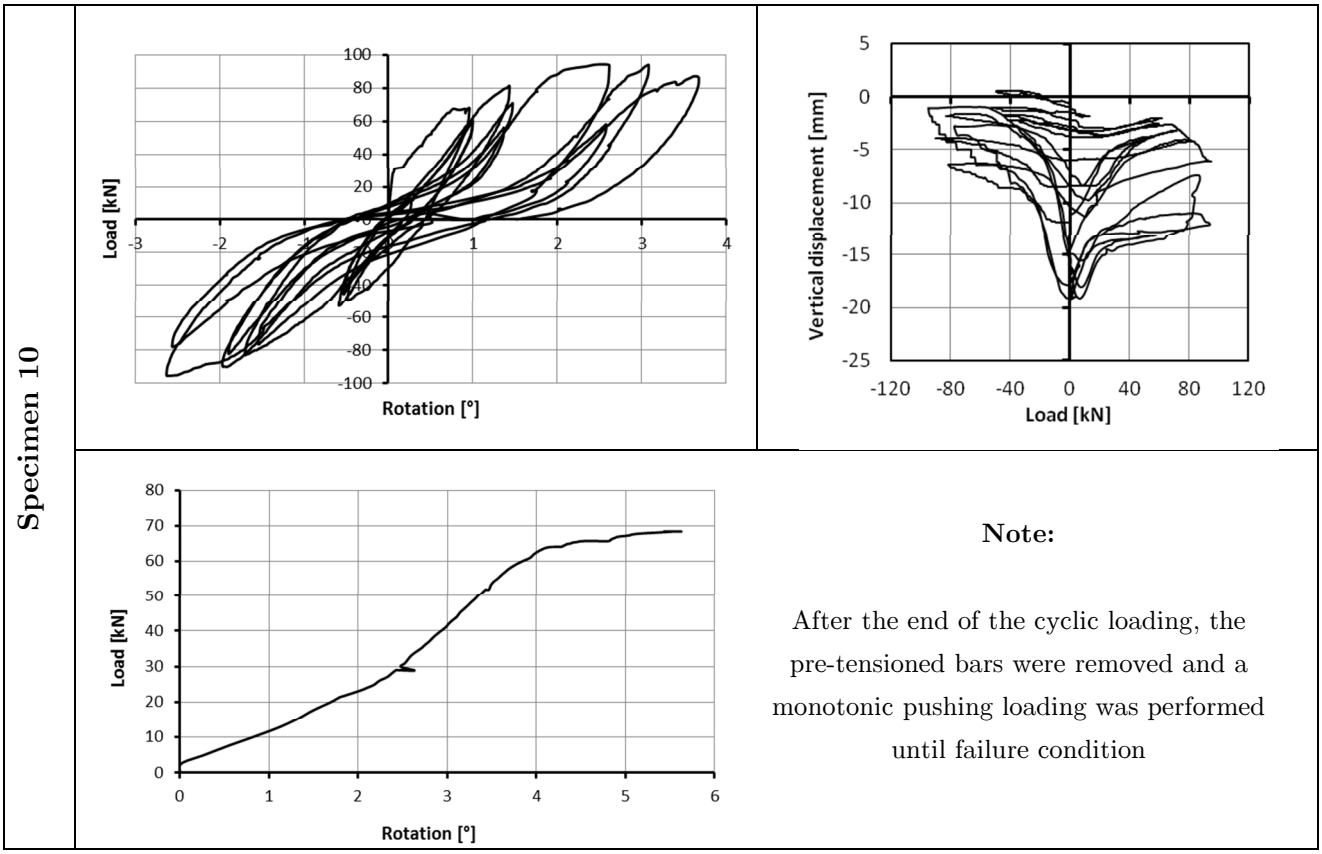

Figure 11-12. T connections: experimental graphs of monotonic (specimen 9) and cyclic loading (specimen 10)

During the monotonic test on specimen 9 the failure was not recorded because the maximum elongation of the instrumentation employed was reached.

Although the specimen was visibly cracked in the two critical sections S, the maximum strength of connection was greater than the analytical one computed without compression along the walls.

The initial pre-tensioning of the bars was intended to simulate a constant dead load on walls of 50 kN (N_p). Actually pre-tensioning increased during the test because of the rocking of the RC floor that tends to open the connection and so to separate the two wall portions (see Figure 11-13). Such compression increment (N_{pp}) is proportional to the distance separation ΔL between walls. This explains the greater strength exhibited by T-connections compared with the theoretical one.

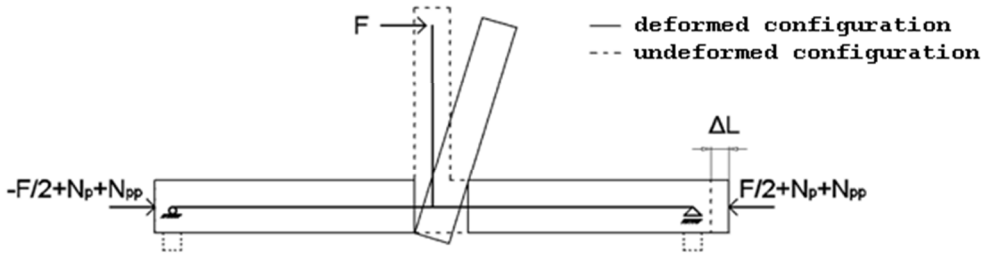

Figure 11-13. Axial force distribution on T-connection

Also in the cyclic phase of the test on specimen 10, the failure was not reached even if large deformations were recorded. Therefore after the cyclic loading the pre-compression bars on the wall element was removed and a monotonic loading has been performed in the pushing direction. The analytical strength in this case was computed without considering the pre-compression force.

11.3. L connections: experimental results and comparisons

The critical section in the wall-to-wall connections is shown in Figure 11-14 and marked with an S letter.

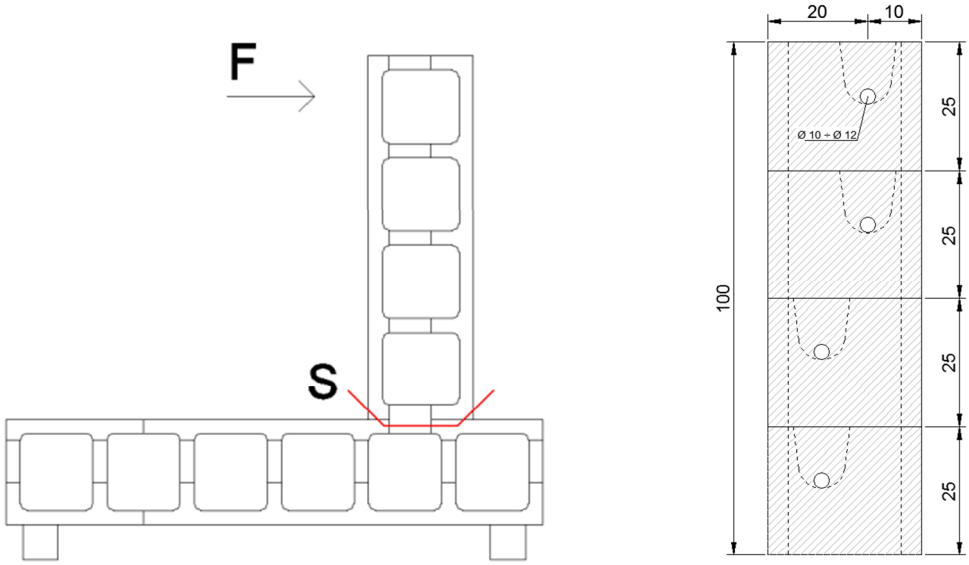

Figure 11-14. Front view of L-connections (left) and S section (right)

Also in this case, the bending moment is applied along the weakest direction of the resistant section. The resistant section is shown in Figure 11-14 (right) and is composed by 4 concrete transverses and wood formwork. Mineralized wood occupies a large portion of section area and gives a non-negligible contribution to the section resistance. A maximum compression wood stress of 3 MPa is considered. Considering the larger area, the reinforcement has a greater arm and can supply a greater resistant moment. The analytical results are summarized in Table 11-3.

Specimen number	Type of block	Reinforcement	Connection type	V_r [kN] analytical	V_r [kN] experim.	Difference [%]
11	I30	Φ12@25/25	Wall-to-wall	25.7	32	19.8
12	I30	Φ10@25/25	Wall-to-wall	22.3	25.4	12.3

Table 11-3. Analytical and experimental results of tests on L connections

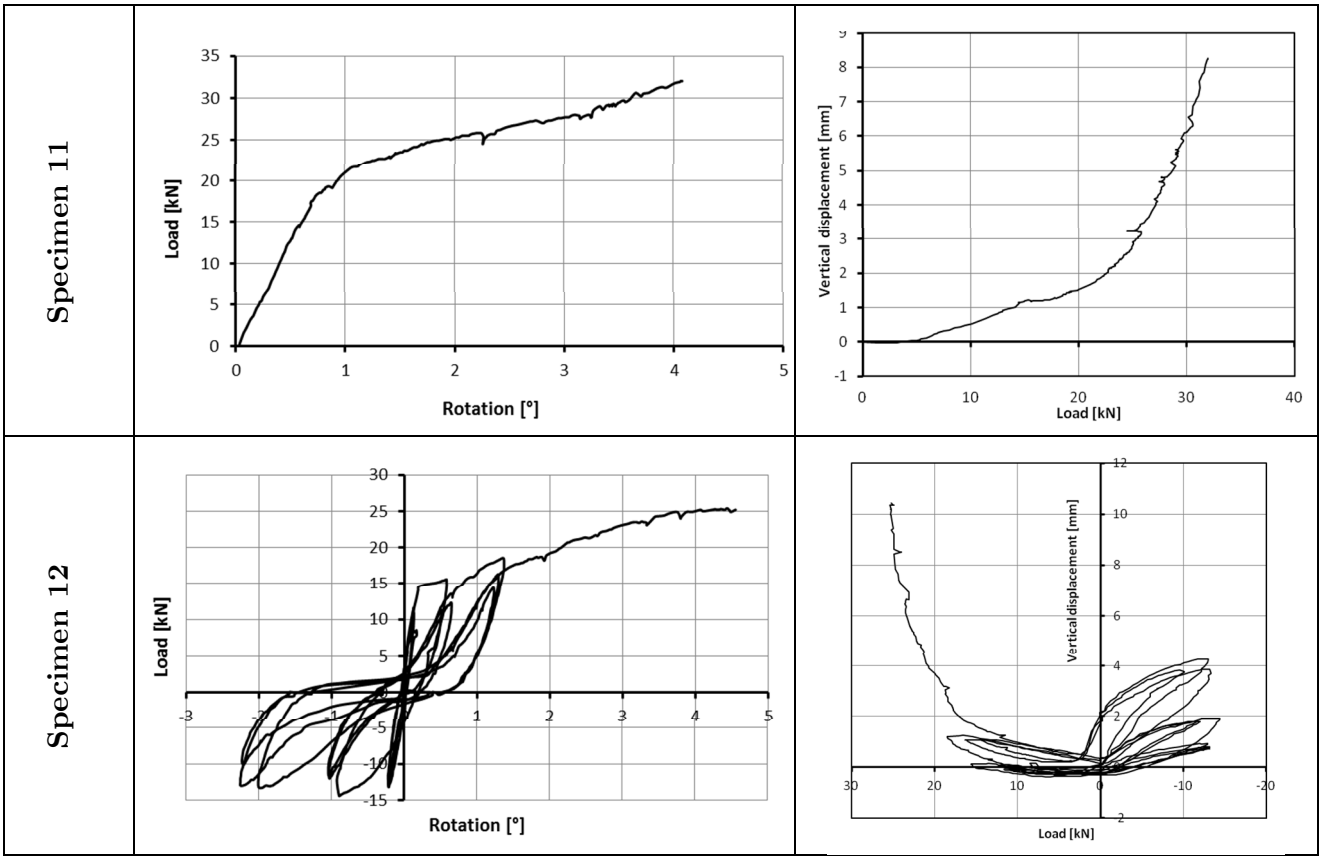

Figure 11-15. L-connections: experimental graphs of monotonic (specimen 11) and cyclic loading (specimen 12)

The interpretation of this test is difficult in terms of maximum strength. The less the magnitude of forces involved, the more complicated the matching of experimental values. This is due to the not negligible resistant contribution given by formwork. Moreover, the small errors in the reinforcement position can affect considerably the predicted strength. With large rotations, the problem can overstep the small deformation field.

In terms of maximum strength, the design force V_d is always conservative in comparison with the experimental one.

It is worth to notice that in the construction practice in rare cases the flexible strength of connections is considered. The aim of these tests was to verify the rotation capacity of connections It was experimentally proved that these kind of connections can easily exceed a drift of 2%, a value that very unlikely can be reached in a wall-to-wall connection even in case of extreme earthquakes.

PART IV – Numerical modeling

Chapter 12. – Introduction to Part IV

Structures in regions of high seismic risk will not respond elastically to the maximum earthquake expected at the site during their usable life. Modern seismic design recommendations intend that buildings respond elastically only to small magnitude earthquakes, but should be expected to experience different degrees of damage during moderate and strong ground motions. The response of reinforced concrete (RC) buildings to earthquake excitations depends on several factors, such as earthquake characteristics, soil quality and structural properties.

The determination of the structural properties of a reinforced concrete building is an essential step in the evaluation if its earthquake response. Typically, initial stiffness, ultimate capacity, and different global and local ductility demands are some of the parameters included in this assessment. In some cases it may be necessary to evaluate the remaining stiffness and load carrying capacity of a building after a strong ground motion. A complete assessment of the seismic resistant design of reinforced concrete structure often requires a nonlinear dynamic analysis. Due to the complex interactions between the various components of real structures, their dynamic characteristic up to the failure cannot be identified solely from dynamic test of scale models. Moreover, the cost of such tests is often substantial, particularly, for the large scale specimens.

Historically, these difficulties have been overcome by static tests on components and on reduced-scale sub-assemblages of structures under cyclic load reversals. Results from these tests are then used in the development and calibration of hysteretic models that permit the extrapolation of the limited test data to other cases and to dynamic response of complete structures. In these integrated studies several models for the nonlinear response analysis of the reinforced concrete structures have been developed. These can be divided into three categories in accordance with the increasing level of refinement and complexity:

Global models: The nonlinear response of a structure is concentrated at selected degrees of freedom. For example, the response of a multistory building may be represented as a system with one lateral degree of freedom at each floor. Each degree of freedom has the hysteretic characteristic of the interstory shear-lateral drift response. Such models are useful in the preliminary design phase for estimating interstory drifts and displacement ductility demands. The reliability of this class of

model in the accurate prediction of global displacements is poor and the recovery of internal members forces from the limited number of degrees of freedom is practically impossible.

Discrete finite element (member) models. The structure is modeled as an assembly of interconnected elements that describe the hysteretic behavior of reinforced concrete members. Constitutive nonlinearity is either introduced at the element level in an average sense or at the section level. Correspondingly, two types of element formulation are possible: (a) lumped nonlinearity, and, (b) distributed nonlinearity member models.

Microscopic finite elements models. Members and joint are discretized into a large number of finite elements. Constitutive and geometric nonlinearity is typically described at the stress-strain level or averaged over a finite region. Bond deterioration between steel and concrete, interface friction at the cracks, creep, relaxation, thermal phenomena and geometric crack discontinuities are among the physical nonlinearities that can be studied with this class of model.

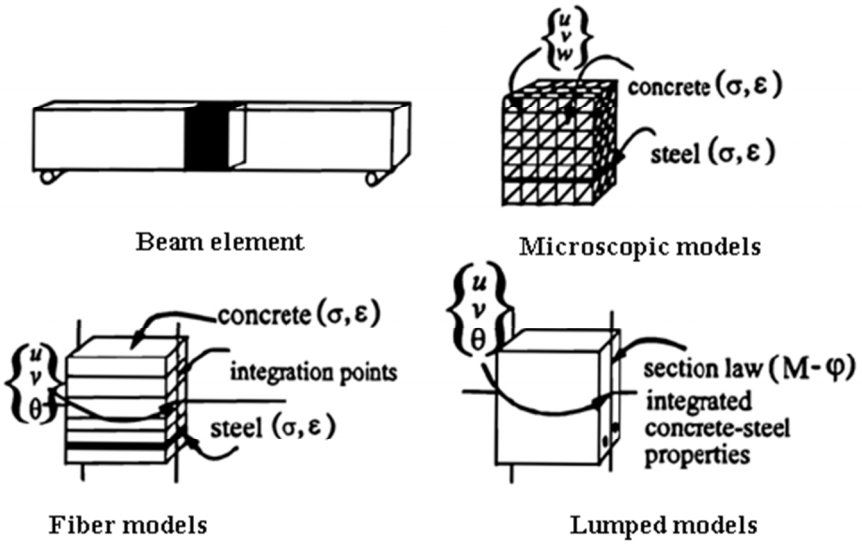

Figure 12-1. Microscopic finite element models (top) and discrete finite element models (bottom)

The fiber model implemented in the commercial software MidasGen 2013 v2.1 belongs to this class of microscopic finite elements models and permits to discretize the section at each integration point with an indefinite number of fiber, assigning to each fiber a material with a particular constitutive law. This software was used in all the numerical simulations described in this Ph.D thesis.

Chapter 13. – Discrete finite element models

The present study concentrates on the second class of models presented in the introduction. Discrete finite elements models are the best compromise between simplicity and accuracy in nonlinear seismic response studies and represent the simplest class of models that still allow significant insight into the seismic response of members and of the entire structure. Global models are based on too crude approximations and yield too little information on the forces, deformations and damage distribution in the structure. Microscopic finite elements, on the other hand, should be limited to the study of critical regions, since these models are computationally prohibitively expensive for large scale nonlinear dynamic analyses, where the model of even a simple frame involves hundreds of degrees of freedom. Before presenting the elements proposed for the modeling of RC walls cast in wooden blocks, an overview of existing discrete models is given until the fiber model implemented in MidasGen 2013 v2.1 and described in (Neuenhofer e Filippou 1997). The overview order of the state-of-the-art is more or less the same reported in (Taucer, Spacone e Filippou 1991).

13.1. State of the art

A review of existing analytical studies relevant to the nonlinear seismic response of RC frames is presented in the following. A concerted effort to model and analyze these structures in the inelastic range of response has been under way for several years and the current state of the art is summarized in this short survey. Respecting a chronological order, lumped plasticity models are presented first and distributed nonlinearity models follow. Stiffness and flexibility formulations are also reviewed and their suitability for the analysis of reinforced concrete members is evaluated.

13.1.1. Lumped models

The modeling of seismic behavior of reinforced concrete structures in the last forty years was the focus of many researchers and led to the development of multiple types of global models. Since the

late 60s were proposed simple models, which over the years have been improved and expanded. This introduction it is focused on the elements for nonlinear analysis of structures, in which the shear strength is enough to ensure the development of inelastic deformation. In this context, global models can be classified in relation to the inelastic deformation distribution, with this criteria may have lumped plasticity elements and distributed plasticity elements. The nonlinear behavior of frame structures of usually concentrated in critical areas corresponding to the beams-columns ends. So one of the first approaches to modeling this behavior has been carried out assuming a zero-length plastic hinges as a rotational springs located at the ends of the beam-column elements, and connected in series or in parallel, depending on the type of connection may have series or parallel models as shown in Figure 13-1.

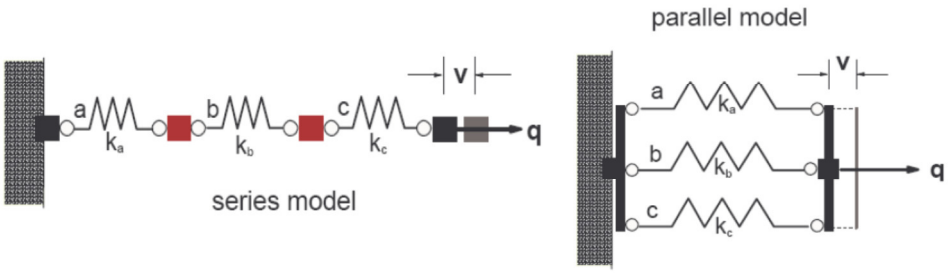

Figure 13-1. Models with springs connected in series (left) and in parallel (right)

The first component model was introduced by (Clough R. 1966), and is shown in Figure 13-2. The model consists of two elements in parallel, one elastic-perfectly plastic, to represent the yield strength, and the other elastic with a reduced stiffness to reproduce the hardening. The element stiffness matrix is the sum of those of the two parallel elements. The advantage of these models, also called "two component model", lies in the independence of the formulation from the moments diagram, while the problem arise from the fact that this kind of elements allow to use only a bilinear moment-curvature relation, so it is incapable of represent the typical degradation of reinforced concrete elements. These models, overestimate the energy dissipation capacity of reinforced concrete structural elements.

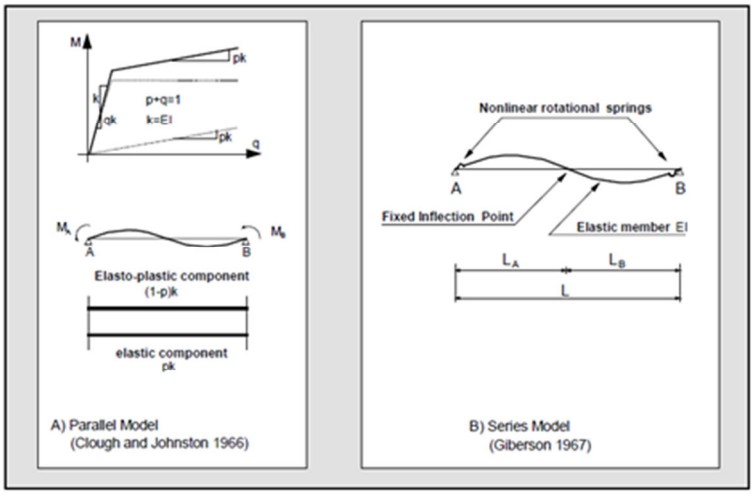

Figure 13-2. Simple lumped plasticity elements: Clough and Johnson model (left), Giberson model (right)

Series models were introduced to overcome the limitations inherent in the parallel models. They were formally introduced by (Giberson M. 1967), the model (see Figure 13-2) consists of two non-linear rotational springs and end of an elastic beam. For each spring is introduced a moment-rotation relationship assuming an antisymmetric linear distribution of moments along the element. In series models the flexibility matrix of each spring is summed with the flexibility matrix of the linear elastic beam. This type of models are much more versatile than the parallels, with series models is possible to describe a more complex hysteretic behavior, selecting an appropriate moment-rotation relationship for springs, but they are limited by the assumption of a constant moments distribution along the element. (Suko M. 1971) proposed to take the contraflexure point from the initial elastic analysis instead of the center of the beam. (Otani S. 1974) proposed a more sophisticated model, shown in Figure 13-3. The Otani's model consists of two deformable parallel elements, one linear elastic and the other non-linear, two rotational springs and two rigid connection at the ends to take into account the finite size of the beam-column node. The rotational springs are used to consider the effects of the reinforcement slip at the nodes.

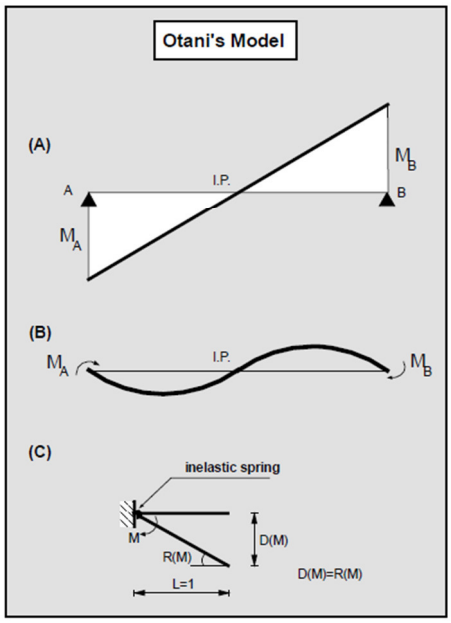

Figure 13-3. Otani's model: A) moment distribution; B) element deformation; C) equivalent inelastic rotational springs

The construction of the flexibility matrix is based on the calculation of the contraflexure point step by step. The element is treated as two cantilever beams, with a free end at the contraflexure point. With this assumption the element is equivalent to two inelastic rotational springs at the ends, whose properties are related to the current position of the contraflexure point. The Otani's model, however, is not capable to evaluate the actual spread inelasticity along the element, depending not only on the current state of the element, but also on the load history.

Concentrated plasticity models have been formulated neglecting the phenomena of axial force-moment interaction. The moment-rotation relationship are defined referring to a constant value of axial force, usually the gravity loads. Actually, the normal stress in the columns due to seismic

action can vary significantly, affecting both the resistance and the stiffness properties of structural elements. Considerable efforts have been made to include the effects induced by the variations of normal stress in simplified models, but this kind of models are not applied extensively. (Ozcebe e Saatcioglu 1989) introduced a concentrated plasticity model, in which the moment-rotation relationship of the springs is characterized by a family of curves, each corresponding to a different value of normal stress. An important step in the modeling of axial force-bending moment interaction, was made with the introduction of multispring models, which are classified between as concentrated plasticity, but actually these differ considerably from those described above, and in somehow are similar to simplified fibers models. The first multispring model was proposed by (Lai S. 1984), it was constituted by a central elastic element, and a series of axial springs at the end zones to simulate the inelastic response (see Figure 13-4). The non-linear deformations are concentrated in the end zone, although their behavior is not defined by the moment-rotation relation, but through a discretization of such zones in areas that represent the springs. In the Lai's model each inelastic element consists of five spring for concrete (four in corners and one in the center) and four for steel. The force-displacement relationship for the steel springs follows an hysteretic model with degradation similar to that assumed on the moment-rotation relationship viewed for others concentrated plasticity models. The elongation of each spring is correlated with the average axial displacement and the section rotation, through the assumption of plane sections remain plain.

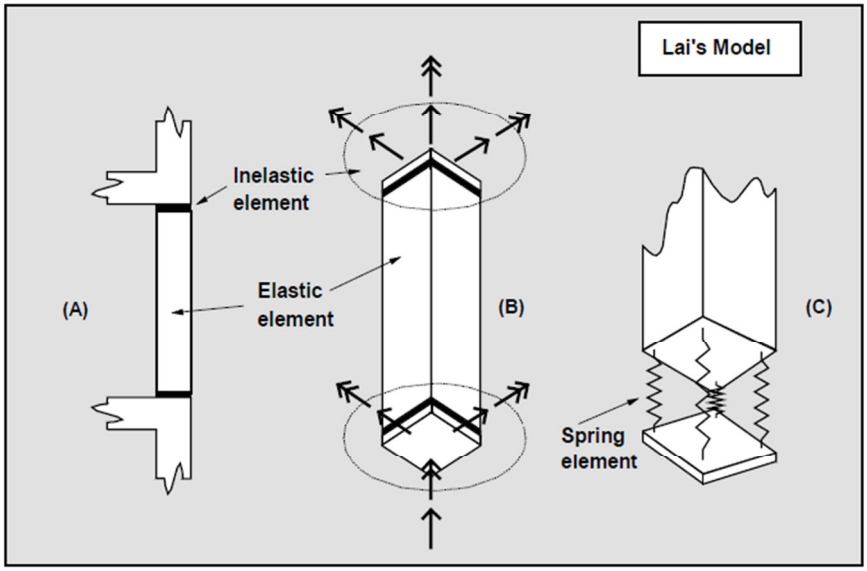

Figure 13-4. Lai's model: degrading inelastic element for reinforced concrete beam-columns under biaxial bending and axial load: A) member frame; B) member model; C) inelastic element

(Saiidi M. 1981), proposed a multispring model with five springs based on (Lai S. 1984). One spring is central to simulate concrete core, while four springs are placed at sides to simulate the behavior of a reinforced concrete element subjected to axial elongation, corresponding to the area represented by each spring. With this model the authors overcame some inherent inconsistencies in the Lai's model, and have performed good comparison with experimental tests. The best feature of multispring models is the ability to simulate with good accuracy the nonlinear behavior of spatial columns, requiring much lower computational effort than fiber models.

The concentrated plasticity models, as seen above, are not able to take into account the gradual spread of inelastic deformation within the elements. A more accurate description of the nonlinear behavior of reinforced concrete elements is possible by using distributed plasticity models. These kind of models assumes that the inelastic deformation may occur in any section, the element response is derived through an integration of sections response along the element. (Takayanagi e Schnobrich 1979), have proposed to divide the element into a finite number of segments (see Figure 13-5), each with constant properties dependent on the bending moment at the midpoint. Each segment is studied through a moment-curvature relation including the effects of degradation due to cyclic loading. Also in this model a proposal to take account the axial-bending interaction is made. The section stiffness is defined, including axial effects, as resulting from predefined interaction diagrams. Analyze the sections response along the element leads to various difficulties, for the greatest calculation time and for the numerical problems related to the arise of unbalanced moments within the element. Equilibrate these moments requires the introduction of complex procedures not necessary when are studied only the end sections. Therefore, several authors have developed concentrated plasticity models able to take into account the gradual spread inelasticity. These models, also called distributed inelasticity have been widely used, and many computer codes have been based on them.

Another element proposed by (Meyer, Roufaiel e Arzoumanidis, Analysis of Damaged Concrete Frames for Cyclic Loads 1983) and later improved by (Meyer e Roufaiel 1987), is divided into three zones, one central elastic and two inelastic ends, varying in length, the so called “effective length”, depending on the load history.

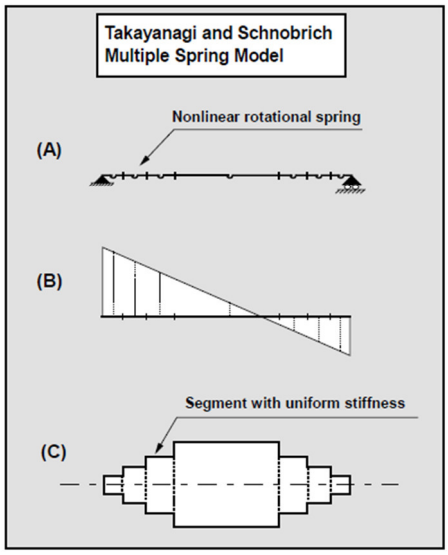

Figure 13-5. Takayanagi and Schnobrich multiple spring model: A) element model; B) bending moment diagram; C) section stiffness distribution

This formulation is independent from the position of contraflexure point, and take into account the coupling of the inelastic deformation in the two nonlinear segments. The properties of these segment are derived by simplified assumptions on the end sections, carried out through hysteretic moment-curvature models. (Keshavarzian e Schnobrich 1985) have adopted the same element, but

taking into account axial-flexure interaction. To consider these effects they followed a similar approach to that proposed by (Takayanagi e Schnobrich 1979). The criteria used by (Meyer, Roufaiel e Arzoumanidis 1983) is part of the formulation of (Filippou e Issa 1988), and (Mulas e Filippou 1990), which added to the element, two rotational springs at the extremities, for take into account the fixed end rotation at the beam-column joint, due to bar pull-out effects. These authors have attempted to define more accurately the moment-rotation relationship of the springs, which was independent from the assumed moment-curvature relationship at the end sections. (D'Ambrisi e Filippou 1999) have included more non-linear springs to account for translational non-linear deformations due to shear. This model is made up of several sub-elements connected in series to distinguish the various aspects that affect the nonlinear behavior of the structural element. A common plasticity model that differs from those just described was carried out by (Kunnath S. et al. 1990), this model can perform local and global damage evaluation as well as non-linear seismic analysis of reinforced concrete structures. (Kunnath S. et al. 1990) did not directly assess the length of the plasticized hinges. The element characteristics will be deducted from the sections by integration, assuming a flexibility distribution piecewise linear (see Figure 13-6).

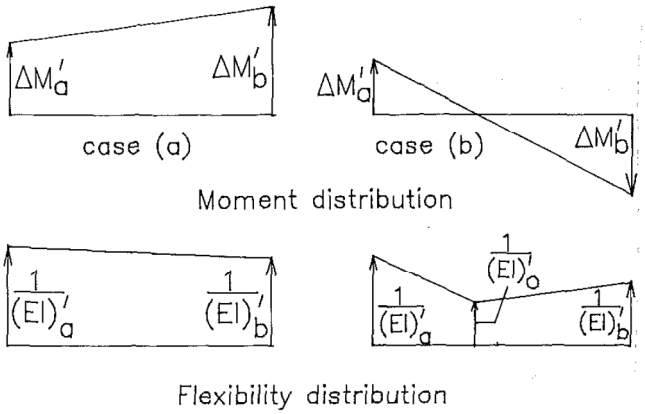

Figure 13-6. Kunnath's model: distributed flexibility model

This distribution is identified by the beam ends flexibility, that come from the moment-curvature relationship, and from the flexibility of the contraflexure point, which is assumed to be equal to the elastic value.

13.1.2. Fiber models

Fiber models carried out a double discretization, in the longitudinal direction defining a predetermined number of sections and in the transverse direction, discretizing in small finite areas the element cross sections. In case of simple planar bending model is sufficient to subdivide the sections into strips perpendicular to the axis of flexion, in the more general spatial cases a double subdivision into small rectangular areas is required (see Figure 13-7). Each fiber, represent a corresponding portion of elementary concrete or reinforcement area , by integration over the cross section is possible to obtain moment-curvature relationship, and thus determines the overall response of the whole element. By the hypothesis of plane sections remain plane, axial deformation

of each fiber $\varepsilon(x,y)$ can be obtained, once knowing curvature χ_x, χ_y and axial deformation ε_0 referred in section centroid.

$$\varepsilon(x,y) = \varepsilon_0 + y \cdot \chi_z - z \cdot \chi_x \qquad [13.1]$$

The characteristics described above are common to all models, so that not changes in different element formulations. What really change in different fiber models is essentially the state determination procedures that depend on different formulation. In fact fiber models, as distributed plasticity models, has the problem, highlighted in previous paragraph, about the arise of unbalanced section forces within the element. After a load step application, nodal displacement are calculated and from these the section forces can be evaluated, but because of the materials nonlinear behavior in all control sections, resisting forces does not match section forces.

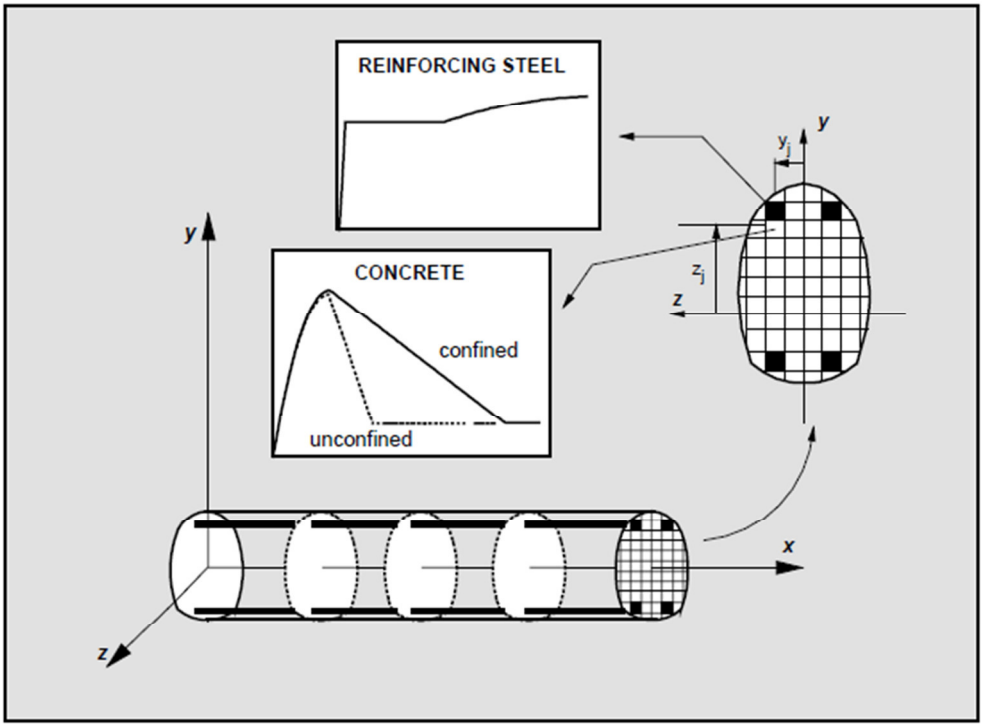

Figure 13-7. Fiber element: distribution of control sections and section subdivision into fibers

In global models, especially those with concentrated plasticity this problem is not treated because only the end sections are taken into account. Fiber models differ therefore in the process used to determine the section resisting forces. Different procedure has been proposed depending on the element formulation, in particular can be found procedure for stiffness based, flexibility based or mixed elements. The early models have been developed on a stiffness based approach, using classical shape functions. A model that use this approach is due to (Aktan, Pecknold e Sozen 1974), in which nodal resisting forces are obtained directly from section resisting forces by applying the virtual work principle. The formulation is compatible, however, it is shown that is inadequate in nonlinear cases because it involves a linear curvature distribution over the length. This assumption is unrealistic for reinforced concrete elements in nonlinear field. The latter models

become increasingly based on a flexibility approach, this class of models uses forces interpolation functions, thus a balanced element is achieved while in stiffness models the compatibility was the basic assumption. One of the first balanced element is proposed by (Kaba e Mahin 1984), based on Aktan's work, this model introduce the displacements interpolation functions updated for each load increment through the flexibility matrix. In this model, however, the numerical problems discussed above have not been solved because the theoretical formulation is not totally consistent with the flexibility approach. Essentially the flexibility approach is more realistic than the stiffness based one, but involves significant problems in determining the nodal resisting forces. Many studies, therefore, have attempted over the years to overcome these problems. (Zeris e Mahin 1988) and (1991), developed a complex iterative procedure to investigate the cross section deformation associated with internal balanced forces, with a shape coincident with forces interpolation functions. Taucer et al. (1991) have proposed a model that is part of a more general mixed approach. The nodal resisting forces are calculated for each element through an iterative procedure. At each iteration, are calculated the residual nodal displacements associated with the unbalance section forces along the element. The main characteristic of this model is that, at each iteration, compatibility and equilibrium are satisfied within the element. Taucer et al. (1991) show that the proposed algorithm is effective even if the structural response is characterized by "softening" as in concrete structures.

Finally some recent developments in fiber models are oriented in the attempts to develop extensions in classical elements including other sources of nonlinear deformation, such as those related to shear stress. In this class of models, the section state deformation is characterized not only by the axial deformation and the curvature in the centroid, but also by the shear deformation evaluated in nonlinear field. Besides the hypothesis of plane sections remain plane, a given distribution of shear deformation is assigned in order to detect the state of deformation of each fiber. Generally a biaxial stress-strain relationships is associated to these elements. This model is very close to a microscopic approach, but compared to that has the same degrees of freedom of a beam element type. In conclusion, fiber models requires a large number of operations to evaluate the element stiffness matrix, the stress and strain state in each section. In other words fiber models are really time consuming in state determination procedures. Although sometimes it incurs in numerical stability problems, many advantages can be identified using these models, such as:

- Catch the actual evolution of plasticization along the element
- Are able to reproduce realistically pinching phenomena
- Describe in detail geometry and position of transverse reinforcement
- Can reproduce the interaction between axial forces and bending moments
- Can be easily implemented spatial elements.

Also the constitutive relationship are more easy to implement because the singles materials are considered instead of moment-curvature relationship.

13.2. Numerical modeling of the construction system based on wooden blocks

As mentioned in chapter 4, the construction system studied in this thesis is composed by reinforced concrete walls with a particular internal grid pattern due to the formwork geometry. Due to the poor mechanical properties of wooden blocks compared with reinforced concrete, the formwork is not considered in the modeling.

In order to model the wall nonlinearity two different types of plasticity have been considered: lumped and distributed. Where possible the use of lumped plasticity is convenient because:

- Reduce the computational effort respect to distributed plasticity model
- Gain more stability during the analyses
- Match in a more direct way with the analytical proposal exposed in chapter 8.

13.2.1. Numerical model for horizontal transverses

The horizontal elements have been modeled with a combination of 3 nonlinear trusses according to the strut-and-tie approach of the analytical proposal. The strut and tie modeling procedure was established according to the assumption that compression is only carried by concrete, and tension is transferred exclusively through reinforcement.

Although the strut-and-tie modeling technique is simple to comprehend, it is a surprisingly complex task to apply in structural analysis. For successful application of this modeling technique the adequate knowledge of the internal force path is needed. But it is dictated by the reinforcement arrangement and the support conditions. Furthermore, the force path may vary significantly for different types of structural failure mechanisms, imposing an additional challenge in identifying a suitable numerical model.

In the case of the horizontal elements the tension path is always more or less the same and predictable because they are not subjected to a direct applied load but they limit the relative displacement between vertical elements. Of course the path could vary with the section characteristics or with the diameter of the bar reinforcement.

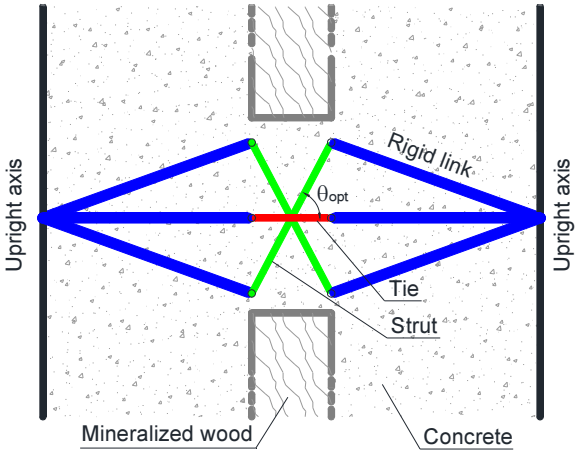

Figure 13-8. Strut & tie model for a single transverse

The only assumption in the model is that the angle between strut and tie for a given section with a given reinforcement remain constant and equal to θ_{opt} defined in Chap. 8. The geometrical properties of struts are calculated according to equations [8.6] and [8.7], whereas the tie has a section equal to the actual reinforcement bar. A panel portion with the detail of elements used in the modeling of horizontal elements is shown in Figure 13-8. Being the strut and tie elements subjected only to axial force, the best practice, computationally speaking, to take into account the nonlinearity is an axial plastic hinge with a force-displacement nonlinear law.

The material models used for strut and tie are, respectively, Mander's model for concrete (described in §13.2.3) and a bilinear model with kinematic hardening for reinforcement.

In the numerical model the pure shear strength of the concrete is taken into account with a suitable increasing factor of the strut-tie mechanism strength. In the model, such over-strength factor has been applied to the compression strength of concrete.

13.2.2. Numerical model for vertical uprights

A fiber model able to take into account the coupling between moment and axial forces in non-linear field is used to model the vertical elements. It is based on the flexibility approach to take advantage of the benefits attributed to this class of fiber model, for example it does not need a very fine discretization or a large number of gauss points in the elements.

A preliminary study, suggested a section discretization with 12 fibers in the direction of maximum wall stiffness and 3 Gauss points along the element length in order to maintain stability and robustness. In the three dimensional simulations presented in chapter 17 the section must be discretized also in the other direction because the presence of a bending moment in the out-of-plane direction is allowed.

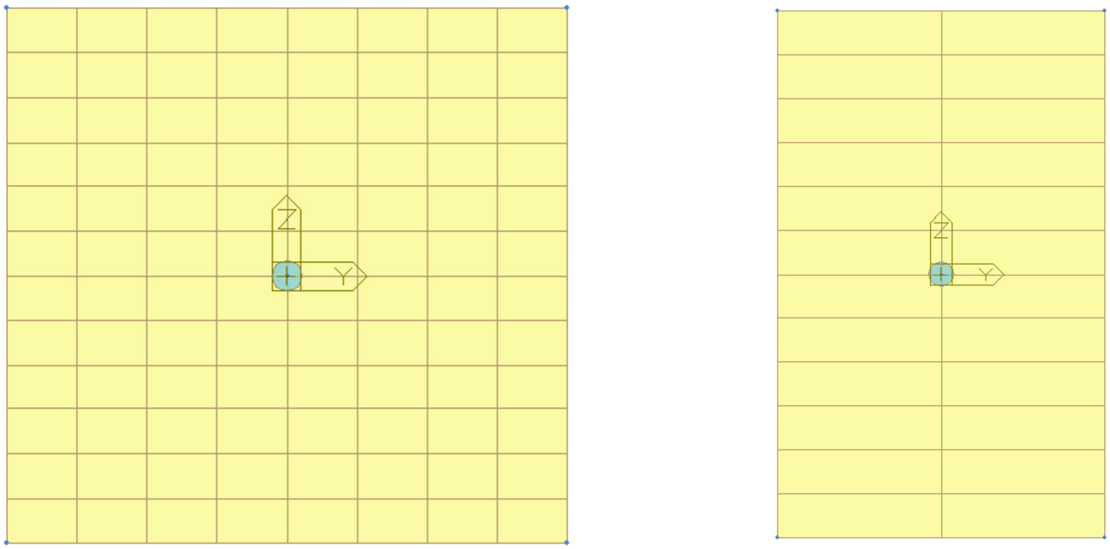

Figure 13-9. I30 section of columns in 3D simulations (left) and N20 section of columns in 2D simulations (left)

Figure 13-9 shows two sections of two different blocks used in two types of simulation: in yellow the concrete fibers and in light blue the reinforcement fibers.

13.2.3. Constitutive laws for materials

(Chang e Mander 1994) proposed a hysteretic material model for the simulation of cyclic behavior of both confined and unconfined concrete. The proposed model was an advanced rule-based model in comparison to other concrete models and the ability to simulate the hysteretic behavior of both ordinary (<6 ksi) and high strength (6-12 ksi) concrete in both cyclic compression and tension. The model incorporates the degradation that occurs due to incomplete unloading cycles in addition to that due to completed unloading cycles. A complete cycle is unloading from the monotonic envelope in one direction to the envelope in the other direction. The effects of both partial and complete reloading to the monotonic envelope is also incorporated. The model pays particular attention to effects of opening and closing of cracks. Chang and Mander noted that most models assumed sudden crack closure with a rapid change in the section modulus, but this assumption is not supported by experimental results obtained on lightly loaded columns. The general shape of the concrete stress-strain curve of their model is shown in Figure 13-10 and has certain characteristics: (1) the initial slope of the curve at the origin is the elastic modulus (E_c), (2) it reaches a maximum value at the peak stress and corresponding strain (ε_c, f'_c), and (3) it has both an ascending and descending branch. Controlling the slope of the ascending and descending branches of the model is important because they are different for confined and unconfined concrete. For unconfined concrete, the slope of the ascending and descending curves becomes steeper. In confined concrete, the slope of the descending branch is dependent on both the level of confinement and strength of the concrete.

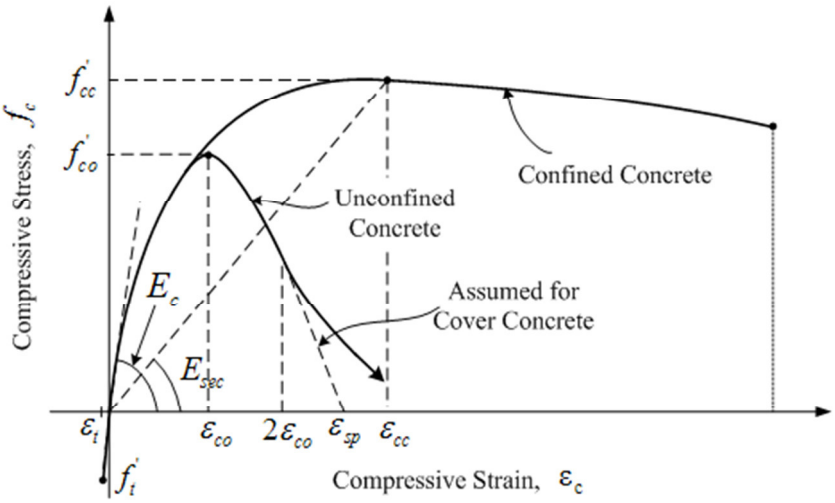

Figure 13-10. Mander's model

The free parameters in the model for unconfined concrete are: f_{c0}, E_c. Mander's formula [13.2] was used to estimate the concrete Young modulus:

$$E_c = 5000\sqrt{f'_{c0}}\ MPa \qquad [13.2]$$

Steel reinforcement of horizontal elements were modeled with a bilinear law (kinematic hardening) whereas a tension stiffening effects was considered in the vertical reinforcement until $f_y/2$ by means of a trilinear curve, according to EC8 §4.3.3.4.1(2) that allows a section stiffness modeling with pre-crack and post-crack branches. In this case the steel Young modulus E_s was increased of 5 times and then decrease to reach the yielding point (ε_y, f_y). The hardening modulus E_h of steel is $E_s/20$ in both cases (horizontal and vertical reinforcement).

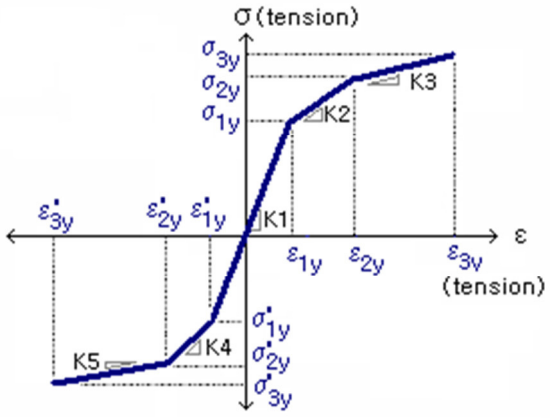

Figure 13-11. Trilinear model for steel reinforcement

Chapter 14. – Numerical simulation of direct shear tests

As first validation of the proposed numerical model the experimental results from direct shear tests reported in §8 have been reproduced. The numerical model of a panel is hereafter reported. It uses the models for uprights and transverses already described.

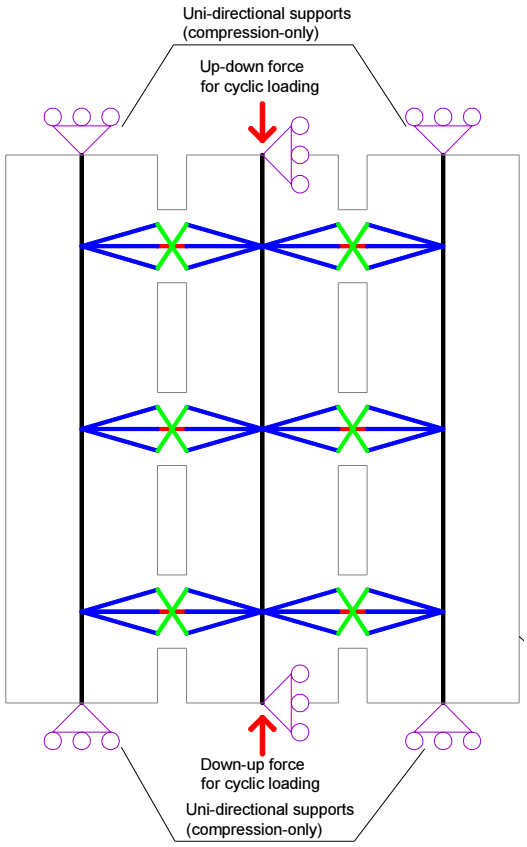

Figure 14-1. Model for direct shear tests simulation

In the following graphs, experimental and numerical results are compared in term of force vs. displacement in vertical direction and in term of energy dissipation. Only the reinforced panels were taken into consideration because this case is coherent with the strut-and-tie approach..

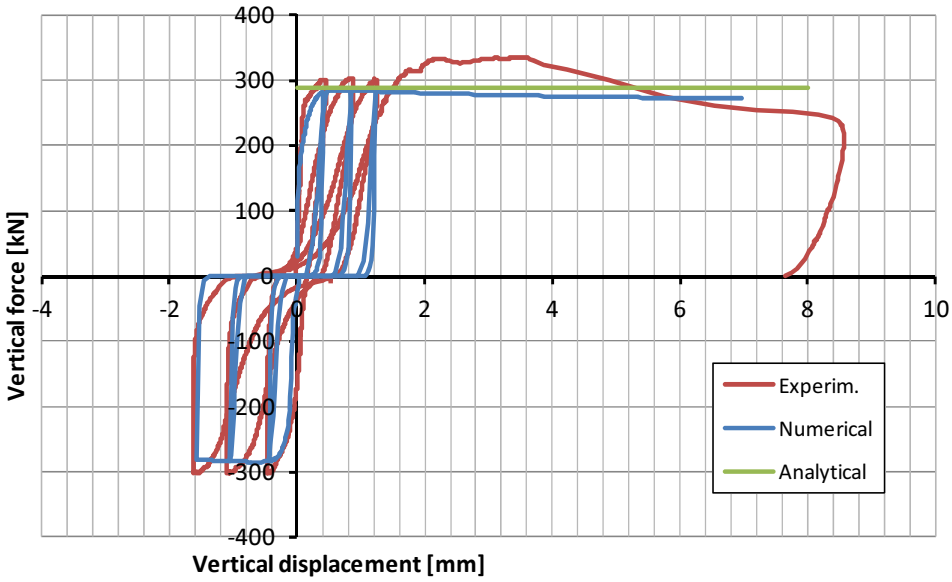

Figure 14-2. N18 ϕ8: force vs. displacement graph

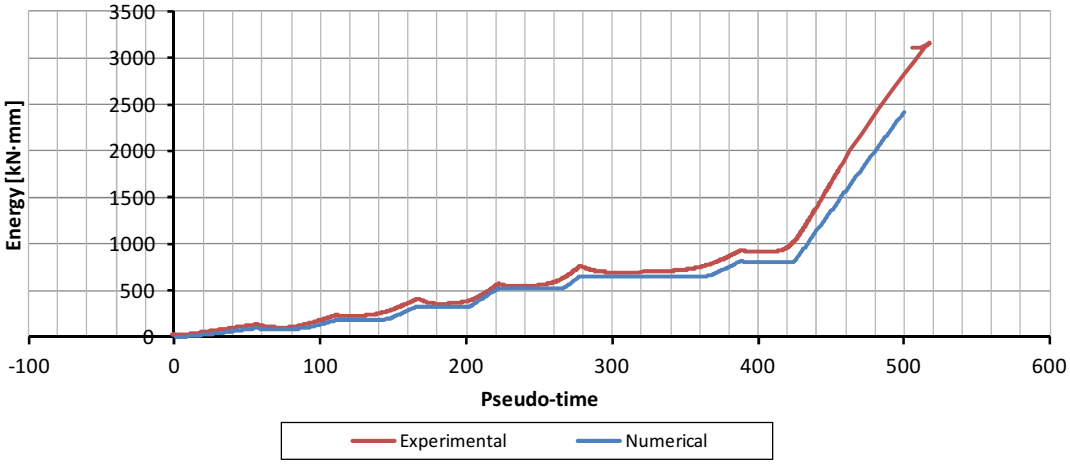

Figure 14-3. N18 ϕ8: Experimental and numerical energy dissipation

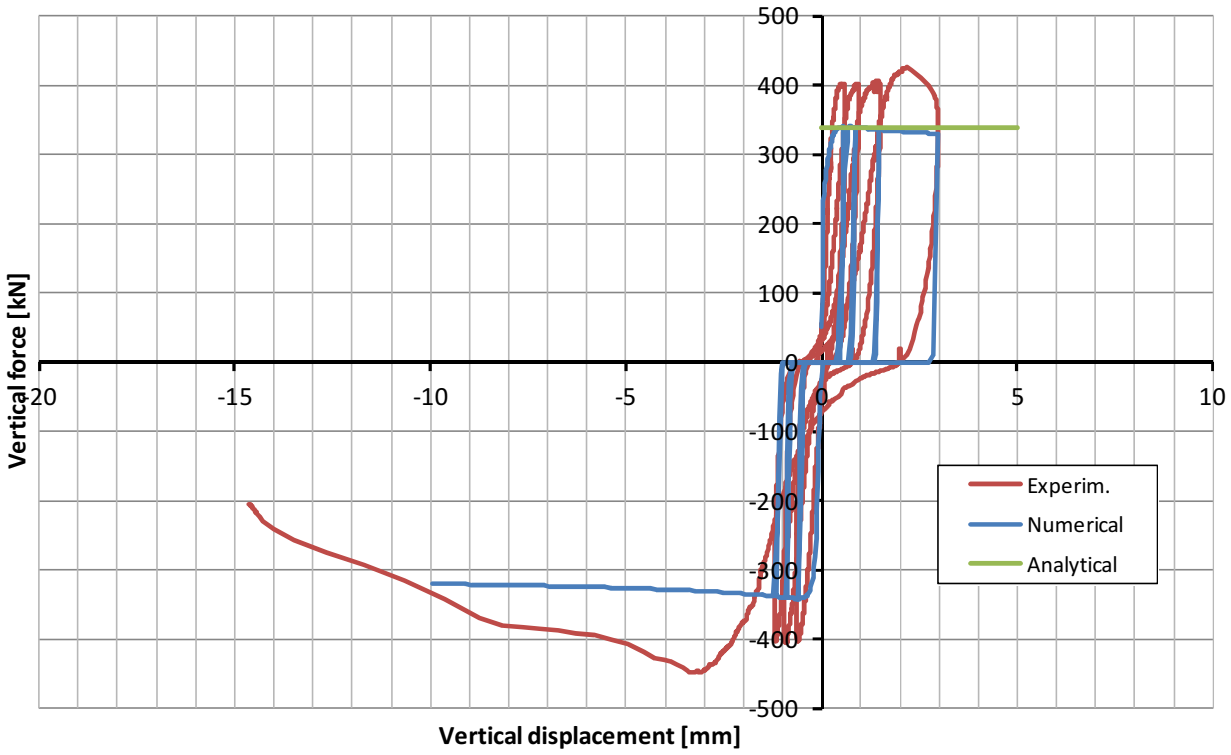

Figure 14-4. N18 ϕ12: force vs. displacement graph

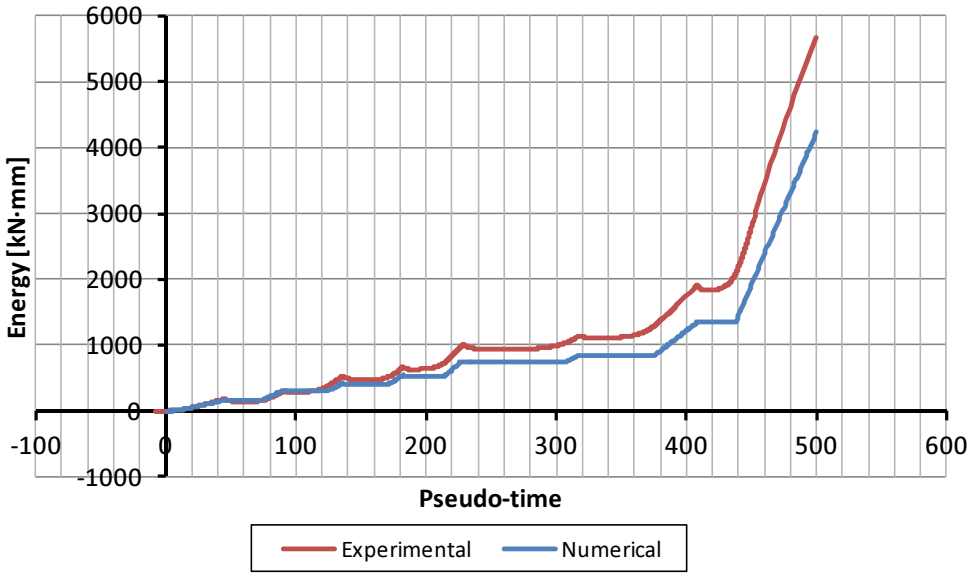

Figure 14-5. N18 ϕ12: Experimental and numerical energy dissipation

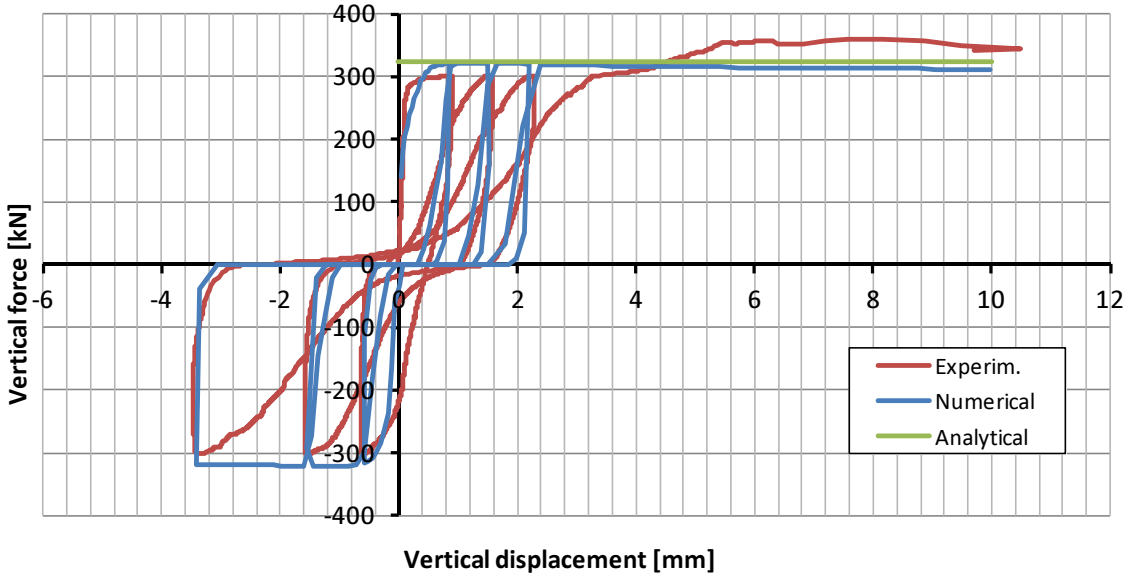

Figure 14-6. N25 ϕ8: force vs. displacement graph

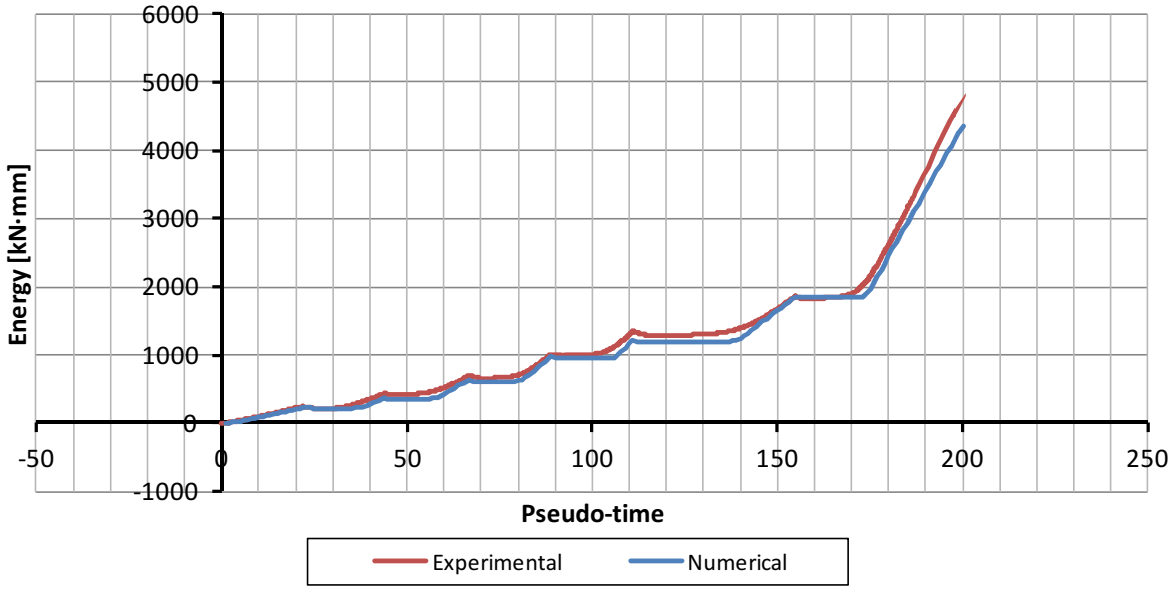

Figure 14-7. N25 ϕ8: Experimental and numerical energy dissipation

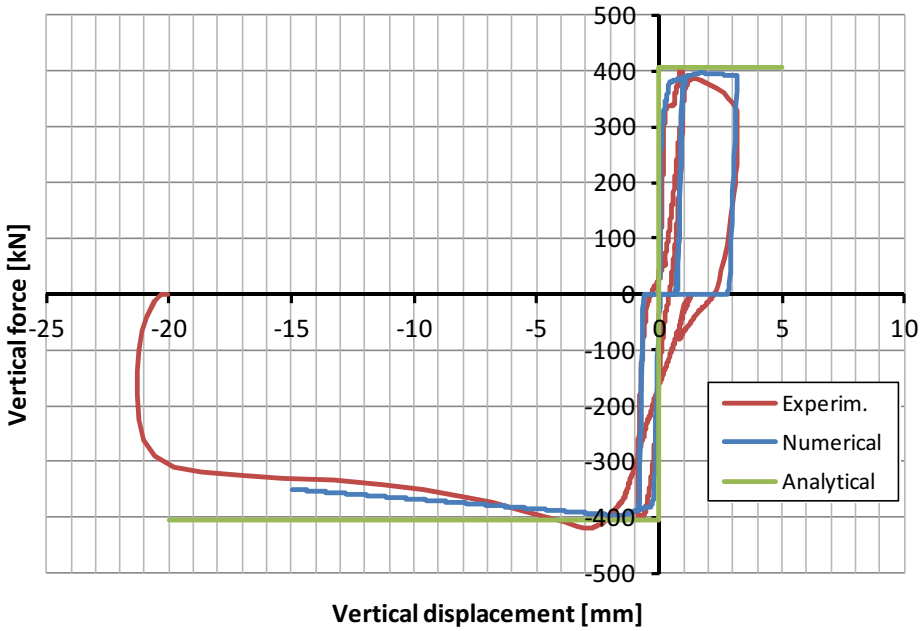

Figure 14-8. N25 ϕ12: force vs. displacement graph

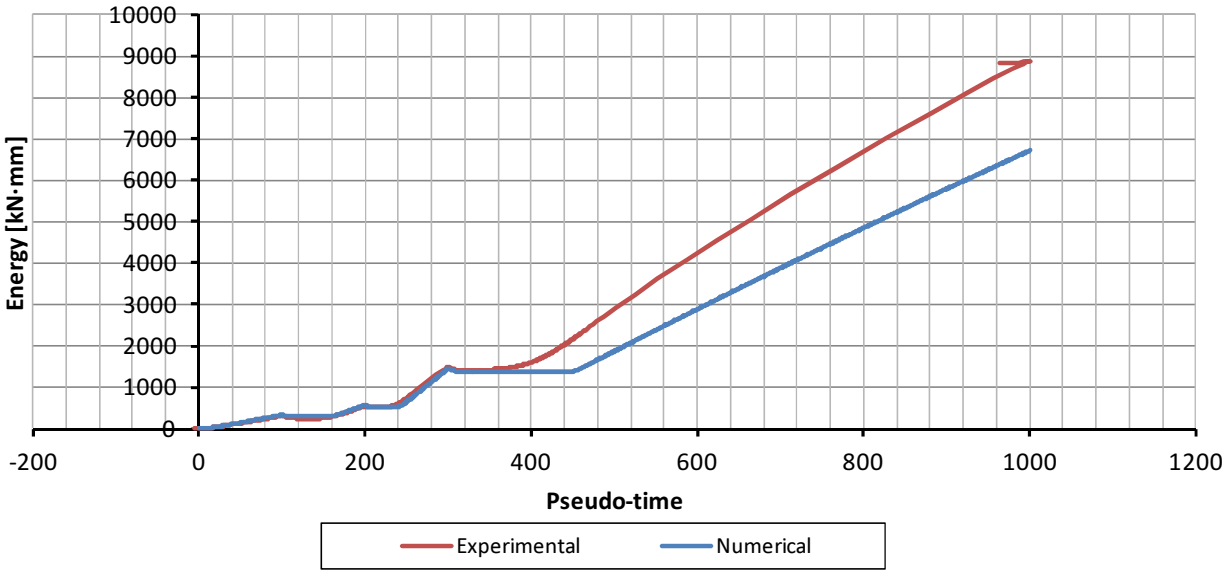

Figure 14-9. N25 ϕ12: Experimental and numerical energy dissipation

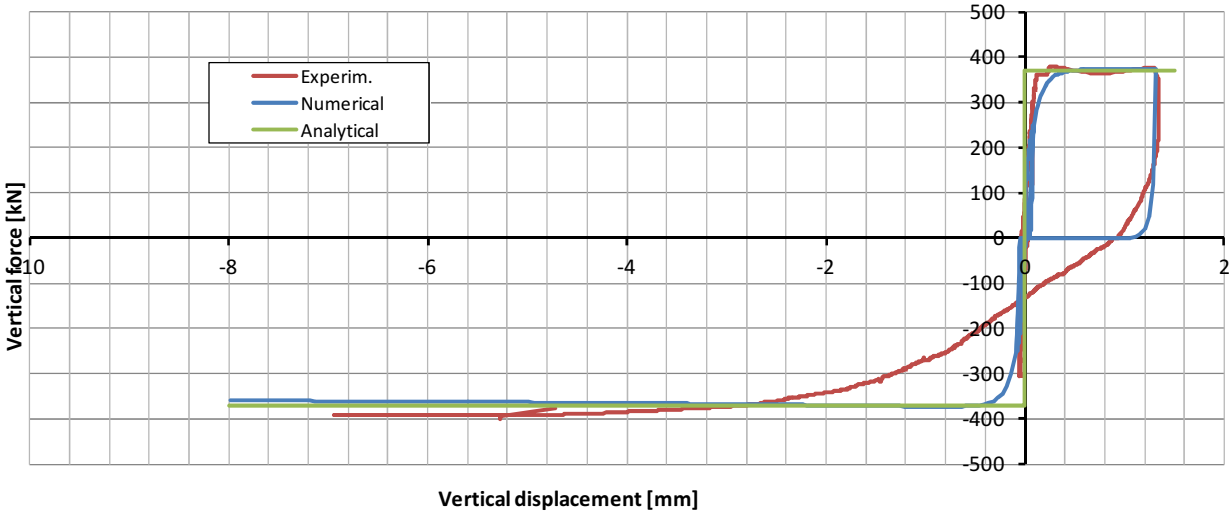

Figure 14-10. I30 ϕ8: force vs. displacement graph

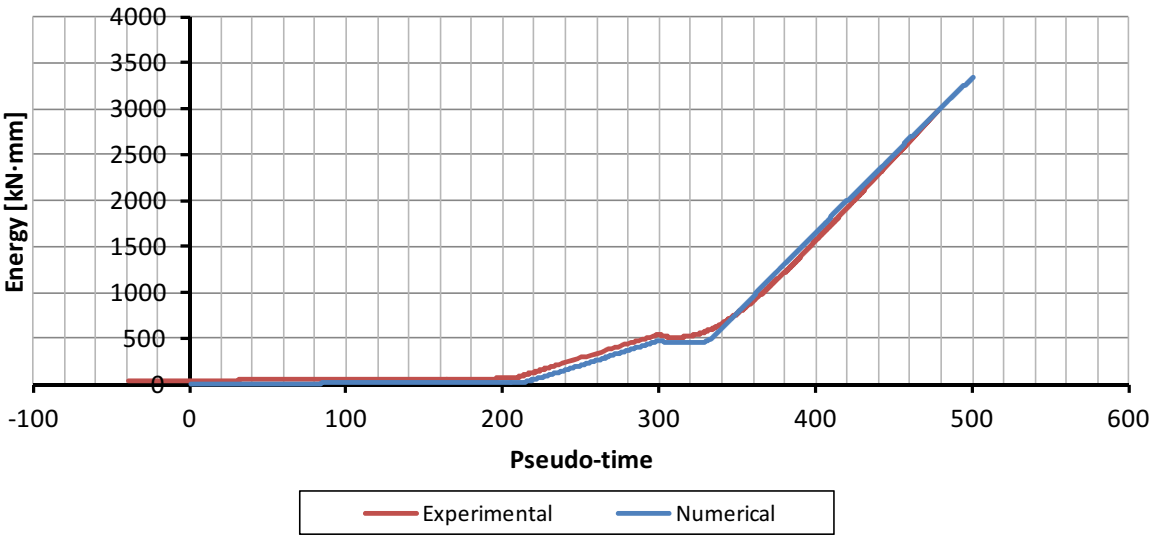

Figure 14-11. I30 ϕ8: Experimental and numerical energy dissipation

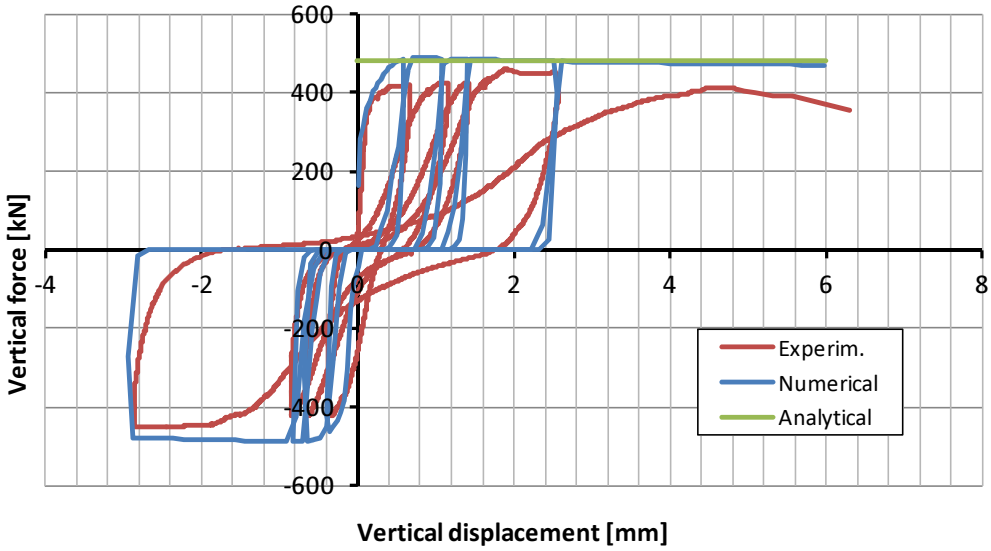

Figure 14-12. I30 ϕ12: force vs. displacement graph

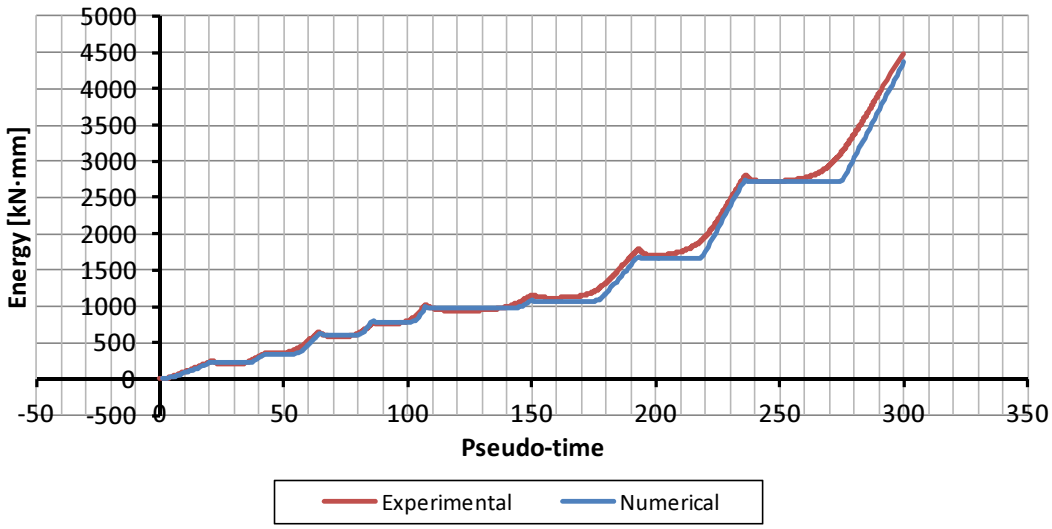

Figure 14-13. I30 ϕ12: Experimental and numerical energy dissipation

In each force vs. displacement graph, the analytical maximum strength is also reported and both numerical and experimental values are always in quite good agreement with such previsions. The comparisons are also good in term of element stiffness being experimental and numerical curves almost juxtaposed in the initial linear elastic branch. The energy dissipation is a very important parameter in seismic analysis at it is always a good practice to compare the results also in terms of this parameter. The energy dissipation is evaluated as the integral of force-displacement curve. It results clear from the experimental curves that, in the unloading phase, there is an elastic recovery testified by the local energy minimums. In the numerical model the unloading is almost vertical with a stiffness very close to the initial one. This generates horizontal branches in the numerical dissipation energy curves, especially in the cycles close to the failure condition.

Chapter 15. – Numerical simulation of tests on simple real scale shearwalls

In this chapter the numerical simulation of tests performed on real scale walls described in chapter 10 is presented. Aim of the simulation is the definitive validation of the numerical model.

15.1. Numerical results and comparisons

Each wall was modeled with a grid of monodimensional elements able to express a nonlinear behavior as described above.

The ribs realized at the two ends of the walls to prevent buckling were modeled as fiber columns with a thickness of 1 meter. The reinforcement was placed in their actual horizontal and vertical direction. The RC floor on the top of the wall was modeled as a continuous beam made of linear elastic material with the concrete Young modulus. In the case of walls with openings the lintel was modeled with the same type of linear elastic beam but with a T cross-section. The dead loads applied on the top of the floor are represented in the model as a constant vertical force of 50 kN applied in the mid-span of the floor. The cyclic shear force was applied in the mid-span of the top linear elastic beam.

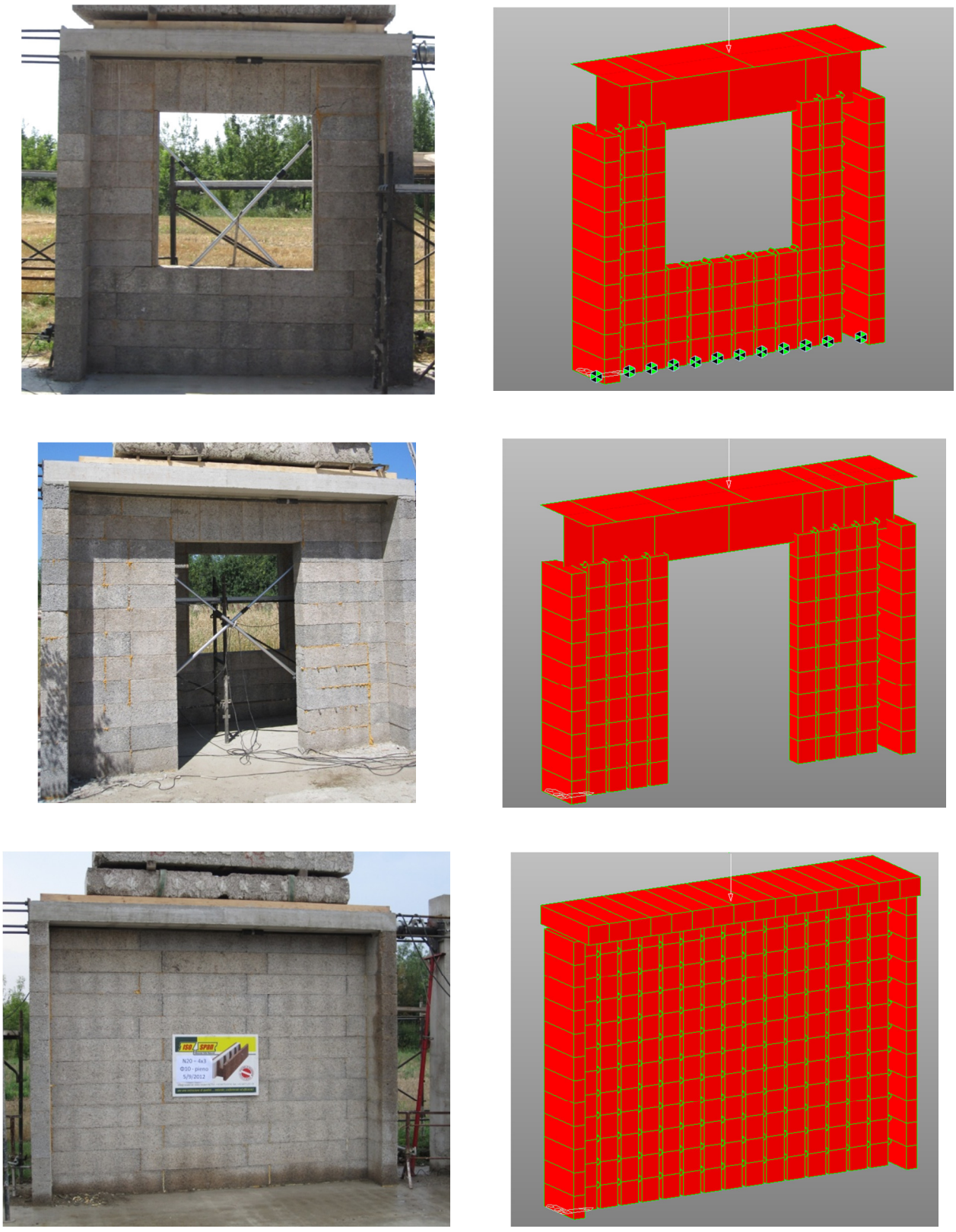

Figure 15-1. General view on wall number 1 (with window), number 2 (with door) and number 5 (without openings): front view of actual specimen (left), model view (right)

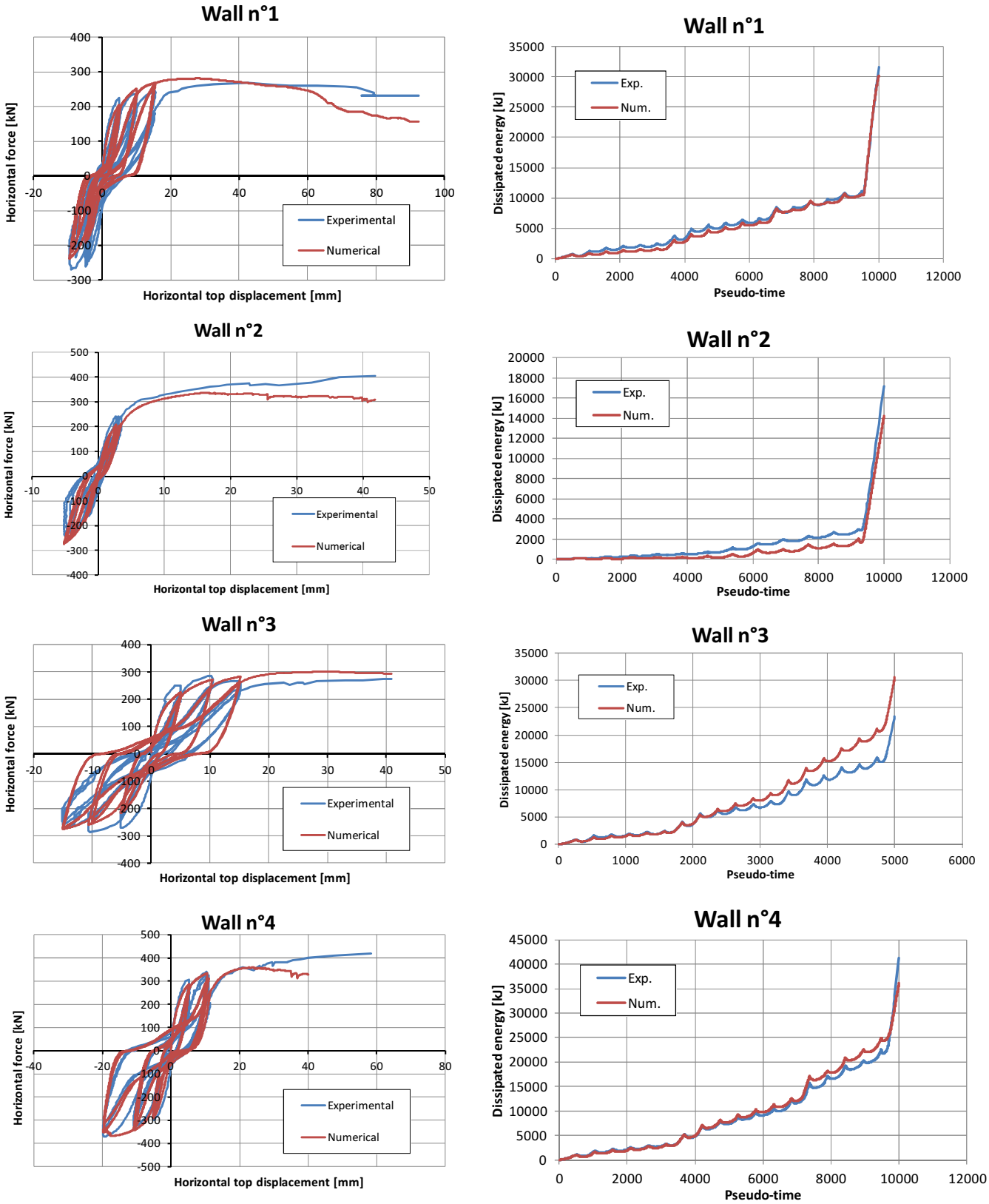

Figure 15-2. Force vs. displacement and dissipated energy vs. pseudo-time curves (walls n°1-4)

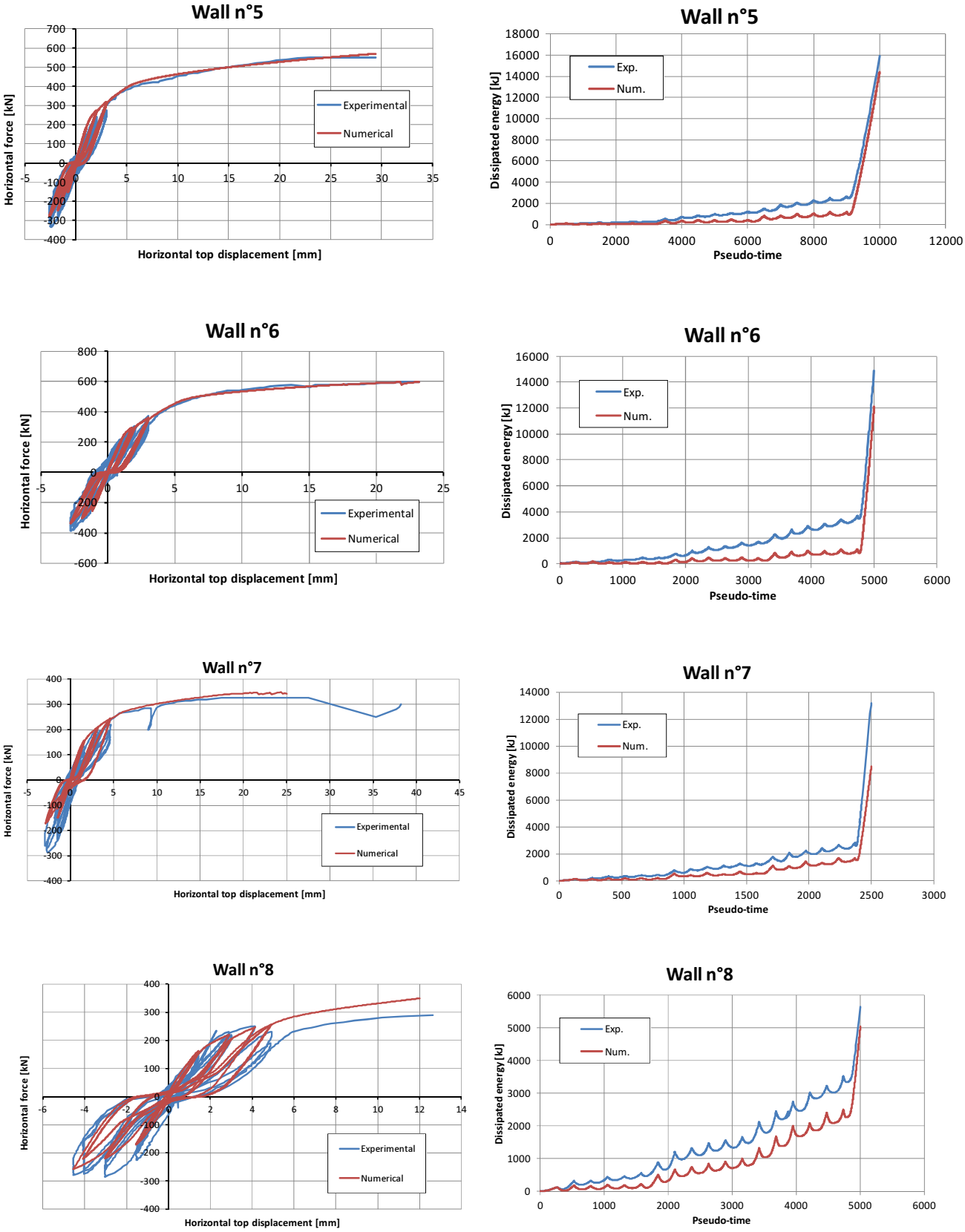

Figure 15-3. Force vs. displacement and dissipated energy vs. pseudo-time curves (walls n°5-8)

These tests evaluate the coherence of numerical modeling with the experiment results in term of hysteric behavior and energy dissipation. In some cases, for example wall number 4, the numerical curve does not reach the same top displacement of the experimental one, because of convergence problems.

Each analysis tries to reach the ultimate experimental displacement, despite the great deformation recorded in the vertical reinforcement. The experimental failure was due to collapse of vertical reinforcement on the actuator side during the last pushing phase. The initial elastic stiffness of the numerical models matches very well the real one. In general, the inelastic branch, clear in all the experiments during the last pushing phase, is very wide in the case of walls with openings. This is due to the large rotation capacity of the plastic hinges at vertical elements ends.

On the other side, the numerical energy dissipation is, in general, conservative if compared with the experimental one, especially in the case of walls without openings. This fact suggests that the model simulates better the energy dissipation due to plastic hinge formation (4 hinges in the case of walls with openings) than the energy dissipation due to internal friction between formwork and RC grid type structure. The model does not take into account the buckling instability of vertical rebars with a developed plastic deformation, typically in the plastic section, between two different loading phases (pushing to pulling or vice versa).

All the experimental hysteretic loops are wider the numerical ones, suggesting a deficiency of the numerical model in the simulation of dissipation energy due to opening and closure of small cracks in the critical sections. This is evident in the case of wall number 6 (without openings) where, even if the hysteretic loops are in the early stage of the displacement range (small cracks, concentrated in one critical section), the real wall is able to dissipate a moderate quantity of energy that is underestimated in the numerical results.

15.2. Conclusions

Although the complexity of the nonlinear model and the variety of elements and plasticity type involved, the numerical results agreed quite well with the experimental ones in terms of maximum shear strength, in terms of displacements and in terms of dissipated energy. All these parameters are very important in the design and in seismic analysis.

The numerical energy dissipation is always conservative in respect to the experimental one, i.e. the model dissipates less than the real wall. There are many effects that can cause this underestimation: e.g. the friction of cracked formwork and the friction between rebars and concrete in the cracked zones.

The good results and robustness of the model permits to increment its complexity in order to model regular and irregular multistory buildings.

Chapter 16. – Numerical analyses of shearwalls

16.1. Description of case studies

The case studies taken as reference in the study on regular buildings has been selected among those built up during the C.A.S.E project for the post-earthquake rebuilding of Abruzzo region – 2009, Italy, described in (AA. VV. 2010), specifically the plan of the three-story building realized by WOOD BETON S.p.a. Company. Figure 16-1 gives some views of the considered buildings.

Figure 16-1. Views of the considered three-story building

The buildings are composed by 4 structurally independent portions with rectangular plan as depicted in Figure 16-1.

Only the lateral portion of the buildings having plan dimensions of 17.5 m x 8.75 m was considered. The inter-story height is equal to 3.05 m. This building portion was realized with Cross-Laminated Timber (CLT) 160 mm thick panels used both for perimeter walls and floors. Floor panels are arranged along the shorter dimension and are supported on the perimeter walls and on an intermediate middle beam. Regarding to the seismic aspects the wall distribution is regular in plan with two seismic resistant walls along the longer side and three seismic resistant walls along the shorter one as shown in Figure 16-2.

Figure 16-2. Plant view of the considered three story building

The wall distribution is symmetrical in both the directions and also the story mass distribution is uniform. Hence the mass center G almost coincides with the stiffness center CR and the torsional effects are negligible.

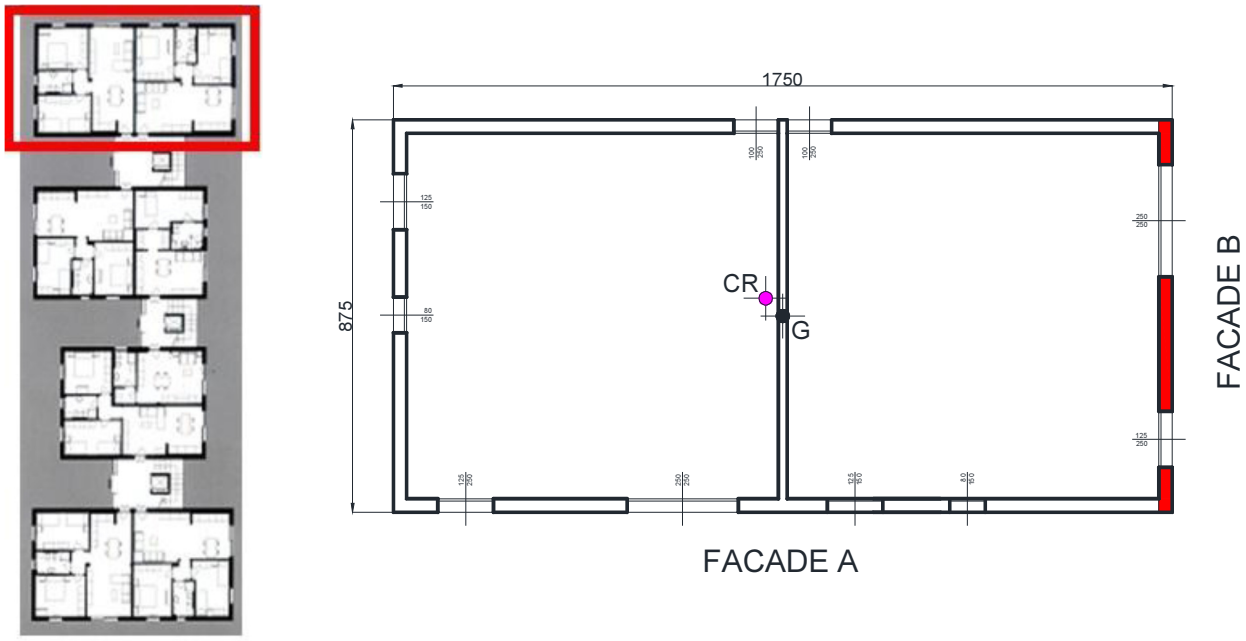

Figure 16-3. Seismic resistant walls distribution with evidenced the walls analyzed with a 2D plane model

Due to the regularity of the building 2D plane models of shearwalls can be used to study the building seismic response along each principal axis of the building. The façade B marked in red in Figure 16-3 was analyzed. The openings distribution on this façade is regular as depicted in the following Figure 16-4. The façade considered was modified in order to generate 3 case studies with different floor number: 3, 4, 5. The seismic response of each case was first analyzed by means of a dynamic linear analysis (modal analysis) and then with static nonlinear (pushover) analyses.

Figure 16-4. Frontal view of the examined façade B

Block type I25 was used to model the façade B and bars Φ12 were used in the horizontal and vertical direction.

16.2. Natural frequency analysis

The mass considered in the model is the self-weight of the structure. The main part of the mass is concentrated at RC floors, that have an influence area of 8.75 x 8.75 m^2.

The natural frequency analysis is useful to identify the modal participating mass for each mode of vibration. The value of the first mode and its eigenvector are used in the pushover analysis. A set of 10 mode were extracted and the results for each building is reported in the following tables.

EIGENVALUE ANALYSIS				
Mode No	Frequency (rad/sec)	Frequency (cycle/sec)	Period (sec)	Tolerance
1	59.4390	9.4600	0.1057	0.0000e+000
2	195.3655	31.0934	0.0322	0.0000e+000
3	344.9018	54.8928	0.0182	0.0000e+000
4	1219.8644	194.1474	0.0052	9.6459e-064
5	1239.9427	197.3430	0.0051	3.9784e-063
6	1307.6624	208.1209	0.0048	2.0017e-060
7	1423.4397	226.5475	0.0044	1.2032e-055
8	1674.3804	266.4859	0.0038	2.0456e-046
9	1721.0444	273.9127	0.0037	2.9369e-043
10	1851.0189	294.5988	0.0034	2.0560e-040

MODAL PARTICIPATION MASSES PRINTOUT												
Mode No	TRAN-X		TRAN-Y		TRAN-Z		ROTN-X		ROTN-Y		ROTN-Z	
	MASS(%)	SUM(%)	MASS(%)	SUM(%)	MASS(%)	SUM(%)	MASS(%)	SUM(%)	MASS(%)	SUM(%)	MASS(%)	SUM(%)
1	83.3551	83.3551	0.0000	0.0000	0.0000	0.0000	0.0000	0.0000	16.9047	16.9047	0.0000	0.0000
2	13.6079	96.9631	0.0000	0.0000	0.0000	0.0000	0.0000	0.0000	70.3865	87.2912	0.0000	0.0000
3	1.7683	98.7314	0.0000	0.0000	0.0000	0.0000	0.0000	0.0000	6.4420	93.7332	0.0000	0.0000
4	0.0004	98.7318	0.0000	0.0000	0.0000	0.0000	0.0000	0.0000	0.0001	93.7333	0.0000	0.0000
5	0.0061	98.7379	0.0000	0.0000	0.0000	0.0000	0.0000	0.0000	0.0345	93.7678	0.0000	0.0000
6	0.0000	98.7379	0.0000	0.0000	0.0000	0.0000	0.0000	0.0000	0.0001	93.7679	0.0000	0.0000
7	0.0224	98.7603	0.0000	0.0000	0.0000	0.0000	0.0000	0.0000	0.1194	93.8873	0.0000	0.0000
8	0.0843	98.8446	0.0000	0.0000	0.0000	0.0000	0.0000	0.0000	0.3732	94.2605	0.0000	0.0000
9	0.0258	98.8703	0.0000	0.0000	0.0000	0.0000	0.0000	0.0000	0.1433	94.4039	0.0000	0.0000
10	0.0196	98.8899	0.0000	0.0000	0.0000	0.0000	0.0000	0.0000	0.1223	94.5261	0.0000	0.0000
Mode No	TRAN-X		TRAN-Y		TRAN-Z		ROTN-X		ROTN-Y		ROTN-Z	
	MASS	SUM	MASS	SUM	MASS	SUM	MASS	SUM	MASS	SUM	MASS	SUM
1	0.1137	0.1137	0.0000	0.0000	0.0000	0.0000	0.0000	0.0000	164693.55	164693.55	0.0000	0.0000
2	0.0186	0.1323	0.0000	0.0000	0.0000	0.0000	0.0000	0.0000	685740.54	850434.09	0.0000	0.0000
3	0.0024	0.1347	0.0000	0.0000	0.0000	0.0000	0.0000	0.0000	62761.325	913195.42	0.0000	0.0000
4	0.0000	0.1347	0.0000	0.0000	0.0000	0.0000	0.0000	0.0000	1.3822	913196.80	0.0000	0.0000
5	0.0000	0.1347	0.0000	0.0000	0.0000	0.0000	0.0000	0.0000	335.9941	913532.80	0.0000	0.0000
6	0.0000	0.1347	0.0000	0.0000	0.0000	0.0000	0.0000	0.0000	0.5434	913533.34	0.0000	0.0000
7	0.0000	0.1347	0.0000	0.0000	0.0000	0.0000	0.0000	0.0000	1163.6474	914696.99	0.0000	0.0000
8	0.0001	0.1348	0.0000	0.0000	0.0000	0.0000	0.0000	0.0000	3635.9000	918332.89	0.0000	0.0000
9	0.0000	0.1349	0.0000	0.0000	0.0000	0.0000	0.0000	0.0000	1396.4733	919729.36	0.0000	0.0000
10	0.0000	0.1349	0.0000	0.0000	0.0000	0.0000	0.0000	0.0000	1191.4510	920920.81	0.0000	0.0000

Table 16-1. Results of natural frequency analysis: 3 stories building

EIGENVALUE ANALYSIS

Mode No	Frequency (rad/sec)	Frequency (cycle/sec)	Period (sec)	Tolerance
1	42.3698	6.7434	0.1483	0.0000e+000
2	144.6664	23.0244	0.0434	0.0000e+000
3	272.5443	43.3768	0.0231	0.0000e+000
4	370.0295	58.8920	0.0170	0.0000e+000
5	1244.7688	198.1096	0.0050	2.2641e-062
6	1394.7290	221.9780	0.0045	9.3293e-056
7	1554.5364	247.4122	0.0040	5.8147e-049
8	1739.3804	276.8310	0.0036	5.9791e-041
9	1777.4394	282.8883	0.0035	2.3094e-039
10	1801.5264	286.7218	0.0035	1.7406e-038

MODAL PARTICIPATION MASSES PRINTOUT

Mode No	TRAN-X		TRAN-Y		TRAN-Z		ROTN-X		ROTN-Y		ROTN-Z	
	MASS(%)	SUM(%)	MASS(%)	SUM(%)	MASS(%)	SUM(%)	MASS(%)	SUM(%)	MASS(%)	SUM(%)	MASS(%)	SUM(%)
1	79.3752	79.3752	0.0000	0.0000	0.0000	0.0000	0.0000	0.0000	0.0015	0.0015	0.0000	0.0000
2	16.0695	95.4447	0.0000	0.0000	0.0000	0.0000	0.0000	0.0000	34.0698	34.0713	0.0000	0.0000
3	3.0038	98.4484	0.0000	0.0000	0.0000	0.0000	0.0000	0.0000	55.8738	89.9452	0.0000	0.0000
4	0.6147	99.0632	0.0000	0.0000	0.0000	0.0000	0.0000	0.0000	0.2538	90.1990	0.0000	0.0000
5	0.0001	99.0632	0.0000	0.0000	0.0000	0.0000	0.0000	0.0000	0.0041	90.2030	0.0000	0.0000
6	0.0065	99.0697	0.0000	0.0000	0.0000	0.0000	0.0000	0.0000	0.3702	90.5733	0.0000	0.0000
7	0.0358	99.1055	0.0000	0.0000	0.0000	0.0000	0.0000	0.0000	0.0506	90.6239	0.0000	0.0000
8	0.0189	99.1244	0.0000	0.0000	0.0000	0.0000	0.0000	0.0000	0.2229	90.8468	0.0000	0.0000
9	0.0133	99.1378	0.0000	0.0000	0.0000	0.0000	0.0000	0.0000	0.3263	91.1731	0.0000	0.0000
10	0.0413	99.1791	0.0000	0.0000	0.0000	0.0000	0.0000	0.0000	0.2889	91.4620	0.0000	0.0000

Mode No	TRAN-X		TRAN-Y		TRAN-Z		ROTN-X		ROTN-Y		ROTN-Z	
	MASS	SUM	MASS	SUM	MASS	SUM	MASS	SUM	MASS	SUM	MASS	SUM
1	0.1445	0.1445	0.0000	0.0000	0.0000	0.0000	0.0000	0.0000	20.2607	20.2607	0.0000	0.0000
2	0.0293	0.1738	0.0000	0.0000	0.0000	0.0000	0.0000	0.0000	466002.43	466022.69	0.0000	0.0000
3	0.0055	0.1793	0.0000	0.0000	0.0000	0.0000	0.0000	0.0000	764234.75	1230257.4	0.0000	0.0000
4	0.0011	0.1804	0.0000	0.0000	0.0000	0.0000	0.0000	0.0000	3471.6771	1233729.1	0.0000	0.0000
5	0.0000	0.1804	0.0000	0.0000	0.0000	0.0000	0.0000	0.0000	55.7112	1233784.8	0.0000	0.0000
6	0.0000	0.1804	0.0000	0.0000	0.0000	0.0000	0.0000	0.0000	5063.7292	1238848.5	0.0000	0.0000
7	0.0001	0.1805	0.0000	0.0000	0.0000	0.0000	0.0000	0.0000	692.0370	1239540.6	0.0000	0.0000
8	0.0000	0.1805	0.0000	0.0000	0.0000	0.0000	0.0000	0.0000	3048.9632	1242589.5	0.0000	0.0000
9	0.0000	0.1805	0.0000	0.0000	0.0000	0.0000	0.0000	0.0000	4463.0811	1247052.6	0.0000	0.0000
10	0.0001	0.1806	0.0000	0.0000	0.0000	0.0000	0.0000	0.0000	3951.7634	1251004.4	0.0000	0.0000

Table 16-2. Results of natural frequency analysis: 4 stories building

EIGENVALUE ANALYSIS

Mode No	Frequency (rad/sec)	Frequency (cycle/sec)	Period (sec)	Tolerance
1	31.0914	4.9483	0.2021	0.0000e+000
2	110.7394	17.6247	0.0567	0.0000e+000
3	216.0356	34.3831	0.0291	0.0000e+000
4	310.3200	49.3890	0.0202	0.0000e+000
5	381.8821	60.7784	0.0165	0.0000e+000
6	1218.6935	193.9611	0.0052	7.8709e-042
7	1223.7679	194.7687	0.0051	6.2763e-041
8	1237.8016	197.0022	0.0051	2.1595e-040
9	1266.1336	201.5114	0.0050	4.8601e-040
10	1316.4609	209.5213	0.0048	8.6117e-037

MODAL PARTICIPATION MASSES PRINTOUT

Mode No	TRAN-X		TRAN-Y		TRAN-Z		ROTN-X		ROTN-Y		ROTN-Z	
	MASS(%)	SUM(%)	MASS(%)	SUM(%)	MASS(%)	SUM(%)	MASS(%)	SUM(%)	MASS(%)	SUM(%)	MASS(%)	SUM(%)
1	76.8379	76.8379	0.0000	0.0000	0.0000	0.0000	0.0000	0.0000	23.3232	23.3232	0.0000	0.0000
2	17.1559	93.9938	0.0000	0.0000	0.0000	0.0000	0.0000	0.0000	56.5084	79.8316	0.0000	0.0000
3	3.8010	97.7948	0.0000	0.0000	0.0000	0.0000	0.0000	0.0000	11.5078	91.3393	0.0000	0.0000
4	1.1913	98.9861	0.0000	0.0000	0.0000	0.0000	0.0000	0.0000	4.7098	96.0491	0.0000	0.0000
5	0.2547	99.2408	0.0000	0.0000	0.0000	0.0000	0.0000	0.0000	0.9086	96.9577	0.0000	0.0000
6	0.0000	99.2408	0.0000	0.0000	0.0000	0.0000	0.0000	0.0000	0.0001	96.9577	0.0000	0.0000
7	0.0007	99.2415	0.0000	0.0000	0.0000	0.0000	0.0000	0.0000	0.0023	96.9600	0.0000	0.0000
8	0.0017	99.2432	0.0000	0.0000	0.0000	0.0000	0.0000	0.0000	0.0061	96.9661	0.0000	0.0000
9	0.0011	99.2443	0.0000	0.0000	0.0000	0.0000	0.0000	0.0000	0.0050	96.9711	0.0000	0.0000
10	0.0001	99.2444	0.0000	0.0000	0.0000	0.0000	0.0000	0.0000	0.0002	96.9713	0.0000	0.0000

Mode No	TRAN-X		TRAN-Y		TRAN-Z		ROTN-X		ROTN-Y		ROTN-Z	
	MASS	SUM	MASS	SUM	MASS	SUM	MASS	SUM	MASS	SUM	MASS	SUM
1	0.1750	0.1750	0.0000	0.0000	0.0000	0.0000	0.0000	0.0000	1102352.0	1102352.0	0.0000	0.0000
2	0.0391	0.2141	0.0000	0.0000	0.0000	0.0000	0.0000	0.0000	2670827.3	3773179.4	0.0000	0.0000
3	0.0087	0.2227	0.0000	0.0000	0.0000	0.0000	0.0000	0.0000	543906.51	4317085.9	0.0000	0.0000
4	0.0027	0.2254	0.0000	0.0000	0.0000	0.0000	0.0000	0.0000	222602.85	4539688.8	0.0000	0.0000
5	0.0006	0.2260	0.0000	0.0000	0.0000	0.0000	0.0000	0.0000	42942.492	4582631.3	0.0000	0.0000
6	0.0000	0.2260	0.0000	0.0000	0.0000	0.0000	0.0000	0.0000	3.8187	4582635.1	0.0000	0.0000
7	0.0000	0.2260	0.0000	0.0000	0.0000	0.0000	0.0000	0.0000	109.1814	4582744.3	0.0000	0.0000
8	0.0000	0.2260	0.0000	0.0000	0.0000	0.0000	0.0000	0.0000	286.9555	4583031.2	0.0000	0.0000
9	0.0000	0.2260	0.0000	0.0000	0.0000	0.0000	0.0000	0.0000	236.2630	4583267.5	0.0000	0.0000
10	0.0000	0.2260	0.0000	0.0000	0.0000	0.0000	0.0000	0.0000	9.6120	4583277.1	0.0000	0.0000

Table 16-3. Results of natural frequency analysis: 5 stories building

The interesting values are reported on the left column and regard the translational motion in X direction, the seismic direction.

For each mode also the eigenvector is computed. Particularly important is the first eigenvector that will be used as load pattern in the pushover analysis.

16.3. Pushover analysis

Figure 16-5 shows a view of the model regarding the cases studied. The reference axes are: X in the horizontal direction and Z in the vertical direction. This is a 2D model and in the figure are also shown the width of the mono-dimensional elements used in the simulation. For example the lintels have a section width of 8.75 m and a fine mesh with a characteristic length of 25 cm is used in order to connect each vertical element of the wall with the corresponding lintel above. No two-dimensional element has been used in the modeling.

Two force distributions were used in order to perform the pushover simulations: one proportional to the masses and the other proportional to the first eigenvector. The structure has not a vertical axis of symmetry and nonlinear laws are involved for materials, therefore the pushover analysis has been performed in positive and negative direction of the horizontal X axis.

This is the classical procedure explained by (Eurocode 8 2004) and by (NTC 2008).

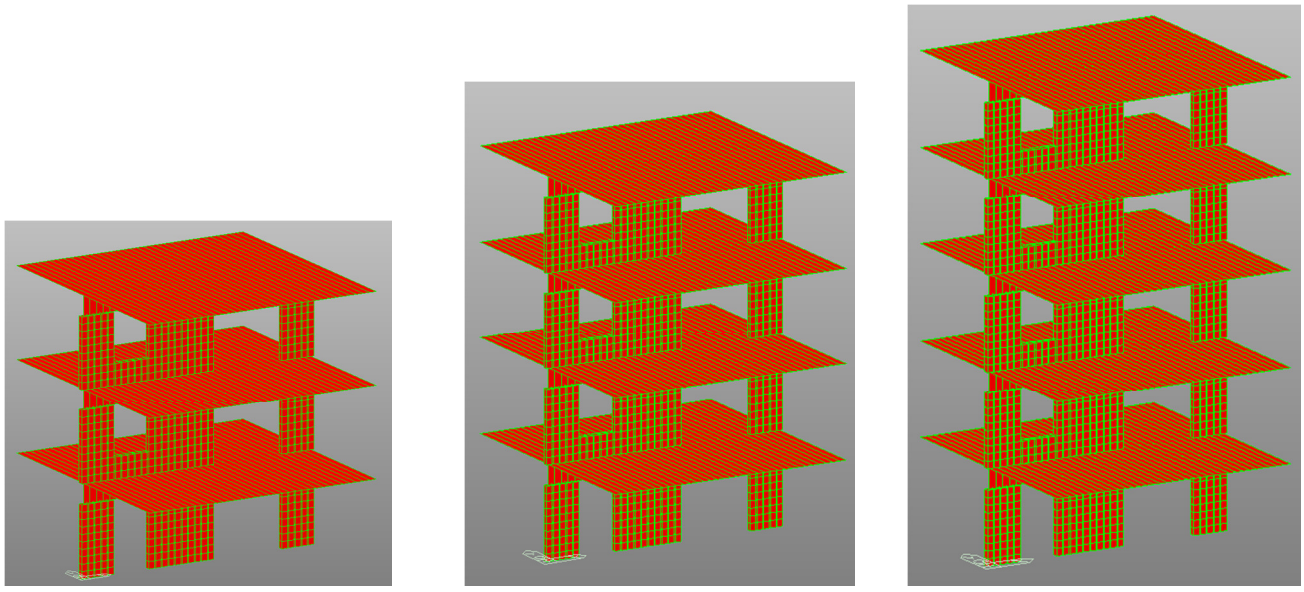

Figure 16-5. The cases studied: 3, 4 and 5 stories buildings

The other 4 and 5 stories buildings were generated copying the last floor above the roof.

The following graphs reports the numerical curves regarding base shear force vs. top displacement.

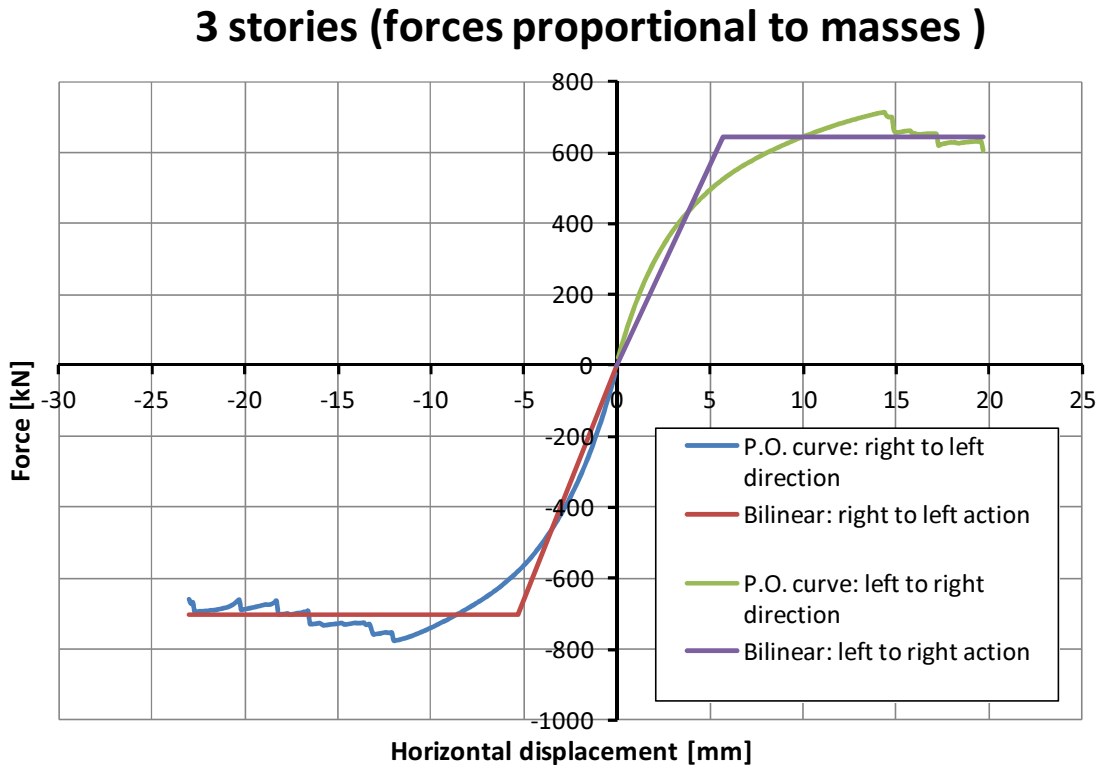

Figure 16-6. Base shear force vs. top displacement (3 stories, forces proportional to masses)

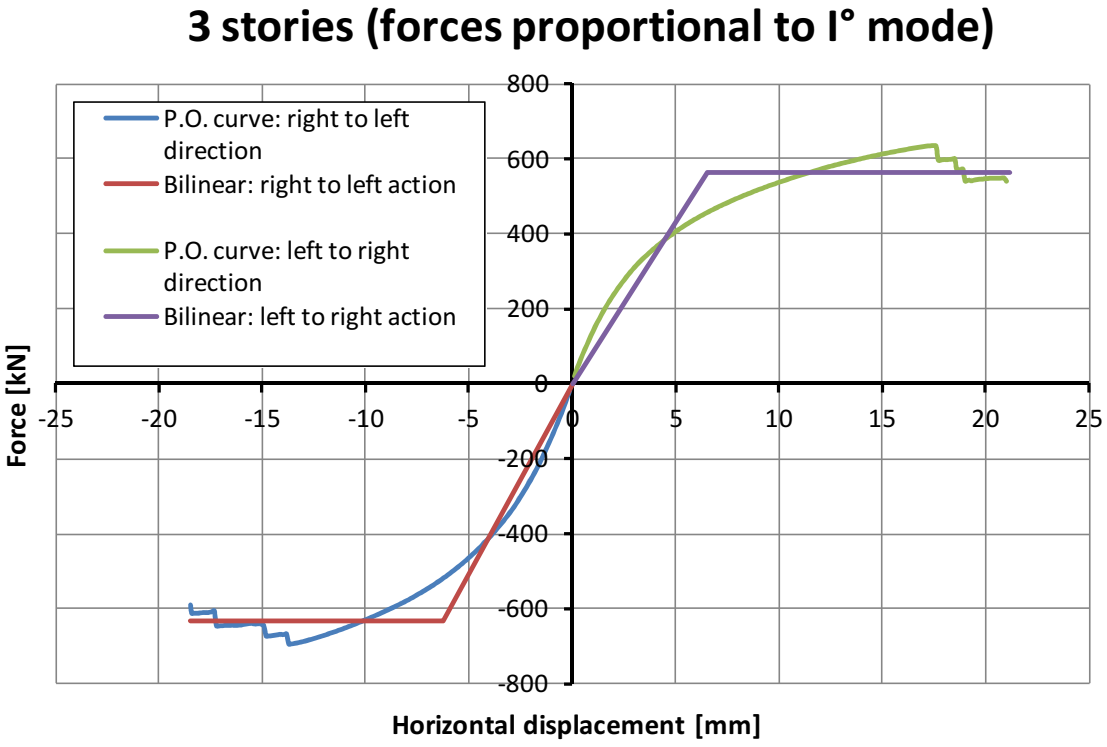

Figure 16-7. Base shear force vs. top displacement (3 stories, forces proportional to I° mode)

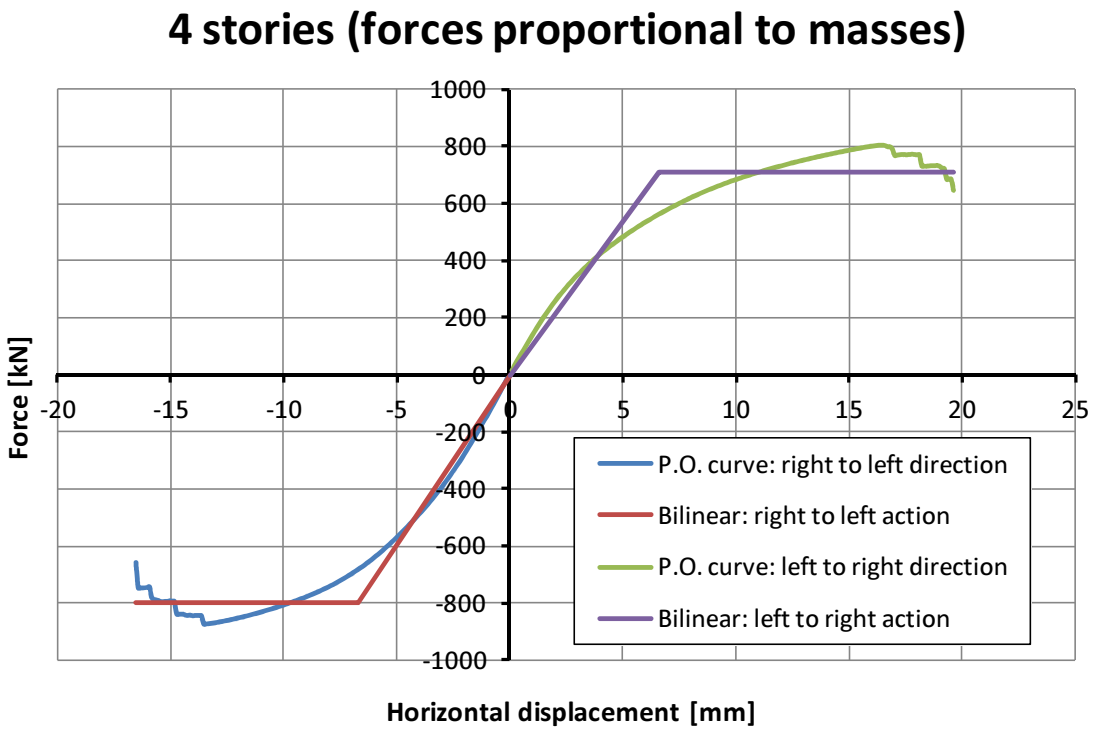

Figure 16-8. Base shear force vs. top displacement (4 stories, forces proportional to masses)

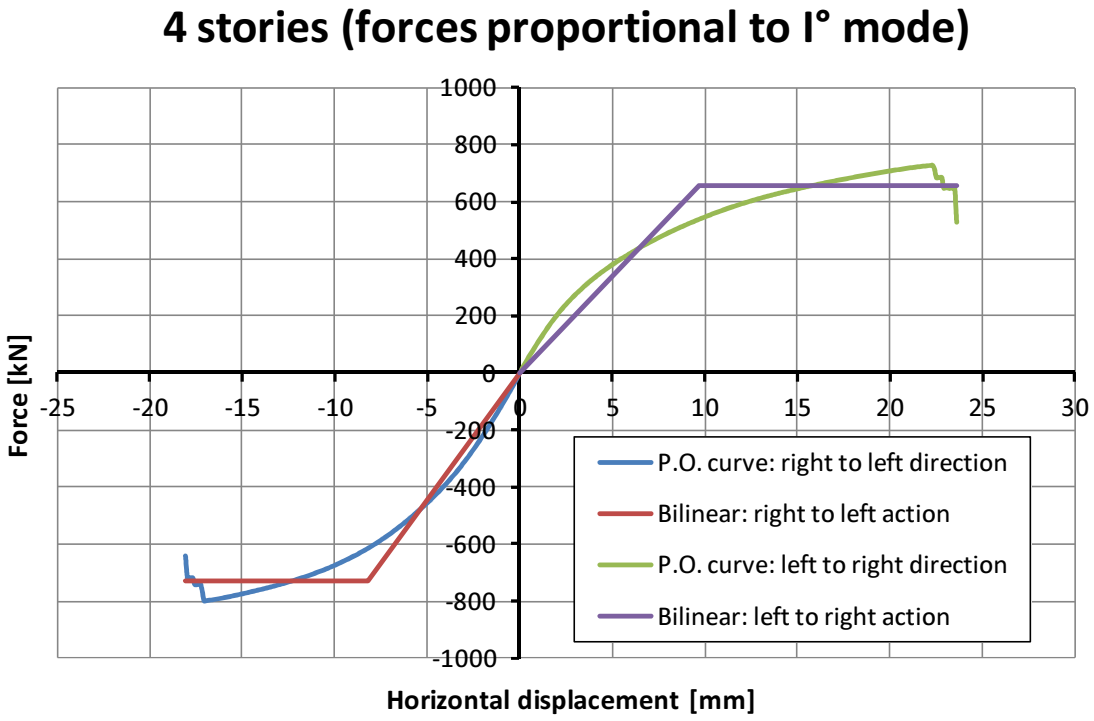

Figure 16-9. Base shear force vs. top displacement (4 stories, forces proportional to I° mode)

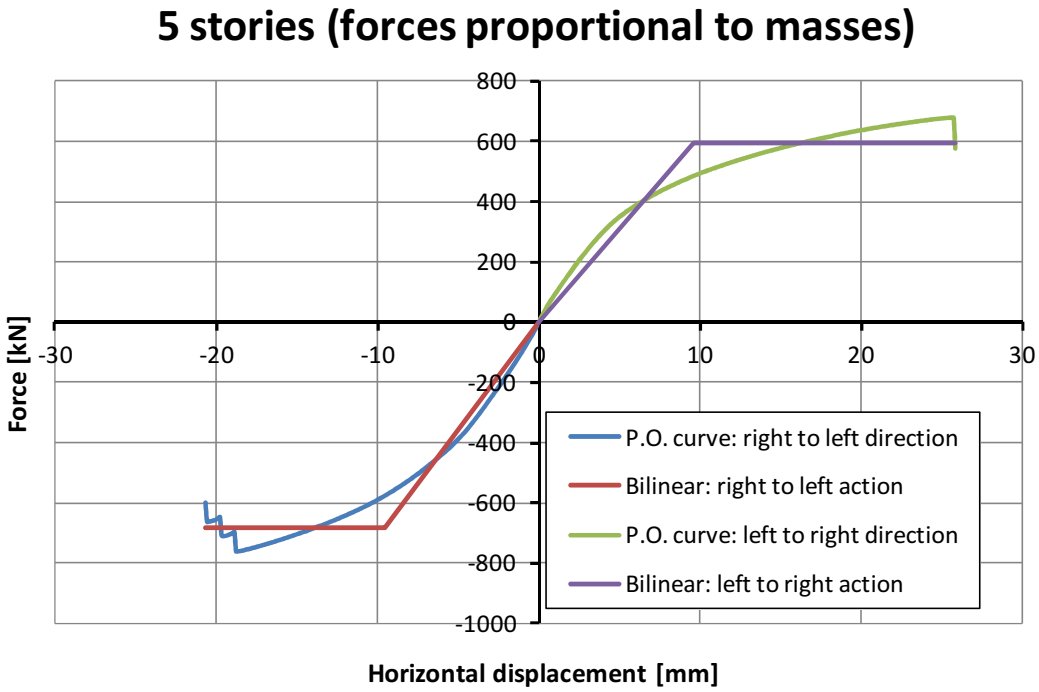

Figure 16-10. Base shear force vs. top displacement (5 stories, forces proportional to masses)

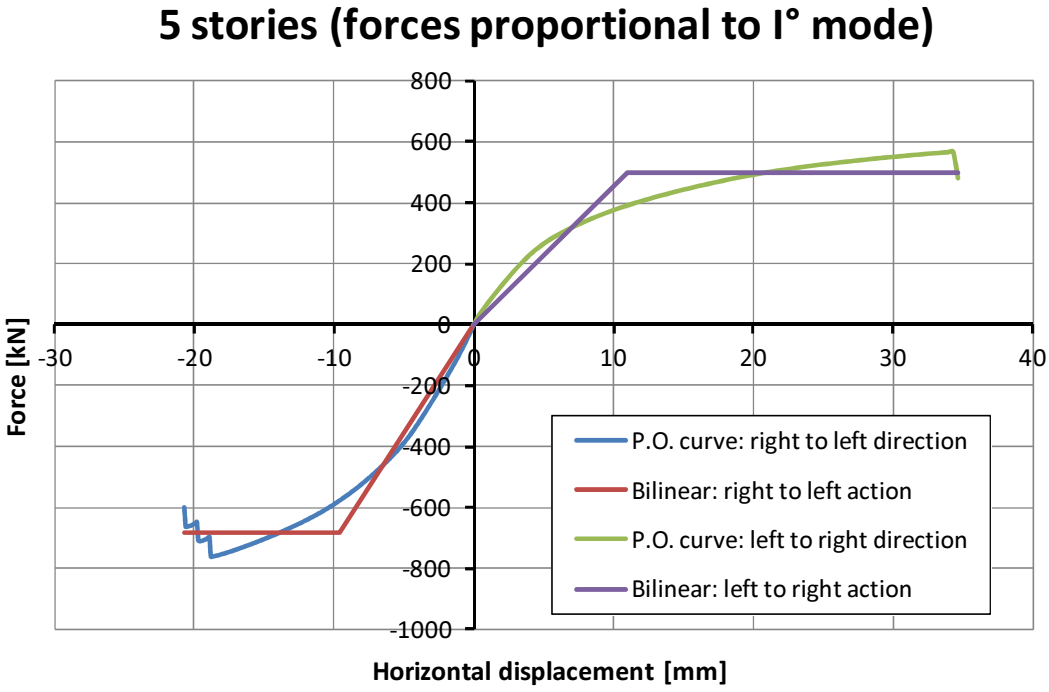

Figure 16-11. Base shear force vs. top displacement (5 stories, forces proportional to I° mode)

The simulation was interrupted when the base shear is equal to 0.85 F_{max}, where F_{max} is the peak shear strength of the capacity curve. This is assumed as failure condition, even if the numerical horizontal displacement can overcome this limit.

The axial stiffness and strength of elements govern the behavior of this kind of structures characterized by a micro-frame internal RC pattern. The bending moment on the single element is very small and the bending moment on wall section can be viewed as a sum of axial forces on the vertical elements. For this reason, an important parameter is the axial deformation of elements.

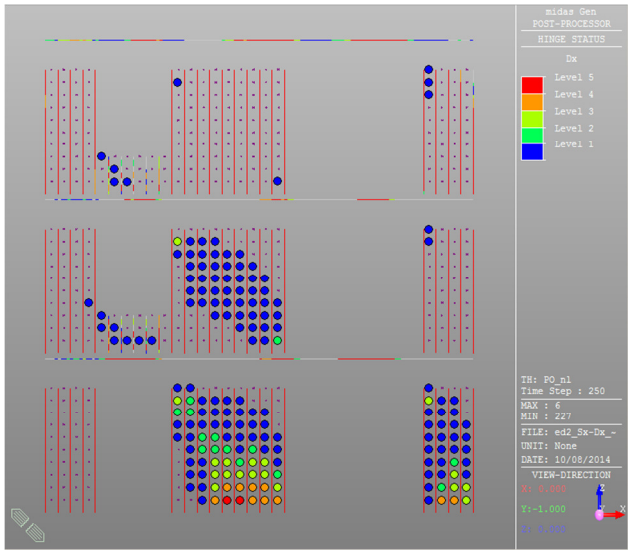

Figure 16-12. Axial compression deformations: 3 stories building

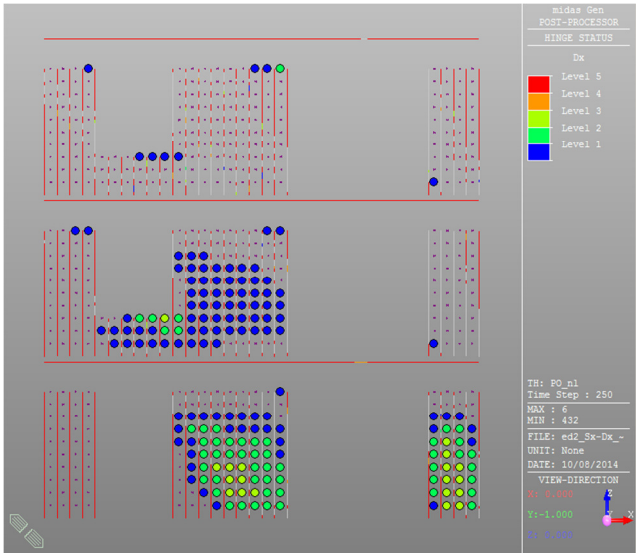

Figure 16-13. Axial tension deformations: 3 stories building

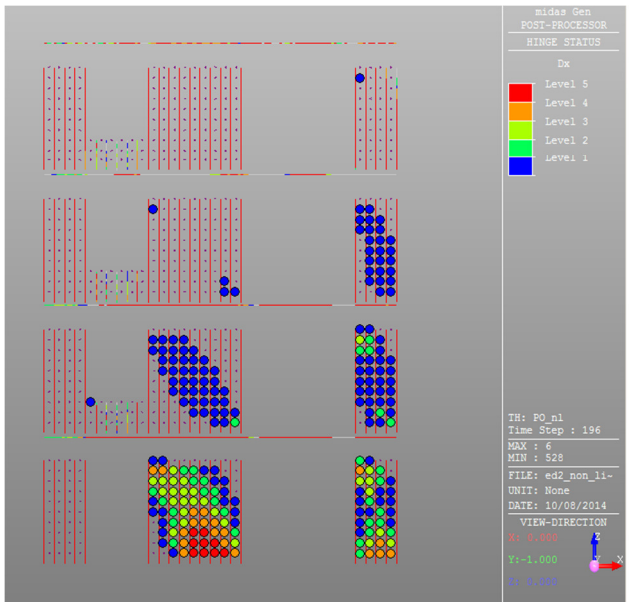

Figure 16-14. Axial compression deformations: 4 stories building

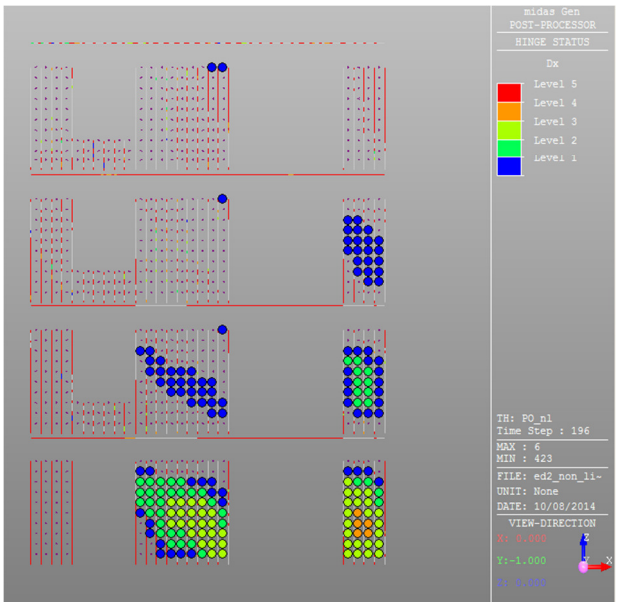

Figure 16-15. Axial tension deformations: 4 stories building

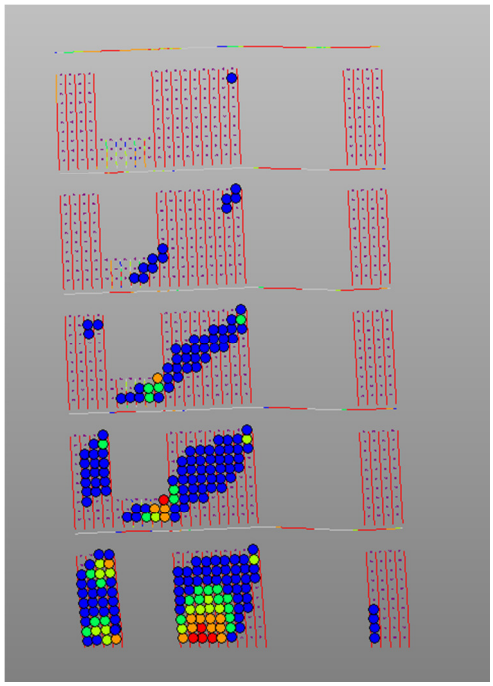

Figure 16-16. Axial compression deformations: 5 stories building

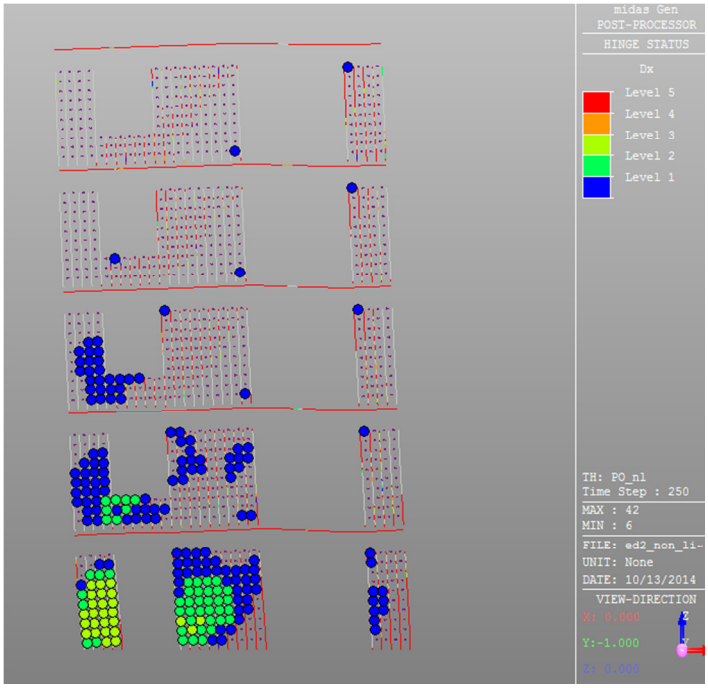

Figure 16-17 Axial tension deformations: 5 stories building

The figures above show the axial deformations (in tension and compression) of columns and transverses, where the compressed element is the strut and the tensioned element is the tie. The contour maps are referred to 5 level of deformations. In all these cases the transverses remain linear, and the main part of the vertical elements overcomes the fifth level of deformation and develops plastic deformations, both in concrete and in steel.

In any case, considering the squat walls with the greater vertical load (e.g. the central wall at ground floor), it is clear the formation of a diagonal band of transverses where is concentrated the higher deformations. This is the same behavior experienced in the case of masonry walls with high compression levels, in this case a shear failure occurs with diagonal cracks.

16.4. Evaluation of q-factor

The evaluation of q-factor uses the pushover curves showed in the chapter above. According to (NTC 2008) the numerical pushover curves are interrupted when the base shear force in the descending branch is equal to the 85% of the peak reached in the ascending branch, F_{max}. Implicitly this is the failure condition assumed. The bilinear passes through $0.6F_{max}$ so the initial stiffness is fixed. F_y, i.e. the plateau value, is found in order to bound the same area of the pushover curve. M_1^* is the modal participation mass of the fundamental mode and the period T^* is calculated with [16.1]:

$$T^* = 2\pi\sqrt{\frac{M^*}{k^*}} \qquad [16.1]$$

M* is the total mass in the case of force distribution proportional to the masses and M_1* in the case of force distribution proportional to the first mode.

The ductility μ* is the ratio between the ultimate and the yielding displacement. The behavior factor is computed with the Vidic's formula:

$$q^* = (\mu^* - 1)\cdot\frac{T^*}{T_C} + 1 \qquad [16.2]$$

because the T^* period is always lesser than 0.4 seconds, the T_C value. This is a typical value for a type 1 elastic spectrum with a ground type A (see Table 3.2 of EC8).

Table 16-4 summarizes the results of q-factor evaluation procedure.

N° of floors	Total mass [ton]	M_1* [%]	M_1* [ton]	Force distribution	Force direction	k* [kN/mm]	T* [sec]	μ*	q*
3	136.6	83.36	113.7	prop. to masses	Right-left	131.6	0.202	4.30	2.67
					Left-right	113.5	0.218	3.46	2.34
				prop. to I° mode	Right-left	102.0	0.210	2.96	2.03
					Left-right	86.3	0.228	3.26	2.29
4	182.3	79.38	144.7	prop. to masses	Right-left	119.1	0.246	2.45	1.89
					Left-right	107.8	0.258	2.97	2.27
				prop. to I° mode	Right-left	88.9	0.254	2.20	1.76
					Left-right	67.9	0.290	2.44	2.04
5	228	76.84	175.2	prop. to masses	Right-left	71.5	0.355	2.16	2.03
					Left-right	61.7	0.382	2.67	2.60
				prop. to I° mode	Right-left	71.5	0.311	2.16	1.90
					Left-right	45.3	0.391	3.14	3.10
							Mean value	2.849	2.244

Table 16-4. Q factor evaluation in the 2D cases by means of pushover analysis

On one hand with a moderate number of stories, 3 for example, the ductility increases because the vertical elements do not reach suddenly a concrete failure; on the other hand increasing the number of stories, 5 for example, the collapse on concrete occurs before but there is an increment in the mass and so in the T^* value that approaches the T_C period. If T^* would be equal to T_C the ductility would be equal to q-factor, this occurs after the acceleration sensitive field delimited by T_C (see (Chopra 1995)).

16.5. Modal analysis of equivalent frame

In analogy with the R_μ factor described in §5.1, q* can be considered as a basic behavior factor that must be multiplied by the overstrength factor Ω_d defined by [5.3]. For each case (3, 4 and 5 stories) an equivalent frame was modeled in order to define the design base shear force V_d. The total mass of the three models is equal to the total masses of the models used in the pushover analysis.

The equivalent frames are derived with the procedure described in (Magenes 2000) and shown in the figure below.

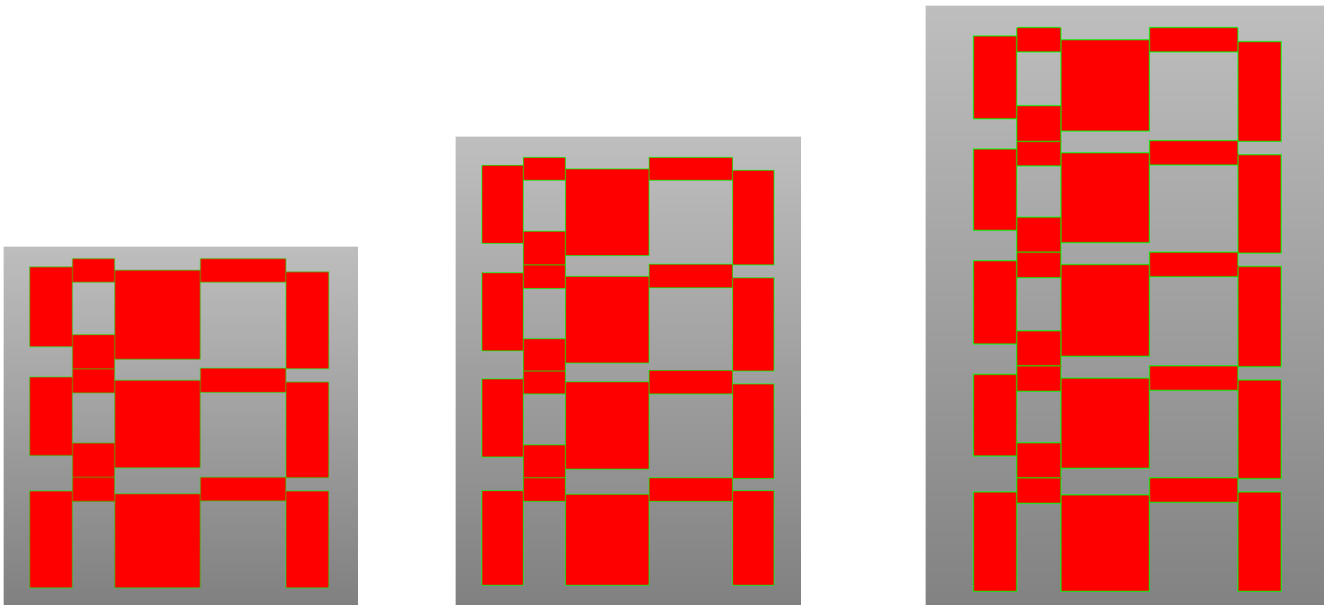

Figure 16-18. Equivalent frames of 2D case study

The load combination used for design is the following:

$$F_d = G + E \qquad [16.3]$$

where G is the action due to gravity loads and E the seismic action.

The elastic response spectrum used is referred to a type A soil, that has the following characteristics (see table 3.2 of EC8): S equal to 1, T_B equal to 0.15 s, T_C equal to 0.4 s and T_D equal to 2 s. The reference peak ground acceleration a_g is 0.25g. The importance factor γ_I was assumed equal to 1, that is typical for an event return period of 50 years (see §3.2.1 of EC8). The viscous dumping assumed is 5%. Three vibration modes are considered with a CQC combination as suggested in §7.3.3.1 of (NTC 2008). The response spectrum used is shown in Figure 16-19.

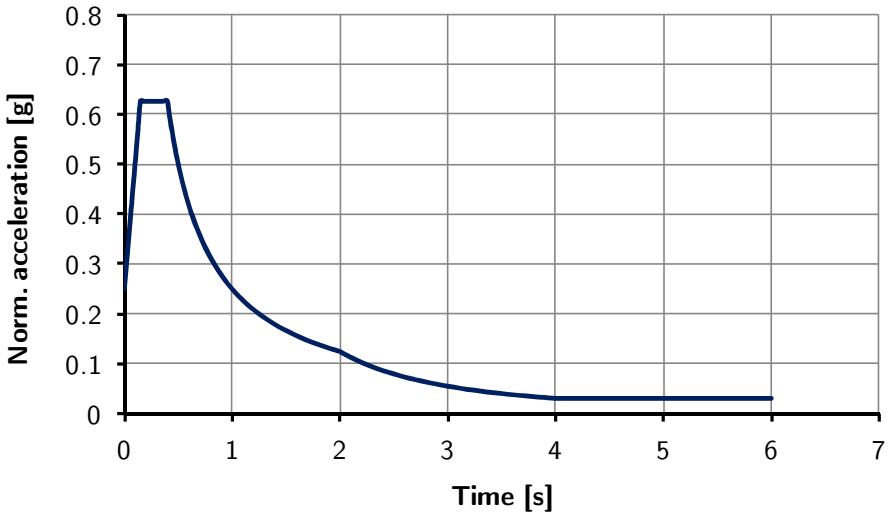

Figure 16-19. Response spectrum used for modal analysis

The horizontal elements are considered as rigid elements. The vertical elements are Timoshenko beams with the characteristics of an I25 block (see chapter 6) reinforced with bars Φ25 in horizontal and vertical directions. The flexural and shear rigidity are divided by 2 in order to take into account the formation of cracked sections, according to §7.2.6 of (NTC 2008). The Young modulus of concrete is 32308 MPa.

For each case the response spectrum is scaled until the section failure of a vertical elements is reached. Interaction diagrams M-N determines the failure condition in vertical elements. The shear strength is always greater than the design shear force. Figure 16-20 shows the bending moment in the 3 cases.

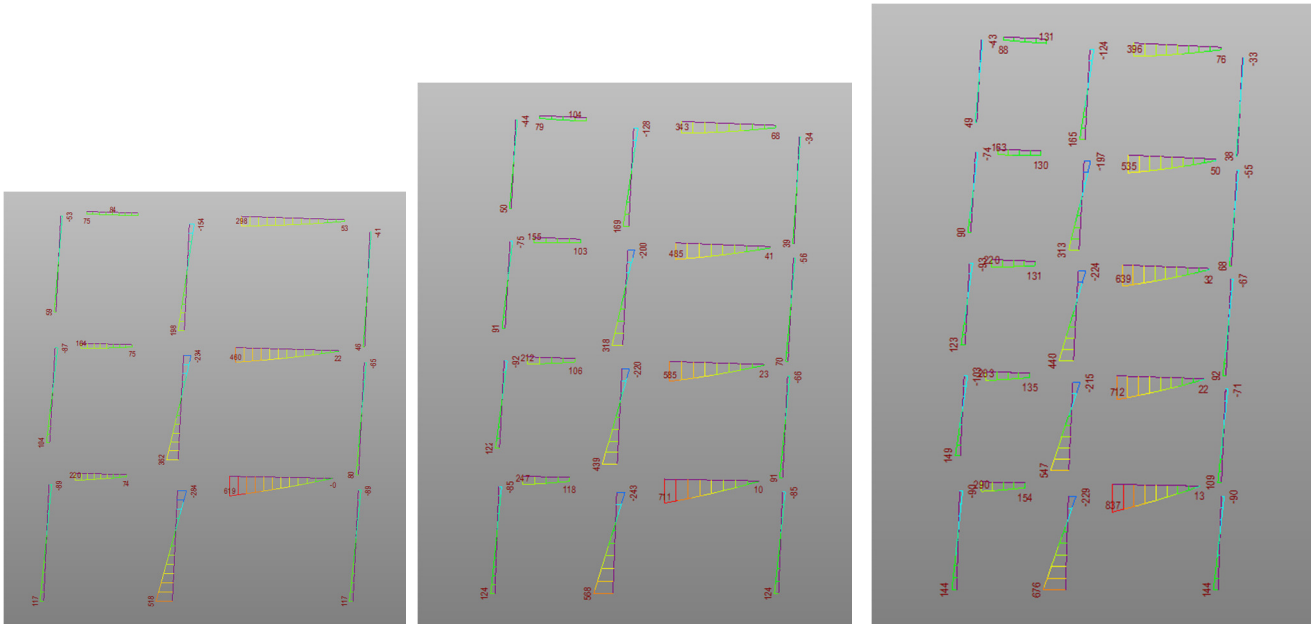

Figure 16-20. Bending moment in the 2D studies

Theoretically, the bending moments at both ends of the vertical elements should be equal when the vertical elements are axially infinitely rigid. The effects of finite axial stiffness is evident in the 5 stories case where the bending moments at ends are different. Hereafter the failure domain of the first element that reach the failure condition is reported.

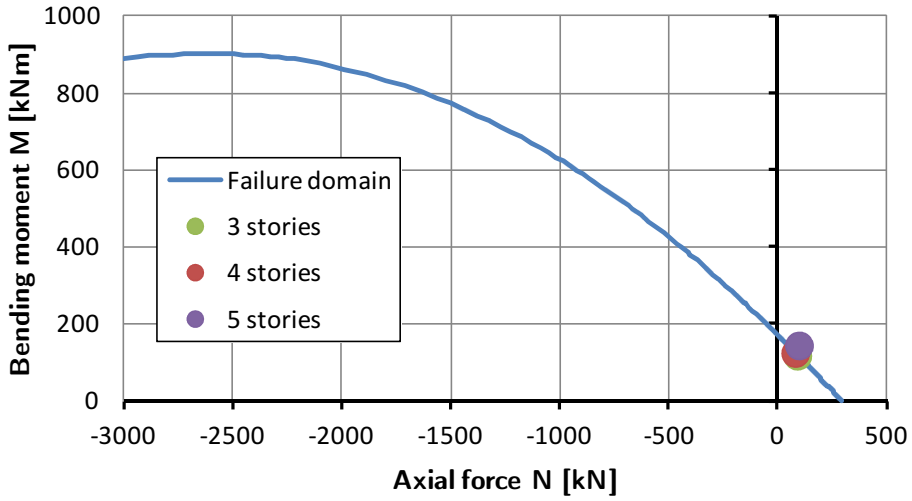

Figure 16-21. Interaction domain of vertical element on bottom left

The aim of this analysis is the determination of K_s. (see equation [5.1]) The greater is V_d, the more conservative is K_s. For this reason, a seismic action from left to right is chosen. The failure condition occurs always in the vertical element placed on ground floor on the left side. The V_y value is the average between the maximum base shear forces of the bilinear curves obtained in the pushover analyses with the force distribution proportional to masses and the other one proportional to the first mode.

N° of floors	Total mass [ton]	Modal Participation mass [%]	V_d [kN]	V_y [kN]	K_s	q*	q
3	136.6	98.8	440	603	1.37	2.33	3.19
4	182.3	97.4	445	685	1.54	1.99	3.06
5	228.0	99.1	496	547	1.10	2.41	2.66
						Mean value =	2.97

Table 16-5. Overstrength factor determination for 3, 4 and 5 stories building

Table 16-5 shows the results of the overstrength factor evaluation. The modal participation mass is the sum of the participation masses of the 3 modes considered. The overstrength factor correct the basic q* factor obtained with pushover analysis in order to obtain a value q useful in the design.

The final q-factor is very close to 3 that is the maximum value accepted by (LL. GG. 2011) in case a valid evaluation procedure based on experimental evidences.

16.6. Conclusions

The evaluation of behavior factor by means of pushover curve treats the whole structure with multiple degree of freedom (MDOF) as a single degree of freedom (SDOF) system with an equivalent rigidity k^* and an equivalent mass m^*. This system has also an equivalent period T^* derived with equation [16.1].

Implicitly, this system has a bilinear force-displacement law with an elastic branch and a perfect plastic post-yielding branch. In this way the elastic stiffness of the whole system is over-estimated and the period T^* is under-estimated. This cause a decrease of the q-factor value for the structure at hand. Even with this underestimation, the mean of behavior factors q* is greater than 2 (see Table 16-4), values proposed for this kind of construction system by (LL. GG. 2011).

The pushover analyses results were also combined with a classical design procedure where a seismic event is applied to the structures in form of response spectrum. The two base shear forces, V_y and V_d, are compared by means of equation [5.3] and the overstrength factor was evaluated. This factor increases q* by means of equation [5.1] giving more realistic values of the final behavior factor q.

In the cases described above the horizontal and vertical reinforcement is maintained constant along the height. Given that, the series of building analyzed can be considered as irregular in elevation because the ratio between actual and required strength is not proportional for adjacent stories. A more accurate design of reinforcement, in the practice, is recommended and can give higher level of ductility with an increment of the behavior factor.

Chapter 17. – Numerical analyses of a multistory building

17.1. Description of the case study

The case study has the same geometries of the three story timber building investigated within the SOPHIE project (A. Ceccotti 2008) in Figure 17-1.

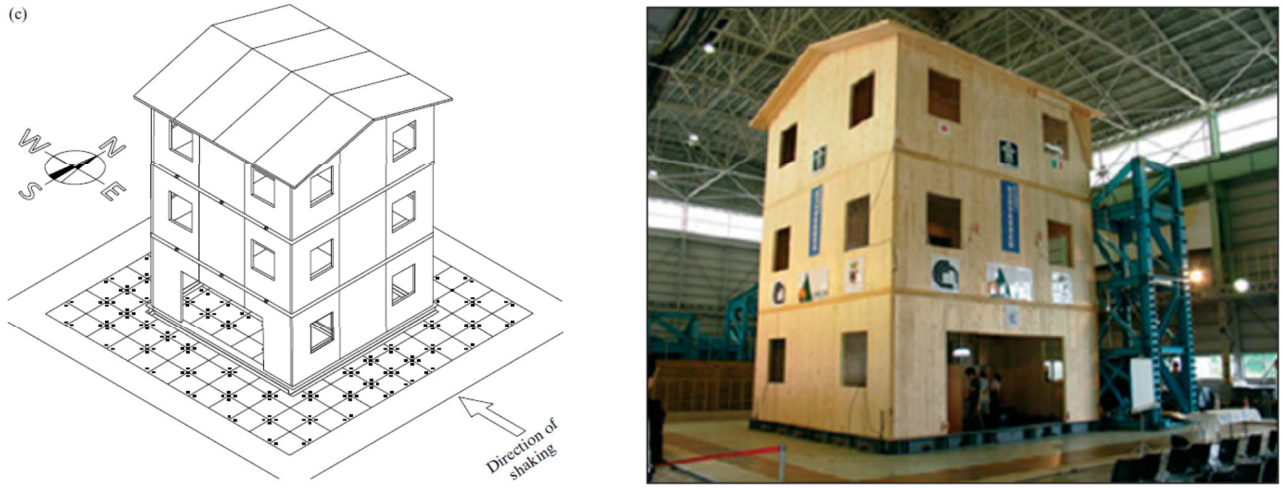

Figure 17-1. Images of SOPHIE project 3-story building

The plan and front views of SOPHIE project building are shown in Figure 17-2.

Some modifications were introduced in the case study building hereafter investigated. In order do not have a weak floor, the ground floor geometry has been repeated at the second and third floor and the windows were converted in doors. Moreover, the internal walls were substituted with a central pillar.

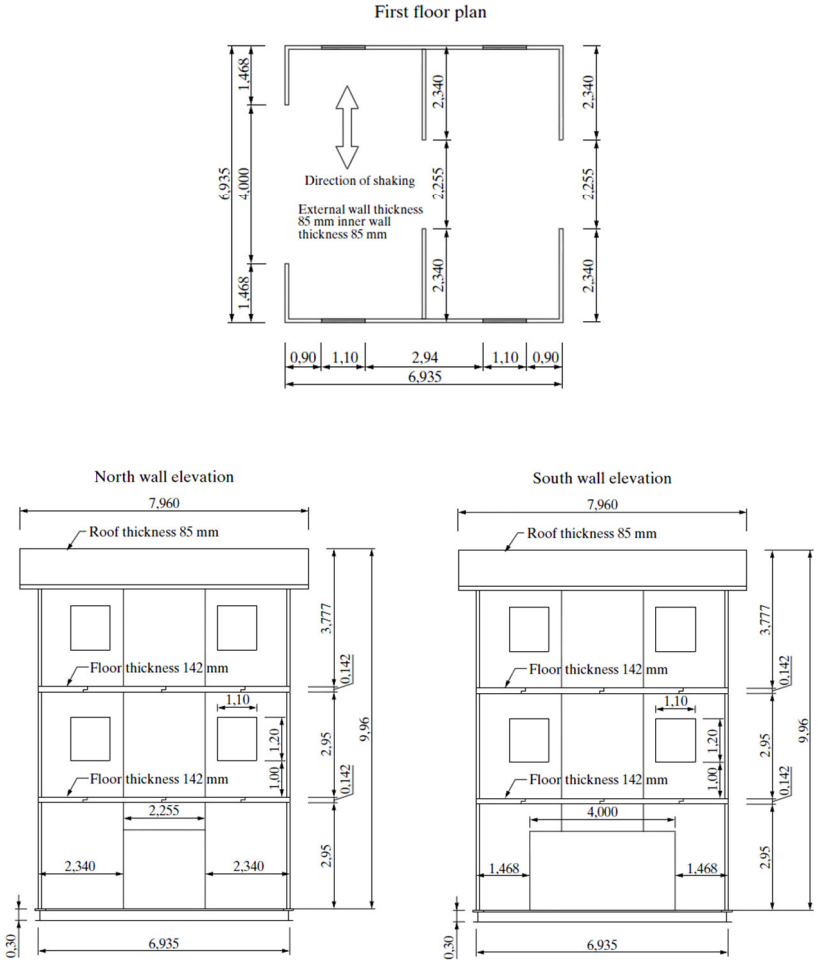

Figure 17-2. Plan and front views of SOPHIE project building (A. Ceccotti 2008)

According to provisions described in §7.4.1, the design characteristics of the materials were:

- Steel B450C, f_{yd}=450/1.15=391 MPa;
- Concrete C30/37, f_{cd}=0.85*30/1.8=14.2 MPa.

Two different numerical models have been done of such building (see Figure 17-3 and Figure 17-4):

- An equivalent frame model to perform linear analyses, following the procedure described by (Magenes 2000)
- A micro-frame model to perform nonlinear analyses according to the procedures described in chapter 13. In the nonlinear model vertical uprights are described with fiber beam elements with a distributed plasticity and transverses are represented with truss elements with concentrated plasticity. The floors are modeled with linear elastic plate elements.

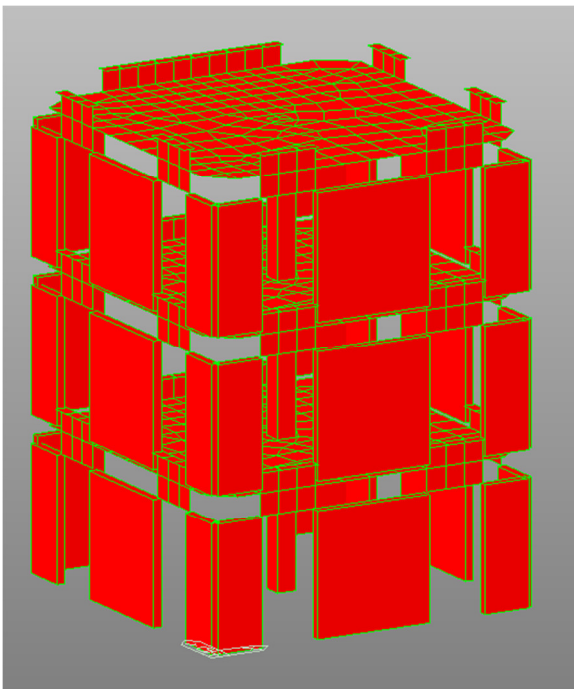

Figure 17-3. Equivalent frame model

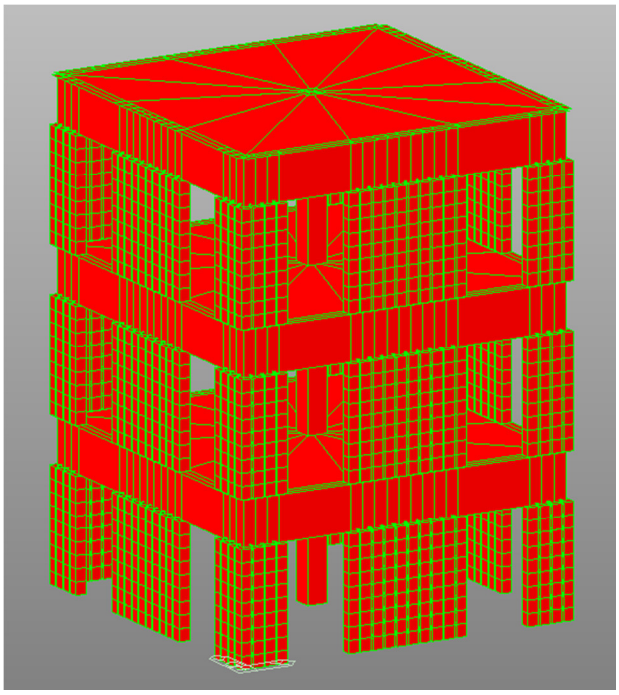

Figure 17-4. Micro-frame model

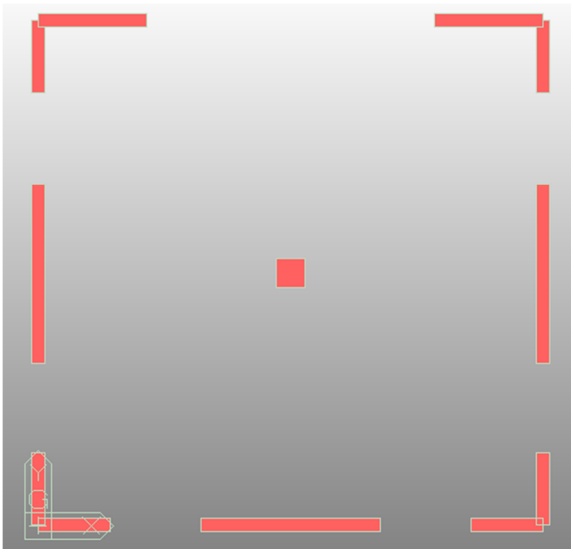

Figure 17-5. Ground plan section of the equivalent frame model

The equivalent frame model have the same concrete area of the micro-frame model using to the definition of effective area given in chapter 7.3.2. The self-weight and mass of the structure is automatically calculated using a weight density of reinforced concrete equal to 25 kN/m^3.

A uniform live load of 2 kN/m^2 on each floors is considered in all the simulation performed. This live load is transformed in equivalent mass and added to the self-weight of the building (dead load). The total mass of the building is about 190 tons. Table 17-1 shows the details of building mass calculation.

FOR EACH FLOOR:					
				Volume	
Plan perimeter	16.5	m			
Height	3	m			
Wall thickness	0.2	m		9.90	m^3
Lintel perimeter	28	m			
Lintel area	0.04	m^2		1.12	m^3
Pillar area	0.16	m^2			
Pillar height	3	m		0.48	m^3
RC slab area	49	m^2			
RC slab thickness	0.2	m		9.80	m^3
			total	21.30	m^3
n° of floors	3				
			total	63.90	m^3

LOADS AND TOTAL MASS					
				Mass	
Density	2.5	ton/ m^3			
		Dead load (mass)		159.8	ton
Live Load on floors	2	kN/m^2/floor			
Slab area	3 x 49	m^2			
Total Live Load	294	kN			
		Live load (mass)		30	ton
			Total mass	189.8	ton

Table 17-1. Mass distribution details

Design forces on shear walls have been obtained by means of a design spectral analysis performed with the equivalent frame model.

For the nonlinear model, two reinforcement distributions have been considered:

- the first with a constant rebar arrangement on all the floors (vertical ϕ12@25 -horizontal ϕ5@25 mm) dimensioned for the strength demand of the ground floor walls;
- the second where the reinforcement is decreasing from the base to the top, correspondingly with the force distribution.

As far as concerning the regularity requirements the following comments hold:

- The first model (constant reinforcement) has to be classified as an "in height irregular building" since according to EC8 §4.2.3.3(4)P the ratio of the actual story resistance to the resistance demand varies disproportionately between adjacent stories;
- On the contrary, the second model (variable reinforcement) instead can be seen as "in height regular building": the regularity in elevation, i.e. the fulfilling of an almost uniform unitary ratio between strength capacity and demand from the analysis at each floor, has been assured by varying the reinforcement as reported in Table 17-2;
- Both the models are plan irregular along the X direction, while are symmetric and then regular along the Y direction.

Floor	**Vertical reinforcement**	**Horizontal reinforcement**
1°	$\phi 12/25$	$\phi 5@25$
2°	$\phi 10/25$	$\phi 4@25^{*}$
3°	$\phi 8/25$	$\phi 2@25^{*}$
* Note: these reinforcement diameters are only theoretical.		

Table 17-2. Reinforcement variations along the height in the regular building case

Therefore the analyses of the two models for the two earthquake directions allow to investigate the dependency of seismic performance on the different combinations of regularities (see Table 17-3).

Earthquake / Reinforcement	**Along X Direction**	**Along Y Direction**
Constant at each floor	In plan reg.: NO In height reg.: NO	In plan reg.: YES In height reg.: NO
Variable – decreasing from ground to top floor	In plan reg.: NO In height reg.: YES	In plan reg.: YES In height reg.: YES

Table 17-3. Different combinations of regularities

17.2. Modal response spectrum analysis

In order to define a design base shear strength (V_d) a spectral response analysis on the linear elastic model has been performed. The elastic response spectrum used is the same one described in §16.5 and reported in Figure 16-19.

Previously modal analysis has been performed in order to obtain periods and shapes of fundamental vibration modes and the corresponding participation masses. The results are reported in Table 17-4.

EIGENVALUE ANALYSIS					
	Mode No	Frequency (rad/sec)	Frequency (cycle/sec)	Period (sec)	Tolerance
	1	49.7743	7.9218	0.1262	0.0000e+000
	2	63.8243	10.1580	0.0984	0.0000e+000
	3	89.9340	14.3134	0.0699	0.0000e+000
	4	154.2881	24.5557	0.0407	0.0000e+000
	5	190.4788	30.3156	0.0330	0.0000e+000
	6	250.2157	39.8231	0.0251	0.0000e+000
	7	264.9096	42.1617	0.0237	0.0000e+000
	8	293.1662	46.6588	0.0214	0.0000e+000
	9	400.0262	63.6661	0.0157	0.0000e+000
	10	683.7931	108.8291	0.0092	5.2592e-025

MODAL PARTICIPATION MASSES PRINTOUT												
	Mode No	TRAN-X		TRAN-Y		TRAN-Z		ROTN-X		ROTN-Y		ROTN-Z	
		MASS(%)	SUM(%)	MASS(%)	SUM(%)	MASS(%)	SUM(%)	MASS(%)	SUM(%)	MASS(%)	SUM(%)	MASS(%)	SUM(%)
	1	79.1614	79.1614	0.0446	0.0446	0.0000	0.0000	0.0173	0.0173	27.0477	27.0477	6.2033	6.2033
	2	0.0403	79.2017	87.0664	87.1110	0.0000	0.0000	26.8472	26.8645	0.0055	27.0532	0.0149	6.2182
	3	7.0301	86.2318	0.0079	87.1189	0.0000	0.0000	0.0000	26.8645	1.1210	28.1742	82.3787	88.5969
	4	11.0599	97.2917	0.0116	87.1305	0.0000	0.0000	0.0254	26.8899	60.6495	88.8237	1.2154	89.8124
	5	0.0027	97.2943	11.1412	98.2716	0.0000	0.0000	68.5259	95.4158	0.0330	88.8567	0.0084	89.8207
	6	2.3547	99.6490	0.0016	98.2732	0.0000	0.0000	0.0034	95.4192	7.2112	96.0679	0.0005	89.8212
	7	0.2610	99.9101	0.0001	98.2733	0.0000	0.0000	0.0094	95.4286	3.6019	99.6699	8.8082	98.6294
	8	0.0001	99.9102	1.6892	99.9625	0.0000	0.0000	4.3226	99.7512	0.0001	99.6699	0.0002	98.6296
	9	0.0668	99.9771	0.0002	99.9626	0.0000	0.0000	0.0008	99.7521	0.1639	99.8338	1.3547	99.9843
	10	0.0000	99.9771	0.0000	99.9626	0.0000	0.0000	0.0002	99.7523	0.0000	99.8339	0.0000	99.9843

Table 17-4. Natural frequency analysis results (the frame model)

The first five modes contains a modal participation mass greater than 90% along the X and Y directions. Given that, these modes are considered in the determination of seismic action on the building according to EC8 §4.3.3.3.1. The "Complete Quadratic Combination with sign" is used to combine the actions due to the 5 modes.

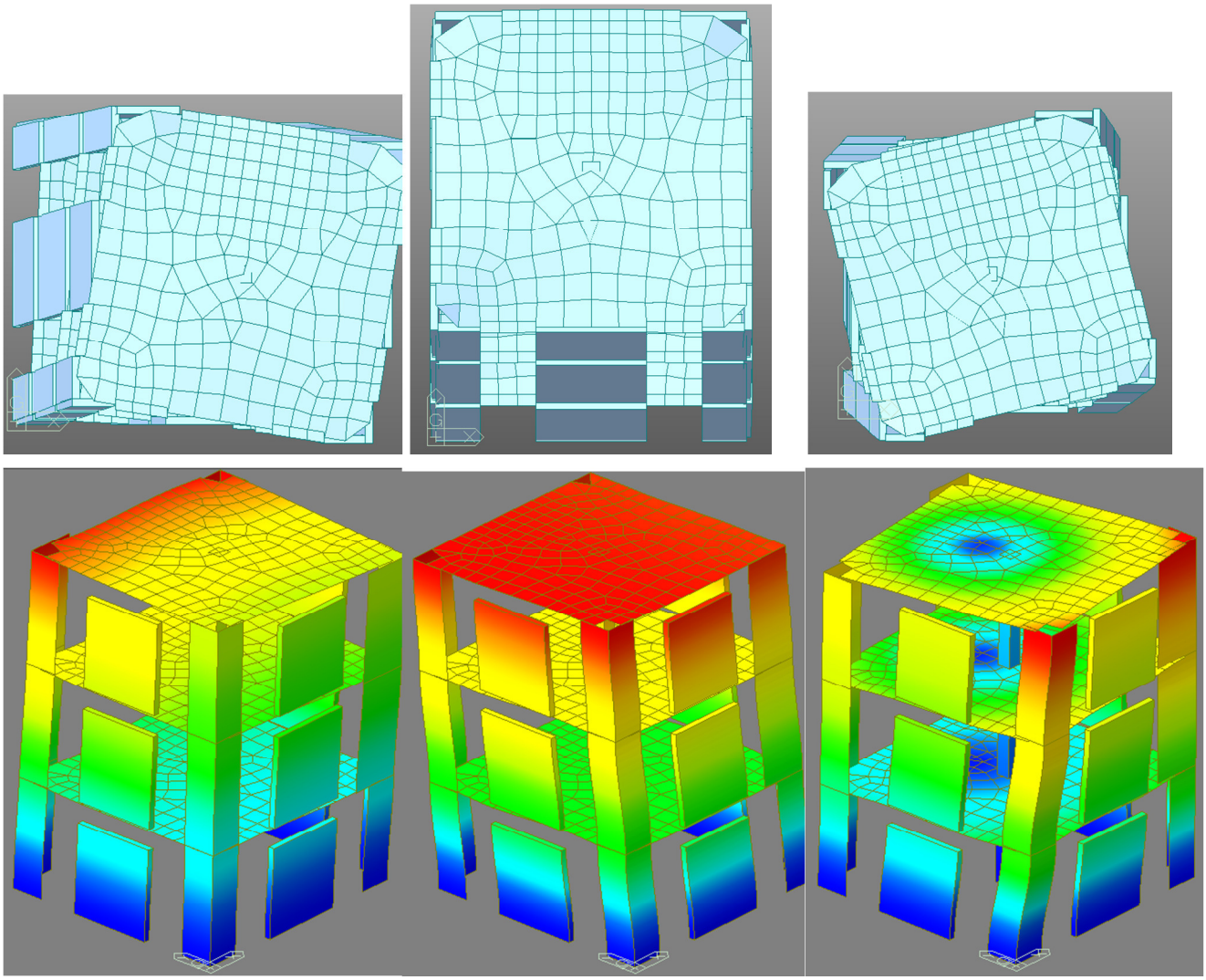

Figure 17-6. Views vibration mode shapes of 3D building: first mode (roto-translational), second mode (translational in Y-direction) and third mode (rotational) described from left to right.

Figure 17-6 shows the modal shapes corresponding to the first three natural vibration modes. The first mode is mixed roto-translational due to the plan asymmetry of the building. The second mode if fully translational along the symmetry axis Y of the building. The contour represents the displacements from blue (zero displacement) to red (maximum displacement). In the first mode (roto-translational), the larger displacements are localized on the weak of the building, in the second mode (pure translational) the displacements are uniform at each floor, whereas in the third case (pure rotational) the center of the at each floor indicates the center of rotation.

This elastic response spectrum has been scaled in order to reach a limit state condition (SLV) under the seismic load combination:

$$F_d = DL + 0.3LL + \psi E \qquad [17.1]$$

where DL is related to dead loads, LL to live loads and E to the seismic load (in one direction).

For the building with constant reinforcement at each floor, once assumed dimensions of walls and reinforcement ratio, the scaling parameter ψ of the seismic action which leads the first element of the structure to his yielding limit has been evaluated, so determining different values of design base shear for X and Y directions: $V_{d,X}$ = 721 kN and $V_{d,Y}$ = 840 kN.

In all the shearwalls (included L-shaped at the corners), the failure condition due to M-N forces was checked by means of interaction diagrams. Shear verifications were conducted with the procedure exposed in §8.5 but they never resulted to be critical.

Then in the building with variable reinforcement the rebar design at each floor was conducted assuring the minimum gap between design forces (demand) and strength (capacity), i.e. searching for an overstrength factor almost unitary at each floor. In this way the reinforcement arrangement already given in Table 17-2 was obtained.

17.3. Torsional behavior

As said before a non-symmetric plan for the building was intentionally chosen in order to induce torsional effects and no-regular behavior when seismic action is applied along X direction. In this condition a preliminary evaluation of elastic torsional stiffness is mandatory.

The adopted procedure is derived by §4.2.3.2 of (Eurocode 8 2004) and was applied to the more realistic micro-frame model assuming an elastic behavior for all the members. For the examination of torsional stiffness a reduced single story model has been considered, being all the stories geometrically identical.

A torsional moment was applied to the rigid floor by means of a couple of opposite distributed forces on the two sides of the building (see Figure 17-7). Named Δx^1 and Δx^2 the displacements of the two opposite sides, the floor rotation φ was evaluated as:

$$\varphi = \frac{\Delta x^1 - \Delta x^2}{L} \qquad [17.2]$$

and the torsional stiffness k_T is the ratio:

$$k_T = \frac{M}{\varphi} = \frac{121.5}{3.83 \cdot 10^{-6}} = 3.17 \cdot 10^{-7}\ kNm/rad \qquad [17.3]$$

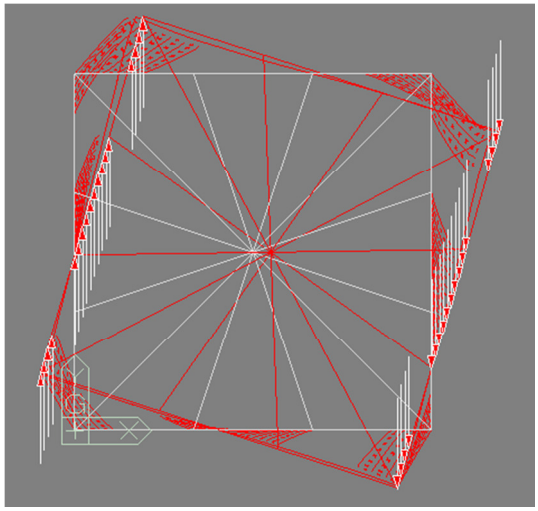

Figure 17-7. Torsion moment applied on RC slab and consequent floor rotation

The center of stiffness must be placed along the symmetry Y axis and the distance e_{0y} between the center of stiffness and the center of the floor can be calculated with:

$$e_{0y} = \frac{\Delta x^1}{\varphi} + \frac{L}{2} = 1.10\ m \qquad [17.4]$$

A force F in X-direction applied to the center of stiffness gives a pure translation Δx in X-direction and allows to evaluate the lateral stiffness k_L as:

$$k_L = \frac{F}{\Delta x} = \frac{100}{9.5 \cdot 10^{-5}} = 1.05 \cdot 10^{-6}\ kN/m \qquad [17.5]$$

The r parameter, defined as:

$$r_y = \sqrt{\frac{k_T}{k_L}} = 5.49\ m \qquad [17.6]$$

has to be compared with the radius of gyration l_s (= 2.85 m) of the floor mass in plan in order to satisfy the EC8 conditions at §4.2.3.2:

$$e_{y0} \leq 0.30\, r_y \qquad [17.7]$$

$$r_y \geq l_s \qquad [17.8]$$

The requirements are both satisfied and consequently the building can be classified as not torsionally flexible.

17.4. Pushover analysis

A uniform distribution of forces was applied at each story level and increased until the "numerical ultimate condition" for the shear walls. This distribution of forces is more conservative than the triangular one as far as concerns the ultimate displacement of the control point.

The correct assumption for failure conditions in pushover analyses is a fundamental point for the derivation of the ultimate displacement and ductility of a structure. Here the pushover analyses were stopped when one of the following conditions occurred:

- The vertical reinforcement strain exceeded 6%
- The concrete softening produced a loss in term of total base shear force of 15%
- The model became not able to reach the convergence criteria (typically due to a strong localized damage of the building).

Considering the assumption for X-Y axes reported in the figures above, west-to-east is the pushing in X positive direction and south-to-north is the pushing in the Y positive direction.

Results from 3 pushover analyses are presented in this section: 1 in the X-direction and 2 in the Y-direction. Indeed, while in +Y and –Y loading direction distinct capacity curves are expected due to symmetry reasons, the two capacity curves for opposite loading along X direction must be identical.

The pushover curves are bilinearized with the same criteria described in §16.3.

17.4.1. Uniform reinforcement model (irregular in elevation building)

Considering the case study with constant reinforcement at each floor the following result were obtained:

	Direction		**D_y^+ [mm]**	**D_y^- [mm]**	**D_u^+ [mm]**	**D_u^- [mm]**	**V_y^+ [kN]**	**V_y^- [kN]**	**V_{peak}^+ [kN]**	**V_{peak}^- [kN]**
Uniform distribution	X		±5.7		±35		±927.1		±994.7	
	+Y	-Y	4.5	-5.4	46.5	-55	1019.3	-1021.2	1081.3	-1076.0

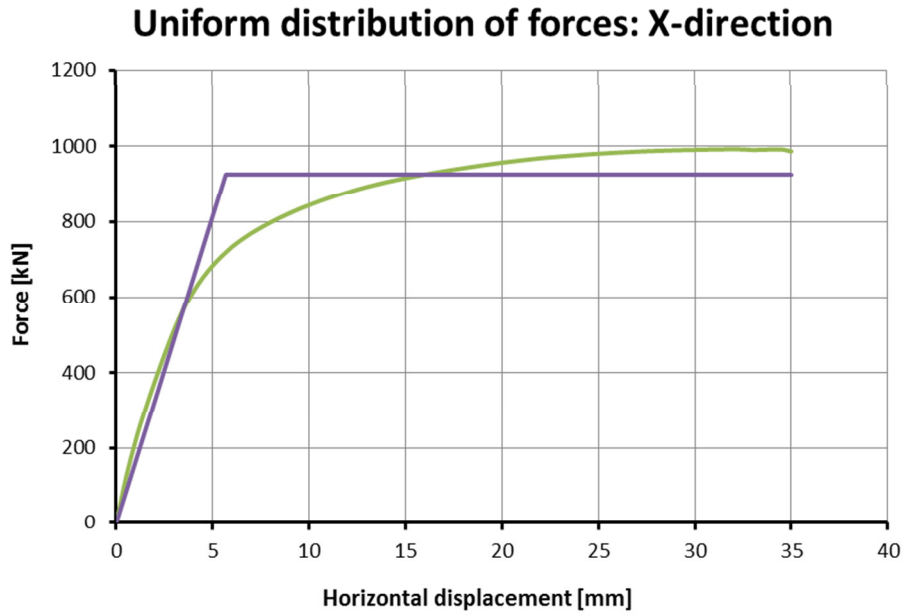

Figure 17-8. Pushover curve in the irregular building case (X-direction)

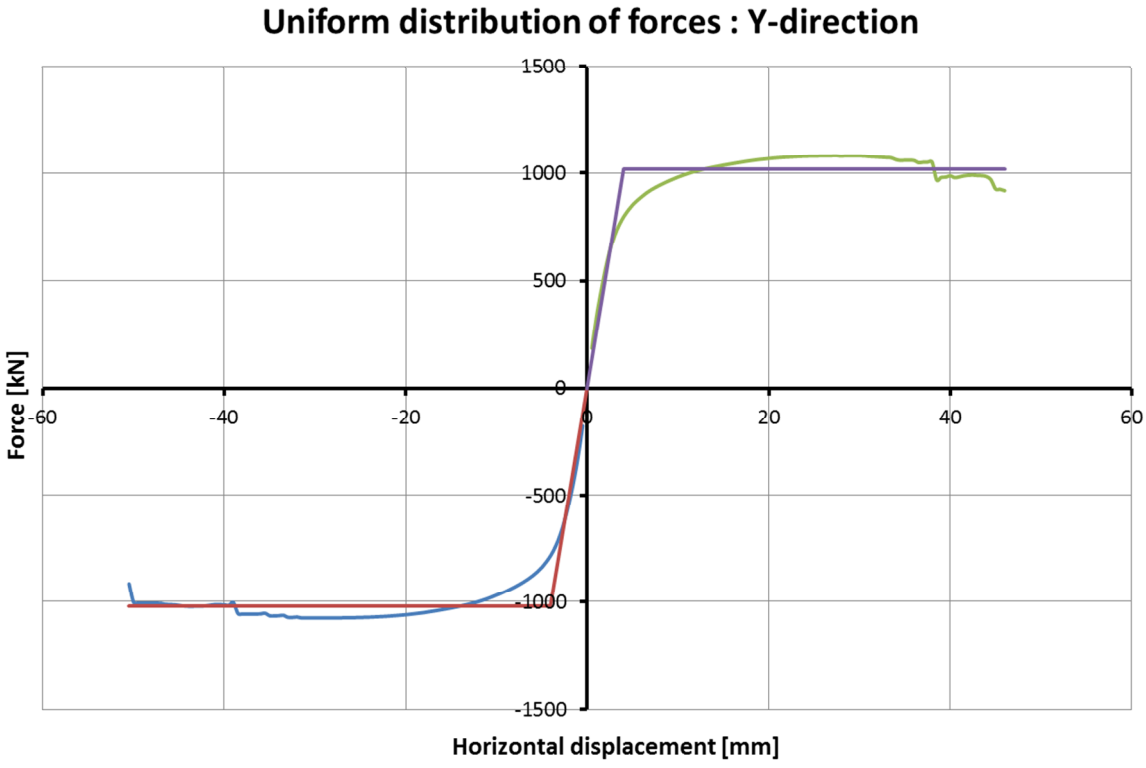

Figure 17-9. Pushover curve in the irregular building case (Y-direction)

The displacement capacity of building in both Y-directions resulted to be greater than in X-direction. It has to be evidenced that analyses along the symmetry axis Y give different result depending on the pushover direction. In both cases failure is governed by the L-shaped piers at the side of the wide opening at ground floor. When pushing in Y+ direction failure is related to

crushing of the concrete compressed uprights, while in Y- direction yielding of vertical steel is the governing phenomena. In the first case failure was obtained for an ultimate top displacement of 46.5 mm and base shear of 1019 kN, in the second case displacement capacity increased to 55 mm but equivalent yielding strength decreased to 1021 kN. For pushing in X direction bending failure of the same piers was obtained. Shear failure was never observed..

In the pushover analysis along the X-direction, the rotation of top floor was not significant in comparison with the total displacement. Figure 17-10 represents the evolution of the top displacements of the four vertex of the top slab. It confirms the high rotational stiffness of the building already drawn in §17.3.

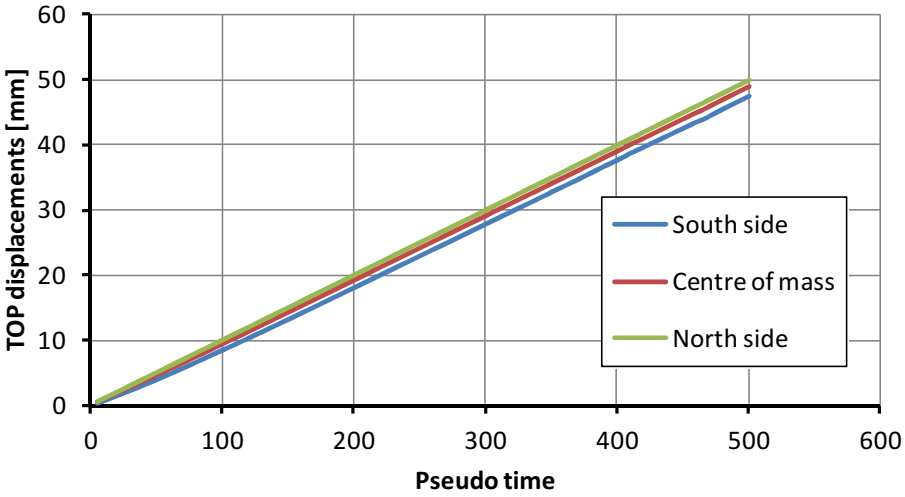

Figure 17-10. Top displacements in pushover analysis: irregular building in elevation

The plot of deformed model at failure condition underlines the formation of a soft floor at the ground level for the building with constant reinforcement (see Figure 17-11). The lateral deformations at first and second floors are almost negligible since they remain in the elastic field. Damaging localizes at ground floor due to the uniformity of steel reinforcement at all the floors.

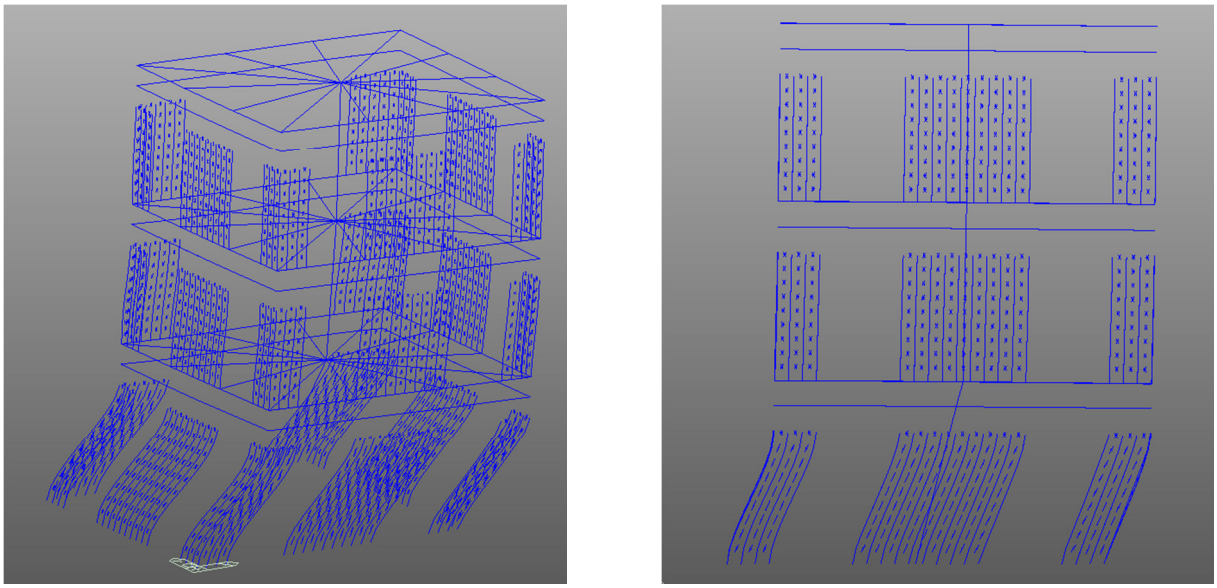

Figure 17-11. Pushover along X-direction and positive Y-direction (irregular building)

17.4.2. Variable reinforcement model (regular in elevation building)

The bi-linearization of pushover curves obtained with the model with variable reinforcement (i.e. with overstrength ratio almost constant at all levels) led to the following results:

	Direction	D_y^+ [mm]	D_y^- [mm]	D_u^+ [mm]	D_u^- [mm]	V_y^+ [kN]	V_y^- [kN]	V_{peak}^+ [kN]	V_{peak}^- [kN]
Uniform distribution	X	±7.1		±47.5		±861.4		±931.9	
	Y	6.2	-5.5	61	-65	978.4	-943.8	1059.3	-1019.7

In comparison with the irregular building, greater displacement capacities were obtained and pushover curves are smoother (i.e. the yielding evolution are less marked) due to progressive and diffuse damaging at all the floors. Moreover, differences between Y+ and Y- pushover directions are reduced.

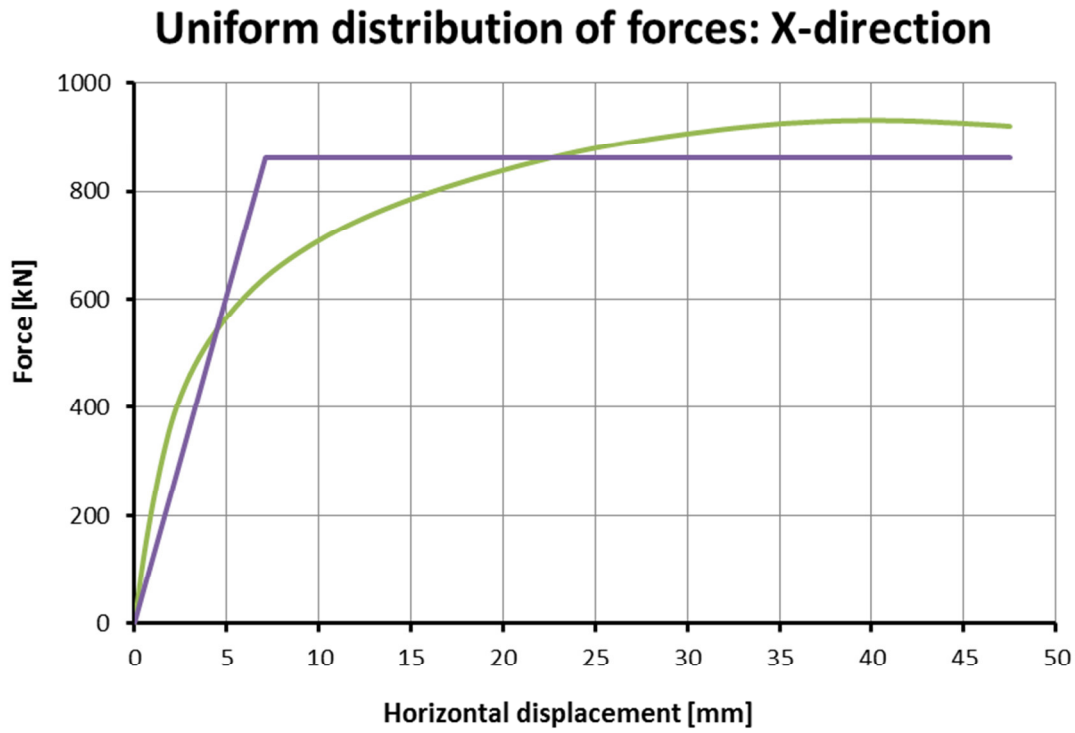

Figure 17-12. Pushover curve in the regular building case (X-direction)

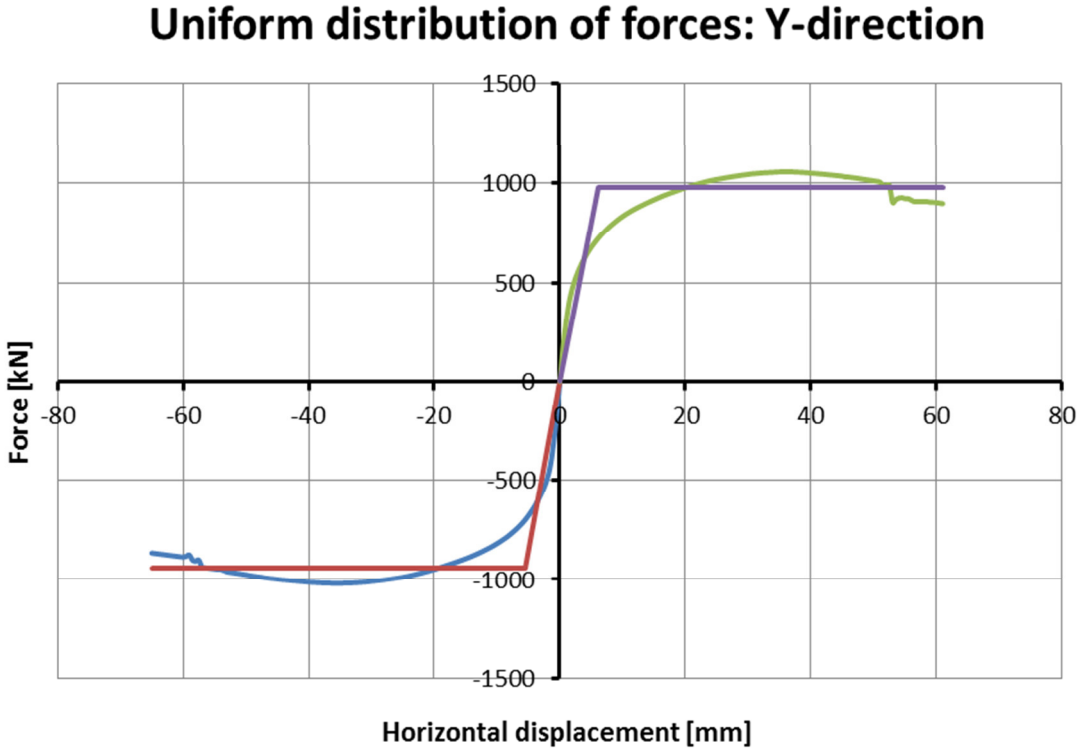

Figure 17-13. Pushover curve in the regular building case (Y-direction)

The damage spreading is also testified by the plots of deformed shapes at failure condition. Even if the main part of distortions remains concentrated at the ground floor, drift at first and second floors is now not negligible.

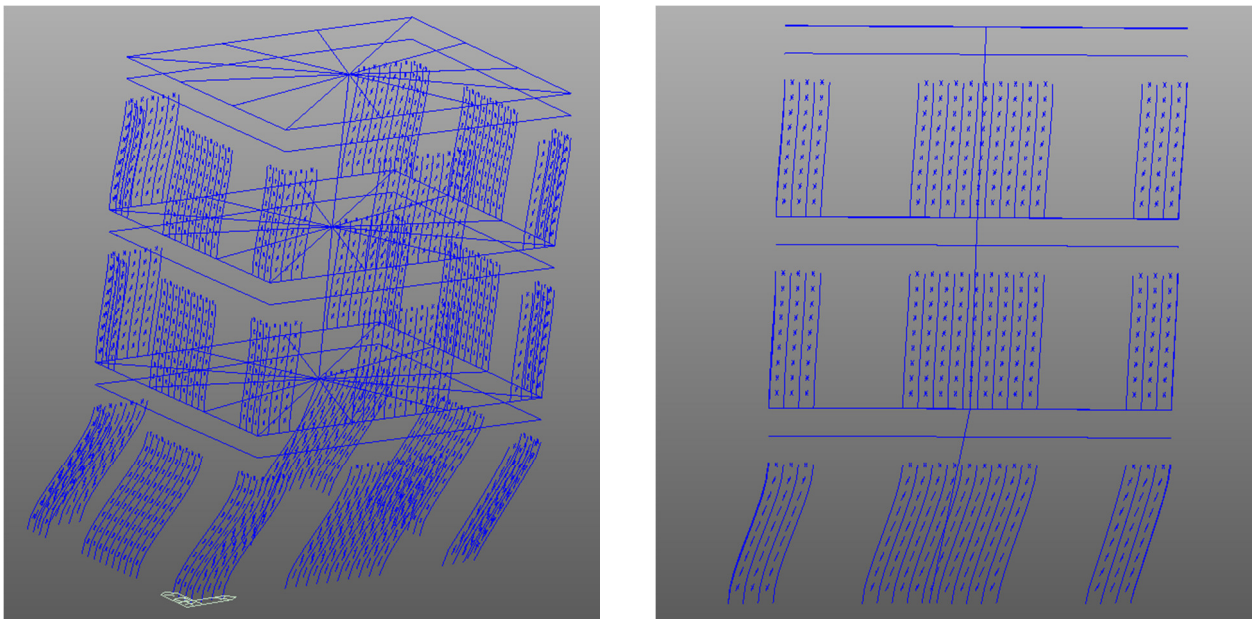

Figure 17-14. Pushover along X-direction and positive Y-direction (regular building)

17.4.3. Overstrength factor

As already explained in §5.1, the overstrength factor K_s, i.e the coefficient accounting for structural redudancy, is the ratio between the ultimate base shear strength V_y obtained with a pushover analysis and the design base shear strength V_d obtained with an elastic analysis.

The overstrength factor K_s has been estimated using the data of the regular and irregular building:

	Direction	V_y^-	V_y^+	V_y^{mean}	V_d	K_s
Irregular in elevation	X	927	927	927	721	*1.29*
	Y	1019	1021	1020	840	*1.21*

	Direction	V_y^-	V_y^+	V_y^{mean}	V_d	K_s
Regular in elevation	X	861	861	861	721	*1.19*
	Y	943.8	978	978	840	*1.16*

K_s average = *1.21*

Table 17-5. Overstrength factor assessment

The regular in elevation building is penalized because the design base shear strength is always the same. Decreasing the reinforcement along the height produces a small drop in term of V_y but a greater displacement capacity.

The Guidelines of the Italian Ministry (LL. GG. 2011) suggest K_s equal to 1.2. The average value of overstrength factor (see Table 17-5) for the buildings analyzed matches very well the Guidelines provision.

The building analyzed is almost regular in plan, indeed his torsional stiffness is relatively high and it is not torsionally flexible (see §17.3). The overstrength factor along the X-direction (plan irregular) is slightly larger because V_d is penalized in that direction. Indeed, the design base shear is calculated with an elastic analysis where the stiffness has the greater weight, while in the nonlinear (inelastic) analysis governs the maximum strength of the vertical members. In the X-direction, this causes a translation of the center of rotation toward the center of mass and, consequently, a mitigation of the eccentricity effects. Of course, the Codes point of view is always conservative and tends to decrease the q-factor in case of irregularity.

17.5. Time-history analyses

In order to define the critical earthquakes that bring the structure to yielding and to failure conditions, a series of 3 ground motion signals was applied to the building and nonlinear time history analyses were performed with the same numerical models used for pushover analyses. In dynamic analysis a equivalent damping has been introduced with the Rayleigh approach, considering a dumping ratio of 5% for T_1 and T_4 (first and fourth modes) as suggested in (Chopra 1995).

17.5.1. Applied seismic events

Three artificially generated earthquakes, called EQ1, EQ2 and EQ3, (see Figure 17-16) have been considered. As demonstrated in Figure 17-16, they are consistent with the elastic response spectrum used for the modal spectral analysis.

According to EC8, §3.2.3.1.2(4), a minimum of three accelerograms is needed in order to perform a significant time-history analysis.

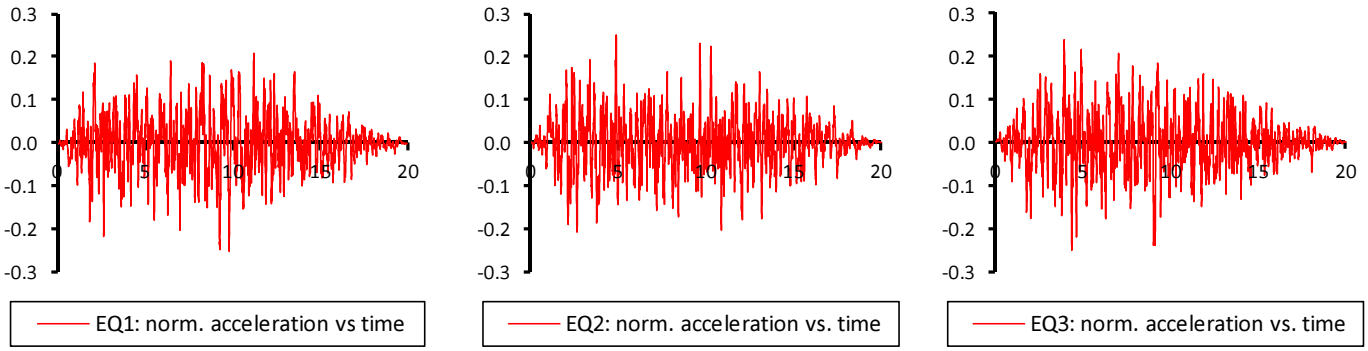

Figure 17-15. Earthquakes used in time-history analyses

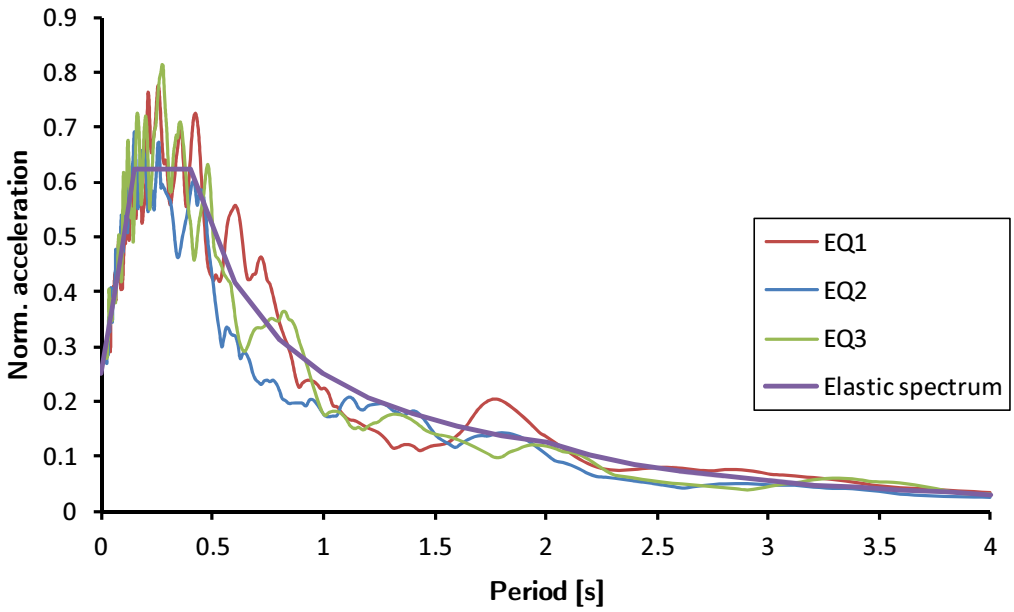

Figure 17-16. Demonstration of spectra compatibility of the artificial earthquakes

17.5.2. Uniform reinforcement model (irregular in elevation)

The artificial earthquakes have been scaled obtaining increasing PGA levels. This procedure is aimed to identify the PGAs that bring the structure to the target displacements determined in the pushover analyses, i.e. D_y and D_u corresponding to yielding and failure condition of the structure. Such PGA levels are indicated as PGA_y and PGA_u respectively. This searching criteria regarding the PGA level that brings the structure to a certain target displacement was adopted because in time history analyses dynamic equilibrium condition at each time step can be always reached even when building completely loses its structural stiffness. Therefore, criterions based on checking the yielding or ultimate condition are not feasible.

For each PGA level, four significant points were selected from the base shear versus top displacement transient curve:

- maximum base shear force and the corresponding top displacement
- maximum top displacement and the corresponding base shear force
- minimum base shear force and the corresponding top displacement
- minimum top displacement and the corresponding base shear force

This four points resume, in a concise way, the simulation results. Different markers are used in following figures for the different PGA/g levels.

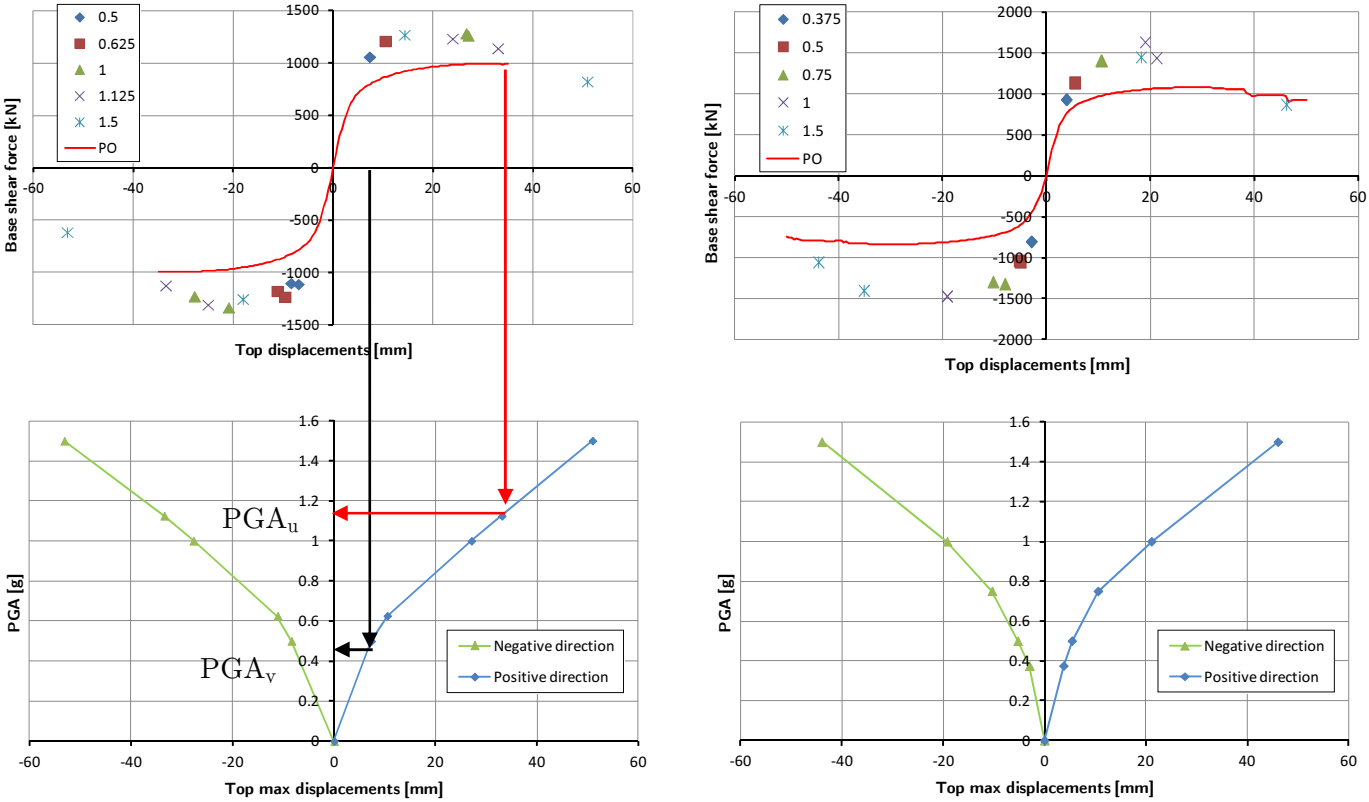

Figure 17-17. EQ1: determination of PGA_y and PGA_u along X-direction (left) and Y-direction (right)

Left side of Figure 17-17 illustrates the procedure used to interpolate the PGA values that bring the building to yielding and failure condition, i.e. PGA_y and PGA_u. From the two target displacements D_y and D_u determined with the pushover analysis, the PGA_y and PGA_u are obtained interpolating the points in the PGA vs. displacement curves. For each of the three seismic motion and for each excitation direction (X or Y) the procedure yields to 2 couples of PGA_y and PGA_u values for positive and negative displacements. For the sake of conservativeness, the greater PGA_y and the smaller PGA_u are chosen, in order to obtain the smaller behavior factor.

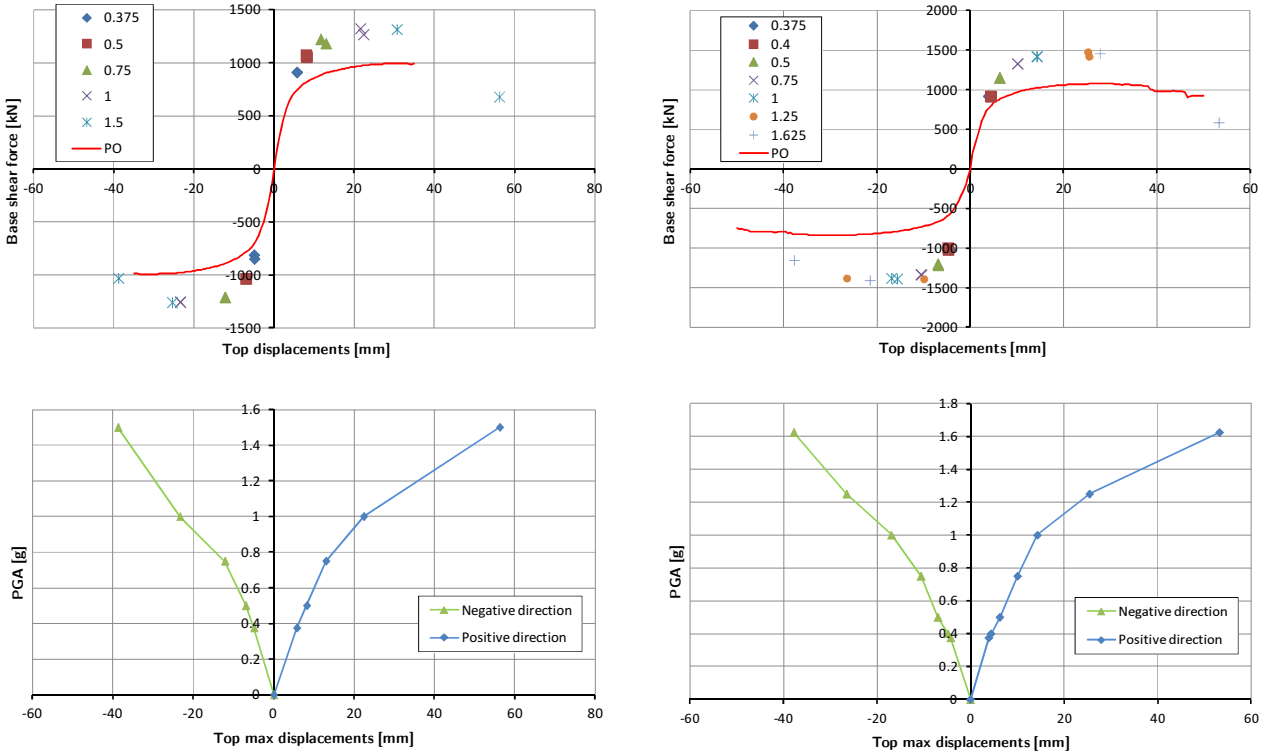

Figure 17-18. EQ2: determination of PGA_y and PGA_u in X-direction (left) and in the Y-direction (right)

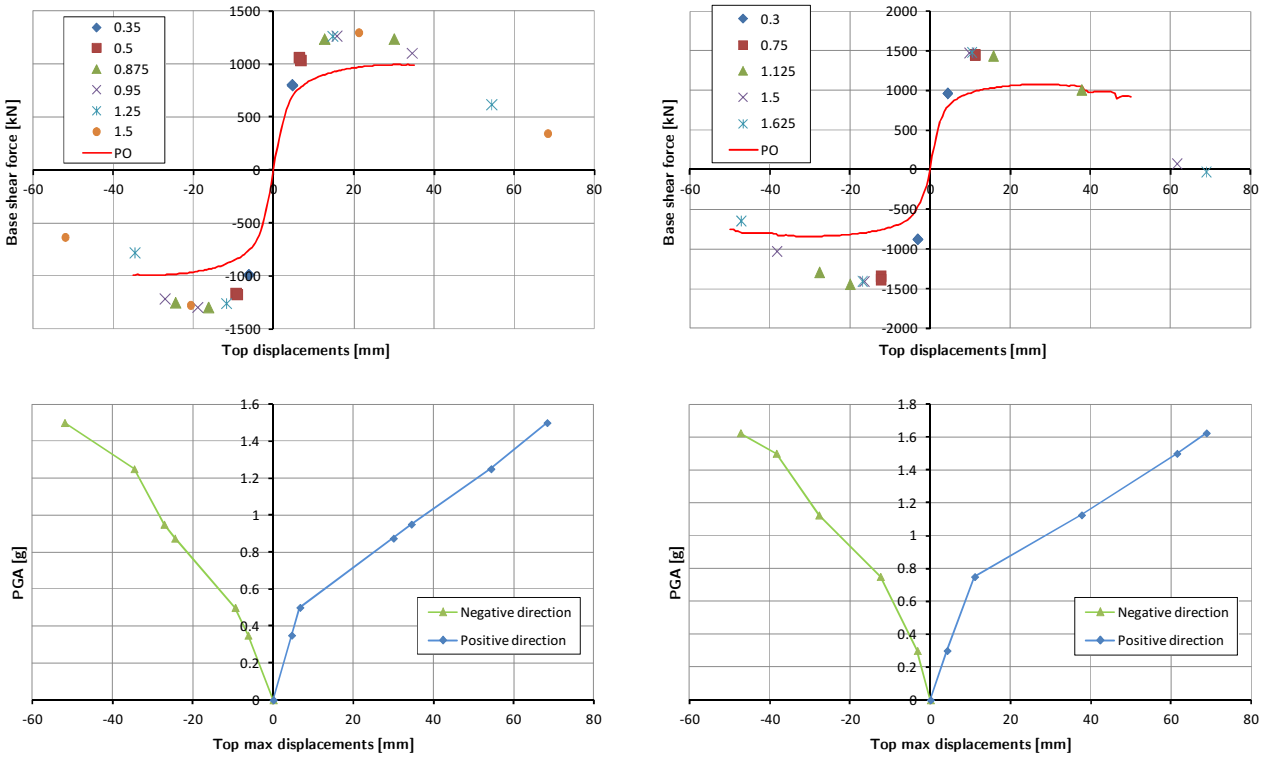

Figure 17-19. EQ3: determination of PGA_y and PGA_u in X-direction (left) and in the Y-direction (right)

In both types of graphs, i.e. force vs. displacement and PGA vs. displacement, the slope variation of curves evidences quite well the PGA level for which the structural behavior shifts from elastic to plastic.

17.5.3. Variable reinforcement model (regular in elevation)

The results obtained for the in elevation regular building are hereafter reported.

The regularity in elevation, i.e. the spreading of no linear damaging and yielding along the entire height of the building, is again testified by the smoother curves representing PGA vs. target point displacement.

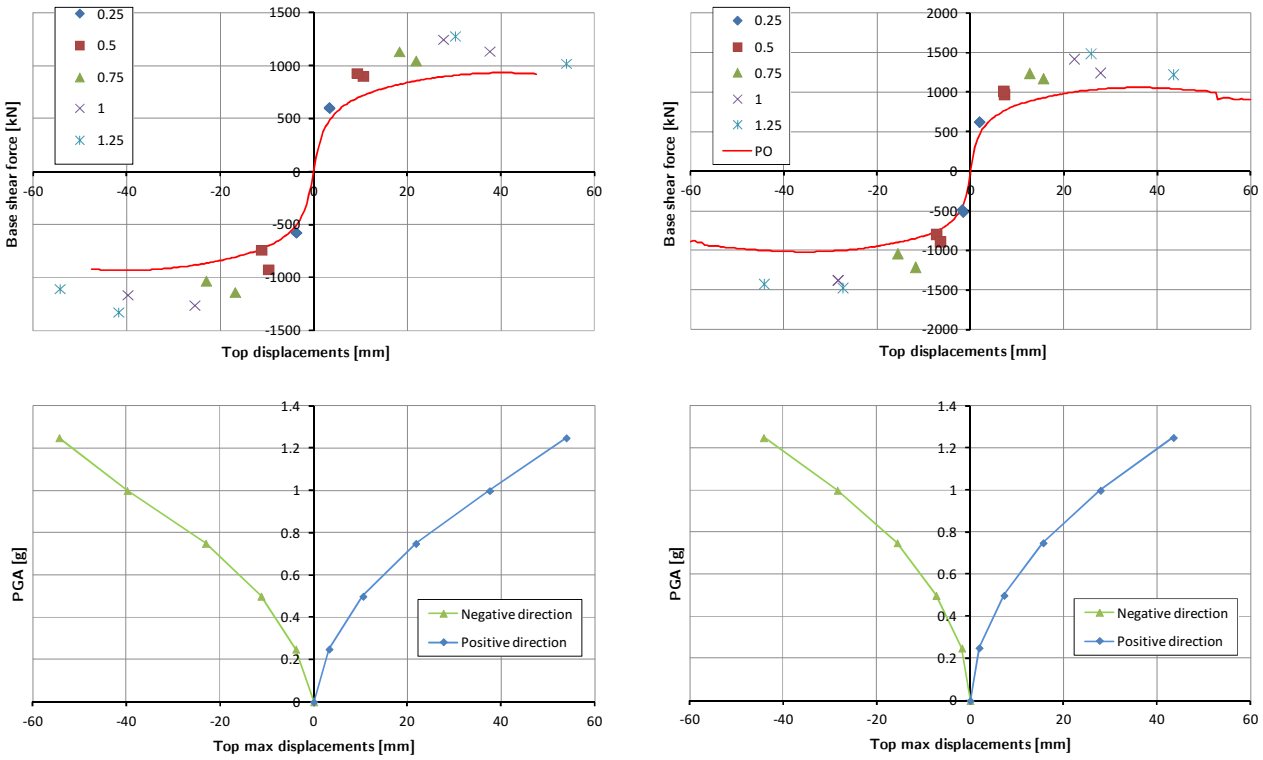

Figure 17-20. EQ1: determination of PGA_y and PGA_u along X-direction (left) and Y-direction (right) in the regular building case

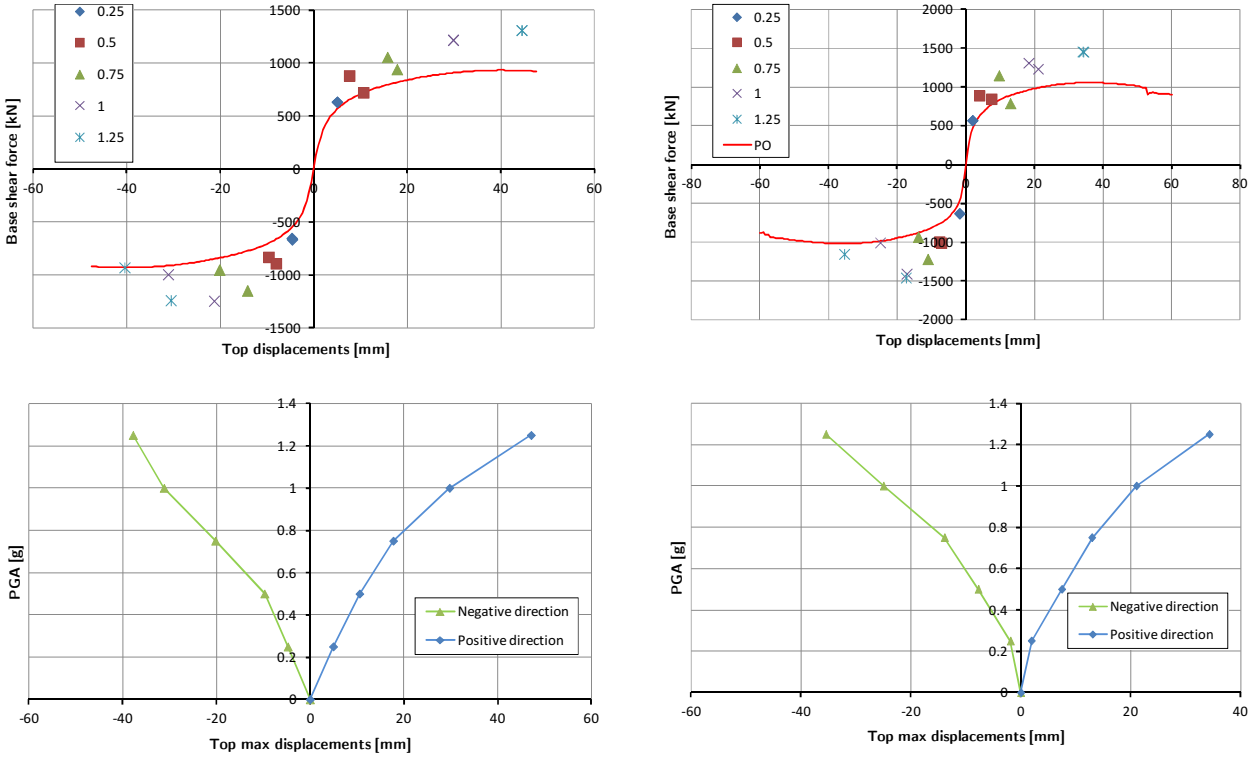

Figure 17-21. EQ2: determination of PGA_y and PGA_u along X-direction (left) and Y-direction (right) in the regular building case

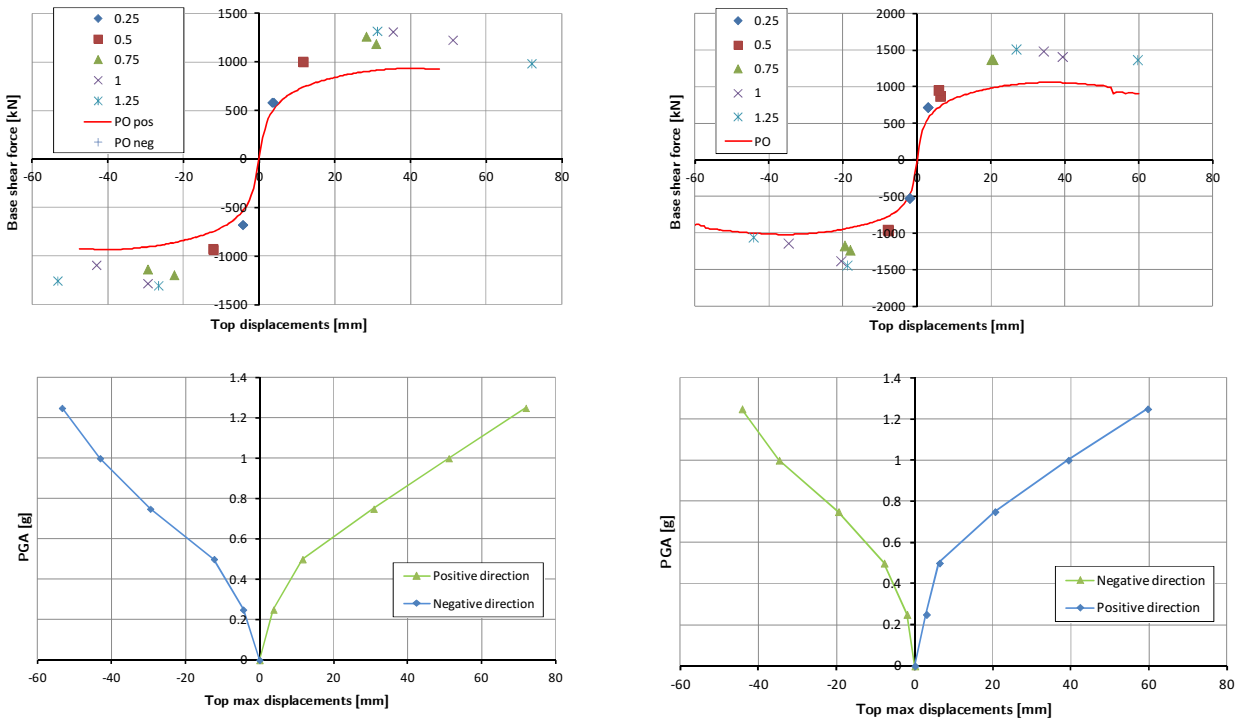

Figure 17-22. EQ3: determination of PGA_y and PGA_u along X-direction (left) and Y-direction (right) in the regular building case

17.6. Evaluation of q-factor and conclusions

The evaluation of q-factor follows the procedure described in §5.1.1.2.1 using NLDA analyses. In §5 it has been introduced that, according to (Fajfar 1996) and equation [5.4], behavior factor q can be written as:

$$q = q^* \cdot \Omega_d = \mathrm{q}_0 \cdot K_s \cdot K_r^h \cdot K_r^p \qquad [17.9]$$

Where:

- q_0 is the basic q factor pertinent to the construction system
- K_s is the overstrength factor (1.2 as suggested by LL.GG. 2011)
- K_r^p account for irreguralities in elevation (i.e. it is 1 for regular buildings and 0.917 for the irregular ones)
- K_r^h account for irreguralities in elevation (i.e. it is 1 for regular buildings and 0.8 for the irregular ones)

Hereafter, factor $q^* = q_0 \cdot K_r^h \cdot K_r^p$ is obtained with the PGA approach as the ratio between PGA_u and PGA_y.

		IRREGULAR BUILDING			REGULAR BUILDING			
Direction		*PGAy*	*PGAu*	$q^*_{irr}=PGAu/PGAy$	*PGAy*	*PGAu*	$q^*_{reg}=PGAu/PGAy$	$K_R=q^*_{irr}/q^*_{reg}$
X	*EQ1*	0.39	1.17	3.00	0.36	1.15	3.19	0.94
	EQ2	0.42	1.19	2.83	0.37	1.30	3.51	0.81
	EQ3	0.43	0.96	2.23	0.33	0.96	2.91	0.77
Mean				**2.69**			**3.21**	**0.84**
Y	*EQ1*	0.52	1.51	2.90	0.42	1.53	3.64	0.80
	EQ2	0.44	1.53	3.48	0.41	1.75	4.27	0.81
	EQ3	0.41	1.26	3.07	0.40	1.27	3.18	0.97
Mean				**3.15**			**3.70**	**0.86**

Table 17-6. Evaluation of q-factor by means of time history analysis

The following considerations can be derived from the analysis of the obtained mean behavior factors:

- in elevation regularity: irregular buildings (i.e. uniform reinforcement) demonstrate a behavior factor that is K_r^h =84÷86% of the regular building (i.e. variable reinforcement sized to the effective strength demand)
- in plane regularity: the ratio between the behavior factors along the X-direction (irregular) and Y-direction (regular) is between K_r^p =2.69/3.15=85% and 3.21/3.70=87%

- overall irregularity: the ratio between the behavior factors for the fully irregular case (X direction – uniform reinforcement) and the fully regular case (Y direction – variable reinforcement) is $K_r = K_r^p K_r^h = 2.69/3.70 = 73\%$

Therefore the code provision for which behavior factor of irregular buildings in elevation have to be penalized by a factor $K_R = 0.8$ is substantially confirmed. The performed analyses highlight that, for the considered building, the relevance of in-plane and in-elevation regularity is almost the same.

Also it has been obtained that regular buildings realized with the examined construction technology can assure a considerable basic q_0 factor, such as they can be classified as DCM (Medium Ductility Class) according to EC8 §5.2.1.

Previous coefficients do not take into account for overstrength factor K_s, which has been already estimated in §17.4.3 by means of pushover analyses.

In order to extend this kind of nonlinear analyses to the study of more complex buildings, continuous models (with bi-dimensional or tri-dimensional elements) are needed and they should be able to describe, even roughly, the local behaviors recognizable in the micro finite element approach.

Chapter 18. – Conclusions

In this Ph.D thesis, the behavior of a *construction system based on reinforced concrete cast in mineralized wooden blocks* has been studied.

The mineralized chip wood blocks used as formworks for the concrete casting lead to the realization of an grid type RC structure that provides good levels of structural efficiency and ductility. Moreover, the blocks provide very good thermo-mechanical properties in term of insulation of external walls and perspiration. The major advantage of "breathing walls" is avoiding the vapor condensation inside the structure.

The lack of any specifications in Building Codes regarding this particular construction system invoked an extensive experimental investigation, particularly focused on the behavior under seismic conditions. In the last six years the researchers of the University of Padua carried out a series of tests on this task and the results are resumed in this thesis and interpreted by means of a newly developed and theoretically well based framework.

The experimental campaign is commented in the third part, where for each type of experiment an analytical proposal for strength evaluation is described. In general, the analytical results are conservative but in very good agreement with the experimental ones. In particular an original strut-and-tie resistant mechanism has been proposed with success for the interpretation of the shear tests. The experiments performed on full scale shearwalls, with and without openings, played an important role, not only to verify analytical formulas but also to test the coherence of modeling with actual behavior. They also allowed the calibration of a nonlinear numerical model able to reproduce the cyclic behavior of the investigated shear walls.

The numerical modeling is treated in the fourth part, where a finite element (FE) model is proposed for vertical (uprights) and horizontal (transverses) elements of the internal micro-frame RC structure. The FE model implements the concepts developed with the analytical framework. Only mono-dimensional elements have been used: fiber elements with distributed damage and plasticity for uprights, truss elements with concentrated plasticity for transverses.

Once tested the coherence of FE modeling with the full scale experiments in term of displacements and dissipated energy, the numerical simulation of typical case-study buildings has been performed and described in last chapters of Part IV. Two-dimensional multistory shearwalls are considered in §16, while a full three-dimensional 3-story building is treated in §17. The aim of these simulations was the numerical evaluation of the behavior factor of regular and irregular buildings realized with the construction system under examination. The behavior factor is a crucial value in the force based approach to seismic design: it summarizes the ductility and dissipative capacities of a structural systems and allows to decrease design forces from seismic action. This value depends on many variables, like for example regularity in plan and in elevation, capacity design, ductility class, construction material, joints behavior. All these characteristics influence the building response under seismic event.

The results vary depending on the different building characteristics. A value of q equal to 3.7 has been obtained in the best scenario of regular building both in plan and in elevation. Obtained results indicate that the Italian Guidelines (LL. GG. 2011), which suggest a q_0 equal to 2 or a maximum of 3 in case of experimental tests supported by appropriate numerical analyses, are conservative. A basic value of the behavior factor q_0 equal to 3,0 seems to be more appropriate for the investigated technology, this value must be further corrected by overstrength and regularity factors.

Appendix

A.1 – Shear equation for transverses with axial compression

The internal forces of an infinitesimal element subjected to compression and shear stress are represented in Figure A-0-1 (right), whereas on the left side the corresponding Mohr's circle is drawn in black.

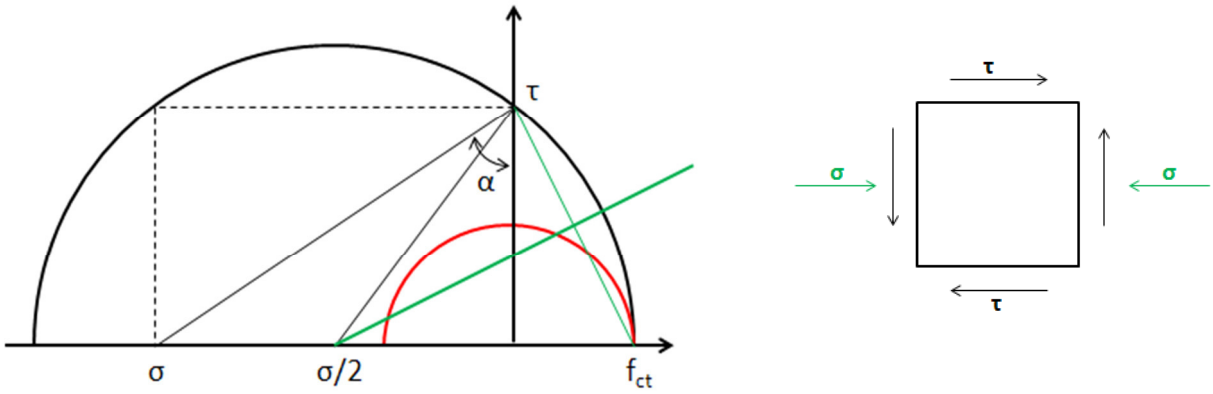

Figure A-0-1. Stresses on an infinitesimal element and its graphical representation with a Mohr's circle

The maximum stress of concrete is bounded to not exceed the tensile strength of concrete f_{ct}. The red circle represents the case α equal to zero, i.e. with no axial stress. Given an angle α that relates τ and σ, the critical circle passing through f_{ct} is to be determined.

The green line has the following equation:

$$y - \frac{\tau}{2} = \frac{f_{ct}}{\tau}\left(x - \frac{f_{ct}}{2}\right) \qquad [A.1]$$

From this equation the determination of the center of circle, σ/2, is straightforward:

$$\begin{cases} y = 0 \Rightarrow -\dfrac{\tau^2}{2f_{ct}} + \dfrac{f_{ct}}{2} = x = \dfrac{\sigma}{2} = -\dfrac{\tau}{2} \cdot \tan\alpha \\ \tan\alpha = -\dfrac{\sigma}{\tau} \end{cases} \quad [A.2]$$

From the equation above, the positive value of τ is obtained:

$$\tau^2 - \tau \cdot f_{ct} \cdot \tan\alpha - f_{ct}^2 = 0 \Rightarrow \tau = f_{ct} \cdot \frac{\tan\alpha + \sqrt{4 + tan^2\alpha}}{2} \quad [A.3]$$

Then, the shear strength for a unit length of wall:

$$v_{r,cls} = \frac{\tau \cdot A_t}{i_t} \Rightarrow v_{r,cls} = \frac{f_{ct} \cdot A_t}{i_t} \cdot \frac{\tan\alpha + \sqrt{4 + tan^2\alpha}}{2} \quad [A.4]$$

that is exactly the [9.8].

A.2 – Reinforcement details of the tested full-scale walls

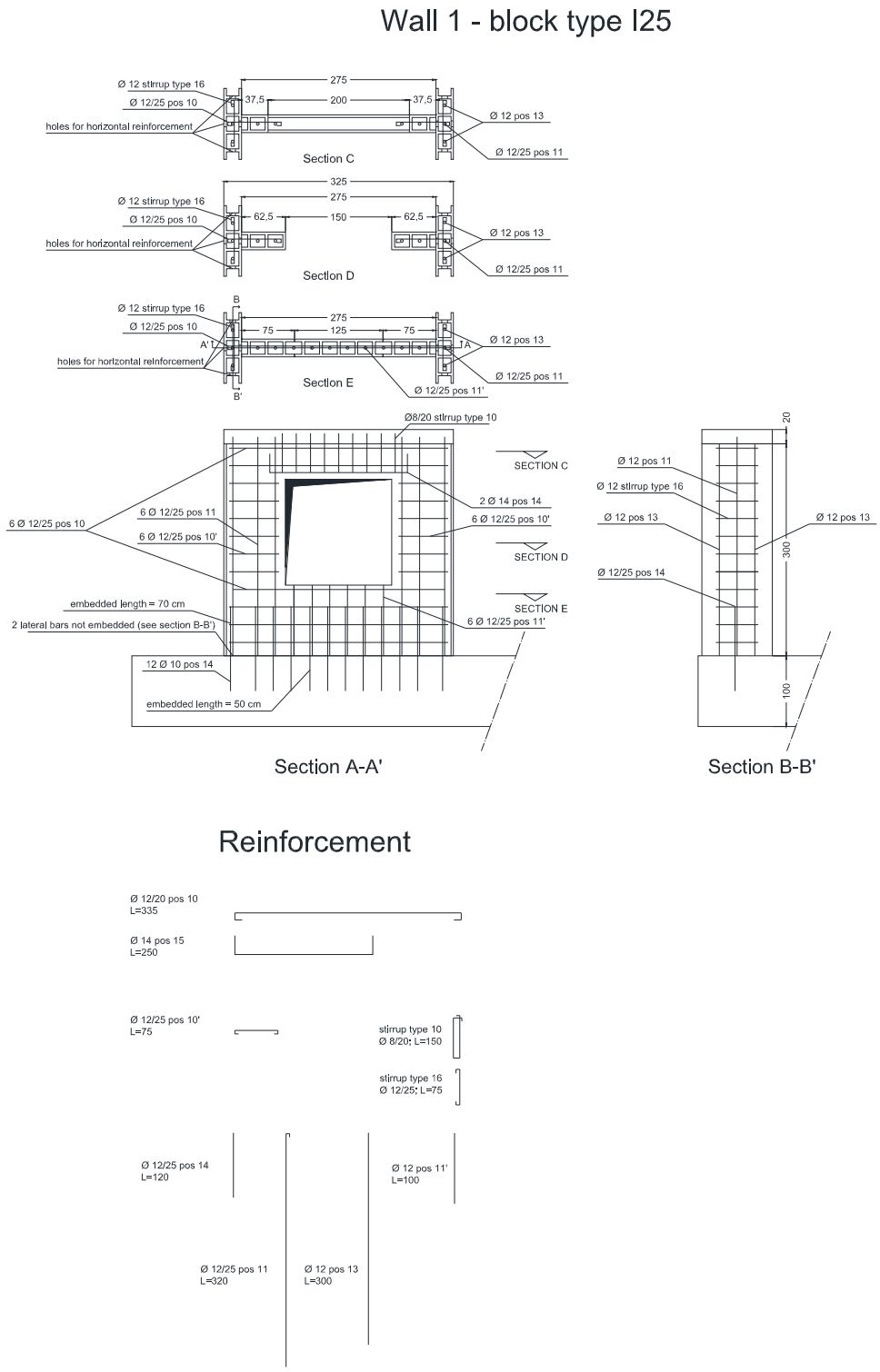

Wall 2 - block type I25

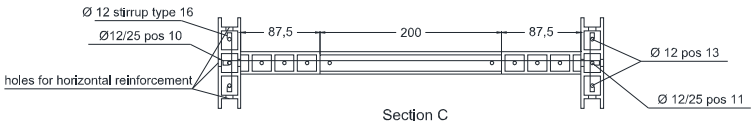

Section C

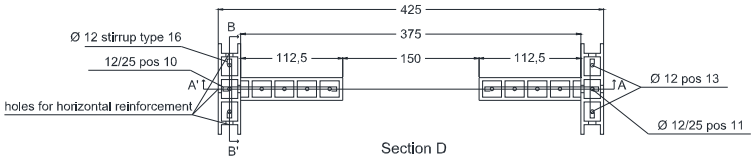

Section D

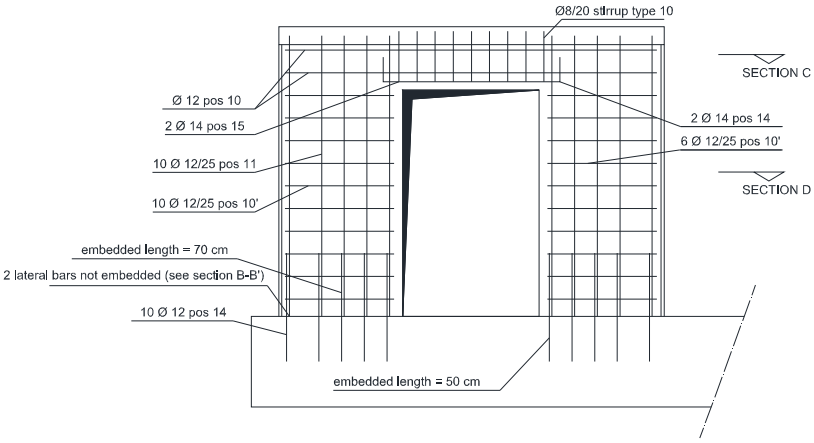

Section A-A'

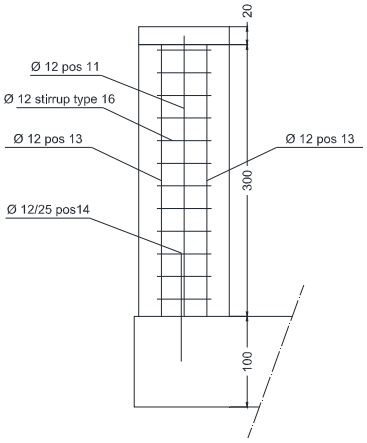

Section B-B'

Reinforcement

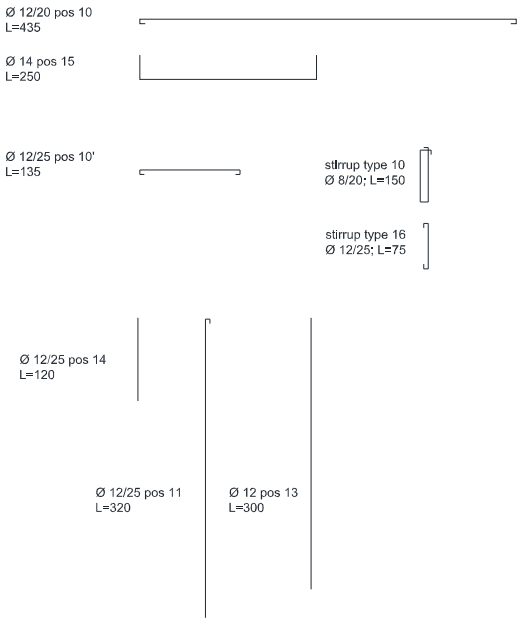

Wall 3 - block type I30

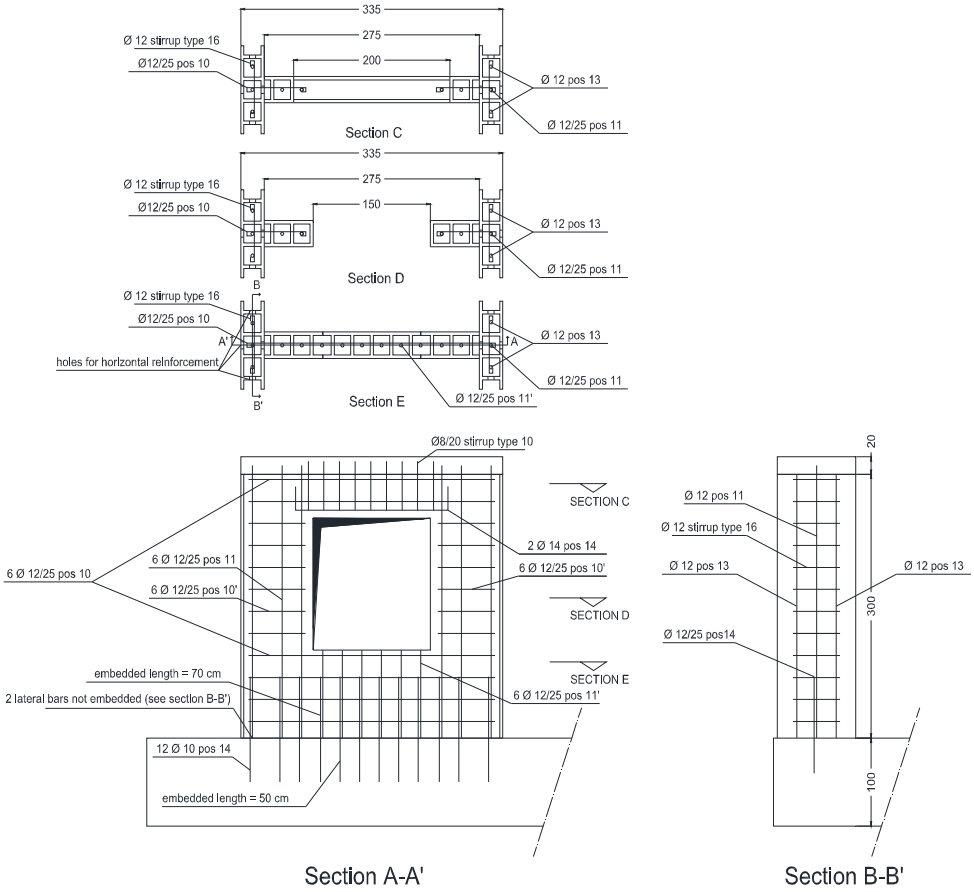

Reinforcement

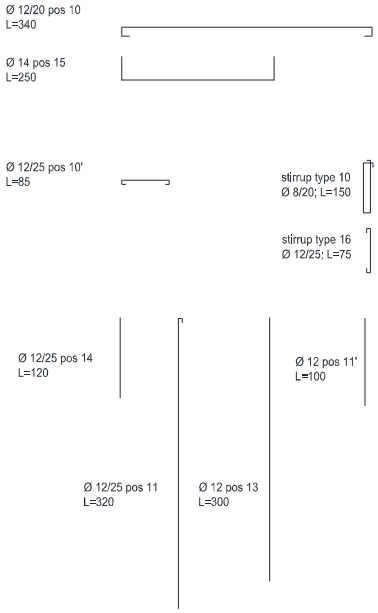

Wall 4 - block type I30

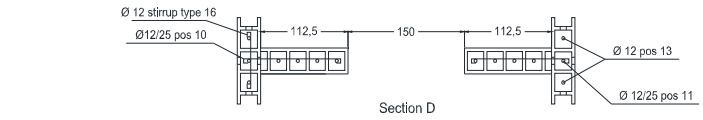

Section D

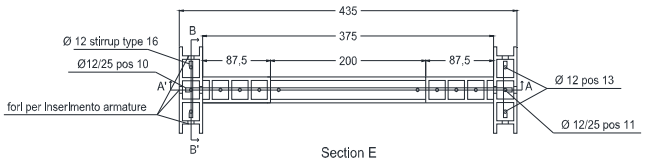

Section E

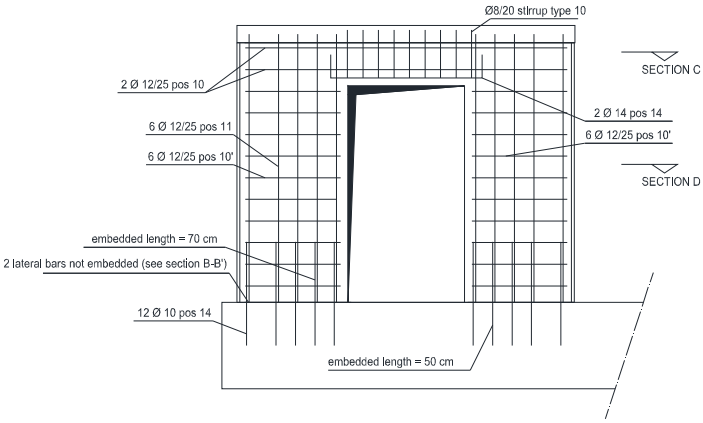

Section A-A'

SEZIONE B-B'

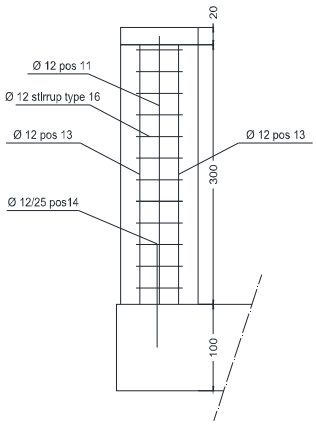

Section B-B'

Reinforcement

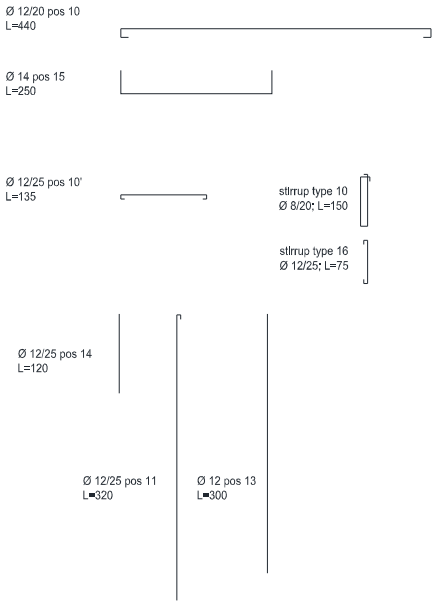

Wall 5 - block type N20

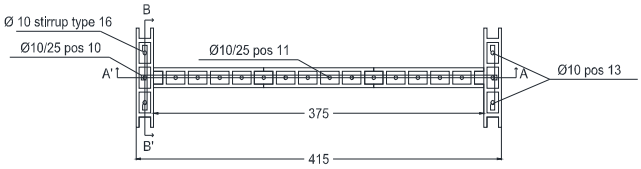

Section A-A'

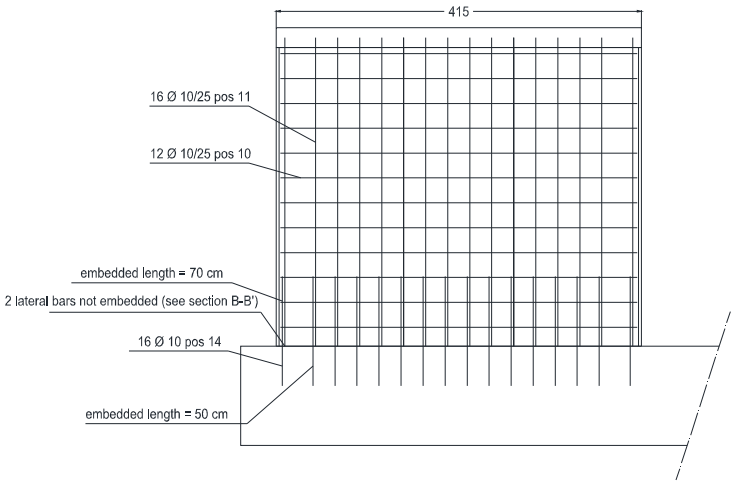

Section B-B'

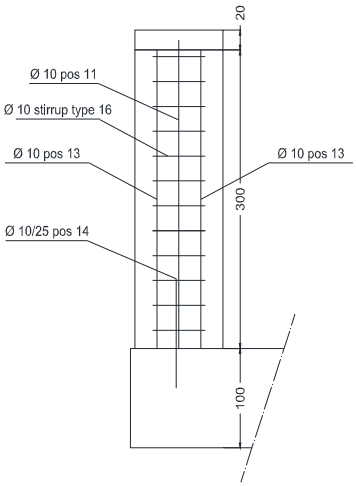

Reinforcement

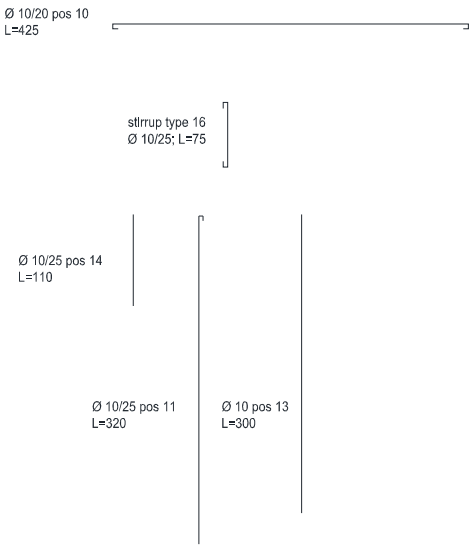

Wall 6 - block type I25

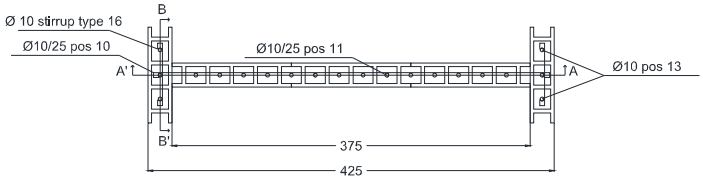

Section A-A'

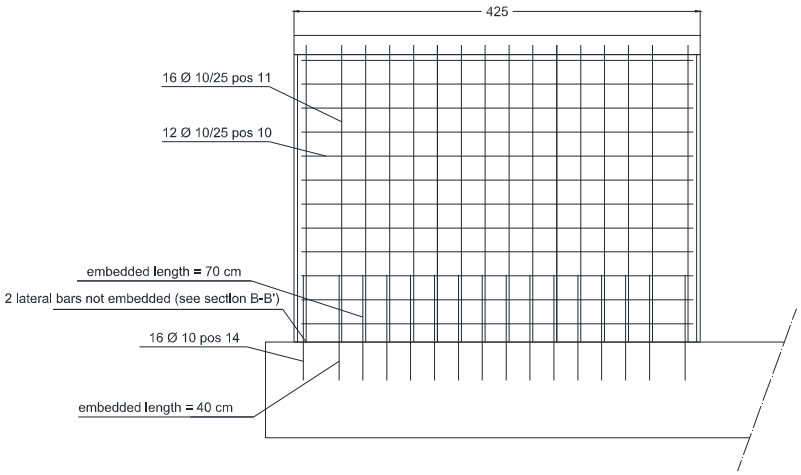

Section B-B'

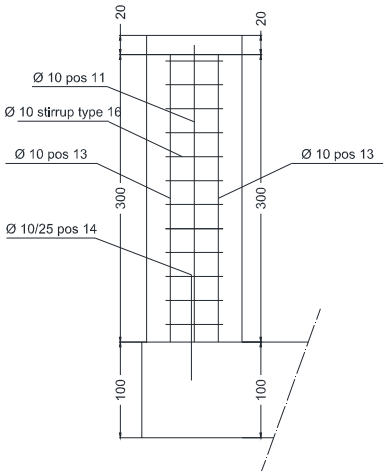

Reinforcement

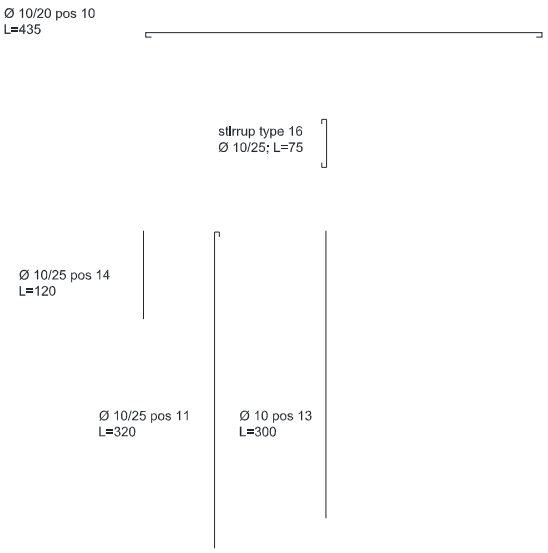

Wall 7 - block type N20

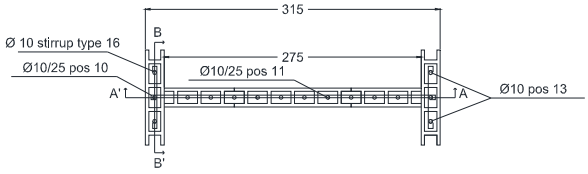

Section A-A'

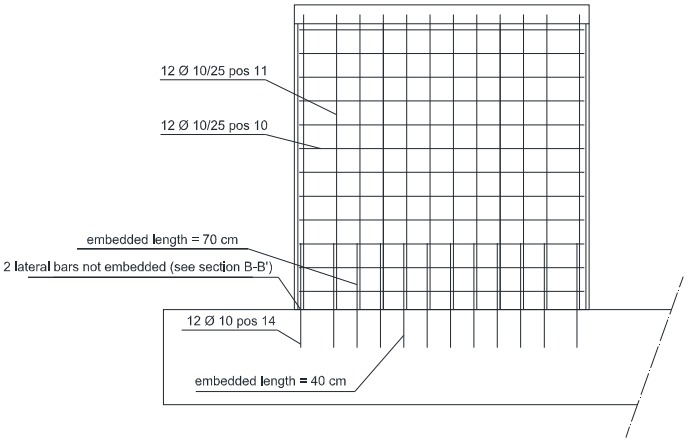

Section B-B'

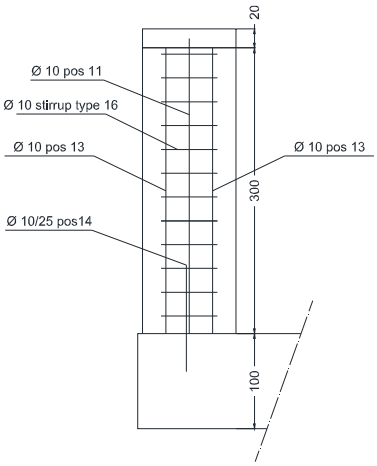

Reinforcement

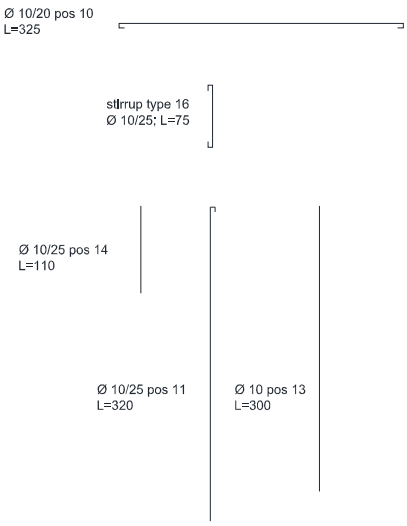

Wall 8 - block type I25

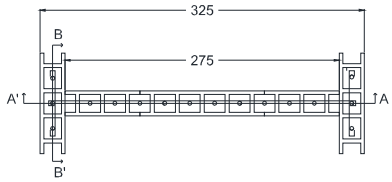

Section A-A'

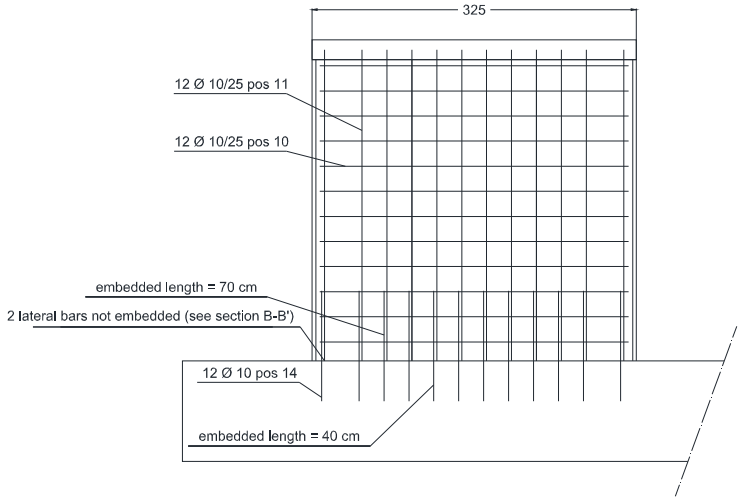

Section B-B'

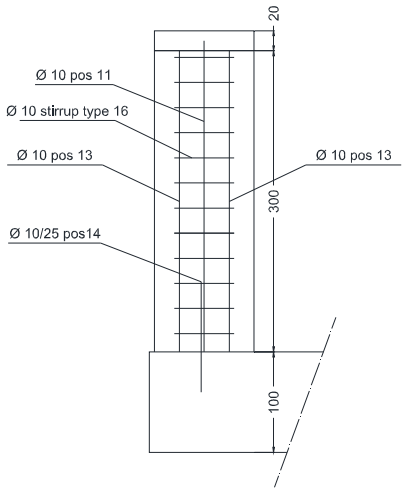

Reinforcement

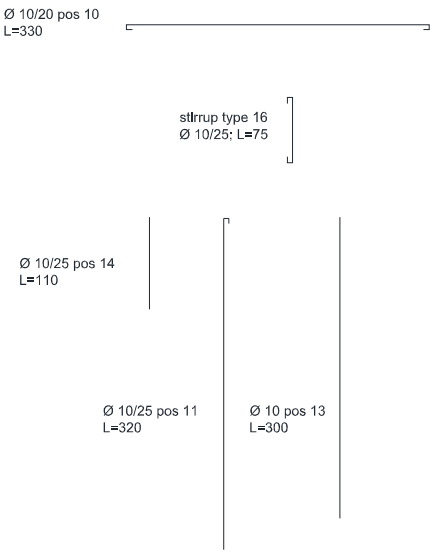

List of figures

References

AA. VV. *L'Aquila. Il progetto C.A.S.E.* Iuss press, 2010.

Aktan, E., D. A. Pecknold, e M. A. Sozen. «R/C column earthquake response in two dimensions.» *Journal of Structural Division, ASCE, 100(10)*, 1974: 1999-2015.

CEB/FIP Manual. *Buckling and Instability.* London: The Construction Press, 1978.

Ceccoli, C., G. Dallavalle, L. Mantovani, e N Tullini. «Indagini sperimentali effettuate su pareti realizzate con blocchi cassero in legno-cemento (in Italian).» *Atti del XIII Convegno CTE.* Pisa, 2000. 327-336.

Ceccoli, C., G. Dallavalle, L. Mantovani, e N. Tullini. «Indagini sperimentali effettuate su pareti realizzate con blocchi cassero in legno-cemento.» *Atti del XIII Congresso CTE.* Pisa, 2000.

Ceccoli, C., P.P. Diotallevi, e N. Tullini. «Identificazione strutturale di un fabbricato a pareti portanti realizzate con blocchi cassero in legno-cemento.» *Atti del X Congresso Nazionale L'ingegneria sismica in Italia ANIDIS.* Potenza-Matera, 2001.

Ceccotti, A., e C. Sandhaas. «A proposal for a standard procedure to establish the seismic behaviour factor q of timber buildings .» *Proceeding of the 11th World Conference on Timber Engineering WCTE.* Riva del Garda, (Italy), 2010.

Ceccotti, Ario. «New technologies for construction of medium-rise buildings in seismic regions: the XLAM case.» *IABSE Structural Engineering International. Tall timber buildings (special ed.)*, 2008: 18:159-165.

Chai, Y.H., e J.D. Anderson. «Seismic response of perforated lightweight aggregate concrete wall panels for low-rise modular classrooms.» *Engineering Structures, Vol. 27*, 2005: 593-604.

Chang, G. A., e J. B. Mander. «Seismic energy based fatigue damage analysis of bridge columns: part 1 - evaluation of seismic capacity.» NCEER-94-0006, Buffalo, 1994.

Chopra, Anil. *Dynamics of structures - theory and applications to earthquake engineering.* Upper Saddle River: NJ: Prentice Hall, 1995.

Clough R., Johnston S. «Effect of Stiffness Degradation on Earthquake Ductility Requirements.» *Transactions of Japan Earthquake Engineering Symposium.* Tokyo, 1966. 195-198.

CNR 10025. *Instructions for design, execution and inspection of prefabricated concrete structures (in Italian: Istruzioni per il progetto, l'esecuzione ed il controllo delle strutture prefabbricate in calcestruzzo).* 1998.

—. *Istruzioni per il progetto, l'esecuzione e il controllo delle strutture prefabbricate in conglomerato cementizio e per le strutture costruite con sistemi industrializzati (in Italian).* 1984.

Coull, A., e Smith B. Stafford. *Tall Buildings Structures: Analysis and Design.* John Wiley & Sons inc., 1991.

D'Ambrisi, A., e F. C. Filippou. «Modeling of Cyclic Shear Behavior in RC Members.» *J. Struct. Eng., 125(10)*, 1999: 1143–1150.

Dolce, M. «Schematizzazione e modellazione per azioni nel piano delle pareti (Italian).» *Corso sul consolidamento degli edifici in muratura in zona sismica.* Potenza (IT), 1989.

Elnashai, S., e A. M. Mwafy. «Overstrength and force reduction factors of multi-storey reinforced-concrete buildings.» *Struct. Design Tall Build. 11*, 2002: 329–351.

EN 15498. *Precast concrete products - Wood-chip concrete shuttering blocks - Product properties and performance.* Brussels: CEN, 2008.

EN-12512. «Timber Structures – Test methods – Cyclic testing of joints made with mechanical fasteners.» 2001.

ENV 1992-1-1:1991. *Eurocode 2 : Design of concrete structures, Part 1-1 : General rules and rules for buildings.* 1991.

ETAG009, European Organisation for Technical Approvals. *Guideline for European technical approval of non load-bearing pemanent shuttering kits/systems based on hollow blocks or panels of insulating materials and sometimes concrete.* Brussels, 2002.

Eurocode 2. *Design of cocrete structures - Part 1-1: General rules - General rules and rules for buildings.* Brussels: CEN, 2004.

Eurocode 3. *Design of steel structures Part 1-1: General rules and rules for building.* Brussels: CEN, 2005.

Eurocode 5. *Design of timber structures – part 1-1: general rules and rules for buildings.* Brussels: CEN, 2009.

Eurocode 6. *Design of masonry structures - Part 3: Simplified calculation methods for unreinforced masonry structures.* Brussels: CEN, 2006.

Eurocode 8. *Design of structures for earthquake resistance, part 1: General rules, seismic actions and rules for buildings.* Bruxelles: CEN, 2004.

Fajfar, Peter. *Design spectra for new generation of code. Proceeding 11th Word Conference on Earthquake Engineering.* Acapulco (Messico), 1996.

FEMA. *NEHRP provisions for the seismic rehabilitation of buildings. Report FEMA 273 (Guidelines) and 274 (Commentary).* Washington DC, 1997.

Filippou, F.C., e A. Issa. «Nonlinear Analysis of Reinforced Concrete Frames under Cyclic Load Reversal.» *EERC Report 83-19, Earthquake Engineering. Research Centre.* Berkeley, 1988.

Gasparini, G., T. Trombetti, S. Silvestri, C. Ceccoli, e D. Malavolta. «Results of pseudo-static tests with cyclic horizontal load on R.C. panels made with wood-concrete caisson blocks.» *Proceedings of the The 14 World Conference on Earthquake Engineering.* Beijing, China, 2008.

Giberson M. «The Response of Nonlinear Multi-Story Structures Subjected to Earthquake Excitation.» *Earthquake Engineering Research Laboratory.* Pasadena, 1967.

Giorgi, Paolo. *Numerical and experimental evaluation of seismic performance of RC buildings with low ductility - Core buildings and RC slab floors.* University of Padua, 2014.

Hidalgo, P.A., C.A. Ledezma, e R.M.. Jordan. «Seismic Behavior of Squat Reinforced Concrete Shear Walls .» *Earthquake Spectra, Vol. 18(2)*, 2002: 287-308.

Hidalgo, P.A., C.A. Ledezma, e R.M.. Jordan. «Seismic Behavior of Squat Reinforced Concrete Shear Walls.» *Earthquake Spectra, Vol. 18(2)*, 2002: 287-308.

Humar, J. L., e M. A. Ragozar. «Concept of overstrength in seismic design.» *In Proceedings 11th WCEE. IAEE.* Acapulco (Mexico), 1996.

ISO 15630-1. *Steel for the reinforcement and prestressing of concrete -- Test methods -- Part 1: Reinforcing bars, wire rod and wire.* 2010.

Kaba, S. A., e S. A. Mahin. *Refined modeling of reinforced concrete columns for seismic analysis.* EERC Rep. No. 84/03, Berkeley: University of California, 1984.

Keshavarzian, M., e W. Schnobrich. «Inelastic analysis of RC coupled shear walls.» *Earthquake Engineering and Structural Dynamics, 13*, 1985: 427-448.

Kunnath S. et al. «Analytical modeling of inelastic seismic response of R/C structures.» *Journal of Structural Engineering, Vol. 116*, 1990: 996-1017.

Lai S., Will G., Otani S. «Model for Inelastic Biaxial Bending of Concrete Members.» *Journal of Structural Engineering, ASCE, 110(ST11)*, 1984: 2563-2584.

LL. GG. *Guidelines for load-bearing permanent shuttering kits/systems based on hollow blocks and lightly reinforced concrete cast in-situ.* Italian Ministry of Public Works, 2011.

Magenes, G. «A method for pushover analysis in seismic assessment of masonry buildings.» *12th World Conference on Earthquake Engineering.* Auckland (New Zealand), 2000.

Malavolta, Daniele. *Strutture a pareti portanti in C.A. caratterizzate da elevate prestazioni sismiche (in Italian).* Bologna, 2008.

Meyer, C., e M. S. Roufaiel. «Analytical Modelling of Hysteretic Behaviour of R/C Frames.» *Journal of Structural Engineering, ASCE, 113(ST3)*, 1987: 429-444.

Meyer, C., M. S. Roufaiel, e S. G. Arzoumanidis. «Analysis of Damaged Concrete Frames for Cyclic Loads.» *Earthquake Engineering and Structural Dynamics vol.11*, 1983: 207- 228.

Miranda, Eduardo, e Vitelmo V Bertero. «Evaluation of strength reduction factors for earthquake-resistant design.» *Earthquake spectra 10*, 1994: 357-379.

Mitchell, D., e P. Paulter. «Ductility and overstrength in seismic design of reinforced concrete structures.» *Canadian Journal of Civil Engineering 21*, 1994: 1049–1060.

Mulas, M.G., e F.C. Filippou. «Analitical procedures in the study of seismic response of reinforced concrete frames.» *Eng. Struct., Vol. 12*, 1990: 37-48.

Neuenhofer, A., e F. C. Filippou. «Evaluation of nonlinear frame finite-element models.» *Journal of Structure Engineering, Vol. 123(7)*, 1997.

Newmark, N. M., e W. J. Hall. «Earthquake Spectra and Design.» Berkeley (Calif.), 1982.

NTC, Italian Ministery of Public Works Decree. *Technical rules for construction.* 2008.

Otani S. «Inelastic Analysis of R/C Frame Structure.» *Journal of the Structural Division, ACSE, 100(ST7)*, 1974.

Ozcebe, G., e M. Saatcioglu. «Hysteretic shear model for reinforced concrete members.» *Journal of Structural Engineering, Vol. 115 (ASCE)*, 1989: 132-148.

Page, A. W. «The strength of brick masonry under biaxial compression-tension.» *Int. Journal of Masonry Construction, Vol. 3(1)*, 1983: 26-31.

Park, R. «Explicit incorporation of element and structure overstrength in the design process.» *In Proceedings 11th WCEE. IAEE.* Acapulco, (Mexico), 1996.

Paulay, T., e M.J.N. Priestley. *Seismic Design of Reinforced Concrete and Masonry Buildings.* Wiley Interscience Press publication, John Wiley & Sons inc., 1992.

Pozza, L., R. Scotta, A. Polastri, e A. Ceccotti. «Seismic behavioiur of wood concrete frame shear-wall system and comparison with code provisions.» *Meeting 45 of the Working Commission W18-Timber Structures, CIB.* Växjö, (Sveden), 2012.

Pozza, Luca. *Ductility and behaviour factor of wood structural system (Ph.D thesis).* University of Padua, 2013.

Saiidi M., Sozen M. A. «Simple Nonlinear Seismic Analysis of R/C Structures.» *Journal of the Structural Division, ASCE, 107 (ST5)*, 1981.

Salonikios, T. N. «Shear strength and deformation patterns of R/C walls with aspect ratio 1.0 and 1.5 designed to Eurocode 8 (EC8).» *Engineering Structures, Vol. 24*, 2002: 39-49.

Salonikios, T.N., A.J. Kappos, I.A. Tegos, e G.G. Penelis. «Cyclic load behavior of low-slenderness R/C walls: Design basis and test results.» *ACI Structural Journal, Vol. 96(4)*, 1999: 649-660.

Salonikios, T.N., A.J. Kappos, I.A. Tegos, e Penelis G.G. «Cyclic load behavior of low-slenderness R/C walls: Failure modes, strength and deformation analysis, and design implications.» *ACI Structural Journal, Vol. 97(1)*, 2000: 132-141.

Suko M., Adams, P. F. «Dynamic analysis of mu1tibay multi-story frames.» *ASCE Journal of the Structural Division, 97(ST10)*, 1971: 2519-2533.

Takayanagi, T., e W. Schnobrich. «Nonlinear Analysis of Coupled Wall Systems.» *Earthquake Engineering and Structural Dynamics, vol.7*, 1979: 1-22.

Taucer, F. F., E. Spacone, e F. C. Filippou. *A Fiber Beam-Column Element for Seismic Response Analysis of Reinforced Concrete Structures.* EERC Report 91-17, Berkeley: Earthquake Engineering Research Centre, 1991.

Tomaževič, M. «The computer program POR.» Report ZRMK, 1978.

Tullini, N. *Interpretazione delle prove sperimentali eseguite su strutture a pareti portanti realizzate con blocchi cassero in legno mineralizzato (in Italian).* Bologna, 2000.

Uang, CM. «EstablishingR (or Rw) and Cd factors for building seismic provisions.» *ASCE 117(1)*, 1991: 19-28.

Vermeltfoort, A. T., T. M. J Raijmakers, e H. J. M. Janssen. «Shear tests on masonry walls.» *Proceedings of 6th North American Masonry Conference.* Philadelphia, 1993. 1183-1193.

Vianello, P. «Modellazione numerica del comportamento di pannelli gettati entro casseri in legno mineralizzato (in Italian).» M.Sc. thesis, Padova, 2009.

Vidic, T., P. Fajfar, e M. Fischinger. «Consistent inelastic design spectra: strength and displacement .» *Earthquake Eng. Struct. Dyn. 23*, 1994: 502-521.

Zeris, C. A., e S. A. Mahin. «Analysis of reinforced concrete beam-columns under uniaxial excitation.» *Journal of Structural Engineering, Vol. 114(4)*, 1988: 804-820.

Zeris, C. A., e S. A. Mahin. «Behavior of reinforced concrete structures subjected to biaxial excitation.» *Journal of structural engineering, Vol. 117(9)*, 1991: 2657-2673.

Acknowledgements

The collaboration with the researcher Eng.-Ph.D Roberto Scotta has been extremely enriching and stimulating. He has injected enthusiasm for the research into me. He has always thought to me the scientific method with his helpfulness and attention.

The opportunity of the visit in Munich has been made possible thanks to Prof. Dr.-Ing Oliver Fischer, who has distinguished for kindness in welcoming me and for commendable support. I hope that the promising collaboration will continue profitably. Thanks also to Anneliese and Erna for their help and friendship during my stay in Munich.

The funding of the Ph.D scholarship has been offered by ISOSPAN GmbH. It has the praiseworthy merit to believe in the partnership between university research and company in order to achieve the scientific and technological progress.

The experimental tests has been carried out thanks to the effective assistance of the Laboratory of Dept. ICEA at the University of Padua, that has provided the test structures and their technical support.

It has been pleasant to collaborate with the engineers Paolo Giorgi, Luca Pozza, Davide Trutalli, Luca Marchi, Enrico Stecca and Lorenzo de Stefani.

I want to thank heartily my father Maurizio, my mother Caterina, my sister Giulia, my grandmother Annamaria, my grandmother Silvana, Piero and Fernanda. All of them have accompanied me with their love, help and encouragement in this experience.

In the end I would like to thank Georg for his important suggestions and remarks.